PREFACE

I am offering the attention of the reader the following report on the scientific activity of the Frank Laboratory of Neutron Physics (FLNP) of the Joint Institute for Nuclear Research (JINR) in 2000. The report consists of two parts. The first is a brief review of the results of experimental and theoretical investigations in condensed matter physics, nuclear physics and applied research. The second contains experimental reports with more information about particular studies. The list of the 2000 publications closes the book.

In 2000 the IBR-2 reactor operated according to the approved working schedule, all of the 8 planned IBR-2 cycles were conducted.

The startup of the first stage of the new Fourier stress diffractometer was accomplished in the reported year. In the autumn cycles, the IBR-2 traditionally operated with a cryogenic moderator. Essential advances have been made in the execution of the IBR-2 modernization project. Namely, the development of the working project of the new movable reflector PO-3 completed and the manufacturing of the reflector started.

The main achievement of the year 2000 is that a group of FLNP scientists received the Russian State Prize for the development and realization of new neutron diffraction methods.

A.V.Belushkin

Acting Director

30 March 2001

1.1. CONDENSED MATTER PHYSICS

Scientific results. Diffraction. The work started in 1997 to investigate doped manganese oxides of the type $La_{1-x}Ca_xMnO_3$, $0 \le x \le 1$, where a certain level of doping triggers the Colossal MagnetoResistance Effect, continued. The effect consists of a dramatic decrease of the electric resistance of the material if an external magnetic field is applied. The reason of the decrease is the phase transition from dielectric to metallic state. The CMR effect may reach a value of 10^7 and higher. Applications of such compounds in technology will be diverse and their effectiveness may be extremely high. In the year 2000, the main direction of research in CMR-materials was carrying out of experiments to obtain information on how homogeneous the states arising at transition from dielectric to metallic phase are. Starting from the classical paper of Wollan and Koehler (Wollan E., Koehler W. *Phys. Rev.* **100** (1955) 545) simultaneous presence in the diffraction patterns of some perovskite manganites of both AFM and FM intensities is interpreted either as a uniform non-collinear (canted) magnetic phase or a spatially separated two phase state: AFM-dielectric and FM-metallic. To choose an acceptable variant for $LaMnO_{3-\delta}$ they carried out experiments in the magnetic field. On the basis of the fact that the dependence of the magnetic AFM and FM intensities on the field strength is non-correlated they came to the conclusion that the low-temperature state is a two-phase state. In the year 2000, similar experiments to investigate one of the canonical CMR compounds $(La_{1-y}Pr_y)_{0.7}Ca_{0.3}MnO_3$ (LPCM-*y*) were conducted (in collaboration with N.A.Babushkina (RRC KI), A.R.Kaul MSU) and P.Fischer (PSI)) for $y=0.75$ and 0.9 being on different sides of the boundary between the metallic and dielectric state. The experiments were done on the diffractometer DMC in an external magnetic field of up to 4 T at the temperature 4 K in PSI (Switzerland). It appears that the behavior of LPCM-75 in the field is analogous to that of $LaMnO_{3-\delta}$ (**Fig.1a**) but the intensity of LPCM-90 peaks changes in a strictly synchronous manner (**Fig.1b**). The experiments contributed essential additions to the phase diagram of LPCM-*y* and helped determine its basic states. Namely, at $y<0.60$ corresponding to the average radius of the A-cation $r_A>1.190$ Å, the LPCM basic state is a homogeneous metallic state with a ferromagnetic ordering. If $y>0.85$, i.e. $r_A<1.182$ Å, the basic state of LPCM is also homogeneous in the main but the type of conductivity is semiconducting and the magnetic moments of manganese form a noncollinear antiferromagnetic structure. In the intermediate region of r_A values there arises a mixed state with spatially separated domains of the mesoscopic size (~1000 Å) demonstrating different types of conductivity and magnetic structure. The physical reasons of formation of a two-phase state in magnetic manganese oxides are the object of further experimental and theoretical research.

In the year 2000, besides LPCM there were investigated other manganese compounds. In particular, preliminary experiments to determine the atomic and magnetic structures of $(Nd,Tb)_{0.55}Sr_{0.45}MnO_3$ and $(Nd,Sr)(Mn,Ru)O_3$ (together with A.Kaul's laboratory, MSU), Ca_2GaMnO_5 and Sr_2GaMnO_5, (together with E.Antipov's laboratory, MSU), study dimensional effects in nanocrystalline samples of $LaMnO_{3-\delta}$ (together with IFM, Ekateringurg), etc. were made.

In particular, the magnetic structure of the $(Nd,Tb)_{0.55}Sr_{0.45}MnO_3$ compound at the lowest temperature reached (~11.4 K) is quite complicated. It includes the ferromagnetic order in the sublattice of Mn cations and the ferrimagnetic order in the lattice of rare-earth cations (Nd,Tb). The magnetic moments of Mn ions are aligned along the *c*-axis of the Pnma unit cell. For the ferrimagnetic sublattice of rare-earth ions, its ferro-component is aligned strictly in the same direction as the Mn-ions moments are aligned, while the antiferro-component is aligned along the *a*-axis, formally forming a «G-type» antiferromagnetic ordering structure (all rare-earth neighbours of the given RE ion do have spins in the opposite direction). The transition temperatures of these two sublattices are not equal (**Fig.2**).

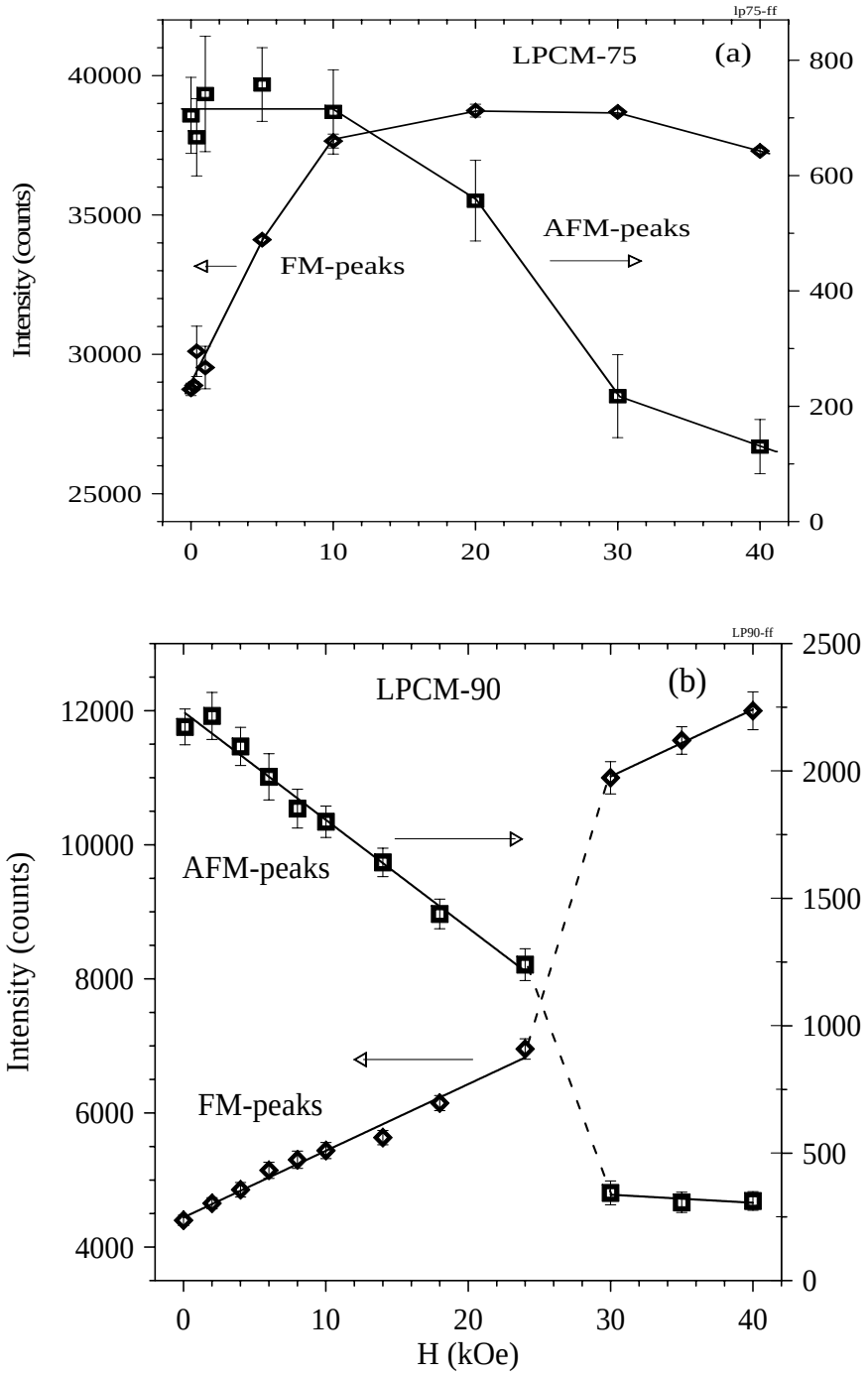

Fig.1. *The dependence of the FM- and AFM-peak intensity on the magnetic field for compositions with y=0.75 (a) and 0.90 (b). In the compositions with y=0.75 changes in the intensity do not demonstrate a synchronous behavior while in the compositions with y=0.90, they are synchronous. In the first case, the sample is in the two-phase state and changes in the intensity of AFM peaks only start to occur at sufficiently large fields. In the second case, the FM- and AFM components are related through the slope angle whose changes lead to synchronous changes of the intensity of peaks.*

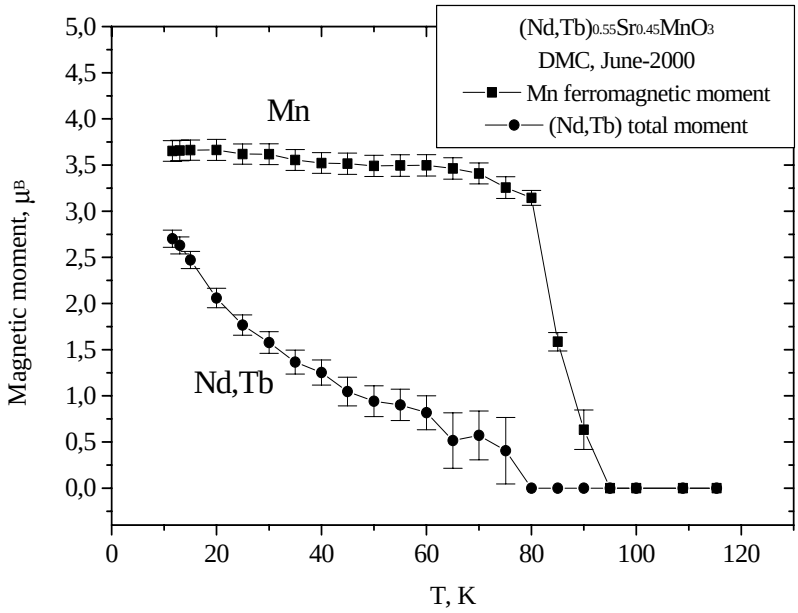

Fig. 2. *The temperature dependence of Mn and rare-earth cations (Nd,Tb) in the compound* $(Nd,Tb)_{0.55}Sr_{0.45}MnO_3$ *as measured in the neutron powder diffraction experiment.*

In the last few years in FLNP investigations of phase separation and magnetic ordering in $La_2CuO_{4+\delta}$ single crystals are conducted. Combined neutron diffraction and μSR experiments (V.Yu.Pomjakushin et al., Phys. Rev. B 58 (1998) 12350) showed that superconductivity and long range magnetic order coexist in these crystals and in addition, in $La_2CuO_{4+\delta}$ crystals with a low oxygen mobility the transition temperature to the superconducting phase coincides surprisingly with that to the static AFM phase. The problem is presently being solved in the framework of the hypothesis of the so-called microscopically phase separated state. It is however not clear yet whether the arising of a spatially inhomogeneous state favors the appearance of superconductivity or on the contrary, the two processes compete. In the year 2000, there were undertaken careful investigations in search of long range magnetic ordering, i.e. the one observed in the diffraction experiment, in a $La_2CuO_{4.02}$ single crystal with T_c=15 K where, as it is found by A.M.Balagurov et al. (Physica C, 272 (1996) 277), no macroscopic separation into phases with a high and low oxygen content exists. It has been shown that down to 2 K, the long range AFM order is absent in this crystal although from the μSR data it follows that the static magnetic order sets on at the temperature equal to T_c. The plans of further investigations into the problem include fluorination experiments of $La_2CuO_4F_\delta$ whose fluorine content may exceed the amount of additional oxygen several times.

On the diffractometer DN-12, investigations of the structure of triple compounds of mercury chalchogenides $HgSe_{1-x}S_x$ at x=0.3, 0.5, 0.6 and an external pressure of up to 3 GPa were conducted (in collaboration with IFM, Ekaterinburg). The extreme terms in the series HgS (x=1) and HgSe (x=0) have essentially different crystalline structures and crystallize in hexagonal and cubic syngonies, respectively. Of interest is to know the influence of pressure on the structure of mixed compounds. In the compound with x=0.3 the phase transition from cubic zinc-blend phase to hexagonal cinnabar phase occurs at P≈1 GPa, the jump in volume being about 12%. The dependence of the hexagonal phase parameters on the pressure is obtained.

On the diffractometer DN-2, structural modulation peculiarities in a single crystal of the ferroelectric-semiconductor $TlInS_2$ were studied in collaboration with several groups from Japan (see Experimental Reports). In the experiment, three-dimensional distributions of the scattered neutrons along the directions [100] and [001] and between the nodes of the directions [101] and [203] were measured at the temperatures: 240 K, 210 K, 203 K, 180 K, and 10 K corresponding to different structural phase states in the crystal. At these temperatures in addition to basic

(commensurable) peaks, satellites with the modulation wave vector **q**=(δ, σ, 0.25) were observed. It appears that the parameters δ and σ depend essentially on the temperature. For example, at T=203 K they turn into zero. The character of changes in the absolute and relative intensities of basic reflexes and satellites points to quasicontinuous changes of the $TlInS_2$ structure.

In the year 2000 a large volume of work in applied materials science was done using the neutron difffraction method. This includes many experiments to determine internal stresses in large-volume industrial products and materials, investigations of nanocrystalline objects, and studies of the texture of minerals. For example, it is shown that marbles possess clear preferred orientations with a much higher degree of the preferred lattice orientation as in dynamically recrystallized carbonate rocks. Hence, it is assumed that the behavior of samples is highly anisotropic at thermal dilatation. This is of interest from the viewpoint of machining and restoration of construction marble materials. In fact, the modeled thermal expansion coefficient α shows a pronounced anisotropy. It is concluded that knowing the texture is a must for the correct determination of the dilatation behavior of marbles (a collaboration with the Institute of Geology and Dynamics of the Lithosphere, Goettingen).

An attempt has been made to determine structural and textural changes of calcite as a function of temperature, mechanical stresses, and time under load. It is confirmed that texture changes due to directed strain and heating up to 250°C are quite small. In contrast, distinct texture changes are observed after a long time under load (20 weeks) at room temperature, which must be attributed to recrystallization processes. It is also shown that the thermal expansion coefficient of calcite α can be determined by neutron diffraction from polycrystalline samples. P-wave velocity measurements in the axial direction of the sample were used to calculate the macroscopic elastic module *E* of the sample and estimate lattice stresses.

Small-angle scattering. The scientific program for YuMO included many directions of condensed matter physics, biophysics and molecular biology, and the physics/chemistry of surfactants, colloids, and polymers, etc. The dependence of the structure and properties of TTABr micelles on the pressure and temperature were studied. It is found that in self-organizing TTABr systems an increase in the salt concentration leads to the phase transition from the ball-like to cylindrical shape of the micelles and to the growth of the radius and length of the cylinder. Increasing temperature produces the opposite effect, the radius and length of cylindrical micelles decrease.

The structure of monoglycerides widely used as emulsifiers and initiators of crystallization of water dissolved fats in food industry is studied. It is determined in what conditions monoglycerides solidification in water occurs, i.e. the gel-phase is formed, and how the formation of a homogeneous monoglyceride-water medium induced by added charged amphifills goes.

Gels and water solutions of N-vinylcaprolactam in heavy water in the presence of ionogenic surface-active substances and pyragallol are studied by small-angle scattering at different temperatures. It is shown that an addition of a thermo-sensitive polymer of different low-molecular substances may affect essentially the temperature behavior and conformation of macromolecules in the polymer.

Polarized neutrons and neutron optics. On the spectrometer SPN experiments to investigate the formation of a field of neutron standing waves in layered nanostructures and the channeling effect of neutron waves in layered structures continued. The prospective applications of these new effects may be the creation of a neutron beam with a super-narrow cross section (100 nm in diameter), formation of extramonochromatic and extracollimated neutron beams, and the use of layered neutron resonators as phase-shifting elements in spin-echo neutron spectrometers. The neutron wave channeling effect was observed in the Cu(30nm)/Ti(150nm)/Cu(100nm) structure deposited on glass. For the neutron moment transfer values 0.997, 0.0134, and 0.0182 $Å^{-1}$ the intensity peaks corresponding to an increase in the neutron density due to coherent summation of waves with different multiplicities of reflection from copper layers. It has thus been shown experimentally that neutron waves are channeled at distances larger than 30 mm. detectable off-specular scattering due to interface roughness is registered for samples with «atomic flat «

interfaces. Thus, magnetic pure spin-flip off-specular scattering can be attributed to the structure of magnetic correlations. These data are quantitatively described within the supermatrix formalism developed for the model of column-like antiferromagnetic domains (**Fig.3**). The reflection and

a)

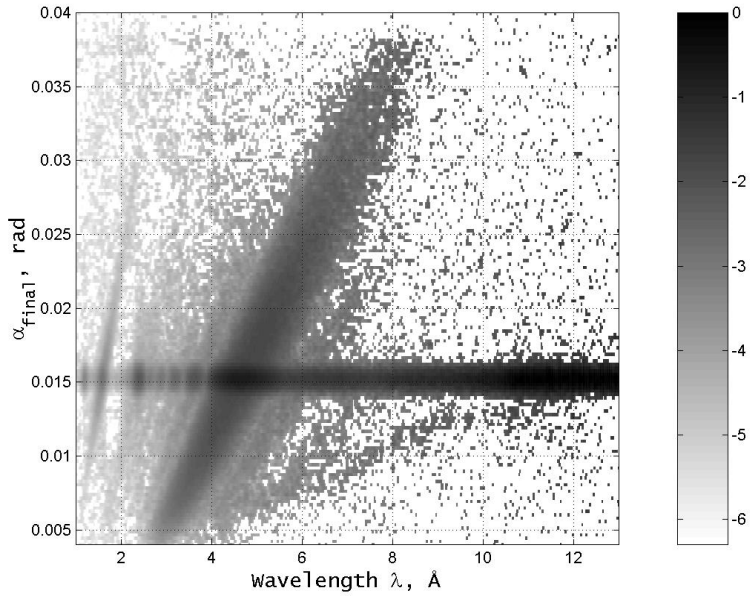

Fig.3. *a) The intensity map of the specular and off-specular scattered neutrons (spin-down) on the Fe/Cr multilayer at H=0.428 kG as a function of li and* aa_f*, the neutron wavelength and outgoing scattering angles, respectively; the incident angle* a_i *= 15 mrad;*

b)

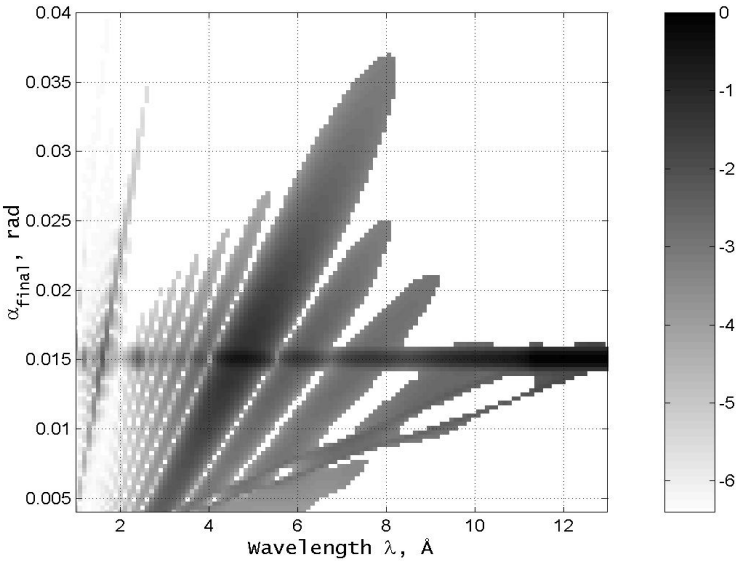

Fig.3. *b) the result of the supermatrix calculation within the model of noncollinear domains.*

polarized neutron off-specular scattering together with a complete data-analysis have been employed to verify atomic spin correlations in Fe/Cr multilayers, a typical system

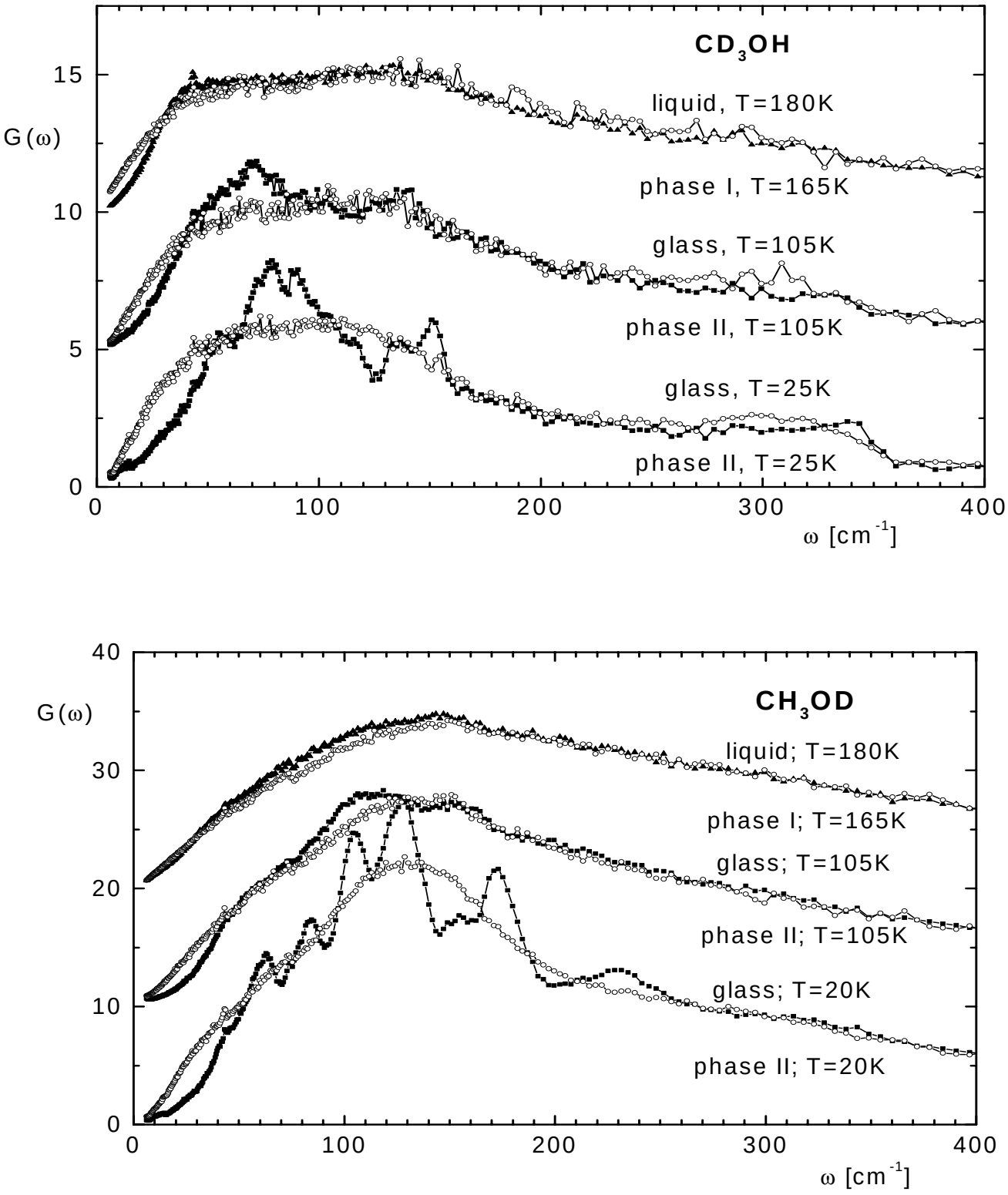

Fig.4. *The temperature dependence of the neutron scattering weighed vibrational spectra of crystalline (full square – phase II, and triangles – phase I), glassy, and liquid (open circles) methanol with partially deuterated subunits.*

showing the GMR-effect. Polarization analysis yields an important result indicating that in-plane magnetisation breaks into rather small column-like domains. For increasing external magnetic fields, within the domains spins in successive Fe-layers have an antiferromagnetic component which tends to zero along with the coupling angle. At the same time, the domain size increases. Within each domain correlations extend through the entire depth of the multilayer. No evolution of the magnetization arrangement in the range of spin-reorientation towards saturation is discussed in view of the nature of the GMR-effect. It is argued that domains may provide an efficient spin-flip mechanism for electron spin-flip scattering - a crucial ingredient of the GMR-effect.

In the spectrometer REFLEX-P-based investigations of thin polycrystalline FeCo-films indications of inelastic neutron scattering into the range of small angles are obtained, which makes it possible to assume the existence of surface or planar magnons in such substances.

Inelastic neutron scattering. On the spectrometers DIN-2PI, KDSOG-M, and NERA-PR investigations of the dynamic properties and phase transitions of metallic, molecular, and ion-molecular compounds were conducted. Most interesting NERA-PR-aided results were obtained in investigations of the dynamic disorder and glass-like phases in solid solutions and compounds containing molecular groups of the type CH_3, CH_4, H_2O or OH. The investigations were traditionally done in collaboration with scientists from Poland and Russia. In the year 2000 in the framework of this theme partial spectra of the density of vibrational states of crystalline or glass-like methanol were determined, the experiments being carried out using selectively deuterated samples of CD_3OH and CH_3OD (**Fig.4**). The obtained data were used to verify the dynamics models of the crystalline and glass-like phases of methanol and also, to determine the microscopic mechanism of arising of the «boson peak» in the low-frequency oscillation spectrum of molecular glass.

In DIN-2PI investigations of water solutions the effect of the dissolved particles on the microdynamics of water molecules entering into their hydrate spheres was determined. The effects of hydrophobic hydration and their influence on the diffuse mobility and rotation-oscillation dynamics of the hydration water molecules were studied. A comparative analysis of two types of hydration reveals the fact that large apolar particles do not destroy the network of hydrogen bonds in the surrounding water.

Investigations of the atomic dynamics of liquid metals and the behavior of impurities in them continued. Studies of Pb-K melts as prospective coolants in fast nuclear reactors of the next generation started. A DIN-2PI diffraction experiment to study a Pb-K melt with a eutectic concentration (9% at. of K) was prepared and performed. An analysis of the structure factor obtained for the region of small neutron momentum transfer reveals the absence of clasterization in this alloy in contrast to what is expected for the eutectic potassium concentration.

Investigations of the structure and dynamic peculiarities of liquids comprising laser-active systems continued. An analysis of the experimental data for liquid phosphorus oxychloride ($POCl_3$) is completed and the information inferred summarized. A search of connections between the microdynamic properties and electron excitation characteristics in this liquid was carried out. Investigations of quantum effects in restricted geometry systems continued. An experiment to study multilayer films of liquid helium on a silica aerogel was prepared and performed. The excitation spectra of liquid helium multilayer films on a silica aerogel at 1.55 K were measured for different thicknesses of helium films (see Experimental Reports).

1.2. NUCLEAR PHYSICS WITH NEUTRONS

1. Introduction

In the reported period the program of investigations in neutron nuclear physics in FLNP covered traditional and relatively new research directions. The fundamental properties of neutrons, spatial parity violation in different nuclear reactions induced by neutrons, highly excited states of nuclei in reactions with resonance and fast neutrons, astrophysical aspects of neutron physics were experimentally investigated and experiments with ultracold neutrons were conducted. An extensive program of studies in resonance neutron induced fission completed.

Development of experimental approaches of investigations in the fundamental field of time-noninvariance effects in the interaction of resonance neutrons with nuclei was under way. At present, polarized neutron transmission through polarized targets seems to be the most convenient tool to conduct direct tests of time-reversal invariance.

Applied research in the field of neutron activation analysis (NAA) and methodological development of neutron and gamma detectors of different types was carried out.

These investigations were mainly done on seven neutron beams of the IBR-30 booster, beams 1 and 11 of the IBR-2 reactor and with the experimental facility «Regata» for neutron activation analysis at IBR-2. In addition, a number of works were conducted in collaboration with nuclear centers of Russia (RRC KI, ITEP, MEPI, PNPI, PEI, RSRIEP), Ukraine (INR NU, Kiev), Bulgaria (INRNE, Sofia), Poland (UL, Lodz; INP, Krakow), Czech (NPI, Řež near Prague), Germany (FZK, Karlsruhe; Tuebingen Univ.; THD, Darmstadt; FRM, Garching), Republic of Korea (PAL, Pohang; KAERI, Taejon), France (ILL, Grenoble; CEC CEA, Cadarache), Belgium (IRMM, Geel), USA (LANL, Los Alamos; ORNL, Oak-Ridge), China (Peking University) and Japan (Kyoto University; KEK, Tsukuba) at their neutron sources.

Interesting possibilities are opening in the framework of a wide international collaboration on the basis of the new n-TOF facility put into operation in CERN at the end of the year 2000, PS-213.

2. Experimental investigations

2.1. Parity violation and time reversal invariance in neutron transmission

2.1.1. Parity violation in compound nuclei. TRIPLE results

Frank Laboratory of Neutron Physics is a member-organization of the Time Reversal Invariance and Parity at Low Energy collaboration (TRIPLE) for the study of the effective weak interaction in nuclei by measuring parity-nonconserving (PNC) asymmetries of neutron p-wave resonance cross sections. The measured PNC asymmetry values lie in the range from 10^{-3} to 10^{-1} for the neutron energy from several eV to 300-2000 eV depending on the target. A high density of states results in the enhancement of the parity violation effect by a factor as large as 10^6 compared to parity violation in the *pp*- scattering. Since compound states have contributions from many single-particle levels, it is possible to use statistical methods to determine the mean square root weak matrix element *M* of each nucleus. To date, the data-taking stage in the Los Alamos National Laboratory has completed and the data-analysis stage is approaching its final phase.

In 2000, analysis of the thorium data extended to the neutron energy above 250 eV where PNC effects of two signs are detected.

The new results show that ten positive-sign PNC effects observed earlier in ^{232}Th in the neutron energy interval below 250 eV can be interpreted as a local doorway state of the statistical nature. The results of the analysis are published by Sharapov et al.[1, 2]. A sizable parity violating off-resonance effect is not expected within contemporary theoretical models. It was experimentally proved by Mitchell et al [3], who analyzed the thorium data between resonances. The obtained

value of the PNC asymmetry P_{off} = (0.5±1.6) ~ 10^{-6} establishes an upper limit for the off-resonance PNC effect that is four orders of magnitude smaller than a typical size of the order of one percent of the PNC-enhanced resonance effect. The indium PNC data were analyzed by Stephenson et al [4]. A total of 36 *p*-wave neutron resonances were studied in ^{115}In [4] to the neutron energy 316 eV and statistically significant asymmetries were observed for nine resonances.

The ***rms*** weak matrix element value $0.67^{+0.16}_{-012}$ meV obtained in the analysis is in agreement with theoretical predictions. A detailed description of the transmission technique of PNC studies at LANL is published by Yen et al. [5]

2.1.2. Current state of work on the project KaTRIn

The project KaTRIn is for the use of an optically polarized Rb – ^{3}He nuclear target as a neutron polarizer and an analyzer of neutron polarization [6, 7]. In the reported period the quality of the polarization ^{3}He cells was improved. A new system for the filling of the cells was developed, manufactured and tested *Fig. 1*. In addition, a prototype of the ^{3}He polarizer of neutrons was installed on beam 2 of the IBR-30 neutron source and trials started. The scheme of the experiment is presented in *Fig. 2*. In the course of the trials the following is done to study the characteristics of the polarizer and complete its design:

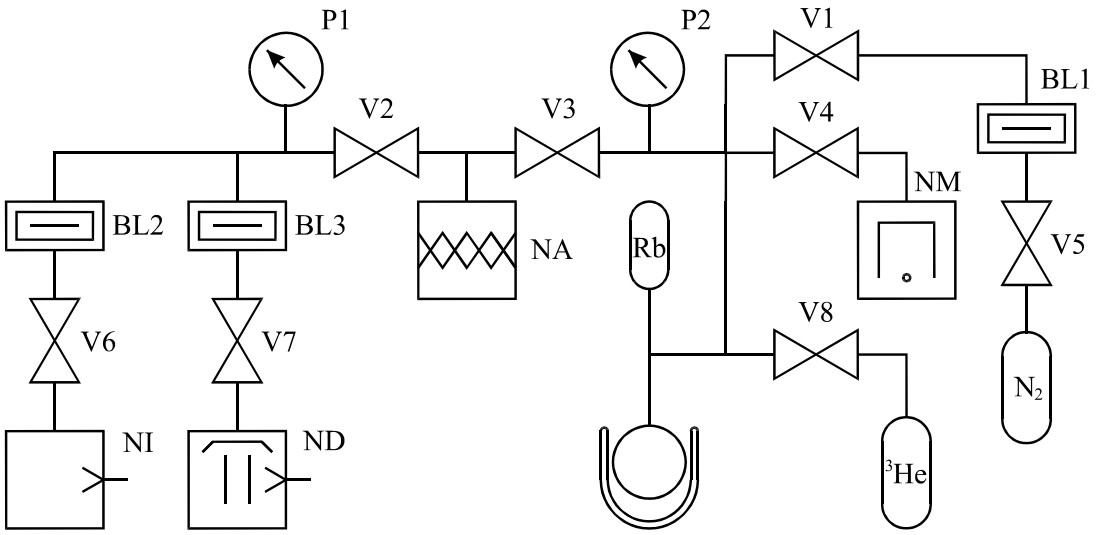

Fig. 1. *The pumping system for the ^{3}He cells. NI – forevacuum pump; ND – diffusion oil pump; NA – sorption pump; BL1, BL2, BL3 – nitrogen traps; P1, P2 – vacuum-meters.*

1. ^{3}He and correspondingly, neutrons are polarized in the absence of a leading magnetic field.
2. The possibility of measurements of P-odd effects at transmission of polarized neutrons through a ^{139}La target without reversing the neutron spin direction is verified.
3. The structure of the polarizer is optimized.

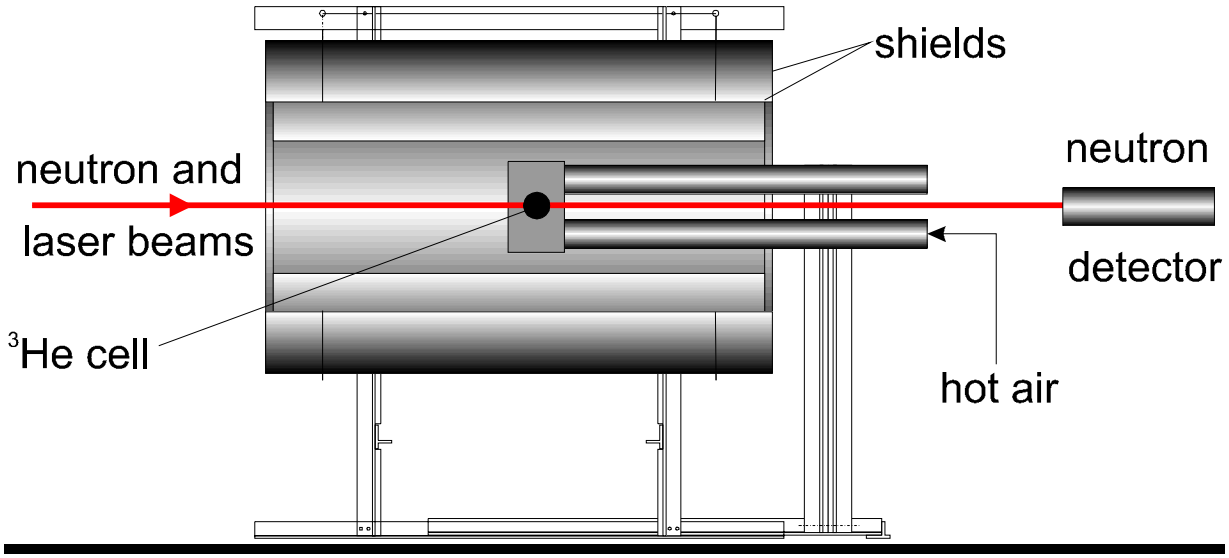

***Fig. 2**. The neutron polarizer prototype*

Work on the second paragraph of the program completed at the end of the year 2000. The stage concerned with the ^{3}He cell and laser pumping of polarization will be executed in the first half of the year 2001.

2.2. Parity violation and interference effects in angular distributions of fission fragments

2.2.1. Investigation of interference effects in angular distributions of fission fragments of heavy nuclei

In 2000, investigations of spatial parity violation and interference effects in the angular distribution of fission fragments from the resonance neutron induced fission of heavy nuclei continued. The existing theories [[8], [9]] make it possible to describe the experimentally measured asymmetry coefficients as a function of the parameters of the s- and p- wave resonances and also, of the matrix elements of the weak interaction for the coefficient a_{pv} that characterizes parity violation. In recent years, experimental investigations of above effects in the resonance energy region were carried out by joint groups of PINP (Gatchina) and FLNP, JINR. Generalized results of all the investigated effects for ^{235}U are published in [[10]]. The experiments with ^{233}U that completed in 1999 are described in [[11]].

Measurements with ^{239}Pu that were initiated in 1999 continued through the year 2000. The advantage of ^{239}Pu over uranium isotopes is that it has a noticeably smaller density of levels. The average distance between resonances is 2.3 eV. This simplifies simultaneous processing of the obtained spectra because the contribution of neighboring resonances to the analyzed section decreases. At the same time, however, this leads to a decrease of the effect as soon as it depends on the distance between the mixing levels.

The ^{239}Pu measurements will continue till the end of June 2001 for which the decommissioning of IBR-30 is scheduled.

2.2.1. Investigation of the angular anisotropy of ^{235}U fission fragments from the aligned target

A set of investigations of the angular anisotropy of fragments from the fission of aligned ^{235}U nuclei induced by resonance neutrons completed providing unique information on the contribution of K-channels to the total and spin-separated fission cross sections and the effect of their interference on the structure of the cross sections. To refine further the obtained data, it is necessary

to know more exactly the superfine electric quadruple interaction constant of the employed monocrystal uranyl rubidium nitrate targets that determines the alignment coefficient of spins in uranium nuclei. To do this, the temperature dependence of the angular anisotropy of alpha- particles on the radioactivity of the investigated samples was measured over the temperature interval $290 - 0.4K$, the experimental data processing is under way, and it is planned to conduct analogous measurements at lower temperatures.

2.3. High-excited states

2.3.1. Investigations of two-step gamma-cascades

In 2000, we continued acquisition, analysis and systematization of the experimental data on nuclear properties in the excitation energy interval corresponding to the nuclear transition from simple low-lying levels to compound states.

The goal is to identify the most general regularities of the process. The volume of the accumulated data allows the assumption that the properties of the excited states below the neutron binding energy, B_n, should be, to a large extent, due to transition from superfluid to usual phase of nuclear matter.

In 2000, the intensity distributions of two-step cascades following the α-decay of ^{40}K, ^{60}Co, ^{80}Br, and ^{185}W compound nuclei were measured. In addition, an analysis of the earlier data obtained for ^{191,193}Os was preformed.

It should be noted that high statistics in joint Dubna - Řež experiments makes it possible to determine the intensity of two-step cascades as a function of the energy of intermediate cascade levels for ^{185,187}W and ^{191,193}Os compound nuclei with an uncertainly not more than 10-20%. This allows one to verify the earlier conclusions based on data with a higher uncertainty and obtain a more detailed picture of processes occurring in nuclei.

Experiments were performed to systematize the phenomena observed earlier and extend the database on the density of levels with a given spin and parity and on the radiative strength functions as most informative parameters of the process under study. We developed and tested the new technique of data analysis to derive not only the total level density but also to determine separately the level density for positive and negative parities from the experimental data. This provided additional evidence in favor of an earlier conclusion about the possibility of rather abrupt changes in the properties of heavy nuclei in the vicinity of the excitation energy 3-4 MeV.

The obtained data are needed for the verification and further development of the level density models that take into account the coexistence and interaction of usual and superfluid phases of nuclear matter over the entire range of nuclear excitation energies below the neutron binding energy, B_n.

2.3.2. Investigations of radiative neutron capture, the nuclear data program

Three sets of measurements of gamma-ray multiplicities in the radiative capture of neutrons by ^{238}U and ^{232}Th nuclei were carried out using a 16-section liquid scintillation detector with a volume of 80 l and a HPGe detector on beam 3 of IBR-30 (123 m base, spectrometer PARUS) [12]. The measurements were conducted to determine the radiative capture cross section of ^{232}Th. Using it as a reference has made it possible to determine the group average radiative cross section and the cross sections in resolved resonance of ^{232}Th with an accuracy of 4-9%. Within the indicated errors, the experimental values are in good agreement with the values calculated with the libraries ENDBF/B-6, JENDL-3, and BROND (Table1, Table2). The measurements will continue in the year 2001 using ^{232}Th filter-samples of different thickness to determine the resonance self-shielding factors.

Table 1

The radiative cross sections in resolved ^{232}Th resonances at neutron energies from 21.5 to 215 eV*

E(eV)	RC(barn)	R_{ENDF}	R_{JENDL}	R_{BROND}
21.79	371.6 ± 12.5	1.05	1.03	1.04
23.46	572.7 ± 19.2	0.98	0.98	0.99
59.51	252.6 ± 10.1	1.13	1.11	1.11
69.19	877.8 ± 30.3	1.00	1.01	0.97
113.03	346.9 ± 16.0	1.14	1.17	1.12
120.85	407.9 ± 16.5	1.05	0.95	1.05
129.19	90.0 ± 8.1	1.00	0.95	0.97
170.39	398.2 ± 19.9	0.95	1.04	0.95
192.70	232.5 ± 18.8	1.17	1.14	1.11
199.40	152.1 ± 12.7	1.12	1.05	1.08

* R_{ENDF}, R_{JENDL}, R_{BROND} are the ratios of the results reported in [12] to the cross section values in the libraries ENDBF/B-6, JENDL-3, and BROND, respectively.

Table 2

The group average radiative capture cross-sections of ^{232}Th

E(eV)	RC(barn)	R_{ENDF}	R_{JENDL}	R_{BROND}
21.5 ÷ 46.5	37.9 ± 1.6	1.00	0.99	1.00
46:5 ÷ 100	21.1 ± 1.0	1.02	1.02	1.01
100 ÷ 215	13.8 ± 0.9	1.05	1.04	1.03

On beam 6 of IBR-3, measurements of the multiplicity spectra of gamma- rays at radiative neutron capture in ^{235}U in the neutron energy range 2 meV ÷ 2 eV completed.

On beam 6 of IBR-30 (500 m flight path, ROMASHKA spectrometer), three sets of measurements of ^{235}U radiative capture spectra of 15 multiplicities were conducted in the neutron range 20 eV to 10 keV, which made it possible to obtain the value of $\alpha = \sigma_\gamma / \sigma_f$, the radiative capture to fission cross section ratio, for over 200 resolved resonances up to the energy 300 eV and the averaged over energy values of α up to the energy 10 keV.

2.3.3. Partial capture cross- section determination by measuring energy shifts of primary gamma-transition

Development of the new neutron spectroscopy method consisting of the measurement of the energy shift of the primary γ-transition, which first allowed the determination of the energy dependence of the partial cross section of radiative neutron capture, continued. In the year 2000, the partial cross sections of ^{58}Ni for γ-transitions to the ground, first, and the second excited states of the daughter nucleus ^{59}Ni were conducted at neutron energies from 10 to 100 keV. This has become possible due to the development of a compact experimental geometry allowing a two times increase in the luminosity of the method in comparison with the time of flight method applied at a similar electrostatic generator operating in the pulsed mode.

The analysis of the results [13] contributed new information about the nature of γ-transitions and radiative strength functions of multipolarity M1 and made it possible to refine spin identification of a number of ð-wave resonance.

Distinct correlation between reduced neutron widths of s-wave neutron resonances and partial γ-widths of transitions to the ground state is discovered. This speaks for the single-particle nature of the investigated γ-transitions.

The partial cross section of γ-transitions to the first excited state is strongly suppressed for s-wave neutron resonances because for γ-transitions between the states with spins 1⁄2 $^{+}$ and 5/2^{-} the multipolarity can be either M2 or E3. For ð-wave neutron resonances with spin 3⁄2^{-}, M1 transitions are possible and for resonances with spin 1⁄2^{-}, E2 γ-transitions can take place. An analysis of the results of our measurements of $\sigma(n,\gamma_1)$ leads to the conclusion that spin identification of resonances in the last compilation by S.I. Sukhoruchkin [14] is not correct. Our results are described well if the compilation of the Oakridge group [15] is accepted.

To the cross section $\sigma(n,\gamma_2)$ there contribute γ-transitions of the same multipolarity as of transitions to the ground state. However, no correlation with reduced neutron widths is observed in this case.

The possibility of analysis of stationary neutron spectra over the energy interval 10 – 150 kev is experimentally verified [16].

2.3.4. Measurements of radiative capture spectra

On beam 5 of IBR-30, spectra of the radiative capture of neutrons with the energy up to 100 eV by the nuclei of the isotopes ^{181}Ta , ^{121}Sb, ^{123}Sb were measured in collaboration with the group of Prof. M Psitula (Lodz, Poland). For antimony isotopes, correlations between population of the excited states and spins of resonances are observed, which allows the use of precision gamma-spectroscopy to study the resonance structure of this nucleus.

2.4. Neutron reactions with emission of charged particles

2.4.1. Investigations of the (n,p), (n,α) reactions on resonance neutrons

On beam 1 of the IBR-30 pulsed source of FLNP JINR, the angular distribution of fission products from the reaction ^{35}Cl(n,p)^{35}S in the region of the resonance E_0=398 eV was measured. This was aimed at determination of the parameters of the angular distribution and extraction from them of partial neutron and proton widths, $\Gamma_{n,p}^{1/2,3/2}$, for the p-wave resonance of ^{35}Cl. A two-section ionization chamber with a grid and a system of acquisition and analysis of multidimensional data were employed in the experiment. Several runs of measurements were conducted. The obtained data are being processed.

2.4.2. Investigations of the (n, p), (n, α) reactions on fast neutrons

At the EG-5 accelerator of FLNP JINR, methodological measurements of the ^{6}Li(n,α)T and ^{235}U(n,f) reactions on neutrons with the energy 4.14, 4.79, 5.24, 5.76 MeV were carried out using a two-section ionization chamber with removable samples and a system of acquisition and analysis of multidimensional data. The goal was to test the created complex of equipment and method for the investigation of the (n,p), (n,α) reactions on fast neutrons. The neutron source was the D(d,n)^{3}He reaction. There was used a solid TiD-target without special cooling and the deuteron current 2-4 μa. The results helped assess the neutron flux and the background conditions of the experiment. Today, equipping of the special channel and the cooling system of neutron producing targets is completed, which will increase the deuteron current by an order of magnitude and as a result, raise the neutron yield.

In collaboration with Peking and Tsinghua Universities (Peking, China) experiments to measure the cross sections and angular distributions of the ^{6}Li(n,α)T, ^{10}B(n,α)^{7}Li, ^{58}Ni(n,α)^{55}Fe, ^{64}Zn(n,α)^{61}Ni reactions for a number of neutron energies in the interval 1-7 MeV were conducted. The experiments were carried out with the Van-de-Graaf accelerator of the Institute of Heavy Ions of Peking University and the two-section ionization chamber with removable samples constructed in FLNP JINR. The measurement of ^{6}Li and ^{10}B was made at E_n=1.8 and 2.6 МэВ with neutrons from the T(p, n)^{3}He reaction. The objective of the experiment

was to investigate the behavior of the angular distribution (differential cross section) of reaction products with changing energy of the incident neutron for light nuclei. The obtained experimental data are being processed. Measurements of ^{58}Ni and ^{64}Zn were made at E_n=6.8 MeV with neutrons from the D(d,n)^{3}He reaction. They were aimed at the study of contributions of the different mechanisms of the reaction (compound nucleus, pre-equilibrium and direct processes). The experimental data are being processed.

Processing of the experimental data on the ^{39}K(n,α)^{36}Cl and ^{40}Ca(n,α)^{37}Ar reactions for neutron energies in the interval 4.5-6.5 MeV completed. The total, partial (α_0, $\alpha_{1,2}$), and differential cross section values are obtained. The obtained data together with the data by other authors were used to analyze the parameters of the reactions in the framework of the spherical optical and dispersion optical model. The results of the analysis show that the two models describe well the parameters of the (n,α) reaction on ^{39}K and ^{40}Ca for the neutron energies below 7 MeV [17, 18, 19].

2.4.3. Program of (n, α) reaction measurements to study explosion nucleosynthesis

In 1999-2000 the procedure was developed and first successful measurements of the ^{147}Sm(n,α)^{144}Nd reaction were conducted on neutron beams of the accelerator ORELA in Oakridge USA. In 2000, the results of interest for astrophysics were obtained and prepared for publication.

The new data on this reaction at energies from 3 eV to 500 keV (***Fig. 3***) were used to verify nuclear statistical models employed to calculate the rapidity of the reactions (including those that are impossible to measure) involved in the scenarios of explosion nucleosynthesis [20].

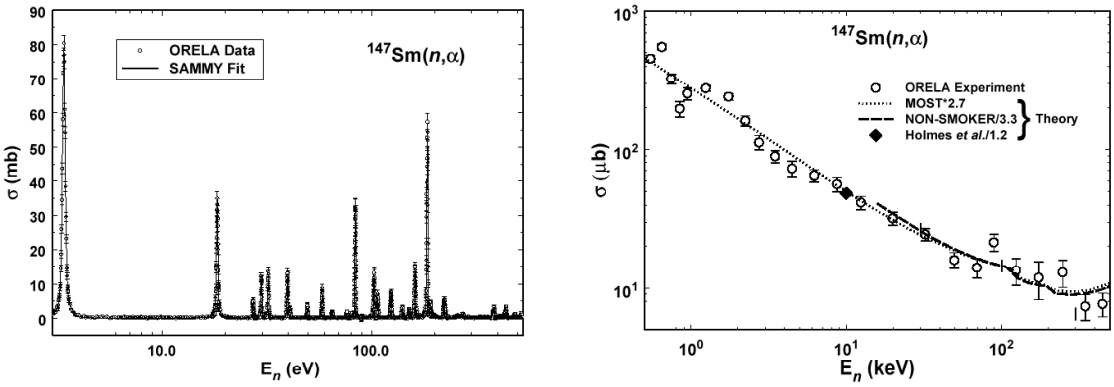

Fig. 3. *The cross section data from [20] for the ^{147}Sm(n,α)^{144}Nd reaction in the region of resolved resonances from 3 to 530 eV (left) and of unresolved resonances from 0.5 keV to 500 keV (right).*

2.5. Physics of ultracold neutrons (UCN), neutron optics

2.5.1. Investigations of "weak" UCN heating at their storage in traps

At the reactor of ILL studies of the mechanism of weak UCN heating continued. The temperature dependence of inelastic UCN scattering with a small energy transfer (~10^{-7} eV), weak heating, on the surface of beryllium or copper was observed. The intensity of scattering on the surface of these materials decreased 2.5 times as the temperature changed from room to liquid nitrogen temperature. The upper and lower limits of the probability of UCN heating with a small energy transfer were refined.

The experimental upper limit of subbarrier UCN transmission through a 14 um vacuum-tight beryllium foil was improved two orders of magnitude to be $(-1.2 \pm 1.0)\cdot 10^{-8}$ per bounce.

2.5.2. Neutron spin optics

The Larmor precession of spin was used as a clock to measure the difference between the speeds of the neutron in vacuum (**V**) and matter (**nV**), where **n** is the refraction index. The experiment was staged on the spin-echo spectrometer IN15 of the Laue-Langevin Institute. The change in the time of flight $\Delta \mathbf{t} = \mathbf{k}(1-\mathbf{n})\dfrac{\mathbf{d}}{\mathbf{V}}$ due to refraction in the sample of thickness **d** gives rise to an additional precession phase, $\Delta\varphi = \omega_L \Delta t$, where $\omega_L = \dfrac{2\mu B}{\hbar}$ - Larmor frequency, μ - neutron magnetic moment, **B** is the magnetic induction. It is the precession phase that is measured in the experiment. The effect was measured for a number of samples of silicon, beryllium, quartz, and pyrolytic graphite. The experimentally obtained values of the refraction index coincide, within several percent, with the theoretical values of $\mathbf{n} = \sqrt{1 - \dfrac{4\pi\rho b}{\mathbf{k}_0^2}}$, where b – coherent scattering length, ρ - nuclear density, $\mathbf{k}_0$ - is the wave number. The measuring accuracy of the delay in the time of flight was $(3\div5)\text{x}10^{-10}$ sec. The sensitivity of the method is so high that even the effect of diamagnetism in the sample material (usually small) affects the results.

2.5.3. UCN diffraction on a moving grid

A quantum experiment to observe a discrete energy spectrum at diffraction of initially monochromatic (ultracold) neutrons on a moving grid was staged on the UCN spectrometer with interference filters in ILL. The quantum experiment is thus made with the help of an instrument based on quantum principles. The basic result is illustrated in *Fig. 4.*

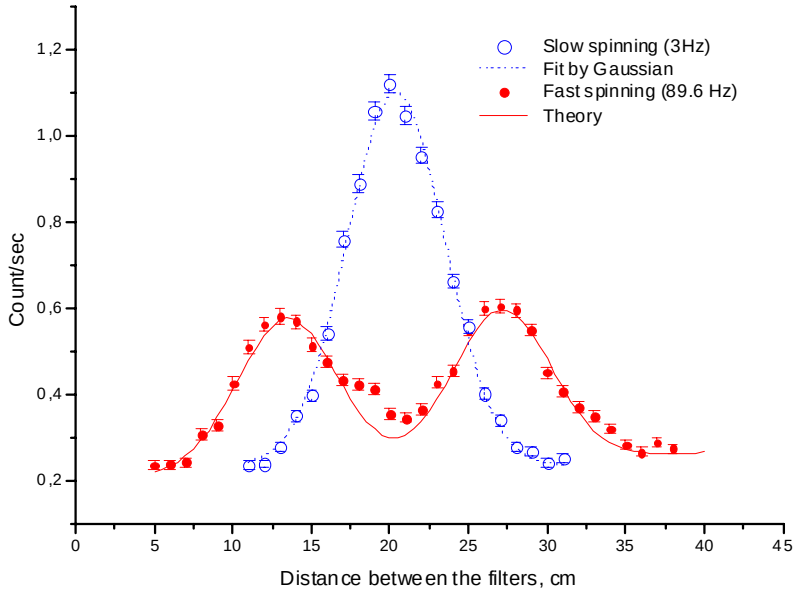

Fig. 4. *The dependence of the counting rate of the UCN detector on the distance between resonance filters.*

In the figure, the open points represent the measured spectrum of neutron transmission through a grid moving at a very small velocity and the corresponding curve is the fitting of the spectrum. The full points represent the measured spectrum of neutron transmission through a fast moving grid, the curve being theoretical.

The essence of the phenomenon can be explained in terms of frequency modulation of the primary beam occurring as the moving periodic structure traverses the neutron beam. The modulation frequency is $\Omega = \pi \mathbf{V}/\mathbf{a}$, where 2a is the period of the grid and V is its linear velocity. In the discussed case, it is a purely phase modulation, $\Omega \approx \mathbf{1.07}\times\mathbf{10}^{7}$ radian/s. (10 MHz).

2.5.4. Neutron scattering on optical inhomogeneities at resonance tunneling

An experiment to observe neutron scattering on optical inhomogeneities at resonance tunneling through an interference filter was performed in ILL. As calculations show, in the conditions of resonance tunneling the cross sections of all processes, including absorption and scattering, increase several orders of magnitude. This is due to a long stay of the neutron in the system. We assume that this fact may lead to the effect of resonance mode mixing in quantum systems comprising three barriers and two potential wells. In accordance with the general principles of quantum mechanics the splitting of quasibound state levels occurs in such systems. The experiment consisted in that the primary neutron spectrum irradiating the system corresponds basically to just one resonance. The scattering on inhomogeneities results in the appearance of neutrons with the energy corresponding to another resonance. The experiment confirmed qualitatively our assumption.

The prospects of the work consist of the development of a new, highly sensitive approach to investigations of the quality of inter-layer surfaces important for applied neutron optics. A better understanding of resonance scattering processes will allow a more reliable interpretation of the results obtained earlier in the experiment of verification of the UCN dispersion law.

3. Theoretical research

3.1. Structure of neutron-excess Λ - hypernuclei

Calculations of different hypernuclei in the 1ð shell (^{12}Be,^{9}He,^{11}He,^{11}Li,^{16}C) were performed by the Skirm-Hartri-Fock method. To obtain the experimental values of the separation energy of the neutron halo in the primary nucleus, fitting of the single-particle potential acting on the neutron was carried out. The halo system is considered to be a neutron in a pure single-particle state immediately outside the core whose ground state is excited both by the neutron and hyperon.

3.2. Correlation between the polarizations of two particles [21]

It is known that if a pair of spinor particles in the singlet state is born in the system in the process of reaction, the polarization of one is strictly determined by the polarization of the other. This means that having measured the polarization of one particle we can be sure that the spin of the other particle has an exactly opposite direction.

In [21] the $\pi^{+}+^{4}$He=p+^{3}He reaction, where the first two primary particles are scalar and have a common spatial parity of –1 while each of the two final particles has the spin s=1/2, is investigated. Since this common parity must conserve, the final particles can be only born in the triplet spin state. Therefore, the spins of the particles correlate. If protons with a given spin projection are separated, the nuclei ^{3}Íå will mainly have the polarization in the same direction in these events. It is true, however, that this will not be a 100% polarization.

3.3. Aaronov-Bom effect [22]

As it is known, as electrons experience scattering on toroidal magnets, the interference of the electron waves that passed through and round the toroid magnet hole takes place. In this case, the interference pattern depends on the magnetic flux enclosed in the toroid. The interference even occurs when the toroid is covered with an electron absorbing material, i.e. the electrons diffracted from the toroid do not come into immediate touch with the magnetic

field in its interior. The calculation of the integral cross section of inelastic scattering on a thin toroid covered with an absolutely black screen and having a hole of the area S gives

$$\sigma_{el} = \int \sigma_{el}(\Omega) d\Omega = 4S \sin^2(\pi e\Phi / hc),$$

where $\sigma_{el}(\Omega)$ is the differential cross section of elastic scattering as a function of the scattering angles Ω, Φ is the magnetic flux, å is the electron charge, h is the Planck constant, and ñ is the velocity of light. This expression is of a somewhat paradoxical character as it provides evidence of dependence on the flux although the flux produces no strength effect on the electron.

The authors show that the strength interaction between the electron and the magnetic field is characterized not by the elastic but transport scattering cross section equal to

$$\sigma_{tr} = \int \sigma_{el}(\Omega)[1 - \cos(\theta)] d\Omega .$$

The calculation of the transport cross section yields a quantity independent of the flux, if the toroid is screened from electrons, and to a quantity dependent on the direct strength interaction with the flux, if the toroid is not screened and electrons penetrate it and experience the action of the Lorentz force from the magnetic field. Thus, the Aaronov-Bom paradox is removed.

3.4. Multilayer systems [23]

Using an earlier developed analytical apparatus of waves multireflection it is possible to find resonances in multilayer systems in a simple analytical form, describe them with the Breit-Wigner formulas, and determine the total width of the resonance together with the partial widths related to the exiting of the multilayer system in one or another direction and also, to absorption.

A mathematical apparatus for the calculation of resonances in magnetic multilayer systems where the magnetization of neighboring levels is not collinear is also developed. In this case, for partial widths there is a possibility of exiting the system with or without spin-flip.

3.5. Coherent wavelength of the neutron [24]

As is known, the coherent neutron length can be defined as a parameter characterizing the preparation of the neutron beam, i.e. its collimation and monochromatization. However, it is also possible to determine the coherent length of the neutron itself that characterizes its own wave packet. The question of how it is possible to separate the neutron's own coherent wavelength then arises. In [24], an attempt to do it is made. The reflection curve of neutrons from thin films at a given angle is known to have an interference behavior depending on the neutron energy, i.e. it has a set of minimums whose position depends on the thickness of the sample and the wavelength of the neutron. The depth of the minimums is mainly determined by the parameters of the beam, scattering on roughness, incoherent scattering, and by absorption. After taking into account all these factors the description of the depth of the minimums is yet not sufficiently good. It turns into a more satisfactory description as soon as the neutron's own coherent length, that appears to be of the order of magnitude of the de Broil packet width found earlier from the description of the UCN storage anomaly, is introduced

3.6. Neutron holography [25]

Holography is described with the wave process. In the case of the neutron, however, we deal with a large number of wave processes. One of them is connected with the de Broil wavelength of the neutron itself. In [25], another wave process, i.e., the one related to spin precession in the magnetic field is investigated. For the given value of the field B and velocity v the wavelength of the neutron itself is $\lambda = vh / \mu B$, where μ is its magnetic moment. Making use of this wave process it is possible to record diagrams without the reference beam.

4. Methodological

4.1. Precision gamma-spectroscopy, the COCOS project

The development of combined correlation gamma-gamma spectroscopy of neutron-nuclear interactions was under way. The method was tested in the experiment of the spectroscopy of the gamma-radiation of fragments from the resonance neutron induced fission of ^{239}Pu carried out on one of the IBR-30 beams, which demonstrated its effectiveness.

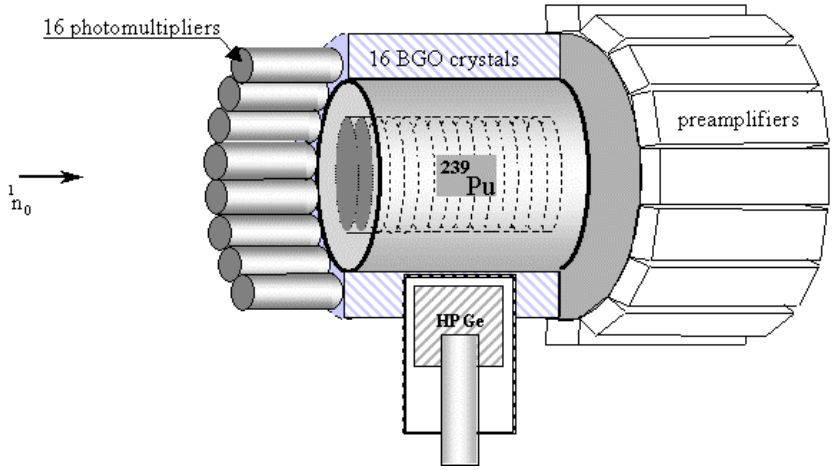

Fig. 5. *The schematic layout of the HPGe-BGO gamma-spectrometer.*

Work to create a 16-BGO-scintillation-block-multidetector for the HPGe-BGO gamma-spectrometer completed **(***Fig. 5***).**

4.2. Investigations with the electrostatic generator EG-5

4.2.1. Neutron spectrometry in gamma-spectrum form

Van de Graaf accelerator-aided experiments to finish off the new method of neutron spectrometry and obtain new data on partial cross sections of radiative neutron capture continued. The experiments were carried out with samples of nickel, copper, and manganese at proton energies higher than the ^{7}Li(p,n) reaction threshold by 100 keV. The energy dependence curves of the partial cross section of the ^{58}Ni(n,γ)^{59}Ni reaction are obtained. The results of measurements of copper and manganese samples are currently being processed.

In addition, the possibility of measuring the neutron energy spectra with the help of the ^{58}Ni(n,γ)^{59}Ni reaction was investigated. Measurements of the spectra of gamma-transitions populating the ground state of the daughter nucleus were carried out for different neutron spectra. It was studied how sensitive the form of the gamma-transition spectrum is to the energy distribution of incident neutrons. It is shown that the employed method makes it possible to study the energy distribution of incident neutrons by investigating the form of the spectrum of primary gamma-transitions from the (n,γ) reaction. Our findings are published in the proceedings of the ISINN-8 conference.

4.2.2. Obtaining of the neutron flux with a Maxwell velocity distribution

A set of experiments to study the possibility of obtaining the neutron flux with a Maxwell velocity distribution for the purposes of further measurements of the neutron capture cross section were carried out at the van de Graaf accelerator.

A graphite prism was used as a moderator. The average neutron flux in the points on the prism surface selected by the Monte-Carlo method was measured by the neutron activation method. Gold plates were used as an activated sample. The measurements yielded relative neutron flux values in different points on the surface of the prism. A comparison of the experimental and

calculated data revealed the existence of an unaccounted contribution to the neutron flux. Additional measurements were conducted (FLNP) and new calculations are presently under way to uncover the reason of the discrepancy (INR).

4.2.3. Calibration of the fast neutron detector HEND

In the year 2000, calibration of the fast neutron detector HEND (High Energy Neutron Detector) designed to work on board the American research apparatus Mars Surveyor Orbiter 2001 as an element of the gamma-spectrometer complex was carried out in cooperation with specialists from DRRI. The work was done under a long-term agreement between the Institute of Space Research, RAS, and JINR specifying that JINR develops the physical concept of the instrument, performs physical and mathematical modeling of its characteristics, and does its efficiency calibration.

The spectrum and the flux of neutrons from the $^{7}Li(p,n)^{7}Be$ reaction over the neutron energy range from 200 to 1000 keV were measured with the help of a ^{3}He high pressure cell counter and a standard SNM-16 counter in a polyethylene jacket. The obtained data were used to determine an absolute efficiency of four detectors.

5. Analytical investigations at IBR-2: neutron activation analysis and radiation research

The instrumental neutron activation analysis method (INAA) at IBR-2 is mainly applied to solve environment protection problems under the auspices of the JINR first-priority project REGATA, IAEA coordination programs, JINR plenipotentiaries' grants, and individual projects. The analytical results of the multielement neutron activation analysis of moss-biomonitors reflecting the level of pollution by heavy-metal and other toxic elements of the investigated territories are sent to the Nordic Committee (Sweden). They are included in the atlas of «Atmospheric Heavy Metal Deposition in Europe» whose publication will be overtaken by the United Nations in 2001. The results of the work carried out in Dubna in the year 2000 were presented at 4 international conferences and are included in the IAEA reports. To prepare the results, GIS techniques (geology computer information systems) are widely used. The final results are presented as color geographical maps of the distribution of elements of high practical importance. A set of CD maps is being prepared.

Under the auspices of the international project (ISTC) studies of the ecological safety of building materials on the example of kinescope broken glass were conducted in cooperation with the Faculty of Safety of Nuclear Facilities of Moscow Construction University. Together with RODON (Sergiev Posad), investigations of the materials used in the solidification of liquid and solid radioactive wastes were carried out. An application for patenting the development and creation of a selenium-containing *Spirulina Platensis*-based pharmaceutical is being prepared together with the Andronikashvily Institute in Tbilisi [26]. The analytical part of work was done using epithermal neutron activation in Dubna in 2000.

The publication of *Tables for Identification of Nuclides Formed in Nuclear Reactors* [27] intensively used in INAA experiments at IBR-2 must be specifically emphasized. The Tables reflect the many-year experience of work with reactor neutrons acquired in the Neutron Activation Analysis and Radiation Research Sector.

On the basis of a radiochemical laboratory of the 3rd class (PTF Regata at IBR-2) practices for students of senior courses of the MSU Interfaculty Center and Dubna University doing a special course in Nuclear Physical Methods of Substance Analysis are organized. In the year 2000, two B.A. and two M.A. degrees in this theme were received and another three M.A. papers are in process and will be ready at the beginning of 2001. Five Candidate-of-Science papers are being

written. Members of the AA and RR sector took active part in the preparation of the international conference *Radionuclides and Heavy Metals in Environment* (2-6 October, 2000, Dubna) held with the support of NATO.

---

[1] E.I. Sharapov, J.D. Bowman, B.E. Crawford, P.P.J. Delheij, C.M. Frankle, M. Iinuma, J.N. Knudson, L.Y. Lowie, J.E. Lynch, A. Masaike, Y. Matsuda, G.E. Mitchell, S. Penttil{\"a}, H. Postma, N.R. Roberson, S.J. Seestrom, H.M. Shimizu, S.L. Stephenson, Y.-F. Yen, and V.W. Yuan, Phys. Rev. **C 61**, 025501(2000).

[2] E.I. Sharapov, J.D. Bowman, B.E. Crawford, P.P.J. Delheij, C.M. Frankle, M. Iinuma, J.N. Knudson, L.Y. Lowie, J.E. Lynch, A. Masaike, Y. Matsuda, G.E. Mitchell, S. Penttila, H. Postma, N.R. Roberson, S.J. Seestrom, H.M. Shimizu, S.L. Stephenson, Y.-F. Yen, and V.W. Yuan, ISINN-8: VIII International Seminar on Interaction of Neutron with Nuclei, Report E3-2000-192, p.86, Dubna 2000.

[3] G.E. Mitchell, J.D. Bowman, B.E. Crawford, P.P.J. Delheij, C.M. Frankle, M. Iinuma, J.N. Knudson, L.Y. Lowie, A. Masaike, Y. Matsuda, S. Penttila, H. Postma, N.R. Roberson, S.J. Seestrom, E.I. Sharapov, S.L. Stephenson, Y.-F. Yen, and V.W. Yuan, Phys. Rev. **C 61**, 045503 (2000).

[4] S.L. Stephenson, J.D. Bowman, F. Corvi, B.E. Crawford, P.P.J. Delheij, C.M. Frankle, M. Iinuma, J.N. Knudson, L.Y. Lowie, A. Masaike, Y. Masuda, Y. Matsuda, G.E. Mitchell, S. Penttila, H. Postma, N.R. Roberson, S.J. Seestrom, E.I. Sharapov, H.M. Shimizu, Y.-F. Yen, V.W. Yuan, and L. Zanini, Phys. Rev. C **61**, 045501 (2000).

[5] Y.-F.Yen, J.D. Bowman, R.D. Bolton, B.E. Crawford, P.P.J. Delheij, G.W. Hart, C.M. Frankle, T. Haseyama, M. Iinuma, J.N. Knudson, A. Masaike, Y. Masuda, Y. Matsuda, G.E. Mitchell, S.I. Penttila, N.R. Roberson, S.J. Seestrom, E.I. Sharapov, H.M. Shimizu, D.A. Smith, S.L. Stephenson, J.J. Szymanski, H. Yoo, and V.W. Yuan, Nucl. Instrum. Methods Phys. Res. A**447**, 472 (2000).

[6] V.R. Skoy, Yu.V. Prokofichev, V.N. Sorokin, N.N. Kolachevsky, Nucl. Instr. Methods, A**402**, 323 (1998)

[7] N.N. Kolachevsky *et al.*, Quantum Electronics, **30**(1), 81 (2000).

[8] Ñóøêîâ Î.Ï., Ôèçèêàòîì Â.Â, ÓÔÍ, 1982, ò. **136**, ñ. 3.

[9] Bunakov V.E., Gudkov V.P., Nucl. Phys., 1983, v.A **401**, p.93.

[10] Alfimenkov V.P.,Chernikov A.N., Lason L. et al. Nucl. Phys., 1999, v.A**645**, p. 31.

[11] Алфименков В.П., Гагарский А.М., Голосовская С.П. и др. ЯФ, 2000, т.63, с.598.

[12] W.Y. Baek , G.N. Kim, M.H. Cho, I.S. Ko, W. Namkung, Yu.V. Grigoriev, H. Faikov-Stanczyk, V.N. Shvetshov, W.I. Furman. Investigation of c-multiplicity spectra and neutron capture cross-sections of ^{232} Th in the energy region 21.5-215 eV. Nuclear Instruments and Methods in Physics Research B **168** (2000) 453-461

[13] Yu.P.Popov, A.V.Voinov, S.S.Parzhitski, A.P.Kobzev, N.A.Gundorin, D.G.Serov, P.V.Sedyshev, M.V.Sedysheva.Proc. ISINN-8, JINR E3-2000-192, p.75-81, Dubna, 2000.

[14] S.I.Suchoruchkin, Z.N.Soroko,V.V. Deriglazov. In: Landolt-Bornstein/ New Series. V.16/B. Table of Neutron Resonance Parameters. (Ed. by H.Schopper). Springer 1998.

[15] C.M.Perey, F.G.Perey, J.A.Harvey, N.W.Hill, N.M.Larson, R.L.Macklin, D.C.Larson. Phys.Rev. C**47** (1993), 1143

[16] A.V.Voinov, Yu.P.Popov, S.S.Parzhitski, A.P.Kobzev, N.A.Gundorin, D.G.Serov, Proc. ISINN-8, JINR E3-2000-192, p.445, Dubna, 2000.

[17] Guohui Zhang, Guoyou Tang, Jinxiang Chen, Zaomin Shi, Guanzhi Liu, Xuemei Zhang, Zemin Chen, Yu.M.Gledenov, M.Sedysheva, G.Khuukhenkhuu. Differential cross-section measurement for the ^{6}Li(n,t)^{4}He reaction at 3.67 and 4.42 MeV. Nucl. Sci. Eng **134** (2000) 312-316.

[18] Xuemei Zhang, Zemin Chen, Yingtang Chen, Jing Yuan, Guoyou Tang, Guohui Zhang, Jinxiang Chen, Yu.M.Gledenov, G.Khuukhenkhuu, M.Sedysheva. Dispersion relations for (n,n), (n,p), and (n,α) reactions on ^{39}K and ^{40}Ca. Phys. Rev. C**61** (2000) 054607.

[19] Xuemei Zhang, Zemin Chen, Yingtang Chen, Guoyou Tang, Guohui Zhang, Jinxiang Chen, Yu.M.Gledenov, G.Khuukhenkhuu. Measurements and Calculations of the ^{39}K and ^{40}Ca (n,α) Cross Sections at E_n = 4.5 to 6.5 MeV. Nucl. Sci. Eng **134** (2000) 86-96.

[20] Yu.M.Gledenov, P.E.Koehler, J.Andrzejewski, K.Guber, T.Rausher. ^{147}Sm(n,α) cross section measurements from 3 eV to 500 keV: Implications for explosive nucleosynthesis reaction rates. Phys. Rev. C**62** (2000) 042801.

[21] В.В.Любошиц, В.Л.Любошиц. Т-инвариантность и поляризационные эффекты в реакциях p + 3He $\rightarrow$ p+ + 4He и p+ + 4He $\rightarrow$ p + 3He . Ядерная физика, 2000, ò.**63**, âûï. 5, ññ. 837-843 (Physics of Atomic Nuclei , 2000, v.**63**, No. 5, pp. 767-773) .

[22] В.В.Любошиц, В.Л.Любошиц. Транспортное сечение рассеяния и эффект Ааронова- Бома на тороидальном соленоиде. Препринт ОИЯИ Р4-2000-48 , Дубна, 2000 ; Журнал экспериментальной и теоретической физики (ЖЭТФ), 2000, т. **118**, вып. 4 (10), сс. 777-786 (Journal of Experimental and Theoretical Physics, 2000, v. **91**, No. 4, pp. 673-681) .

[23] V.K.Ignatovich, F.V.Ignatovitch, D.R.Andersen, Algebraic description of multilayer systems with resonances. Particles and Nuclei Lett. **3** [100], pp. 48-61, 2000.

[24] D.A.Korneev, V.I.Bodnarchuk, S.P.Yaradaikin, V.F.Peresedov, V.K.Ignatovich, A.Mennelle, P. Gaehler, Reflectometry studies of the neutron coherent properties. Physica B, v. **276**, p. 973, 2000.

[25] В.К.Игнатович, в Материалах семинара, посвященного 80 летию со дня рождения М.И.Подгорецкого, с. 67-84. ОИЯИ, Дубна, 2000.

[26] L.M. Mosulishvili, Ye.I. Kirkesali, A.I. Belokobylsky, A.I. Khizanishvili, M.V. Frontasyeva, S.F. Gundorina, C.D. Oprea: Epithermal neutron activation analysis of blue-green algae Spirulina Platensis as a matrix for selenium-containing pharmaceuticals. Preprint of JINR, E14-2000-225, Dubna, 2000 (submitted to J. Radioanal. Nucl. Chem.)
[27] T.M.Ostrovnaya: Tables for Identification of Nuclides Formed in Nuclear Reactors. Preprint JINR, E14-XXX, 2000, pp. 1-YYY.

2. NEUTRON SOURCES

2.1. THE IBR-2 PULSED REACTOR

In the year 2000 the IBR-2 reactor operated in accordance with the approved working schedule. It operated for the physical experiment 8 cycles (~2073 h), including three with a cryogenic moderator, at W=1.5. Over the period there were 6 emergency shutdowns. Details of IBR-2 operation are summarized in Tables 1 and 2.

Table 1

The parameters of IBR-2 operation in the period from January 1, 2000 to January 1, 2001

Cycle	1	2	3	4	5	6	7	8	*Total*
Time of cycle	*16.01 – 27.01*	*14.02 - 25.02*	*13.03 – 24.03*	*10.04 - 21.04*	*15.05 - 26.05*	*23.10 - 3.11*	*13.11 - 24.11*	*04.12 - 15.12*	
Operation for physical experiment, h	266	260	269	256	263	253	258	248	**2073**
Operation of movable reflector, h	277	271	278	278	275	268	273	274	**2194**
Generated energy, MWh	405	394	406	399	393	385	394	378	**3154**
Number of emergency shutdowns,	1	1	-	2	1	-	-	1	**6**
including caused by:									
▪ Voltage drops	-	1	-	1	1	-	-	1	**4**
▪ Equipment malfunctioning	1	-	-	1	-	-	-	-	**2**
▪ Electronic equipment malfunctioning	-	-	-	-	-	-	-	-	**0**
▪ Personnel fault	-	-	-	-	-	-	-	-	**0**

Table 2

The parameters of the IBR-2 reactor state as of 01.01.2001

No.	Parameter (beginning from startup)	Fact	Rated
1	Total operating time for physical experiment, h	38567	
2	Total generated energy, MWh	71360	85000
3	MR-2P mechanical operating time, h	13866	18000
	MR-2P generated radiation, MWh. *(for flux density in the center of blade $5 \cdot 10^{13}$ n/cm^2 for neutrons with E>0.1 MeV)*	23694	36000
4	Maximum fluence on reactor jacket in the center of active zone (10^{22} n/cm^2):		
	• for En > 0.1 MeV	3.11	3.72
	• for En > 0.8 MeV	1.35	
5	Maximum fuel burn (%):		
	• pellet TVEL	5.36	6.5
	• spigot TVEL	5.76	8,2
6	Reactivity resource (%)	0.64±0.05	
7	Total number of emergency shutdowns	430	550

The 2000 Plan of Maintenance Work was executed in the scheduled period, June-September. During the period the movable reflector MR-1 decommissioned in 1987 was removed from the operative storeroom, which makes it possible to move MR-3 to the storeroom for the time of modernization.

In the year 2000 a diesel generator for 100 kW was bought from FRG and was erected outside the reactor building to provide reliable power supply for the IBR-2 reactor in case of break down of the regular power supply system. The startup of the diesel generator is scheduled for the 1st quarter of 2001.

The year 2000 saw essential advances in the modernization of the IBR-2 reactor as a result of signing of the Agreement on IBR-2 Modernization between the Atomic Energy Ministry of the Russian Federation and the Joint Institute for Nuclear Research on February 14, 2000 and Contract No. 6.06.19.19.00.950 of 15.03.2000 for the execution of research and construction work in IBR-2 modernization in the year 2001.

In the year 2000:

1. Working documentation of the movable reflector MR-3 is prepared.
2. Strength and elasticity investigations of the alloy ХН77ТЮРУ-ВД (ЭИ 437 БУ-ВД) in the thermally treated state are conducted (Report 23.6365).
3. Technical project (TP) and working documentation (WD) of fuel assemblies (FA) of IBR-2M are prepared.
4. Work to develop TP for the modernization of basic reactor equipment continued.
5. Development of the executive mechanisms of the control and emergency system (CES) started.
6. Manufacturing of the main and auxiliary reactivity modulators, MRM and ARM, and of the MR-3 jacket started in NIKIET.
7. Manufacturing of the following MR-3 blocks started in JINR:
   - cart;
   - platform;
   - technological frame;
   - transmission shaft;
   - dismountable shielding.

   The working schedule to manufacture MR-3 is presented in Fig 1.
1. Industry is prepared for the production of TVEL of the new loading, the necessary amount of plutonium dioxide is produced and its industrial tests are being carried out.
2. A complete set of items for TVEL of IBR-2M is produced and shipped to the Industrial Enterprize Maiak.
3. Documentation on transport of 2 decommissioned fuel assemblies (DFA) of IBR-2 for the purpose of examination after their 5% burn is prepared.
4. The possibility of using the step motor to trigger the emergency system was demonstrated on the test-rig. The results on the speed of response are inspiring.
5. Work to develop technical requirements for the CES electronic equipment of IBR-2 started in IAE (Swierk, Poland).

In the year 2000 financing of works on the project of IBR-2 modernization proceeded according to the financing plan (see Table 3).

No.	Work	Responsible	2000	2001	2002	2003
	MR-2P					
1.	Manufacturing of MR-2P					
1.1.	MMR and AMR	NIKIET				
1.2.	Jacket	NIKIET				
1.3.	Cart	CWS JINR				
1.4.	Transmission shifts	CWS JINR				
1.5.	Technological frame	CWS JINR				
1.6.	Platform	CWS JINR				
1.7.	Removable shielding	CWS JINR				
1.8.	Reduction gear	CWS JINR				
1.9.	Front support	CWS JINR				
1.10.	Piping arrangement	CWS JINR				
1.11.	Sensors	FLNP				
1.12.	Speed gear-box	FLNP				
1.	Assembling on test-rig	FLNP				
2.	Test-rig trials	FLNP				
3.	Moving of MR-3 to bldg. 117	FLNP				
4.	On-site assembling and tests in bldg. 117	FLNP				

Fig.1. Working schedule of the execution of the MR-3 Project

Table 3

The financing plan of the project "IBR-2 Modernization" for the year 2000 (k$)

Work	JINR		MAE		Σ	
	Plan	**Fact**	**Plan**	**Fact**	**Plan**	**Fact**
MR-3	73	**86**	136	**106**	209	**192**
TVELs	24	**34**	136	**160**	160	**194**
Basic equipment	95	**73**	28	**5**	123	**78**
Total	192	**193**	300	**271**	492	**464**

2001 Objectives:

1. Provide beam time in the volume of 2000 h for physical measurements (8 cycles per year, including 3 cycles with CM).
2. Manufacture MR-3.
3. Continue works on fuel loading.
4. Prepare technical project of modernization.

2.2. The IREN Project

The working schedule of the IREN project corrected in accordance with the recommendations of the JINR directorate formulated at the 87th Session of the Scientific Council is implemented in the main points during the year 2000.

The BINP in Novosibirsk completed the construction and tests of the accelerating tubes, buncher and the SLED system for the linac LUE-200 on time. In two test runs conducted with an accelerating tube prototype an acceleration of about 30 MeV/m was obtained, which is sufficiently close to the rated value. The final stage of test measurements carried out in October with participation of JINR experts showed that the shape of the electron energy spectrum differs from the expected. The achieved beam power is only is only 60% of the rated value. Regular financing enabled the shipment of two accelerating tubes to JINR in September. The buncher and the SLED system are due at the end of February, 2001. The design and construction of a powerful RF load and beam diagnostic elements has started in BINP in accordance with the terms of a recently signed contract. Copper tubes for the construction of a solenoid for the magnetic focusing system of the linac were partly ordered or produced. By the end of the first quarter of the year 2001 they will be delivered to JINR. Designing and manufacturing of a set of high-voltage supplies for this system started in BINP in October, 2000. Certain success is achieved in designing and modeling of a pulsed electron gun. By the end of this year a thermo-stabilization and a vacuum systems will be mounted on a full scale RF stand that FLNP assigned for testing of the accelerating tubes of LUE-200.

The contract with a known German firm, PPT, for designing and construction of two modulators for feeding of klystrons 5045 SLAC in LUE-200 is concluded and the designing will be completed in December 2000. It is financed from a long term German loan to the Russian Federation. The conditions of supply of two 5045 SLAC klystrons are agreed upon with the DOE of the USA in the respective agreement signed by JINR and DOE in 1993.

The «Mayak» plant completed the construction and received a license for the fuel elements of the multiplying target of IREN. They will remain at the plant until everything is ready for assembling of the new active zone in the reactor hall of the former IBR-30.

Specialized Moscow institutes, RINM and NIKIET, in close collaboration with JINR developed the technical project of the assembly of IREN in 2000. However, a short delay in financing as well as the necessity to do extra calculations of IREN safety caused by recently introduced stricter requirements for nuclear hazardous facilities in the Russian Federation resulted in a four-month shift of the completion date of the first stage of the technical project. This will obviously lead to a delay in receiving of the license for the decommissioning of the IBR-30 reactor and the construction of the IREN facility. However, there is still a possibility to have this license by the date of the final shutdown of IBR-30 at the end of June 2001.

3. THE IBR-2 SPECTROMETERS COMPLEX AND COMPUTATION INFRASTRUCTURE

Organization of investigations and instrument developments. In the year 2000, as in the few previous years, under theme 1031 neutron scattering investigations in condensed matter physics were mainly conducted at the reactor IBR-2. In addition to IBR-2, members of the FLNP Division of Neutron Investigations of Condensed Matter working under the auspices of theme 1031 carried out experiments with the electrostatic generator EG-5 and X-ray diffractometers in FLNP and in some other neutron laboratories in Europe under the terms of the accepted proposals.

During the reported year IBR-2 operated for eight working sessions. The experimental time of the reactor spectrometers was distributed following experts recommendations taking into account the submitted proposals and the existing long-term agreements. The 2000 list of spectrometers operating in the user mode included ten instruments: HRFD, DN-2, DN-12, SKAT, YuMO, SPN, REFLEX-P, KDSOG, NERA, and DIN.

The most important result of the year is the startup of the first stage of the new neutron Fourier diffractometer FSD for investigations of internal stresses in materials and engineering products. By the spring 2000 all basic units of FSD, including the biological shielding, mirror neutron guide, fast Fourier chopper, beam control systems, sample table, and the goniometer devices, had been installed and tested on channel 11 of the IBR-2 reactor. The first high resolution FSD measurements were carried out with a +90° element of the detector MultiCon in the May cycle of the reactor, and by the October 2000 the first –90° element of the detector MultiCon and a lithium glass-based detector in the back-scattering position were installed in FSD. In all the detectors the rated resolution of *d*-spacing is reached (**Fig.1**) (see Experimental Reports).

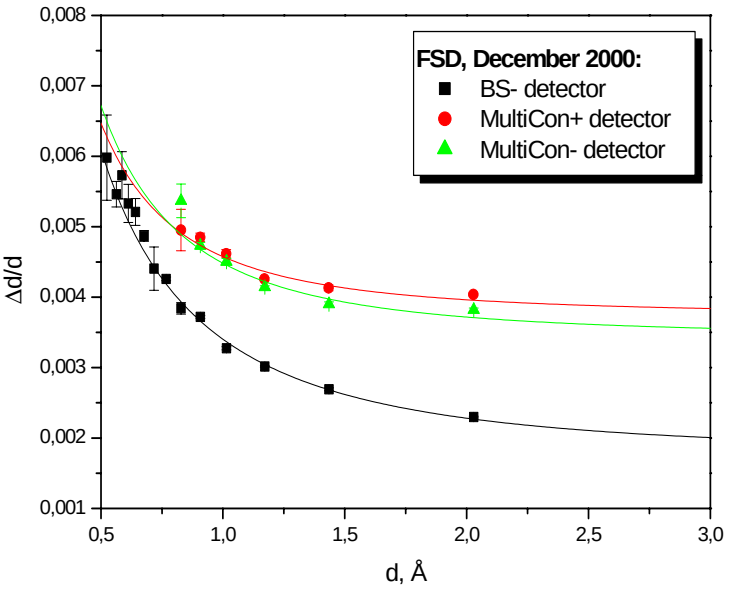

Fig. 1. *The FSD resolution function with the detectors BS^- and $MultiCon^{\pm}$ determined in the diffraction from the powder α-Fe at V_{max}=6000 rot/min.*

At SKAT, a second set of collimators with an angular dispersion of 45' was used for the first time in October-2000. The predicted intensity gain was obtained as well as the predicted worsening of the *d*-spacing resolution. It is proved that collimators with an angular dispersion of 45' are applicable for many kinds of samples, except polyphase rock samples with low-symmetrical constituents like phyllosilicates and feldspars.

The first tests at temperatures up to 600°C were performed with a high-pressure chamber. In the chamber, temperature stabilization close to this limit is possible though negative effects (generation of cracks) are observed in some cases. They are related to internal stresses due to weak

thermal conductivity of geological materials. Reducing the temperature gradient during heating seems to solve the problem. Furthermore, the ultrasonic system of the chamber has been changed to allow ultrasonic measurements even at high temperatures.

In the small-angle scattering spectrometer YuMO a second detector is installed and tested extending essentially the transfer momentum interval over which the neutron scattering spectrum is measured simultaneously (**Fig.2**).

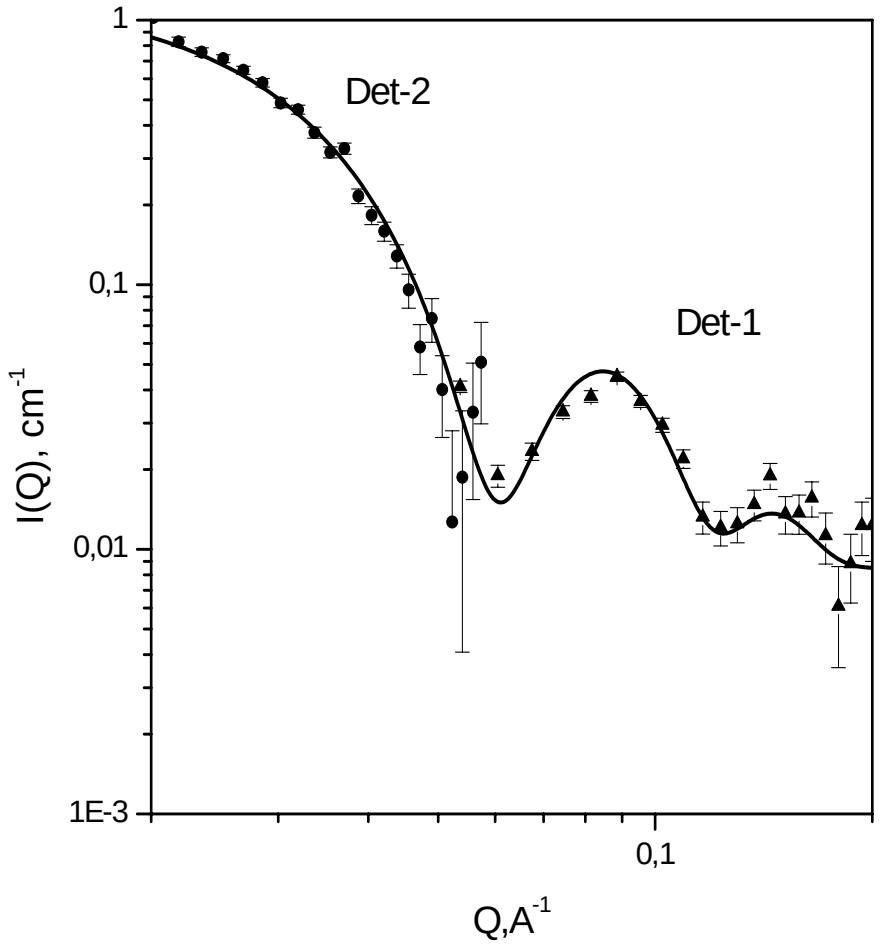

Fig.2. *Small-angle neutron scattering on a diluted solution of apofferitin, the protein consisting of a spherical shell with a known size (Rout=62E and Rin=41E), as a function of the scattering vector Q. The experimental points are measured with two detectors at 11.95m and 5.27m from the sample position. The calculated curve is also shown.*

In the REFLEX-P spectrometer the new low-background detector on the basis of a ZnS screen was approbated and started operation for the physical experiment. An ~50 times reduction of the background helped carry out unique experiments of the registration of surface phonons and magnons in thin films on the level of sensitivity $2 \cdot 10^{-7}$ of the basic elastic scattering process.

In the frame of the modernization project of the polarized neutron spectrometer SPN a supermirror neutron polarizer was built and tested. Compared to the existing standard polarizer it has a considerably larger wavelength interval (~2.6 times) over which the polarization efficiency exceeds 95%. The new polarizer will increase essentially the polarization efficiency of measurements at larger wavelengths (10 times for the wavelengths 3÷7 Å) and will also raise the luminosity of the spectrometer.

On the spectrometer REFLEX-P experiments to study the effect of the «neutron gun», a special deepening (canyon) in the neutron moderator on the side of the spectrometer, were performed. They show, as it has been expected that the neutron flux from the depth of the canyon is noticeably larger than from the flat surface. The integral spectrum gain is 3.5, but in some intervals of the spectrum it is up to a factor of 5.5. The effect can be successfully applied to increase the luminosity of spectrometers that require small areas (~10 mm) of the radiating surface of the moderator (see Experimental Reports).

A transition to VME control electronics completed at some of the IBR-2 spectrometers (HEFD, DN-2, DN-12, YuMO), which is a step towards a higher level of experiment automation.

Work within the theme was focused on three main directions:

- development of the FLNP information and computing infrastructure
- creation and putting into operation of the VME data acquisition and control systems
- development of the IBR-2 spectrometer complex

Local area network and computing infrastructure. At present the realization of the first stage of the project «Measurement and Computational Complex (MCC)» allows us to create a modern basic network and a computing infrastructure of FLNP with characteristics and possibilities on the level of leading European centers. It comprises a high performance four-processor file-server Enterprise 3000 (only two processors are presently available), a cluster of 17 Workstations SUN20 and ULTRA5/10 with a common disk space of 60Gbyte, X-terminals, ~200 personal computers, network printers and a radial-structure local computing network with the commutation equipment enabling the data transfer rate up to 100Mbit/s via fibre-optic communication lines and twisted pairs. Access to the centralized computing resources of JINR is provided via the Orange Ridge ATM/Ehernet switching node at a rate of 155Mbit/s.

In the year 2000, the following work aimed at further development of the information and computer infrastructure of the IBR-2 complex was carried out:

- Data traffic in the FLNP local network was optimized and the data transfer rate increased significantly (Internet).
- Two segments of the network were changed over to twisted pairs (central segment in building 119 and Nuclear Physics Department segment).
- The number of X-terminals and the disk space of the SUN-cluster were increased.

Data acquisition and control systems. In the first stage of the project the architecture and electronic modules of unified VME data acquisition and control systems for the IBR-2 spectrometers were developed. At present, unified VME systems for data acquisition, spectrometers equipment, including step motors, goniometers, refrigerators, furnaces, etc., for control of the experiment as a whole are installed on the main IBR-2 spectrometers.

The spectrometer electronics is installed in VME crates and it includes purchased standard blocks (processor E17 with a memory module, hard and floppy disk subsystems, input/output register, ADC/DAC block, network interface) and blocks developed in FLNP specifically for neutron time-of-flight experiments. The digital systems for registering and accumulating of data represent a unified set of identical (from the viewpoint of hardware) blocks for all the IBR-2 spectrometers. The systems carry on distinction in parameters, functional capabilities, encoding, correction and preliminary data processing specific for each spectrometer on the level of microprograms, electronic tables, *etc.* These blocks are the interface block intended to receive data from PSDs; block for encoding the point detector number; block for encoding the neutron time of flight; processor block and **a** histogram memory.

The instrument and sample environment control systems consist of the following unified subsystems:

- Control systems for executive mechanisms (step motors, etc.);
- Regulation systems based on the Euroterm, LTC or DRC regulators;
- Analog parameter acquisition systems;
- Systems for control of logical parameters.

All the instruments are equipped with the FLNP standard Sonix control software which runs on VME-side in the OS-9 environment. The Sonix has a modular structure. The current set of available Sonix programs consists of the following modules or tasks: Join - script interpreter, Tofa - DAQ control, Unipa - neutron beam and some sample environment parameters supervision, Motor -

goniometer and other stepper-motor driven setup control, Temp - heater/refrigerator control, Graph – visualization protocol of the temperature etc, Vsp - one-dimensional spectra visualization (both on-line and off-line)

To satisfy needs of particular instrument these tasks are very much configurable. Thus exactly the same version of modules are used for all instruments. The OpenG2 program based on PV-WAVE package are adapted to visualize spectra for all of these instruments both for one- and multi-dimensional detectors. This program provides visualization, preliminary data processing, and some analysis of data, measured on IBR-2 reactor.

In 2000 the VME data acquisition and control systems on the YuMO, DN-2, FSD and DN-12 spectrometers were put into test operation. Positive results were achieved on the all spectrometers, however, at the YuMO and DN-2 spectrometers some problem involving data accumulation from PSD arose. In course of the first autumn cycles several non-trivial errors in electronics were found, which revealed them selves only when working with high count rates on the beam. During these cycles the errors were corrected and we hope that they were last ones.

The new generation detector electronics for gas linear and PSD detectors as well as for point detectors has been constructed and installed on the YuMO, DN-2, SPN and DN-12 spectrometers.

At JINR FLNP in collaboration with HMI, Berlin, the development of the main DAQ board for MSGC detector was completed as far as possible with simulation and routing programs as well as the CPLD programming and the development and debagging software. A prototype of the board is ready. FLNP is presently continuing the adjustment and testing of the DAQ board by means of a software event generator. HMI is preparing the testing of the DAQ hardware and software with the MSGC detector prototype in 2000/2001.

The reliable operation with all temperature devices, close cycle refrigerators, cryostats and other sample environment devices has been provided.

The work on improvement of existing VME systems on the spectrometers HRKD, NERA-PR, SCAT and EPSYLON was continued.

- Development of new detector system based on ZnS scintillator will start.

4. EXPERIMENTAL REPORTS

4.1. CONDENSED MATTER PHYSICS

Diffraction

Long Scale Phase Separation Versus Homogeneous Magnetic State in $(La_{1-y}Pr_y)_{0.7}Ca_{0.3}MnO_3$
V.Pomjakushin, A.Balagurov, D.Sheptyakov, V.Aksenov, P.Fischer, L.Keller, O.Gorbenko, A.Kaul, N.Babushkina

Effect of Partial $^{16}O \rightarrow {}^{18}O$ Substitution on the Magnetic Structure of $(La_{0.25}Pr_{0.75})_{0.7}Ca_{0.3}MnO_3$
D.V.Sheptyakov, V.Yu.Pomjakushin, V.L.Aksenov, A.M.Balagurov, N.A.Babushkina, O.Yu.Gorbenko, A.R.Kaul

X-Ray and Neutron Diffraction Studies of a New Aurivillius Phase $Bi_{2.53}Li_{0.29}Nb_2O_9$
A.M.Balagurov, A.I.Beskrovniy, S.G.Vasilovsky, L.S.Smirnov, M.Sarrion, L.Mestres, M.Herraiz

Peculiarities of Incommensurate Phase in Ferroelectric-Semiconductor $TlInS_2$
A.I.Beskrovnyi, B.R.Gadjiev, N.Yamamoto, N.Mamedov, S.Iada, H.Uchiki, S.Kashida

Neutron Diffraction Study of the Strain/Stress Behaviour on Dolomite Rock
Ch.Scheffzuk, W.Walther, A.Frischbutter, R.A.Zhukov

Texture - an Indicator of Rock Metamorphism and Deformation Processes in the Continental Crust
A.N.Nikitin, T.I.Ivankina, N.V.Zamyatina, V.I.Kazansky, K.V.Lobanov, A.V.Zharikov

Structural Study of Ternary Mercury Chalcogenide Systems $HgSe_{1-x}S_x$ (x=0.3, 0.5, 0.6) under High Pressure
V.I.Voronin, V.P.Glazkov, D.P.Kozlenko, S.V.Tikhomirov, B.N.Savenko, I.F.Berger, V.V.Shchennikov

Fullerene Molecule Strain in RbC_{60}
V.L.Aksenov, Yu.A.Ossipyan, L.Forro, S.Khasanov, V.V.Chernyshev, V.S.Shakhmatov

Symmetry Groups of Carbon Nanotubes
V.L.Aksenov, Yu.A.Ossipyan, V.S.Shakhmatov

Fourier Stress Diffractometer (FSD): First Results
G.D.Bokuchava, V.L.Aksenov, A.M.Balagurov, E.S.Kuzmin, A.V.Tamonov, V.V.Zhuk, V.V.Zhuravlev, V.A.Trounov, V.A.Kudrjashev, A.P.Bulkin

Effect Anisotropic Thermal Expansion on the Physical Weathering of Marbles
K.Ullemeyer, S.Siegesmund, T.Weiss, E.K.Tschegg

Small-Angle Scattering

Influence of Particle Concentration on Ferrofluids Microstructure Studies by SANS
M.V.Avdeev, Maria Balasoiu, Doina Bica, L.Rosta, G.Torok, L.Vekas

Small-Angle Neutron Scattering from Tetradecyltrimethylammonium Bromide in NaBr Aqueous Solutions
G.Eckold, N.Gorski

Strucrutal Characterization of Unilamellar Lipid Vesicles with Anchored Alkylglycosides at High Water Excess for Studying Cell Recognition Processes
P.Jorchel, J.Gorshkova, G.Klose, H.Schmiedel

Low Energy Excitations in Solid State Electrolyte $Cu_{2-x}Se$
N.N.Bickulova, S.Danilkin, V.A.Semenov, A.Skomorokhov, Z.A.Jagofarova, E.L.Jadrowski

Investigations of Mechanism of Membrane Proteins Crystallization in Lipidic Cubic Phase
G.Bobarykina, R.Efremov, V.Gordeliy, A.Islamov, A.Kuklin, G.Bueldt

The Study of the Unbinding of Membranes by SANS
V.Gordeliy, U.Gorshkova, A.Islamov, V.Haramus

Water Moderator of a Reactor IBR-2 with a Canyon on a Lateral Surface. A Design and Physical Parameters
A.A.Beliakov, V.I.Bodnarchuk, D.A.Korneev, V.F.Peresedov, E.P.Shabalin, S.P.Yaradaikin

DMPC Membrane Swelling by Nonionic Surfactant $C_{12}E_8$: X-Ray Diffraction Study
M.A.Kiselev, D.Lombardo, P.Lesiuer

Structure Factor of DMPC Unilamellar Vesicles: SAXS Study at Synchrotron
M.A.Kiselev, D.Lombardo, A.M.Kisselev, P.Lesieur

Neutron Optics

Neutron Wave Channeling in the Structure Cu(30nm)/Ti(150nm)/Cu(100nm)/glass
V.L.Aksenov, Yu.V.Nikitenko, A.V.Petrenko, V.V.Proglyado, F.Radu, V.G.Syromyatnikov

Neutron Spatial Beam-Splitting and Polarization Analysis in Reflectometry
V.L.Aksenov, S.V.Kozhevnikov, Yu.V.Nikitenko

RBS Investigation of Multilayer Structures
A.P.Kobzev, A.Z.Kiss, A.Simon

Inelastic Scattering

Surface Excitations in Thin Helium Film in Silica Aerogels
I.V.Bogoyavlenskii, A.V.Puchkov, H.J.Lauter, A.Skomorokhov

Structural and Magnetic Phase Transitions in $Rb_{1-x}(NH_4)_xMnF_3$ Provskites ($0.75 \leq X \leq 1$)
I.Natkaniec, J.Rubin, L.Smirnov

Phonons in Coarse Grained and Plastically Deformed Vanadium
S.Danilkin, M.Jung, H.Wipf

Quasielastic Scattering Investigation of Liquid Phosphorus Oxychloride $POCl_3$
A.G.Novikov, O.V.Sobolev

Inelastic Neutron Scattering and Hydration Kinetics in Aqueous Solutions
A.G.Novikov, M.N.Rodnikova, O.V.Sobolev

The Effect of Pressure on Hydrogen Tunneling in α-Mn
V.E.Antonov, V.P.Glazkov, D.P.Kozlenko, B.N.Savenko, V.A.Somenkov, V.K.Fedotov

Neutron Diffraction Study of Pyridinium Perrhenate at Ambient and High Pressures
L.Bobrowicz-Sarga, J.Wasicki, A.I.Beskrovnyi, P.Czarnecki, I.Natkaniec, W.Szczepanski

Isotopic Effects on Dynamics of Crystalline and Vitreous Methanol
I.Natkaniec, K.Holderna-Natkaniec, K.Parlinski

Computer Simulation and Neutron Scattering Investigation of Dynamics of Urea: $CO(NH_2)_2$ and $CO(ND_2)_2$
I.Natkaniec, K.Parlinski, K.Holderna-Natkaniec, J.Mayer

4.2. NEUTRON NUCLEAR PHYSICS

Fundamental Properties of the Neutron

Investigation of the Neutron-Electron Interaction
E.L.Enik, L.V.Mitsyna, V.G.Nikolenko, S.S.Parzhitskii, A.B.Popov, G.S.Samosvat, R.V.Khariuzov

Investigation of Interference Minima near s-Wave Resonances of ^{238}U
T.L.Enik, L.V.Mitsyna, G.S.Samosvat, V.V.Sinitsa

Fission

Parity Violation and Interference Effects in Angular Distributions of Fission Fragments
V.P.Alfimenkov, N.A.Bazhanov, L.Lason, Yu.D.Mareev, V.V.Novitskii, L.B.Pikelner, T.L.Pikelner, M.I.Tsulaia, A.N.Chernikov

Improving Explosive Nucleosynthesis Models via (n,α) Measurements
P.E.Koehler, Yu.M.Gledenov, J.Andrzejewski, K.H.Guber, S.Raman, T.Rauscher

Nuclear Structure

Level Density and Radiative Strength Functions of Dipole Transitions below B_n in $^{185,187}W$ and $^{191,193}Os$
V.A.Bondarenko, J.Honzanko, V.A.Khitrov, A.M.Sukhovoj, I.Tomandl

Applied Research

Weekly Cycles of Element Pollutants in Air of the Greater Cairo Area (Egypt) Studied by Neutron Activation Analysis
M.V.Frontasyeva, A.B.Ramadan, T.Ye.Galinskaya

Study of Trace Elements in Annual Segments of Moss Biomonitors Using Epithermal Neutron Activation Analysis: Link with Atmospheric Aerosol
Ye.V.Yermakova, M.V.Frontasyeva, E.Steinnes, K.A.Rahn

LONG SCALE PHASE SEPARATION VERSUS HOMOGENEOUS MAGNETIC STATE IN $(La_{1-y}Pr_y)_{0.7}Ca_{0.3}MnO_3$

V. Pomjakushin[1,2], A. Balagurov[1], D. Sheptyakov[1,2], V.Aksenov[1], P. Fischer[2], L. Keller O.Gorbenko[3], A. Kaul[3], N. Babushkina[4]

[1] *Frank Laboratory of Neutron Physics, JINR 141980, Dubna, Russia*
[2] *Laboratory for Neutron Scattering ETHZ & PSI, CH-5232, Villigen PSI*
[3] *Chemical Department. Moscow State University, 119899, Moscow, Russia*
[4] *RSC "Kurchatov Institute",123182 Moscow, Russia*

The magnetic structure of the colossal magnetoresistance perovskite manganites $(La_{1-y}Pr_y)_{0.7}Ca_{0.3}MnO_3$ for y from 0.5 to 1.0 has been studied by neutron powder diffraction in the temperature range from 10 to 293 K and in external magnetic fields up to 4 Tesla at DMC/SINQ, DN12/IBR2 and HRFD/IBR2 [1-2]. This family has a fixed optimal electron doping and variable

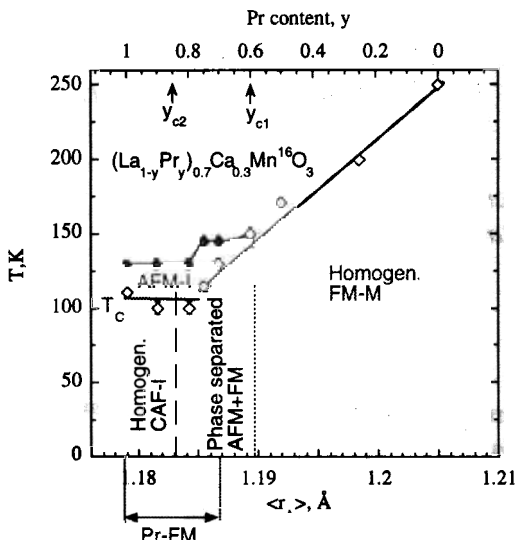

***Fig. 1**: Phase diagram of the $(La_{1-y}Pr_y)_{0.7}Ca_{0.3}MnO_3$ shows temperatures of magnetic ordering of Mn-ions. The bottom x-axis shows average A-cation radius $<r_A>$. The low temperature state is homogeneous for y>0.8 (canted antiferromagnetic insulator CAF-I) and for y<0.6 (ferromagnetic metal FM-M). In addition, a ferromagnetic contribution of the Pr-moments parallel to the ferromagnetic component of Mn-moments is found for y>0.6. The moment of Pr scales with the ferromagnetic Mn-moment rather than with the Pr-concentration and thus presumably induced by Mn.*

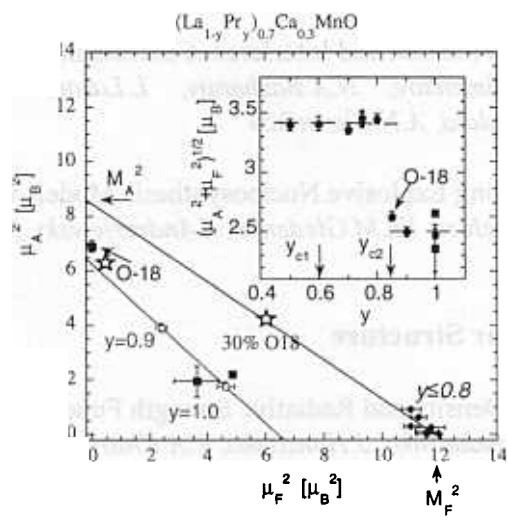

***Fig. 2**: The squares of the antiferromagnetic component μ_A^2 as a function of the ferromagnetic (F) magnetic moment component μ_F^2 with Pr-concentration y as a parameter. The lines are the linear LS-fits to the data points for y≤0.8 and y>0.8. The ^{18}O-enriched samples (y=0.75) are also shown. 75%-enriched sample has no F-component at all (O-18), serving as a reference of pure antiferromagnetic state. The stars show samples with partial isotope substitution: 30% and 55%. The insert shows the total magnetic moment as a function of the Pr-concentration.*

A-cation radius $\langle r_A \rangle$ which is linearly connected with the Pr-concentration y. It is believed that the principal effect of decreasing $\langle r_A \rangle$ is a decrease in the charge carrier bandwidth W, which is proportional to T_C in the double exchange model. Our data show that the phase diagram has a border region of concentrations $0.6 \leq y \leq 0.8$ separating the homogeneous FM metallic and canted AFM (pseudo CE-type) insulating states. In this region the low temperature magnetic state is macroscopically (>10^3 Å) incoherently spatially separated into AFM an FM phases. The FM phase has a small non-collinearity of C-type, presumably due to interfaces to the AF-phase. The macroscopical clusters can be induced by disorder on the carriers hopping amplitude caused by natural dispersion of the A-cation radius near the metal-insulator transition around y=0.7 [3]. For the concentrations $y \geq 0.9$ the long range ordered magnetic state is homogeneous with a canted AF structure. The total long-range ordered magnetic moment of the Mn-ion shows a step like decrease from $\mu_{Mn}=3.4\mu_B$ to $2.5\mu_B$ as a function of Pr-concentration at the transition to a homogeneous canted antiferromagnetic (CAF) state (Fig.2). The canting angle is significantly increased on doping, while the total magnetic moment stays constant for $y \geq 0.9$. The spatial inhomogeneities can still be present for $y \geq 0.9$, according to the reduced μ_{Mn}-value, but the Mn-spins between the homogeneously CAF-ordered moments have to be either short range ordered or paramagnetic. The ^{18}O-isotope substitution for y=0.75 acts like increase of y: the effective bandwidth is decreased due to JT-polaronic effect. The sample with 75% substitution of ^{18}O (O18) reveals the ordered magnetic moment close to the natural isotope samples with y>0.8. This places O18 in the region above the concentrational transition at yc2.

REFERENCES

[1] A. Balagurov, V.Pomjakushin, D.Sheptyakov et al, Phys. Rev. **B** 60, 383 (1999).

[2] A.Balagurov, V.Pomjakushin, D.Sheptyakov, V.Aksenov, P. Fischer et al, Accepted in Phys. Rev. **B** (2001).

[3] A.Moreo et al, Phys. Rev. Lett. **84**, 5568 (2000).

Effect of partial $^{16}O \rightarrow {}^{18}O$ substitution on the magnetic structure of $(La_{0.25}Pr_{0.75})_{0.7}Ca_{0.3}MnO_3$

D.V. Sheptyakov[a,b], V.Yu. Pomjakushin[a], V.L. Aksenov[a], A.M. Balagurov[a], N.A. Babushkina[c], O.Yu. Gorbenko[d], A.R.Kaul[d]

[a]*FLNP JINR, Dubna, Russia*
[b]*Laboratory for Neutron Scattering ETHZ & PSI, 5232 Villigen PSI, Switzerland*
[c]*RRC Kurchatov Institute, Moscow, Russia*
[d]*Chemistry Department, Moscow State University, Moscow, Russia*

The magnetic structure and phase diagram of $(La_{1-y}Pr_y)_{0.7}Ca_{0.3}MnO_3$ compound with $0.5 \leq y \leq 1$ have been systematically studied by neutron powder diffraction **[1-3]**. For composition with y=0.75 (LPCM-75), the analysis was performed on two samples, one containing the natural mixture of oxygen isotopes (99.7% ^{16}O-sample, metallic at T≤100 K), and the other one 75%–enriched by ^{18}O (^{18}O-sample, insulating in all temperature range). At first it was found that both samples have identical crystal structures at room temperature. At the temperature lowering, the sample with ^{16}O undergoes subsequent antiferromagnetic (T_{AFM}=150 K) and ferromagnetic (T_{FM}=110 K) transitions, while in the sample with ^{18}O the pure AFM ordering (T_{AFM}=150 K) was found. To get a better insight into the crossover between the FM+AFM metal and AFM insulator states we decided to study LPCM-75 samples with partial oxygen isotope substitution.

Altogether 11 samples with different values of the $r=^{18}O/(^{16}O+^{18}O)$ ratio were prepared and studied macroscopically **[4]**, and three of them with r=0.30, 0.55 and 0.63 were examined by neutron diffraction. Experiments were performed at the IBR-2 pulsed reactor with DN-12 diffractometer, which is specially designed for microsamples studies. Despite of small amount of samples (about 100 mg each) good enough quality diffraction patterns were measured in 2.5 – 4 hours at several temperatures. The values of magnetic moments were refined with the use of FullProf program.

It was found that at low temperature compositions with r=0.30 and 0.55 possess the same type of the magnetic structure as ^{16}O sample: phase separated FM + AFM (pseudo-CE), while in the composition with r=0.63 only AFM state (just as in ^{18}O sample) appears. The temperature dependencies of FM and AFM magnetic moments for r=0 [1], 0.30 and 0.55 are shown in **fig.1**. The dependence of μ_{AFM} for r=0.63 and 0.75 is practically the same as for r=0.55.

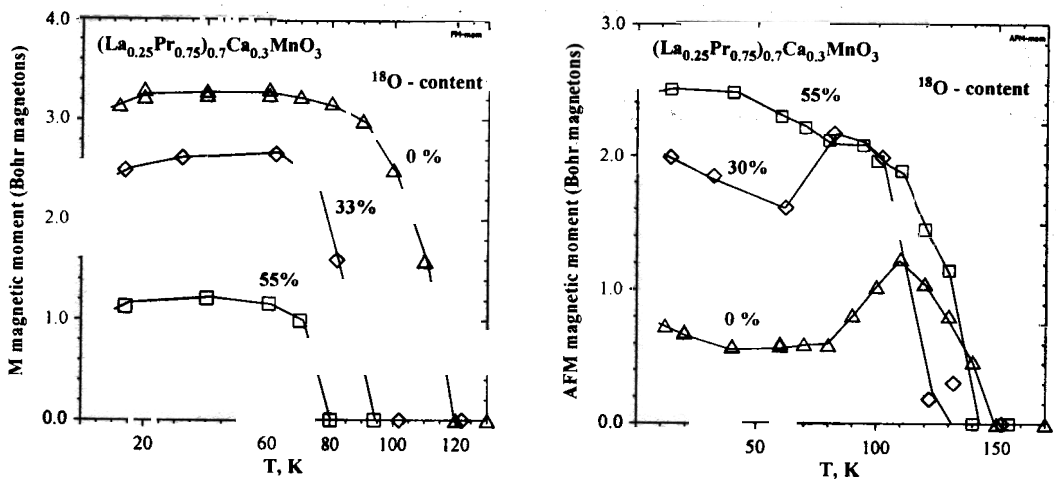

Fig.1. The temperature dependencies of FM (left part) and AFM (right part) magnetic moments of LPCM-75 with partial $^{16}O/^{18}O$ isotope substitution. The AFM moment lowering below the temperatures when FM phase appears is typical for phase separated state **[5]**.

One can see from fig.1 that T_{AFM} is more or less the same for all r, while T_{FM} decreases with r. The extracted from diffraction peaks intensity behaviour of the phase transition temperatures is displayed in **fig.2**.

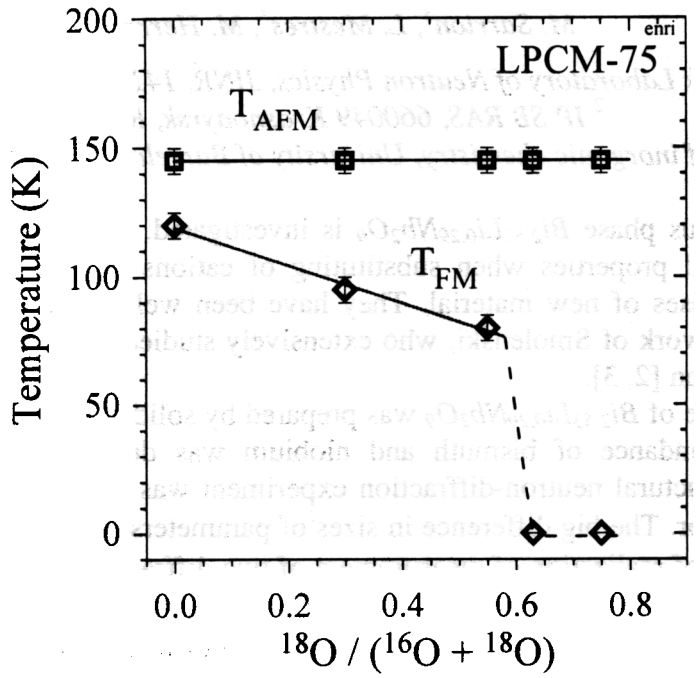

Fig.2. Dependence of T_{FM} and T_{AFM} phase transition temperatures on ^{18}O content in LPCM-75 samples. Points for r=0 and 0.75 are taken from Ref. [1].

The measurements of electrical resistivity and magnetic susceptibility show **[4]**, that samples with partial $^{16}O \rightarrow {}^{18}O$ isotope substitution behave as a percolation-type two-phase system consisting of the FM metal and AFM insulator. A critical value of ^{18}O for metal-insulator transition was found close to r=0.40. From the temperature behavior of magnetic moments values, the relative amounts of both magnetic phases at low temperature were estimated: 15% AFM + 85% FM for r=0; 50% AFM + 50% FM for r=0.3; and 98% AFM + 2% FM for r=0.55. These values are in good agreement with magnetic susceptibility data.

There are some attempts for explaining of so strong isotope effects in both LPCM-series and others manganites with CMR-effect (see, for instance, **[6]**) but details of this phenomenon are still far from clear understanding.

This work has been done with the help of RFBR program (project 00-02-16736).

References

1. A.M. Balagurov, V.Yu. Pomjakushin, D.V. Sheptyakov et al., Phys. Rev. B 60, 383 (1999).
2. A.M. Balagurov, P.Fischer, V.Yu. Pomjakushin et al., Physica B 276-278, 536 (2000).
3. A.M. Balagurov, V.Yu. Pomjakushin, D.V. Sheptyakov et al., Eur. Phys. J. (2001) accepted.
4. N.A.Babushkina, A.N.Taldenkov, L.M.Belova et al., Phys. Rev. B 62, R6081 (2001).
5. A.M. Balagurov, V.Yu. Pomjakushin, D.V. Sheptyakov, J.Phys.Soc.Japan, (2001) accepted.
6. N.M.Plakida, JETP Letters, 71, 720 (2000).

X-ray and neutron diffraction studies of a new Aurivillius phase

$Bi_{2.53}Li_{0.29}Nb_2O_9$

A. M. Balagurov[1], A. I. Beskrovniy[1], S. G. Vasilovskij[1,2], L. S. Smirnov[1], M. Sarrion[3], L. Mestres[3], M. Herraiz[3]

[1] *Frank Laboratory of Neutron Physics, JINR, 141980 Dubna, Russia*
[2] *IP SB RAS, 660049 Krasnoayrsk, Russia*
[3] *Departament of inorganic chemistry, University of Barselona, 08028, Barselona, Spain*

New Aurivillius phase $Bi_{2.53}Li_{0.29}Nb_2O_9$ is investigated. Structures of this type show hide variability of physical properties when substituting of cations of metal [1]. This opens greater possibilities at syntheses of new material. They have been well known as ferroelectric materials since the pioneering work of Smolenski, who extensively studied their ferroelectric properties as a function of composition [2, 3].

Powder sample of $Bi_{2.53}Li_{0.29}Nb_2O_9$ was prepared by solid-state reaction from Bi_2O_3, Li_2CO_3 and Nb_2O_5. The abundance of bismuth and niobium was determined by a method of x-ray fluorescence. The structural neutron-diffraction experiment was carried out in the FLNP, JINR at the IBR-2 pulse reactor. The big difference in sizes of parameters of an elementary cell (a=24.84 Å, c=5.45 Å) has served of realization of measurement of two diffractometers. On diffractometer DN-2 the neutron-diffraction date was measured in the range from 1 Å to 12 Å with the medium resolution. On diffractometer HRFD was received neutron-diffraction date in the range from 1 Å to 3.2 Å with high resolution. X-ray measurements were beforehand executed within the range of angle of scan from 6^0 to 80^0.

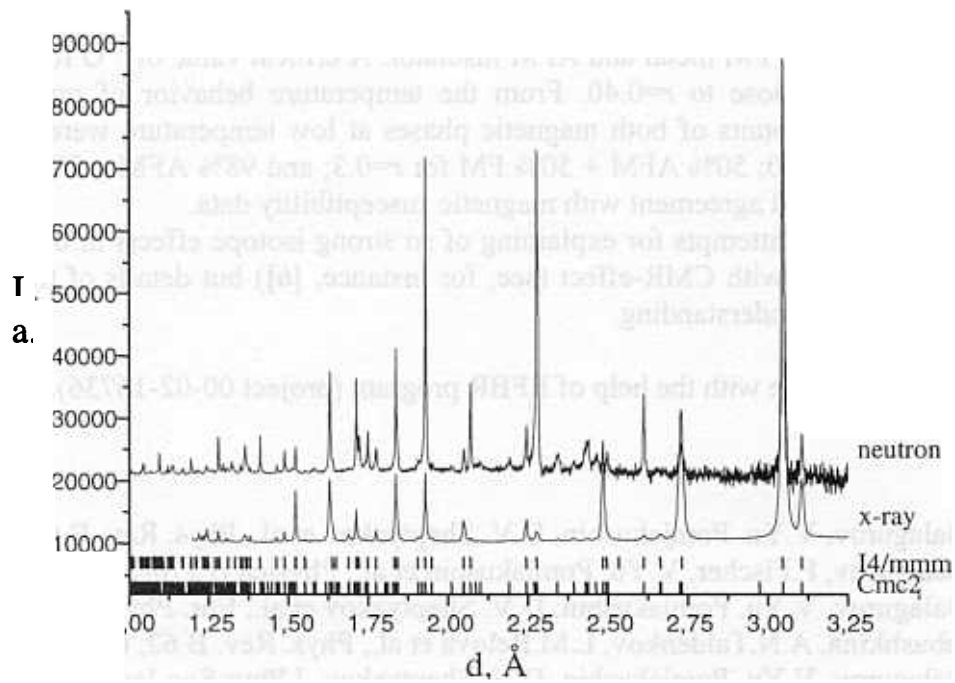

Fig.1

It was early show, the x-ray and neutron diffraction patterns showed that crystallographic structures phases of $Bi_2CaNb_2O_9$ and $Bi_2SrNb_2O_9$ are ortorombic with space group $Cmc2_1$. However, structure of $Bi_2BaNb_2O_9$ is tetragonal with space group $I4/mmm$ [4, 5].

Figure 1 shows the x-ray and neutron powder diffraction patterns at room temperature and afforded initial indexing the peaks. From figure it is visible, that only space group $Cmc2_1$ describes all observably peaks.

Said above creates premises for suggestion that as initial terms when undertaking revision on method Rietveld possible use positions of atoms, determined for structures of $Bi_2CaNb_2O_9$ and $Bi_2SrNb_2O_9$ [4].

Under two temperatures (T=10 K and T=290 K) determined parameters of elementary cell, position of atoms in structure, sites and thermal factor in изотропном approach. Result Rietveld refinement profiles is brought on figures 2 and 3.

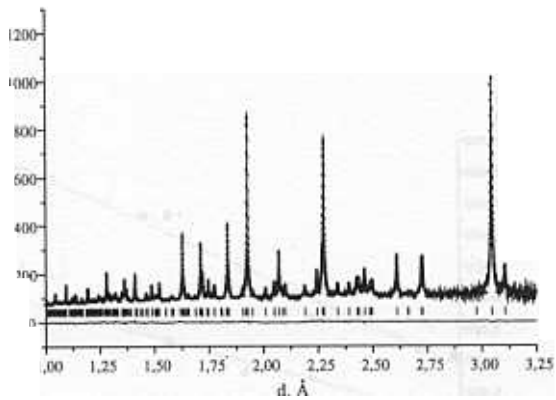

Fig.2. HRFD, T=10 K

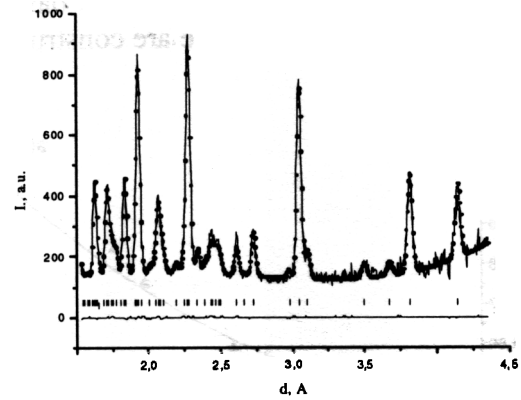

Fig.3. DN-2, T=290 K

In the structure to manage localize a position of atoms lithium. The possible variant of replacement of bismuth by lithium in bismuthic-oxide layer (position 8 (b)) was checked during specification of crystal structure. As a result of calculation the factor of population of lithium in position 8 (b) is received equal to zero. The received data give the basis to assume, that replacement of a bivalent ion with trivalent bismuth and univalent lithium results in occurrence of structural vacancies in the perofskite layer that can create favorable conditions for development of ionic conductivity on structural vacancies (fault ion conductivity).

On the received coordinates a bond valence method [6], calculation of valency V_{ij} for cations is calculated:

$$V_{ij} = \sum_{i}^{v} s_{ij}(R_{ij}) \tag{1}$$

where v – coordination number.

Dependence of valent effort s_{ij} on length of communication R is determined as:

$$s_{ij} = \exp\left[(R_{1j} - R_{ij})/b\right] \tag{2}$$

where R_1 - length of communication of individual valence, and the empirical parameter b is equaled 0.37 Å.

Atom	Bond valence		
	T=10 K	T=290 K	Model
Bi	3.03	2.89	3
(Bi/Li)	1.89	1.81	1.88
Nb	4.94	5.14	5

Arrangements of octahedrons in structure are distorted. Except this, noticeably garbling of their form. Below given lengths of communications of atoms, falling into octahedron.

Bond type	L, Å	
	T=10 K	T=290 K
Nb-O(1)	2.131	2.136
Nb-O(2)	1.868	1.831
Nb-O(4)	1.925 2.019	1.882 2.039
Nb-O(5)	1.957 2.054	1.992 2.085

For reception of more detailed information about sample, on difractometer DN-2 powder neutron diffraction data were collected at high temperature. Phase transitions in this area of temperatures it is not noticed. On the basis of the received data dependences of parameters of an elementary cell on temperature are constructed.

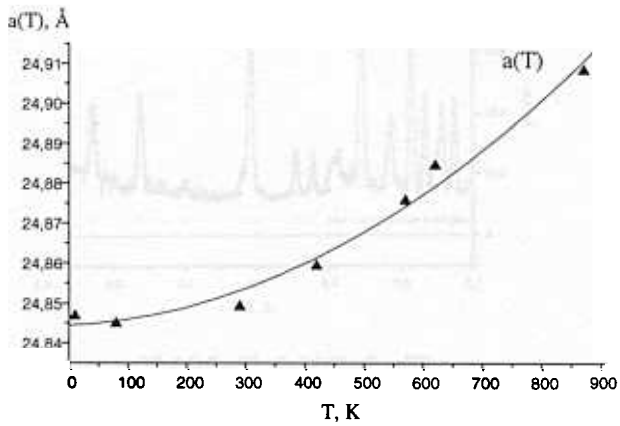

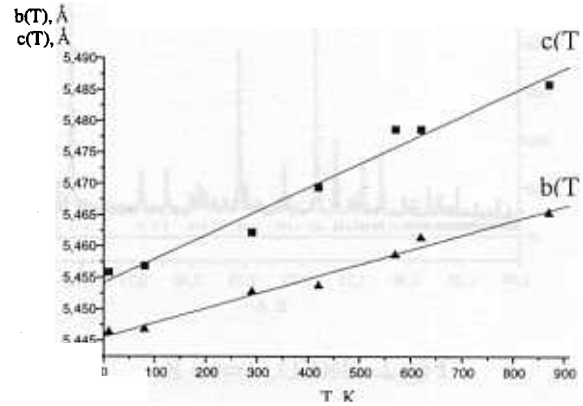

From the given dependences it is visible, that ortorhombic distortion of structure is increased with rise in temperature. It contradicts the data, which are given in [4] for $Bi_2(Sr, Ca)Nb_2O_9$.

1. K. S. Aleksandrov, B. V. Beznosikov, Crystals of type perouvskite, «Saince», Novosibirsk, 1999.
2. V. A. Isupov, Properties of the ferroelectric Aurivillius phases of type $A_{m-1}Bi_2M_mO_{3m+3}$, J. Unorgan. Chem, 1994, т. 39, №5, с. 731-737.
3. G. A. Smolenscki, Sov. Phys. Solid. State, 1959, 3, 651.
4. S. M. Blake, M. J. Falconer, M. McCredy, Cation disorder in ferroelectric Aurillius phases of the type $Bi_2ANb_2O_9$ (A = *Ba, Sr, Ca*), J. Matter. Chem., 1997, 7(8), 1609-1613.
5. Y. Shimacama, Y. Cubo, Crystal structure and ferroelectric properties of $Bi_2ATa_2O_9$ (A = *Ba, Sr, Ca*), Phisical Review B, v. 61, №10, 6559-6564.
6. V. S. Urusov, Theoretical chemistry of crystals, M., MSU, 1987.

PECULIARITIES OF INCOMMENSURATE PHASE IN FERROELECTRIC-SEMICONDUCTOR $TlInS_2$

A.I. Beskrovnyi[a], B.R. Gadjiev[a], N.Yamamoto[b], N.Mamedov[b], S.Iida[c], H.Uchiki[c] and S.Kashida[d]

[a] *Frank Laboratory of Neutron Phisics, Joint Institute for Nuclear Research, Dubna, Moscow region, Russia*

[b] *Department of Physics and Electronics, University of Osaka Prefecture, Osaka, Japan*

[c] *Department of Electrical Engineering, Nagaoka University of Technology, Nagaoka, Japan*

[d] *Department of Environment Science, Faculty of science, Niigata University, Niigata, Japan*

Incommensurate phases in ferroelectrics-semiconductors have a series of peculiarities. The most important one is a great influence of equilibrium and non-equilibrium carriers on the structure of incommensurate phase and possible change of the latter.

In this work we present the results of the full symmetry analysis of the succession of phase transitions of high-symmetry-commensurate-incommensurate type in ferroelectric-semiconductor $TlInS_2$ together with the results of temperature-dependent neutronography of this material. It is shown that the succession of high-symmetry-incommensurate-commensurate phase transitions in $TlInS_2$ is of improper ferroelectrical type.

In terms of a theoretical consideration the succession of high-symmetry-incommensurate-commensurate phase transitions in improper semiconductor-ferroelectric $TlInS_2$ shall be described by the irreducible representation of the space group C_{2h}^6 for the modulation wave vector $\vec{q} = (0,0,0.25)$ [1,2,3,4,5].

The full symmetry consideration in the framework of the theory of Landau shows that the functional of the thermodynamic potential of the $TlInS_2$ -type compounds can be written in the form

$$F = \iint_D f(x,z,\varphi(x,z),\varphi'_x,\varphi'_z)dxdz, \text{ were } f = \frac{\alpha}{2}\rho^2 + \frac{\beta}{4}\rho^4 + \gamma\rho^8\cos n\varphi(x,z) - \delta_1\rho^2\frac{\partial\varphi(x,z)}{\partial x} - \\ - \delta_2\rho^2\frac{\partial\varphi(x,z)}{\partial z} + \frac{k_1}{2}\rho^2\left(\frac{\partial\varphi(x,z)}{\partial x}\right)^2 + \frac{k_2}{2}\rho^2\left(\frac{\partial\varphi(x,z)}{\partial z}\right)^2 + \frac{\upsilon}{2}\rho^2\left(\frac{\partial\varphi(x,z)}{\partial x}\right)\left(\frac{\partial\varphi(x,z)}{\partial z}\right) \quad (1)$$

The suddle equation corresponding to the functional (1) is represented by the expression

$$k_1\frac{\partial^2\varphi(x,z)}{\partial x^2} + k_2\frac{\partial^2\varphi(x,z)}{\partial z^2} + \nu\frac{\partial^2\varphi(x,z)}{\partial x\partial z} + n\gamma\rho^{n-2}\sin n\varphi(x,z) = 0 \quad (2)$$

The differential equation (2) is of hyperbolic type if $\nu^2 - 4k_1k_2 > 0$, of parabolic type if $\nu^2 - 4k_1k_2 = 0$ and of elliptical type if $\nu^2 - 4k_1k_2 < 0$.

In hyperbolic case the spatial distribution of the order parameter has the form

$$\psi(\xi,\eta) = 4arctg\left\{\frac{h'}{k'}sn\left[\left(\frac{16c}{6+4cd}\right)^{1/2}\frac{1}{k'}\xi\right]sn^{-1}\left[\left(\frac{16}{d}\right)\frac{1}{h'}\eta\right]\right\}. \quad (3)$$

The further analysis shows that in terms of Landau theory there takes place the $C_{2h}^6 \Rightarrow P_{1\bar{1}}^{C/2c} \Rightarrow P_{11}^{C2} \Rightarrow C_2^3 \Rightarrow S_2^1 \Rightarrow C_0^1$ succession of phase transitions in these materials as temperature decreases.

In the neutronographic experiments the tree-dimensional distributions of the diffraction intensity along the directions [100] and [001], and between directions [4, 0, 4] – [4, 0, 6] are measured at the

temperatures 240K, 210K, 203K, 180K and 10K, chosen preliminary as possibly corresponding to the different phase states of $TlInS_2$.

The analysis of the two-dimensional cross-sections of the diffraction intensity at 240K shows that between directions [4, 0, 4] and [4, 0, 6] there are observed the corresponding Bragg peaks of the main lattice only. As temperature goes down to 203K, besides the main reflexes a satellite with $d = 1.942\text{Å}$, and Miller indices (4, 0, 4.5) emerges in between the (4, 0, 4) and (4, 0, 6) peaks. Further cooling down to $T = 180K$ leads to the tripling the number of satellites. Positions of these satellites with $d_{hkl} = 1.768\text{Å}$, 1.796Å, $1.928\ \text{Å}$ relate fairly well with the calculated positions of the satellites with $d_{4,0.5,5} = 1.759\text{Å}$, $d_{405.25} = 1.799\text{Å}$ and $d_{404.75} = 1.926\text{Å}$, respectively. At 100$K$ (Fig.1) the intensities of the just-mentioned satellites become significantly increased and a satellite with $d_{404.5} = 1.883\text{Å}$ appears in the intensity distribution. At last, at $T = 10K$ (Fig.2) the intensities of all the previous satellites become stronger again without positional change noticeable with the accuracy of the experiment. At the same time the (406) peak becomes approximately four times weaker in intensity. As follows from Fig. 1 and 2, the positions of the satellites are on the line that connects the (4, 0, 4) and (4, 0, 6) Bregg points.

With lowering the temperature, there also are some changes in the sector of the reciprocal space lying between [4, 0, 4], [4, 0, 6] directions. The peak having $d_{50.57.25} = 1.382\text{Å}$ at 240K corresponds to the structure with modulation wave vector $\vec{q} = (0, q_y, 0.25)$ and $q_y \approx 0.5$. At 203K this peak disappears indicating the change of the modulation vector. At 180K already two peaks, with $d = 1.383\text{Å}$ and $1.488\ \text{Å}$, respectively, appear in the above zone. Their intensities decrease as temperature goes down to $T = 100K$. Further changes take place with lowering the temperature below 100K. At 10K, besides the already observed couple of peaks a third one appears, having the $d = 1.099\text{Å}$.

In the cross-section (hol) the reflex $(00l)$ relative intensities are temperature independent. There is no additional diffraction peaks in the zone $\Delta k \approx 0.5$ at temperatures 240K and 210K. At 180K a solitary weak peak emerges in the neutronogram remaining unchanged upon further decreasing the temperature. As temperature comes down to 10K one more additional peak appears. In the neighborhood of $(h,0,0)$ peaks the temperature reduction effect can be easily made out only at 10K in the form of the significantly increased intensity of the (8, 0, 0) peak. Besides this, the (16, 0, 0) feflection becomes slightly observable at 100K and 10K. In this zone with $\Delta k \approx 0.5$ the additional peak appears first only at 180K. At 100K the number of the additional peaks triples and at 10K the intensities of these peaks is weakened.

To overall, we have shown that $TlInS_2$ crystals, which have an average space group of symmetry C_{2h}^6 in high-temperature phase, at $T = 240K$ are in incommensurate state with modulation wave vector $\vec{q}_{inc} = (q_x, q_y, 0.25)$. The parameters q_x and q_y exhibit significant temperature dependence. Within experimental accuracy these parameters do not exceed 0.005 at 203K. The magnitude of the third component does not change in the entire range of the accessed temperatures. According to the obtained data the $TlInS_2$ compound is in incommensurate phase already at 240K. The modulation wave vector is $\vec{q} = (0, q_y, q_z)$ and q_y is a strongly temperature dependent parameter $(q_y(T = 240K) \propto 0.5,\ q_y(T = 203K) \propto 0)$. At the same time, the q_Z is practically temperature independent. It seems important to figure out that the obtained neutron-scattering data are unambiguous about the successive structural changes and the modulation wave vector rotation with decreasing the temperature. These results permit the possibility of incommensurate-incommensurate phase transition and two-dimensionally modulated incommensurate phase on the phase diagram of $TlInS_2$. However, the results of the presented theoretical results on $TlInS_2$ require further experimental efforts, especially structural investigations in more detail.

Literature:

1. Vakhrushev S.B. Incommensurate phase transition in $TlInS_2$ crystal, JETP Letters, 1984, v.39, No. 6, pp. 245-247.

2. Kashida S., Kobayashi Y. X-ray study of the incommensurate phase of $TlInS_2$, J. Phys.: Condensed Matter, 1999, v.11, pp. 1027-1035.

3. Henkel W. High-pressure Raman study of the ternary chalcogenides $TlGaS_2, TlGaSe_2, TlInS_2 and TlInSe_2$, Phys. Rev. B, v.26, No.6, pp. 3211-3221.

4. Gashimzade F.M., Gadjiev B.R. Dielectric permittivity in incommensurate phase of $TlGaSe_2$, FTT, 1985, v.27, No.8, pp.2286-2290.

5. Gadjiev B.R., Seidov Yu. M. Incommensurate-incommensurate transition in subsuquant phase transitions in layered $TlInS_2$, ФТТ, 1996, т. 38, в.1, с. 3-13.

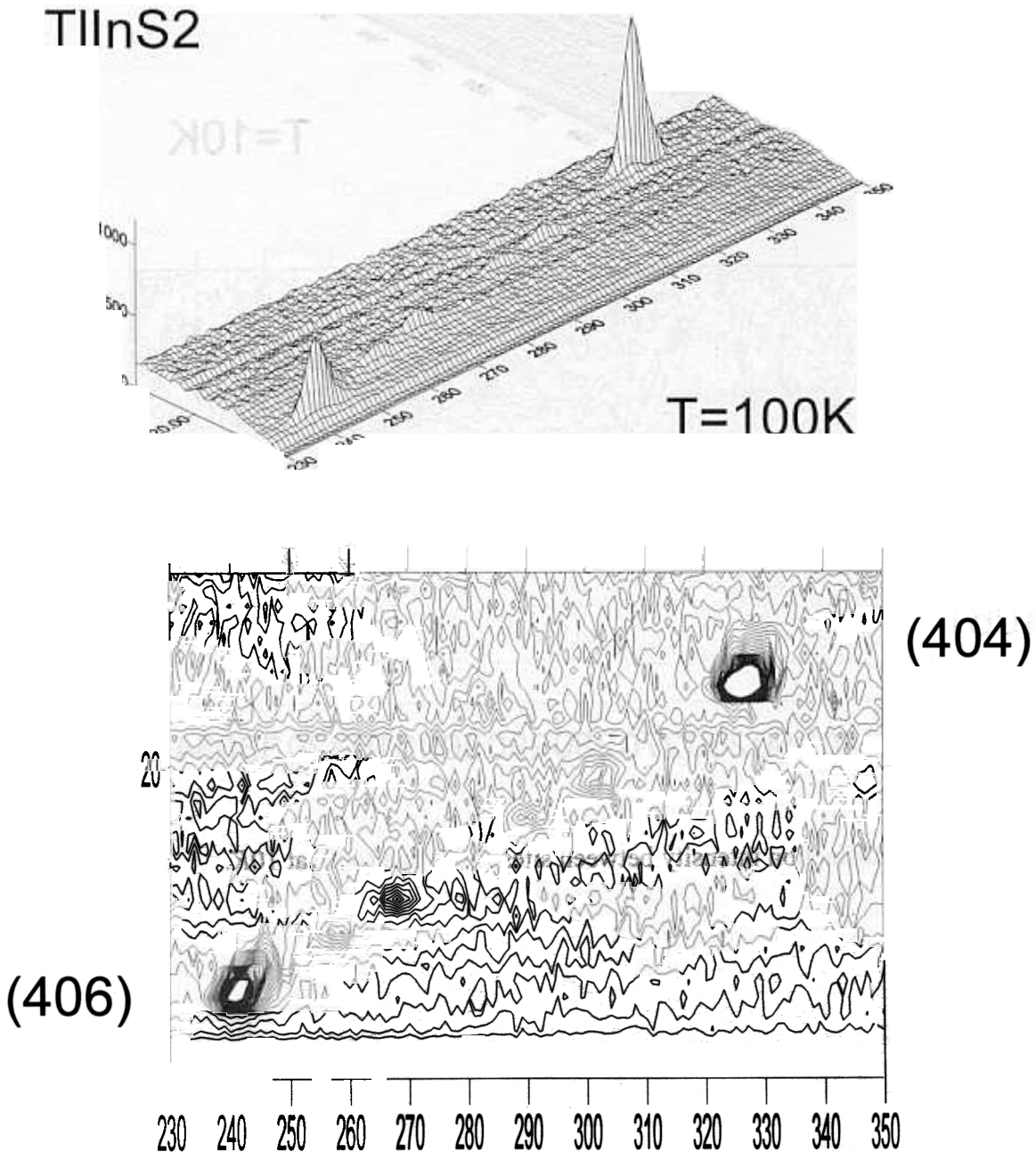

Fig.1 Maps of diffraction intensity between sites (404) and (406) at 100K

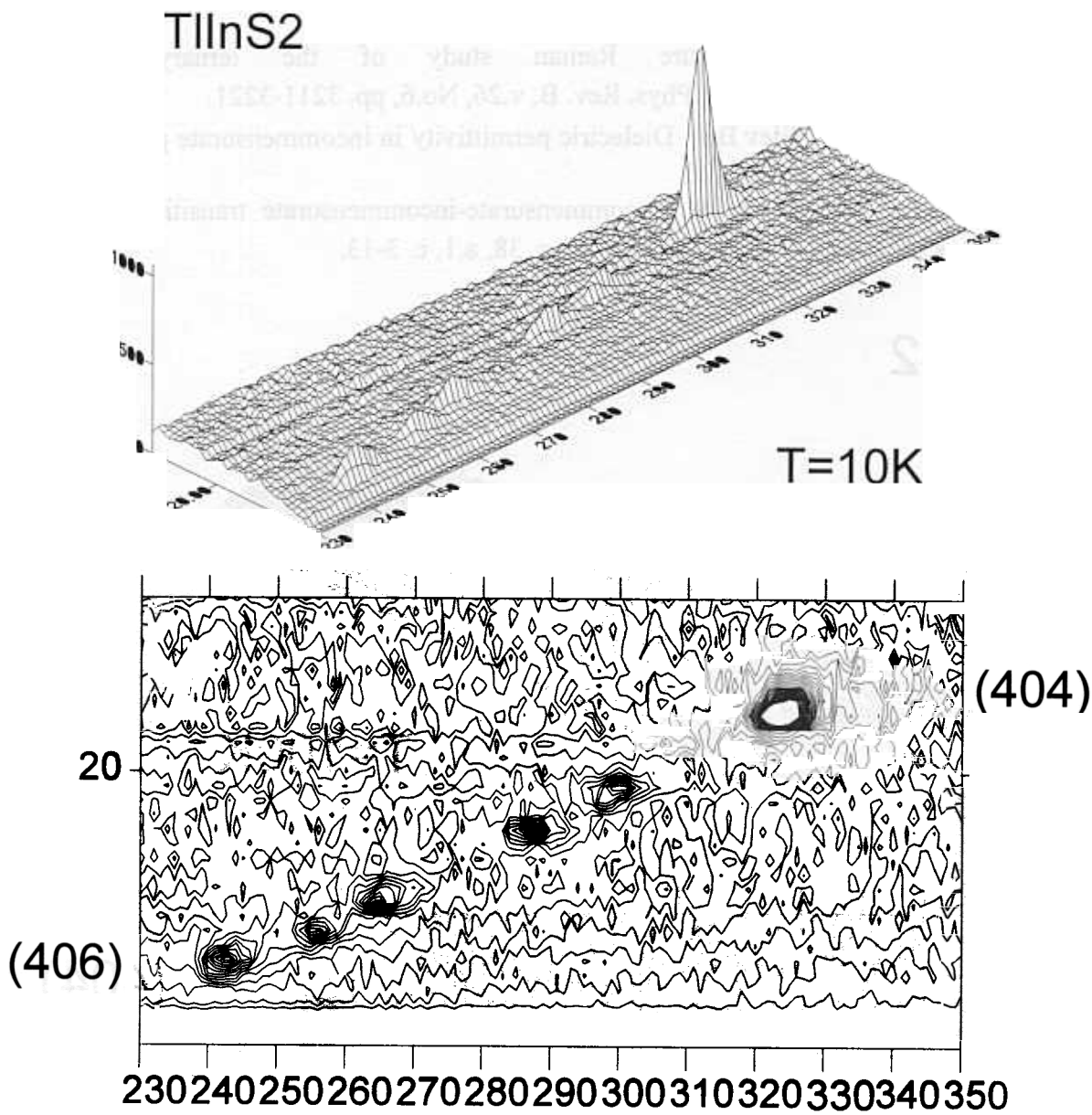

Fig.2. Maps of diffraction intensity between sites (404) and (406) at 10*K*.

Neutron diffraction study of the strain/stress behaviour on dolomite rock

Ch. Scheffzük [1,2], K. Walther[1], A. Frischbutter[1] and R.A. Zhukov [3]
[1] *GeoForschungsZentrum Potsdam, Telegrafenberg, 14473 Potsdam, Germany*
[2] *FLNP, Joint Institute for Nuclear Research, 141980 Dubna, Russia*
[3] *Tula State University, 300 600 Tula, Russia*

Introduction and sample orientation

Diffraction methods for strain/stress studies are well established in materials sciences [1]. Only recently geological materials became the subject of strain/stress investigations using diffraction methods. However, the study of geological problems is more complicated. One reason is the diversity of fabric elements, influencing the strain/stress properties of rocks, e.g. its polyphase composition, the occurrence of various macro- and microstructures like foliations, bedding planes, joints and crystallographic preferred orientations. Even the deformation history of rocks, which is often characterized by repeated superimposed deformation events accompanied by temperature and/or pressure is of importance. Consequently, the deformation history and the deformation parameters of geological materials are mostly unknown. In contrast to X-rays, neutron diffraction allows investigation of large sample volumes (several cm^3) due to the high penetration depth of neutrons. First experiments were carried out on sandstone using angle dispersive neutron diffraction as well as time-of-flight neutron diffraction in order to investigate applied and residual stresses [2]. Fundamental investigations of the strain/stress behaviour using diffraction methods in the laboratory - combined with microstructural investigations using optical and electron microscopy - are essential for a better understanding of rock mechanics.

The investigation of the strain-stress behaviour of monomineralic natural dolomite under uniaxial applied stress by neutron time-of-flight diffraction is the subject of this study. Next to calcite, the trigonal-rhombohedral ($\bar{3}$) dolomite ($CaMg(CO_3)_2$) is the most important rock forming mineral in carbonate rocks. The dominating morphological lattice planes are the rhombohedrons $\{10\bar{1}1\}$, special forms are pinacoids $\{0001\}$ and hexagonal prisms $\{hki0\}$. In contrast to calcite, which under load is twinning on *e*-planes $\{01\bar{1}2\}$, the most important twin plane of dolomite is the *f*-plane $\{02\bar{2}1\}$. The deformation mechanisms are described in [3] in more detail.

The sample (G3) was prepared from a core (⌀ 60 mm, depth: 1018 m below surface level) of borehole GUBEN 16/64 in the Niederlausitz (Germany). The sample is a grey, massive, oolithic dolomite, weakly developped flaser-bedding is indicated by thin layers of fine-grained, massive dolomite. The diameter of the ooids approximates 1 mm, most ooids are perfectly concentric. Only within a few distinct layers (thicknesses: several mm) the ooids are flattened, obviously due to the overburden pressure of the surface rock. Individual sparritic dolomite crystals embedded in a micritic dolomite matrix form the matrix between the ooids. The nuclei of the ooids are sometimes filled with dolomite monocrystals, too. The ooids itself consist of concentrically arranged layers of micritic dolomite-felt. Under the microscope, relics of muscovite and quartz can be detected,

embedded within the matrix and enclosed within ooids as well. The mineralogical composition of the sample was determined by quantitative X-ray phase analysis: 92% dolomite, 3% quartz and accessory phases. All these observations indicate synsedimentary deformation and subsequent diagenetic recrystallization.

Experimental setup, sample preparation and results

For the experiments we used a sample cylinder ($\varnothing$=30 mm, l=60 mm). For d_0-determination, powder was prepared from the same sample (grain size ≤ 64 μm), heated for 24 h up to 400°C and slowly cooled down to room temperature. The experiments were carried out at room temperature at the diffractometer EPSILON at beamline 7A of the pulsed reator IBR-2 at JINR Dubna. Due to the long flight path of 102.38 m a rather good spectral resolution of $4x10^{-4}$ is achieved. The diffractometer is equipped with the uniaxial pressure device EXSTRESS, which is able to apply loads up to 100 kN under *in situ* conditions. Stresses up to 150 MPa are applicable for the actual sample dimensions.

The neutron-TOF-pattern (Fig. 1), normalized with respect to the energy distribution, was measured with a time channel width of 32 μs. Taking into account the asymmetry of the diffraction peaks two superposed GAUSSIANs with different half widths were used for the peak fit procedure [4]. The FWHM of the (0006) peak is in the order of 36 time channels, the $(10\bar{1}4)$ peak comprises about 27 channels, the $(11\bar{2}3)$ peak about 20 channels. Strain/stress experiments were carried out in four steps up to 45 MPa. Each loading state for applied stress measurement was interrupted by a stress-free state for residual strain measurements. The peak positions of all three lattice planes obviously change with different intensity towards lower time channels with increasing load (Fig. 2). Determining the corresponding values of the Young's modulus by linear regression, we obtained 101 GPa for the $(11\bar{2}3)$ reflection, 63 GPa for the (0006) reflection and 292 GPa for the $(10\bar{1}4)$ reflection.

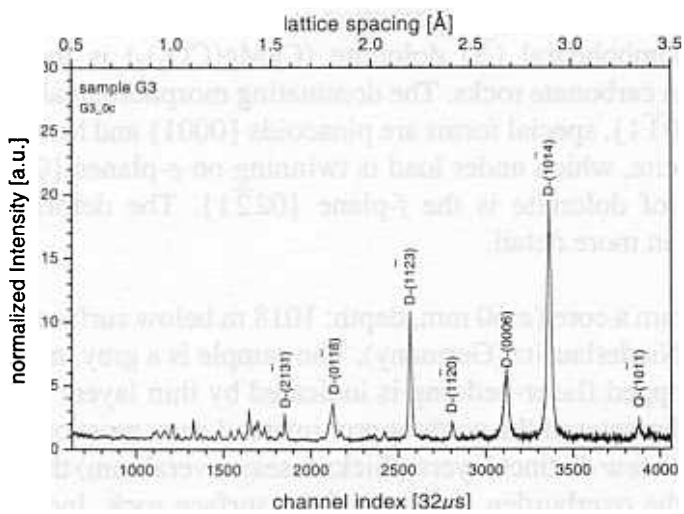

Fig. 1: Neutron time-of-flight diffraction pattern of the dolomite sample investigated.

The patterns determined at the relaxed positions of the sample are similar regarding the behaviour of the three reflections. Differences are valid only in scale (Fig. 3). This evolution is restricted to less than one time channel for the $(11\bar{2}3)$ and $(10\bar{1}4)$ reflections.

Nevertheless, all considered lattice planes indicate the same gap of compressive pseudostrain by a period of extension (stage 2). Assuming that the virginal state (◆ in Fig. 3) of the sample is more or less stress-free, the strain of the relaxed states of the sample was calculated using the virginal state as d_0. There are only weak changes regarding the evolution of the FWHM during the deformation experiment. This is demonstrated on behalf of the $(11\bar{2}3)$ peak, which is free of superimpositions. The FWHM of the $(11\bar{2}3)$ peak only slightly increases with increasing load.

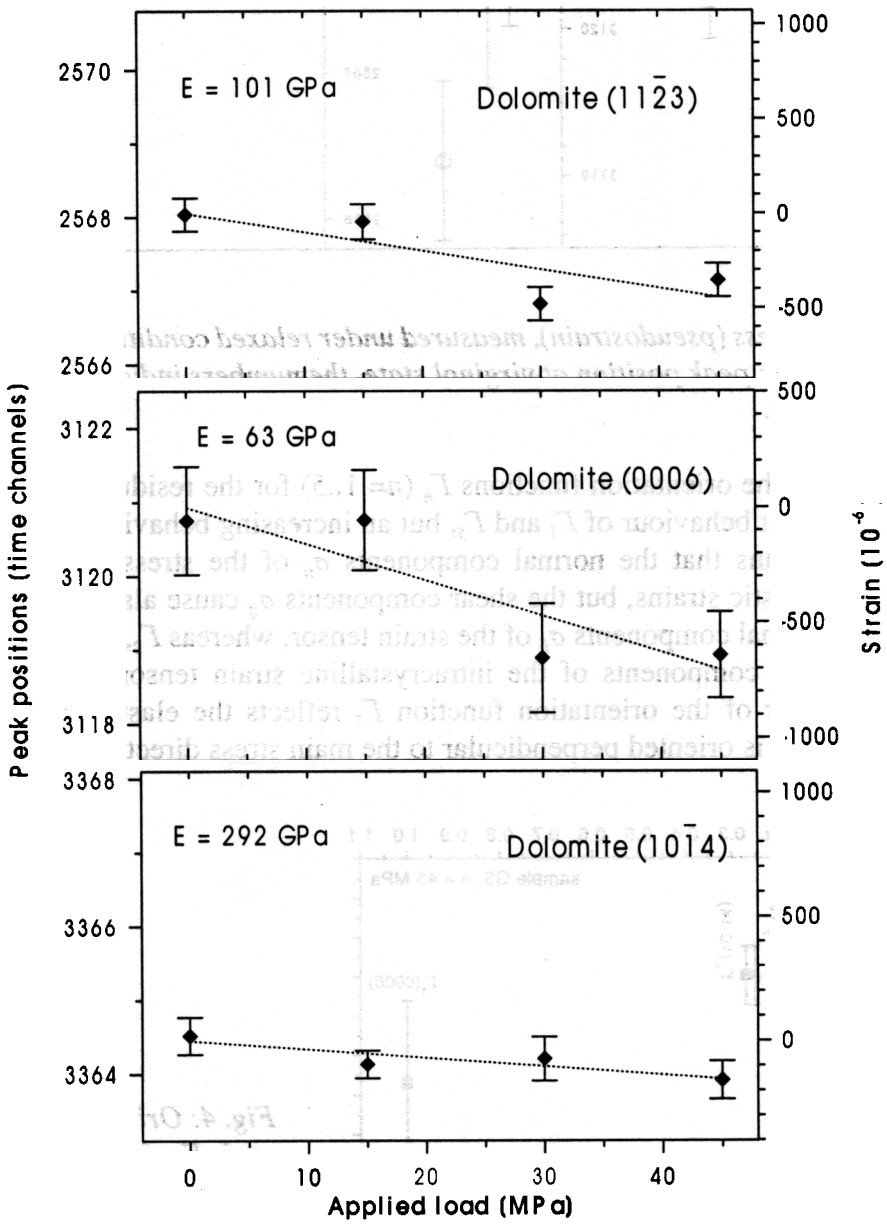

Fig. 2: Strain-stress relation for the $(11\bar{2}3)$, (0006) and $(10\bar{1}4)$ Bragg reflections of dolomite (sample G3), measured by stepwise increase of applied load. The Young's modul are enclosed.

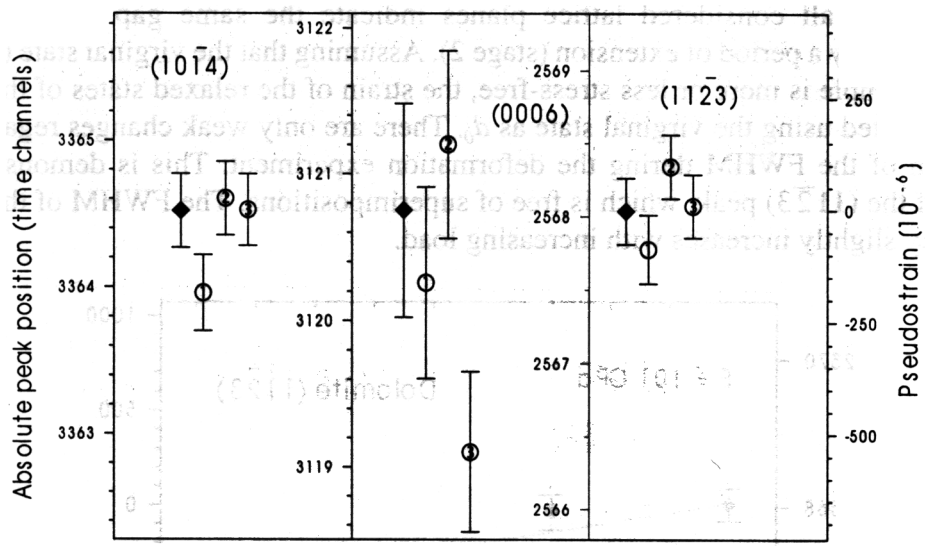

Fig. 3: Residual stress (pseudostrain), measured under relaxed conditions after each state of applied load. (◆: peak position at virginal state, the numbers indicate the order of the state of relaxation).

By calculation of the orientation functions Γ_n (n= 1..5) for the residual strain values we observed a constant behaviour of Γ_1 and Γ_5, but an increasing behaviour of Γ_2, Γ_3 and Γ_4 (Fig. 4). This means that the normal components σ_{ii} of the stress tensor cause only intracrystalline elastic strains, but the shear components σ_{ij} cause also plastic strains. Γ_1 represents the normal components σ_{ii} of the strain tensor, whereas Γ_2, Γ_3 and Γ_4 represent elastic and plastic components of the intracrystalline strain tensor. Furthermore, the constant behaviour of the orientation function Γ_5 reflects the elastic character in the direction σ_3, which is oriented perpendicular to the main stress direction σ_1.

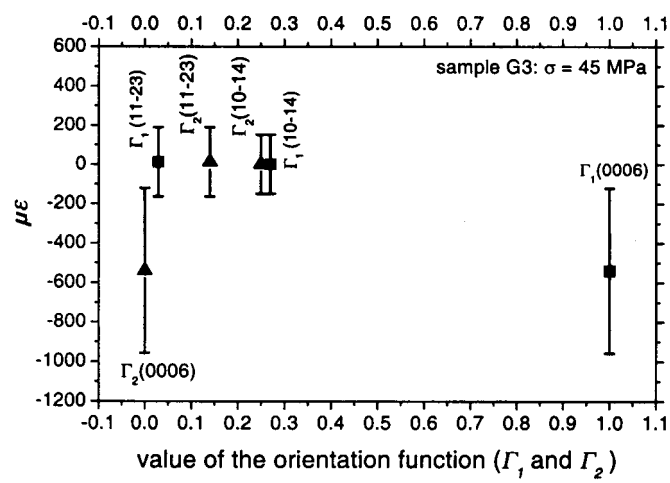

Fig. 4: Orientation functions Γ_1 and Γ_2 for residual stress values of the dolomite sample G3.

Discussion

Our results indicate that neutron time-of-flight diffraction is a useful tool for *in situ* experiments concerning the strain/stress behaviour and residual stress measurements on

dolomite rocks. The actual experimental set up allows us to make use of only two dolomite reflections for strain/stress studies: $(11\bar{2}3)$ and $(10\bar{1}4)$, because other reflections are either weak (measuring time), superposed or out of range. The Young's modulus, determined from the strain-stress curve for the dolomite $(11\bar{2}3)$ reflection, agrees well with published data for isotropic polycrystalline aggregates [5], but disagrees with published values for the dolomite (0006)- and $(10\bar{1}4)$-reflections. The discrepancy may arise from the entirety of macro- and microstructural features of the studied sample, from the superimposition of diffraction peaks and from resulting complications in data analysis.

The work has been founded by the German BMBF (projects DUBPOT-3 and DUBPOT-9). We gratefully acknowledge further support of FLNP/JINR Dubna and GeoForschungsZentrum Potsdam.

REFERENCES

1. M.T. Hutchings and A.D. Krawitz (Eds.), Measurement of Residual and Applied Stress Using Neutron Diffraction. NATO ASI Series **E216**: 588 p. (1992).
2. A. Frischbutter, D. Neov, Ch. Scheffzük, M. Vrana and K. Walther, Lattice strain measurements on sandstones under load using neutron diffraction. *J. Struct. Geol.* **22** (11/12), 1587-1600 (2000).
3. D.J. Barber, H.C. Heard and H.-R. Wenk, Deformation of dolomite single crystals from 20-800°C. *Phys. Chem. Minerals* **7**, 271-286 (1981).
4. K. Walther, Ch. Scheffzük and A. Frischbutter, Strain-stress-experiments on dolomite using neutron TOF diffraction. *Physika semli*, in preparation.
5. K.H. Hellwege, Landolt-Börnstein - Zahlenwerte und Funktionen aus Naturwissenschaften und Technik. - Neue Serie, Band 1b: Physikalische Eigenschaften der Gesteine. [Springer Verlag Berlin, Heidelberg, New York: 604 p., 1982].

TEXTURE – AN INDICATOR OF ROCK METAMORPHISM AND DEFORMATION PROCESSES IN THE CONTINENTAL CRUST

A.N. Nikitin[a], T.I. Ivankina[a], N.V. Zamyatina[a], V.I. Kazansky[b], K.V. Lobanov[b] and A.V. Zharikov[b]

[a] *Joint Institute of Nuclear Research, Frank Laboratory for Neutron Physics, 141980, Dubna, Russia*

[b] *Institute of Geology of Ore Deposits, Petrography, Mineralogy and Geochemistry, Russian Academy of Sciences, 109017, Moscow, Russia*

Introduction

Crystallographic preferred orientation (texture) of rock-forming minerals is the main controlling factor of rock anisotropy, among other factors like shape preferred orientation and microcracks. Textures can produce pronounced directional dependence of elastic properties. Hence, texture determinations contain information on the seismic anisotropy and can be helpful to understand the nature of seismic boundaries in the continental crust. Texture measurements of naturally deformed rocks combined with the results of deep seismic sounding may allow reconstruction of the paleotectonic stress state at deep crustal levels. Texture analyses give us a key for the understanding of texture development and, consequently, for the restoration of geological evolution processes.

In this paper we report results of texture determinations carried out on core samples from the Kola superdeep borehole SG-3 and their surface analogues. These measurements carry on earlier texture and anisotropy investigation of deep crustal rocks [1] and will be useful for the geodynamic modelling [1] of the crustal structure at the Pechenga ore region (Kola Peninsula) [2].

Sample description

The core samples were collected from selected sections of the SG-3 core distance (8.5 – 11.5 km). The surface analogues were collected about 50 km northeast from the SG-3 drilling site in a reference area located south from the Mustatuntury ridge. The core and surface samples (two gneisses, four amphibolites) are characterized by identical mineralogical and chemical composition and mineral density. The average mineralogical composition of the core samples (black bars) and surface samples (white bars) are presented in Fig.1.

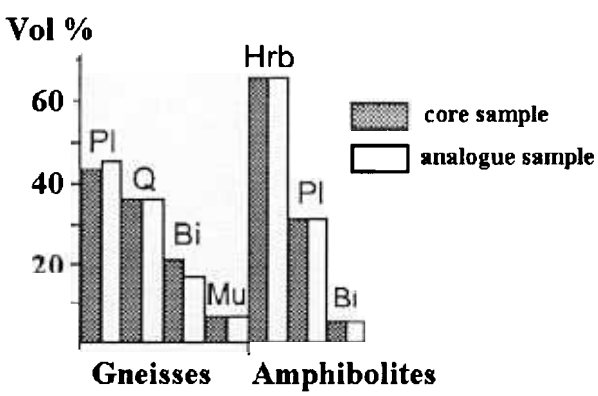

Fig. 1. Mineralogical composition of Kola rock samples:
Pl – plagioclase, **Q** – quartz,
Bi – biotite, **Mu** – muscovite,
Hrb – hornblende.

The experiments were performed on cubic samples with 30 mm edge length. The sample reference system corresponds to the geographical coordinates (azimuth and declination).

Experiment and results

Texture measurements have been carried out at the neutron texture diffractometer SKAT at the pulsed reactor IBR-2. The measuring time for the each sample was 36 hours, the exposition time at one sample position was 30 min. As an example, the time-of-flight diffraction pattern of the core gneiss sample K9002 is shown in Fig.2. The K9002 sample constitutes of plagioclase – 55%, quartz – 26%, biotite and muscovite– 16%, additional minerals – 3%.

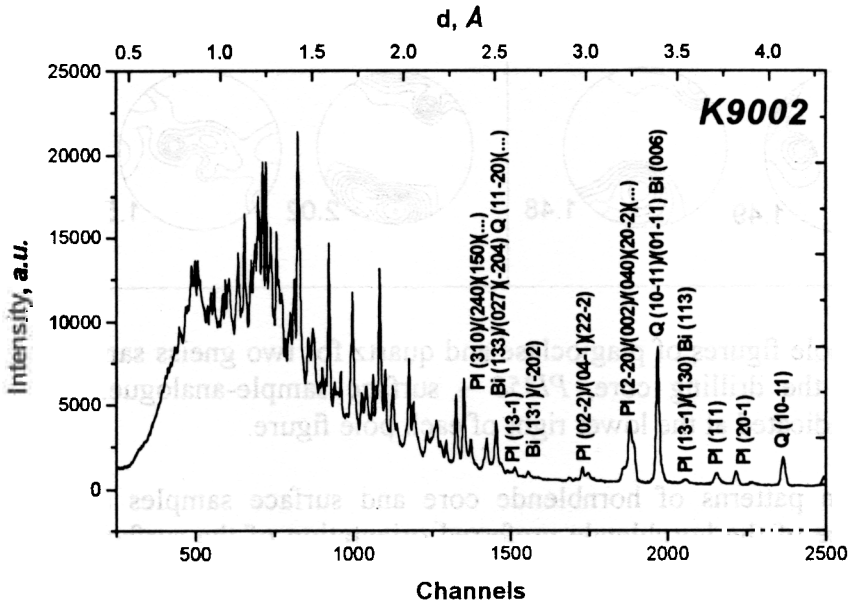

Fig. 2. Diffraction pattern of sample K9002. Some Bragg reflections as well as the overlapping conditions are indicated. Pl – plagioclase, Q – quartz, Bi – biotite.

Since the samples consist of low symmetrical minerals, texture analysis of such polyphase rock is not trivial due to complex diffraction patterns with many overlapping peaks. Nevertheless, a sufficient number of plagioclase and quartz pole figures (for gneisses) and hornblende and plagioclase pole figures (for amphibolites) could be extracted from the diffraction spectra. Since counting statistics of biotite and muscovite reflections are insufficient, pole figures for these mineral phases were not extracted from the diffraction pattern.

Based on the experimental pole figures, the orientation distribution functions (ODF`s) and pole figures of the main crystallographic planes (100), (010) and (001) of the predominant mineral phases have been calculated. The results of texture analysis display a well developed textures of all mineral phases.

In the gneiss samples preferred orientation patterns of plagioclase are more pronounced compared to the quartz patterns. Pole figures of the plagioclase crystallographic planes (001), (010), (100) of core sample *K9002* and its surface analogue *Pl358* are shown on Fig. 3. It was observed that patterns of both samples are similar, but the degree of preferred orientations of sample *Pl358* is weaker compared to sample *K9002*.

Fig. 4 displays pole figures of two amphibolite samples: *K8933* - selected from the drilling core SG-3 and *Pl356* – the surface equivalent. It is obvious, that the prevailing rock forming mineral hornblende (65-70 %) possesses the more pronounced stronger preferred orientations compared to plagioclase textures. The texture of quartz could not be calculated because of the low volume fraction (~ 4 %) of this mineral.

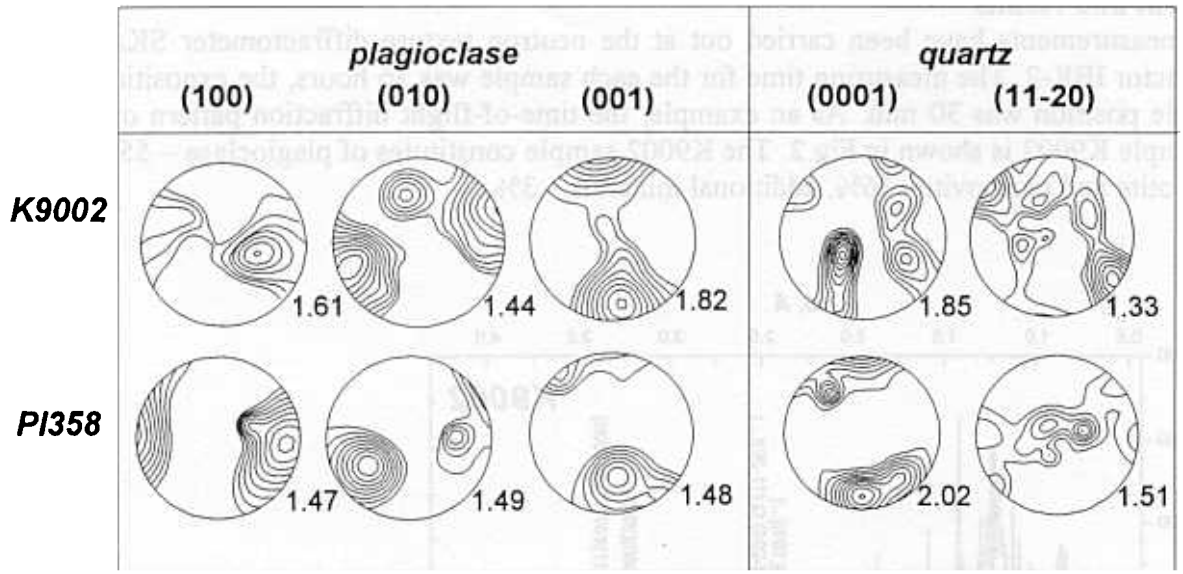

Fig. 3. ODF - derived pole figures of plagioclase and quartz for two gneiss samples: *K9002* – gained from the drilling core, *PI358* – surface sample-analogue. The maximum intensity is indicated at the lower right of each pole figure.

The preferred orientation patterns of hornblende core and surface samples as well are comparable. However, the degree of the hornblende preferred orientation of the surface sample is higher compared to the core sample. In the case of plagioclase, differences in the preferred orientation of core and surface sample is not so clear as for the hornblende textures.

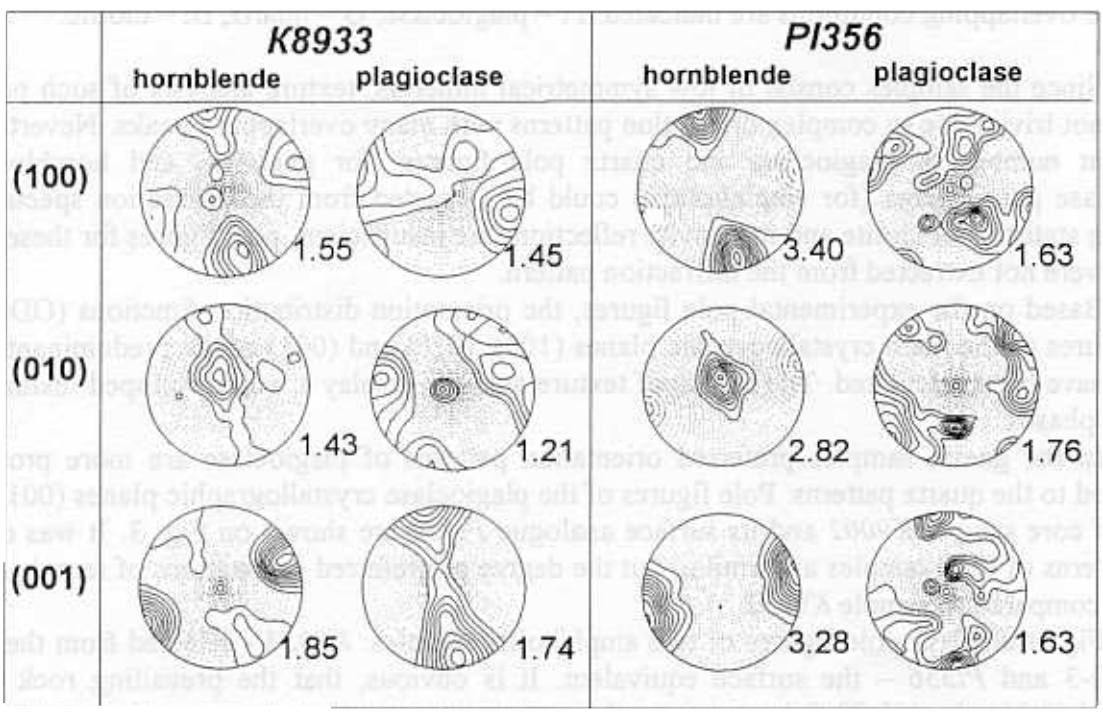

Fig. 4. ODF - derived pole figures of hornblende and plagioclase for two amphibolite samples: *K8933* – gained from the drilling core, *PI356* – surface sample-analogue. The maximum intensity is indicated at the lower right of each pole figure.

Comparing the plagioclase pole figures (gneisses and amphibolites as well) from different levels of the SG-3 section, it can be found that plagiogneisse K9002 and amphibolite K8933, belonging to the allocated section, are characterised by identical patterns. It should be also noted that texture formation took place of about 550-630°C (amphibolite metamorphic facies), as indicated by plagioclase-hornblende geothermometer. This represents an additional forcible evidence for analogy between the samples collected from the Kola SG-3 and Mustatunturi area.

Acknowledgements
This study has been performed in the framework of the UNESCO International Geological Correlation Programme (Project 408) and with financial support from the Russian Foundation for Basic Research (Project № 00-05-64244).

References

[1] Nikitin A.N., Ivankina T.I., Ullemeyer K., Locajicek T., Pros Z., Klima K., Smirnov Yu.P., Kusnetzov Yu.I. Texture controlled elastic anisotropy of amphibolites from the Kola superdeep borehole Sg-3 at high pressure. Fizika Zemli. 1 (2001)

[2] Three-dimensional models and geodynamics of the Pechenga ore region and adjacent areas. In: Kola Superdeep. Scientific Results and Research Experience. M.: TECHNONEFTEGAZ, 130-155 (1998)

STRUCTURAL STUDY OF TERNARY MERCURY CHALCOGENIDE SYSTEMS $HgSe_{1-x}S_x$ (x=0.3, 0.5, 0.6) UNDER HIGH PRESSURE

V.I.Voronin[1], V.P.Glazkov[2], D.P.Kozlenko[3], S.V.Tikhomirov[3], B.N.Savenko[3]
I.F.Berger[4], V.V.Shchennikov[1]

[1] *Institute for Metal Physics, RAS, Ural Division, 620219 Ekaterinburg, Russia*
[2] *Russian Research Center "Kurchatov Institute", 123182 Moscow, Russia*
[3] *Frank Laboratory of Neutron Physics, JINR, 141980 Dubna Moscow Reg, Russia*
[4] *Institute of Solid State Chemistry, RAS, Ural Division, 620219 Ekaterinburg, Russia*

Mercury chalcogenides HgX (X=O, S, Se, Te) attract great deal of attention due to a number of pressure-induced phase transitions accompanied by the changes in electronic structure [1]. Structures of binary systems HgSe and HgS under high pressure have been extensively studied by X-ray diffraction [2-4]. HgS (the cinnabar) at ambient conditions has a hexagonal structure, space group $P3_121$ (the cinnabar phase). This phase is characterized by spiral atomic chains, parallel to c-axis. HgSe at ambient conditions has a zinc blende cubic structure, space group $F\bar{4}3m$. Under pressure HgSe converts to the cinnabar phase at $P \sim 10$ kbar [2]. Both HgS at $P \sim 130$ kbar and HgSe at $P \sim 200$ kbar transform to NaCl-type cubic structure, space group $Fm3m$ [4]. At higher pressures ($P \sim 400$ kbar) HgSe transform to orthorhombic structure, space group $Cmcm$.

An effect of high pressure on the structure of ternary systems $HgSe_{1-x}S_x$ have not been studied yet. One may expect that these compounds will undergo a sequence of the phase transitions similar to that for pure HgS or HgSe. In [6] it was found that electrical resistance of $HgSe_{1-x}S_x$ systems ($0.1 < x < 0.6$) increases rapidly in 2-3 orders of magnitude at pressure $P \sim 4 - 8$ kbar depending of S content. This effect was attributed to a semimetal-semiconductor electronic transition and it was suggested that this change of electrical resistance corresponds to the structural phase transition from cubic zinc-blende phase to cinnabar hexagonal phase. At $P \sim 100$-150 kbar the decrease of electrical resistance of $HgSe_{1-x}S_x$ compounds was observed [7]. This effect may correspond to semiconductor-metal electronic transition and it was suggested that it is accompanied by a structural phase transition to NaCl-type cubic phase.

To study structural changes in ternary mercury chalcogenide systems $HgSe_{1-x}S_x$ (x = 0.3, 0.5, 0.6), neutron diffraction experiments have been performed with the DN-12 spectrometer at pressures up to 30 kbar and ambient temperature using sapphire anvil high pressure cells. The scattering angle was $2\theta = 90°$.

Diffraction patterns of $HgSe_{0.7}S_{0.3}$ measured with the DN-12 spectrometer at $P = 0$ and 17 kbar are shown in fig. 1. Diffraction patterns of $HgSe_{0.5}S_{0.5}$ and $HgSe_{0.4}S_{0.6}$ look similar. For all the investigated systems a phase transition from the cubic zinc-blende phase to the hexagonal cinnabar phase was observed at $P \sim 10$ kbar in agreement with electrical resistance measurements [6]. In the high pressure cinnabar phase Hg atoms occupy $3a$ sites (u, 0, 1/3) and Se/S atoms occupy $3b$ sites (v, 0, 5/6) of the space group $P3_121$ with $u = 0.72(1)$ and $v = 0.47(1)$. As a result of the phase transition, the unit cell volume per molecular unit undergoes a jump with relative volume reduction of $\Delta V/V \sim 12$ %. From diffraction data lattice parameters and interatomic distances as functions of pressure were obtained. Lattice parameters a and c as functions of pressure for the cinnabar high pressure phase of $HgSe_{1-x}S_x$ systems (x=0.3, 0.5, 0.6) are shown in fig. 2.

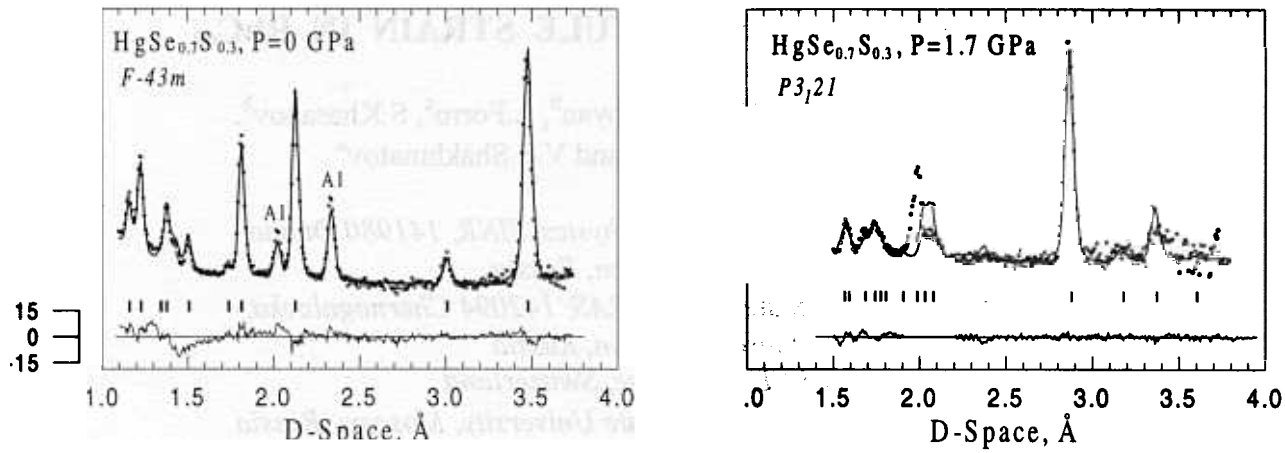

Figure 1. *Diffraction patterns of $HgSe_{0.7}S_{0.3}$, measured with the DN-12 spectrometer at P=0 (zinc blende cubic phase) and P=17 kbar (hexagonal cinnabar phase) and processed by the Rietveld method.*

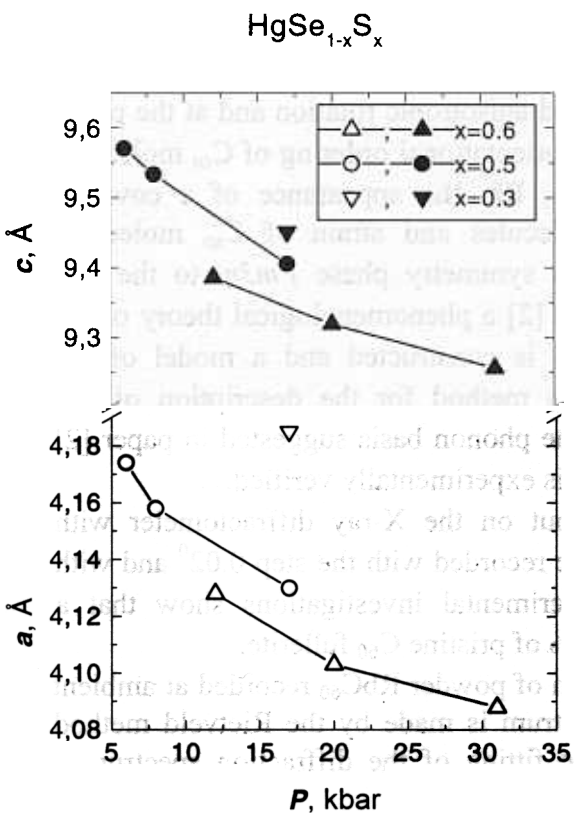

Figure 2. *Lattice parameters a and c as functions of pressure for the cinnabar high pressure phase of $HgSe_{1-x}S_x$ systems (x=0.3, 0.5, 0.6).*

The work has been supported by Russian Foundation for Basic Research, grant № 00-02-17199.

1. I.M.Tsidilkovsky, V.V.Schennikov, I.G.Gluzman, Soviet Phys. of Soild State, 24, 2658 (1982).
2. M.I.McMahon, R.J.Nelmes, Phys. Stat. Sol. (b) 198, 389 (1996).
3. A.Werner, H.D.Hocheimer and K.Strössner, Phys. Rev. B 28, 3330 (1983).
4. T.L. Huang and A.L.Ruoff, Phys. Rev. B 31, 5976 (1985).
5. N.G.Wright, M.I.McMahon, R.J.Nelmes, A.San-Miguel, Phys. Rev. B 48, 13111 (1993).
6. V.V.Shchennikov, N.P.Gavaleshko, V.M.Farsunyak, V.I.Osotov, Soviet Physics of Solid State, 37, 2398 (1995).
7. V.V.Shchennikov, N.P.Gavaleshko, V.M.Farsunyak, Soviet Physics of Solid State, 35, 389 (1993).

FULLERENE MOLECULE STRAIN IN RbC_{60}

V.L.Aksenov[a], Yu.A.Ossipyan[b], L.Forro[c], S.Khasanov[b],
V.V.Chernyshev[d] and V.S.Shakhmatov[a]

[a] *Frank Laboratory of Neutron Physics, JINR, 141980 Dubna, Moscow Region, Russia*
[b] *Institute of Solid State Physics RAS, 142094 Chernogolovka, Moscow Region, Russia*
[c] *EPFL, Lausanne, Switzerland*
[d] *Lomonosov Moscow State University, Moscow, Russia*

Strain displacements of carbon atoms in a C_{60} molecule in the *Pnnm* phase of the RbC_{60} fulleride are first determined by X-ray diffraction. The measurements show that the polymeric bond length between carbon atoms of two nearest molecules C_{60} is equal to 1.69 (1) Å, the rotation angle of the molecule about the polymeric direction is $47.0(3)^0$ [1].

In most fullerene crystals, orientational phase transitions are observed. At high temperatures, C_{60} molecules experience retarded anisotropic rotation and at the phase transition temperature, the rotation ceases and orientational ordering of C_{60} molecules takes place. In AC_{60} fullerides, where A=K, Rb, the appearance of a covalent (polymeric) bonds between nearest C_{60} molecules and strain of C_{60} molecules following the phase transition from the high symmetry phase *Fm3m* to the low symmetry phase *Pnnm* are observed. In papers [2] a phenomenological theory of the structural phase transition in fullerides AC_{60} is constructed and a model of the orientational phase transition together with a method for the description of C_{60} molecule strain are proposed. In this article, the phonon basis suggested in paper [2] for the description of fullerene molecule strain is experimentally verified.

Structural investigations are carried out on the X-ray diffractometer with $CuK_{\alpha 1}$ radiation (λ =1.5406 Å). The spectra are recorded with the step 0.02^0 and with the fixed exposition time 30 sec. Our experimental investigations show that a polycrystalline sample of RbC_{60} contains ~13 % of pristine C_{60} fullerite.

In Fig. 1, the X-ray diffraction spectrum of powder RbC_{60} recorded at ambient temperature is shown. The fitting of the spectrum is made by the Rietveld method using a modernized MRIA program. For the fitting of the diffraction spectrum a number of the models are used.

The results are following. On the basis of the symmetry theory [2] of fullerene molecule strain at the orientational phase transition in AC_{60} crystals it is possible to obtain deformational displacements of carbon atoms in the C_{60} molecule in diffraction experiments (see Fig. 2). Double bond lengths of strained C_{60} molecule range from 1.37 Å to 1.55 Å and single bonds lie in the interval from 1.18 Å to 1.59 Å. The length of a broken double bond in the molecule is 1.55(2) Å and the distance between the carbon atoms of two nearest molecules is equal to 1.69(1) Å.

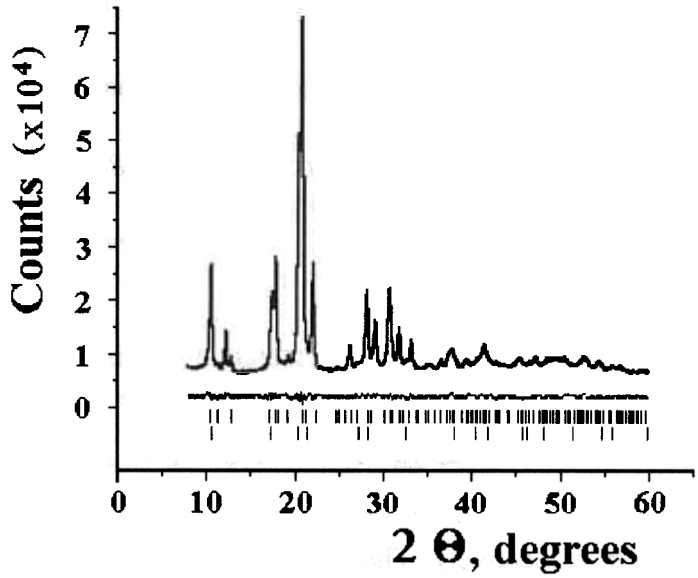

Fig. 1. The X-ray diffraction spectrum of RbC_{60} (and ~13 % of pristine C_{60}) at 300 K.

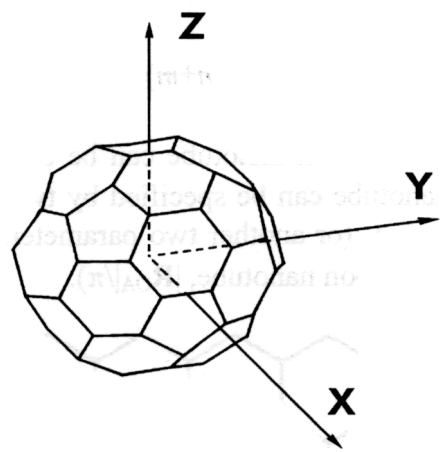

Fig. 2. The strain of C_{60} molecule of RbC_{60} fulleride in the polymer- like *Pnnm* phase.

The reported work has been performed under the auspices of the State Scientific and Technical Program «Fullerenes and Atomic Clusters», N20002.

References

1. Aksenov V.L., Ossipyan Yu.A., Forro L., Khasanov S., Chernyshev V.V., Shakhmatov V.S. Fullerene molecule strain in RbC_{60}, Physics Letters A, 2000, v.268, pp. 395-398.
2. Aksenov V.L., Ossipyan Yu.A., Shakhmatov V.S. *JETP Letters*, **64**, 120 (1996); *JETP*, **86**, 591 (1998).

SYMMETRY GROUPS OF CARBON NANOTUBES

V.L.Aksenov[a], Yu.A.Ossipyan[b] and V.S.Shakhmatov[a]

[a] *Frank Laboratory of Neutron Physics, JINR, 141980 Dubna, Moscow Region, Russia*

[b] *Institute of Solid State Physics RAS, 142094 Chernogolovka, Moscow Region, Russia*

The structure of carbon nanotubes of different types is investigated and the symmetry groups of them are proposed. A carbon nanotube of zigzag type, $(n,0)$, where n- an integer number, has the D^1_{2nh} symmetry group or D^2_{2nh} group for odd or even n, respectively. Tubes of armchair type, (n,n), has also two groups, D^3_{2nh} and D^4_{2nh}, for odd or even n, respectively. The latter groups are isomorphic to previous ones but are different from them by the translation vector along axis of tube. A nanotube of general type (n,m) ($n>m$ and $m\neq 0$) has the symmetry group $D^{n',m'}_N$ if the number $N=2(n^2+m^2+nm)/(n-m)$ is an integer. The basic translation vector in this case is defined by the numbers n' and m' which comply the equation

$$n'(2n+m) + m'(n+2m) = 0.$$

The structure of carbon nanotube can be understood using a plane shown in Fig. 1. The carbon nanotube can be specified by two numbers n and m which define the vector $\mathbf{R}_{OA} = n\mathbf{a}_1 + m\mathbf{a}_2$ (or another two parameters, for example, the chiral angle, ψ, and the diameter of carbon nanotube, $|\mathbf{R}_{OA}|/\pi$).

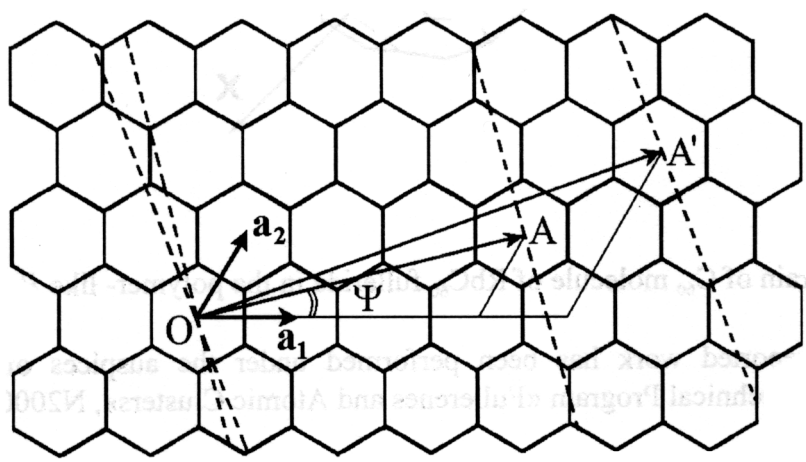

Fig. 1. A two-dimensional graphene sheet for construction of the carbon nanotubes. Carbon atoms are located at each vertex of the honeycomb cell. $\{\mathbf{a}_1,\mathbf{a}_2\}$ are the unit vectors of the hexagonal lattice. $\mathbf{R}_{OA} = 3\mathbf{a}_1 + 1\mathbf{a}_2$ defines the (3,1) nanotube and $\mathbf{R}_{OA'} = 4\mathbf{a}_1 + 2\mathbf{a}_2$ defines the (4,2) nanotube.

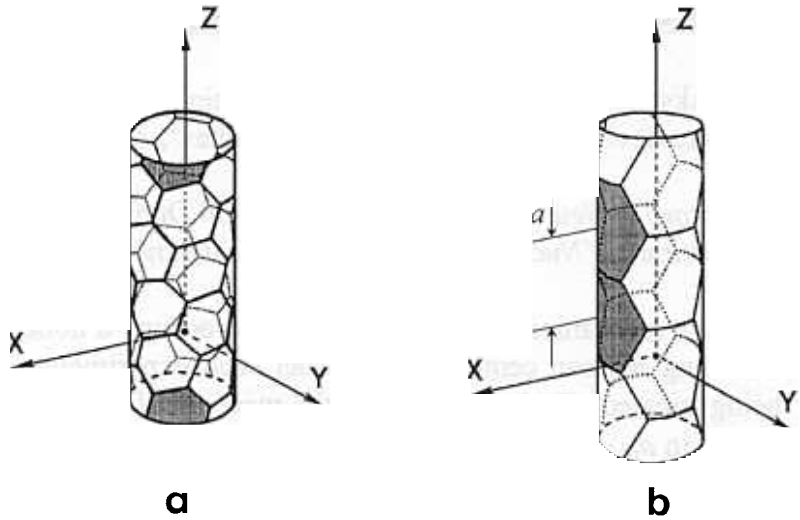

a b

Fig. 2. a). The structure of (4,2) carbon nanotube. b). The structure of (2,2) carbon nanotube. The shaded hexagons are separated by the basic translation vector, **t** ($|\mathbf{t}| = a$), along Z axis.

Two different carbon nanotubes are shown in Fig. 2. The symmetry elements of the (2,2) carbon nanotube are written as [1]

$$\{E, (C_4|\mathbf{t}/2), C_4^2, (C_4^3|\mathbf{t}/2)\}\otimes\{E, U_1, (U_2|\mathbf{t}/2), U_3, (U_4|\mathbf{t}/2)\}\otimes$$

$$\otimes\{E, I\}\otimes\{E, \mathbf{t},..., \mathbf{t}^k,...\},$$

where E is the identical element, $(C_4|\mathbf{t}/2)$, C_4^2 and $(C_4^3|\mathbf{t}/2)$ are the rotations about Z axis at 90^0, 180^0 and 270^0, respectively, $\mathbf{t}/2$ is the accompanied nonprimitive translation, U_1,..., $(U_4|\mathbf{t}/2)$ are the rotations at 180^0 about axes perpendicular Z axis, I is the inversion operation, **t** is the unit translation vector of one-dimensional subgroup of translations, the symbol $\otimes$ denotes direct production of subgroups. The proposed symbol of this group is D_{4h}^4.

For the (4,2) carbon nanotube the symmetry elements are following

$$\{E, (C_{28}|\tau), (C_{28}|\tau)^2,..., (C_{28}|\tau)^{27}\}\otimes\{E, U_1, (U_2|\tau),..., (U_{28}|\tau^{27})\}\otimes$$

$$\otimes\{E, \mathbf{t},..., \mathbf{t}^k,...\},$$

where $\tau = \mathbf{t}\sqrt{\frac{27}{28}}$. The symbol of this group is $D_{28}^{4,-5}$.

The work has been performed under the auspices of the State Scientific and Technical Program «Fullerenes and Atomic Clusters», N20002.

References

1. Aksenov V.L., Ossipyan Yu.A., Shakhmatov V.S. Symmetry groups of carbon nanotubes, Particles and Nuclei, Letters, N1[98]-2000, pp.44-47.

FOURIER STRESS DIFFRACTOMETER (FSD): FIRST RESULTS

G.D.Bokuchava[a], V.L.Aksenov[a], A.M.Balagurov[a], E.S.Kuzmin[a], A.V.Tamonov[a], V.V.Zhuk[a], V.V.Zhuravlev[a], V.A.Trounov[b], V.A.Kudrjashev[b], A.P.Bulkin[b]

[a] *Frank Laboratory of Neutron Physics, JINR, 141980 Dubna, Russia*
[b] *Petersburg Institute of Nuclear Physics, 188350 Gatchina, Russia*

Experiments to study mechanical internal stress start to occupy a noticeable position in the research programs of leading neutron centers. To conduct such experiments, specialized neutron diffractometers are being created. Such devices should meet the following requirements: high luminosity, high resolution in d_{hkl}-spacing, fixed scattering angles $2\theta=\pm 90°$, sufficiently wide range of d_{hkl}, specific sample environment (goniometers, collimators, loading devices, etc.). The experience of application of neutron diffraction to study residual stresses with the HRFD diffractometer in Dubna arouse much interest on the side of science and Russian industry [1, 2]. Therefore, the new project for the creation of a neutron diffractometer dedicated *exclusively* to residual stress studies started on beam №11a of the IBR-2 pulsed reactor in FLNP JINR. Channel 11 of IBR-2 is divided in two neutron beams: beam 11a for the FSD diffractometer and the ISOMER instrument for nuclear physics studies will be installed on beam 11b (fig. 1).

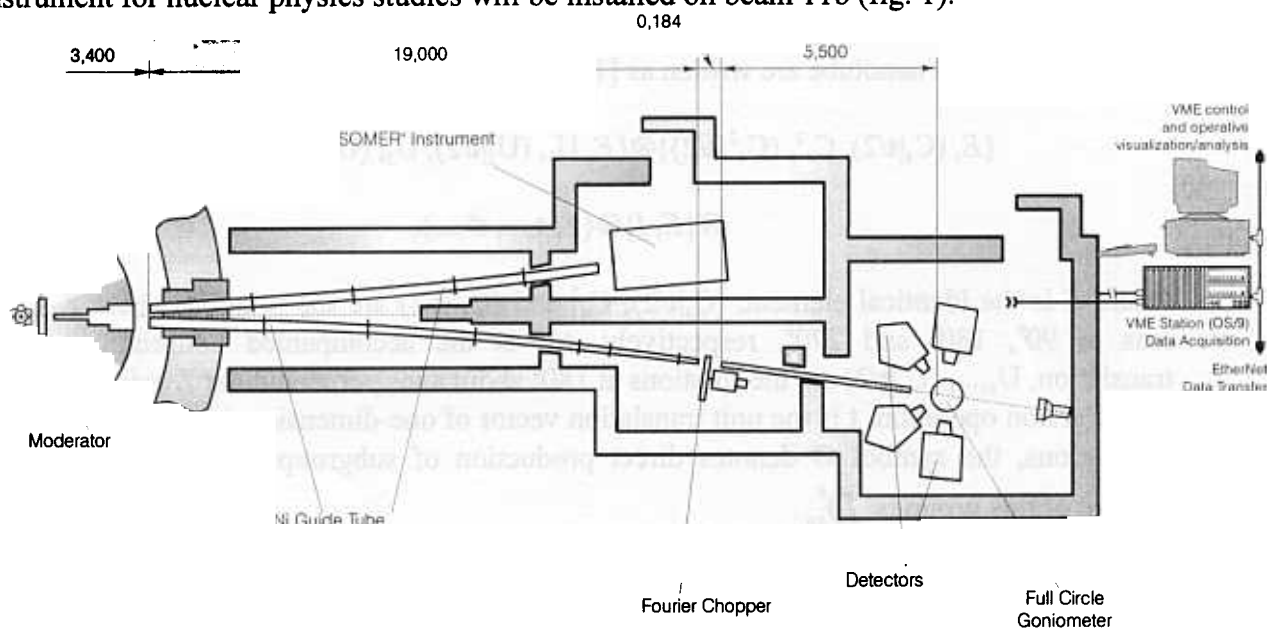

Fig. 1. The layout of the FSD diffractometer at the IBR-2 pulsed reactor.

After installing the mirror neutron guide produced in PNPI (Gatchina) the first test experiments on FSD were carried out in May, 1999: the vertical and horizontal profiles of the direct beam at the mirror neutron guide exit and at the sample site were investigated, the integral neutron flux at Fourier chopper site and at the neutron guide exit were estimated, the first diffraction spectra from standard samples in the low-resolution mode (usual time-of-flight regime without the Fourier chopper) were registered (fig. 2).

In November 1999 the Fourier chopper made in PNPI (Gatchina) was installed in FSD. One of the major parameters of the Fourier diffractometer using the correlation technique is the Fourier chopper contrast factor. With the help of the ^{3}He-detector at the scattering angle $2\theta\approx 90°$ neutron diffraction spectra from the standard sample Al_2O_3 in the low-resolution mode (usual time-of-flight regime) were measured at different positions of the Fourier chopper rotor. The dependence of the (210) diffraction peak integral intensity (d=2.086 Å) versus the rotor position x is shown in fig. 3. The Fourier chopper contrast factor was defined as R=max(I)/min(I) and the effectiveness factor

Q(R)=1-1/R, where I is the diffraction peak integral intensity The Fourier chopper contrast dependence on the wavelength is given in table 1.

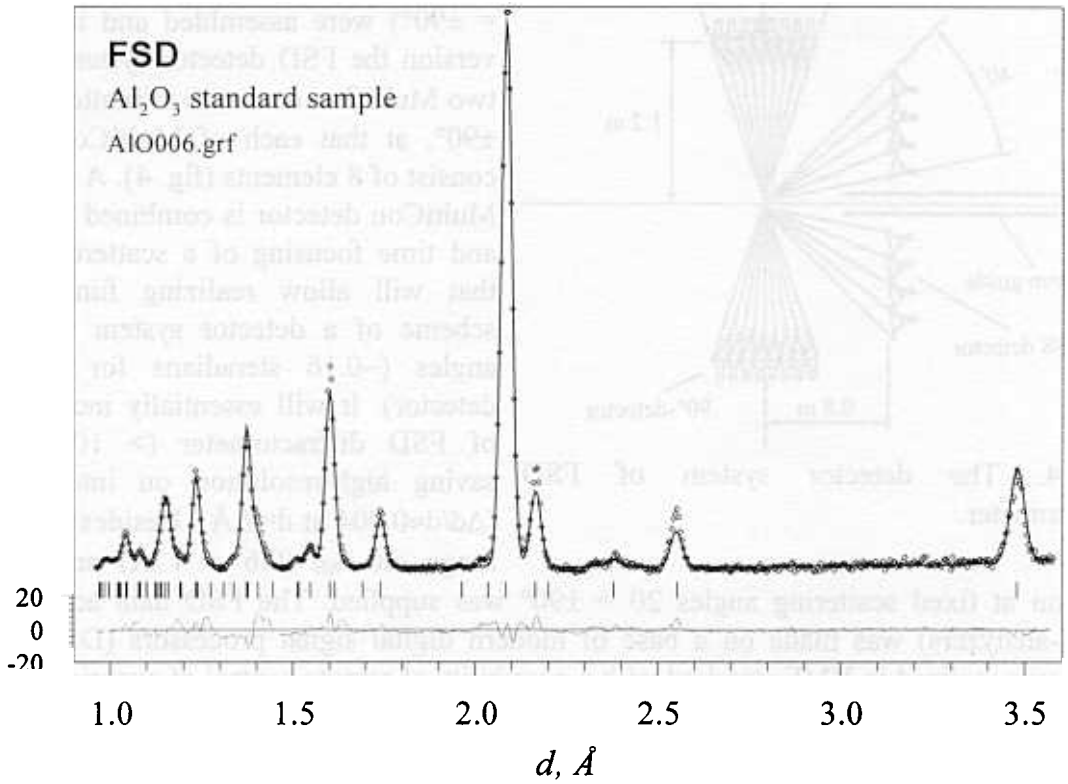

Fig. 2. Part of the neutron diffraction pattern from the Al_2O_3 standard sample measured on FSD in the low-resolution mode (usual time-of-flight regime without the Fourier chopper). The experimental points, the profile calculated by the Rietveld method and the difference curve are shown.

Table 1. The Fourier chopper contrast dependence on the wavelength.

d, Å	λ, Å	R	Q(R)
2.086	2.949	72.352	0.986
1.613	2.281	58.809	0.983
1.392	1.968	51.819	0.981
1.252	1.770	41.067	0.976

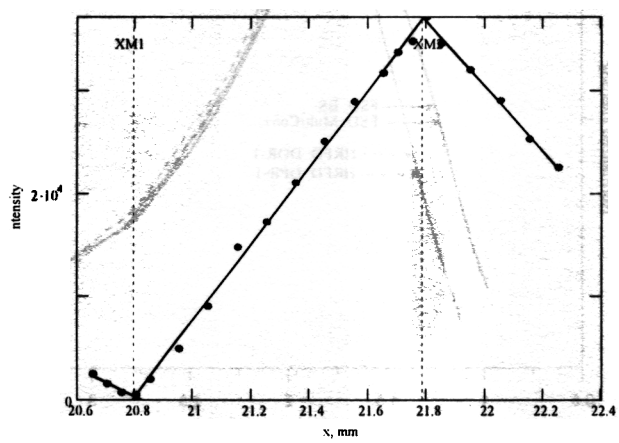

Fig. 3. The dependence of the (210) diffraction peak intensity (d=2.086 Å) versus the rotor position *x*. ^{3}He-detector (2θ≈90°), sample Al_2O_3, T=3 min.

For good Fourier chopper performance contrast value should be R ≥ 20. In our case this value is exceeded in 2-3 times depending on a wavelength. Thus the carried out test measurements have confirmed high contrast of the Fourier chopper, which gives a possibility to obtain a good quality of high-resolution spectra.

After first experiments in low resolution mode backscattering BS- detector (2θ = -141°) composed of 16 ^{6}Li scintillation elements (analogue of DPR-1 detector existing on HRFD) was

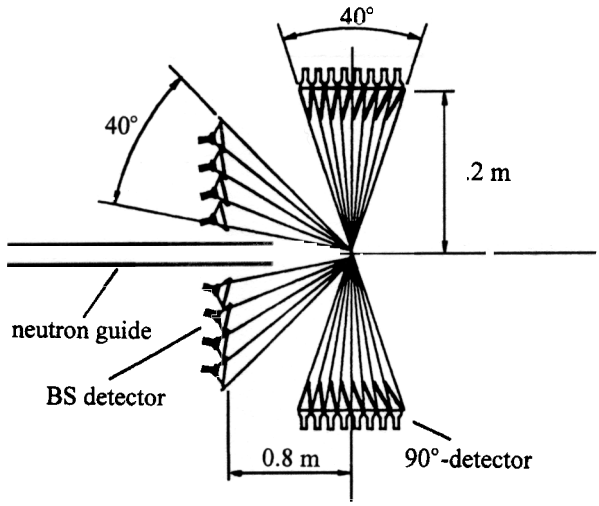

Fig. 4. The detector system of FSD diffractometer.

installed on FSD. Additionally ZnS scintillator based two 1st elements of MultiCon detector (2θ = ±90°) were assembled and installed. In final version the FSD detector system will consist of two MultiCon detectors at scattering angles 2θ = ±90°, at that each of MultiCon detectors will consist of 8 elements (fig. 4). A peculiarity of the MultiCon detector is combined use of electronic and time focusing of a scattered neutron beam that will allow realizing fundamentally new scheme of a detector system with large solid angles (~0.16 steradians for each MultiCon detector). It will essentially increase luminosity of FSD diffractometer (> 10^5 n/cm^2/sec) at saving high-resolution on interplanar spacing ($\Delta d/d \approx 0.004$ at d=2 Å). Besides the wide enough range on d_{hkl} (0.6 ÷ 4 Å) and possibility of operation at fixed scattering angles 2θ = ±90° was supplied. The FSD data acquisition system (RTOF-analyzers) was made on a base of modern digital signal processors (DSP). The control system was realized in VME standard with a possibility of remote control of experiment.

A comparison of neutron intensity spectral distributions for FSD and HRFD diffractometers was made with the help of neutron scattering on standard vanadium sample. On FSD mirror neutron guide has greater radius of curvature in comparison with HRFD diffractometer in order to obtain appropriate neutron spectral distribution. It was found that for FSD neutron intensity spectral distribution is shifted towards shorter wavelengths by $\Delta\lambda \approx 0.2$ Å (fig. 5). This fits well to FSD required characteristics since lattice parameters of most studied materials at FSD are rather small so the available d_{hkl}-range should be shifted to smaller values. Integral neutron flux with Fourier chopper measured at the sample position gives quite high value $F \approx 3\times10^5$ neutr./cm^2/sec. The value of Fourier chopper transmission was found ≈ 1/4.5.

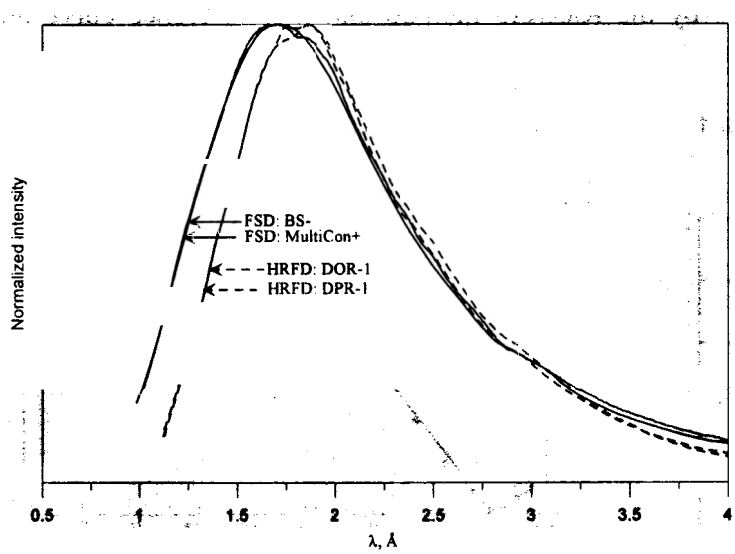

Fig. 5. Comparison of neutron intensity spectral distributions for FSD and HRFD diffractometers. For FSD spectral distribution is shifted by $\Delta\lambda \approx 0.2$ Å towards shorter wavelengths.

The first neutron diffraction patterns from α-Fe standard sample measured on FSD in high-resolution mode by BS- and MultiCon± detectors are shown in fig. 6. After registering first neutron diffraction spectra in high-resolution mode some important experiments were carried out in order to investigate FSD main parameters. Thus FSD resolution function was measured on annealed α-Fe powder by all three detectors at maximal Fourier chopper speed V_{max}=6000 rpm (fig. 7). Results of experiments shown that all detectors have sufficiently high-resolution: $\Delta d/d \approx 2.3\times10^{-3}$ for BS- detector and $\Delta d/d \approx 4\times10^{-3}$ for both 1st elements of MultiCon± detectors at d=2 Å. This outcome confirms fitness of FSD diffractometer for residual stress studies with required accuracy.

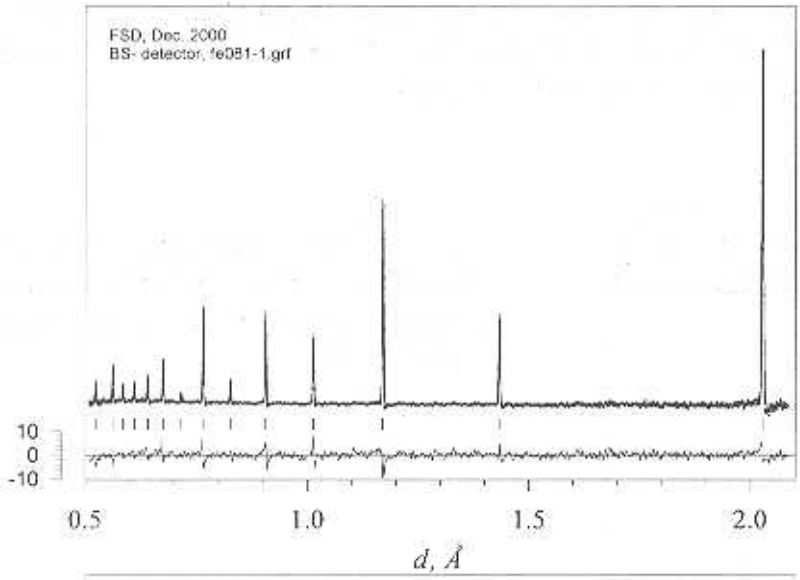

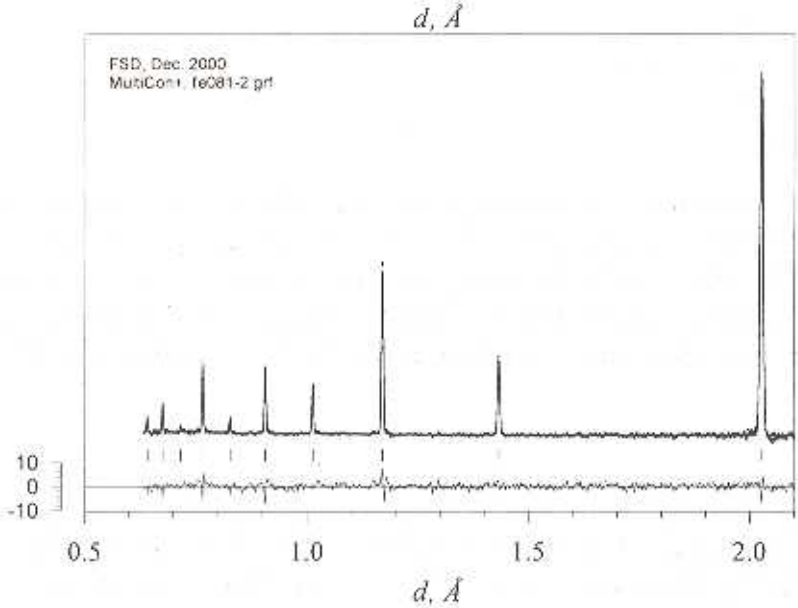

Fig. 6. Part of the neutron diffraction pattern from the α-Fe standard sample measured on FSD in the high-resolution mode by BS- (top) and MultiCon+ (bottom) detectors. The experimental points, the profile calculated by the Rietveld method and the difference curve are shown.

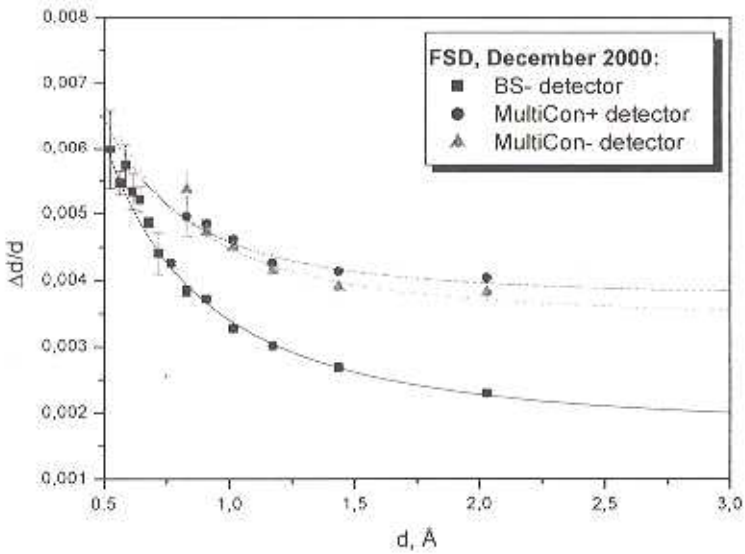

Fig. 7. FSD resolution function measured on the α-Fe powder at maximal Fourier chopper speed V_{max}=6000 rpm.

One of the peculiarities of RTOF technique is diffraction peak width (fig. 8) dependence versus maximal Fourier chopper speed. This feature gives possibility to vary a necessary resolution and luminosity of diffractometer depending on problem to be solved.

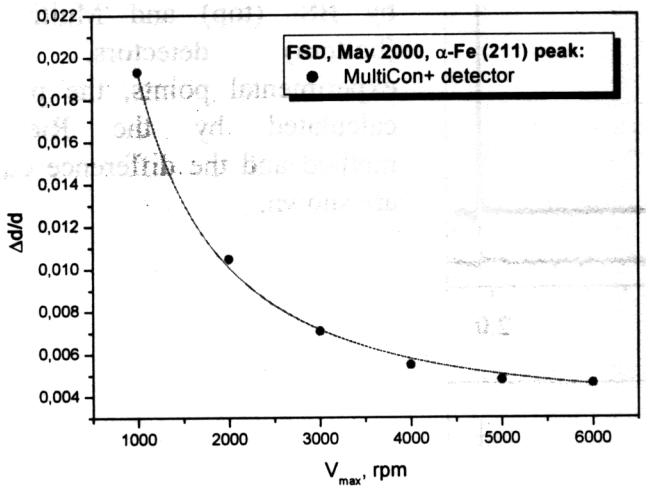

Fig. 8. FSD resolution function dependence versus maximal Fourier chopper speed (α-Fe, peak (211), d=1.1711 Å).

Thus the first stage of FSD construction was completed successfully, that enables to continue work on the further diffractometer development. Currently the designing work on the sample environment (goniometers, collimators, loading devices, furnaces, etc.) and precise sample positioning system is in progress. The existing devices will be adapted to fit the FSD diffractometer. Further work on manufacturing the rest working counters of large area MultiCon detector now is conducted.

REFERENCES

[1] V.L. Aksenov, A.M. Balagurov, V.G. Simkin et al., *J. Neutron Research*, v. 5, p. 181, (1997).

[2] V.L.Aksenov, A.M.Balagurov, G.D.Bokuchava et al., Proc. of National Conference on Application of X-rays, Synchrotron Radiation, Neutrons and Electrons for Material Studies, May 25-29, 1997, Dubna, Russia, vol. 1, pp.69-74 (in Russian).

EFFECT OF ANISOTROPIC THERMAL EXPANSION ON THE PHYSICAL WEATHERING OF MARBLES

K. Ullemeyer[a,b], S. Siegesmund[c], T. Weiss[c] and E.K. Tschegg[d]

[a]*Frank Laboratory of Neutron Physics at JINR, 141980 Dubna, Russia*
[b]*Geological Institute, University of Freiburg, D-79104 Freiburg, Germany*
[c]*Institute of Geology and Dynamics of the Lithosphere, University of Göttingen, D-37077 Göttingen, Germany*
[d]*Institut für Angewandte und Technische Physik, TU Wien, A-1040 Wien, Austria*

Introduction

Marbles as building stones often show complex weathering phenomena, which can be of enormous economic importance (see Fig. 1). In addition to the influence of climate and chemical substances (acid rain, biofilms), the highly anisotropic thermal expansion coefficient of calcite and dolomite and therefore their textures have significant influence on mechanical weathering [1]. Marbles with distinctively different fabrics were selected to investigate the relationship between the anisotropy of the thermal expansion α and the residual dilatation behaviour after heating and cooling. In order to understand and to quantify these effects, rock fabric studies were carried out. Based on the calcite and dolomite textures, the directional dependence of thermal dilatation was modeled and compared with the experimental data to identify constraints on the observed weathering phenomena.

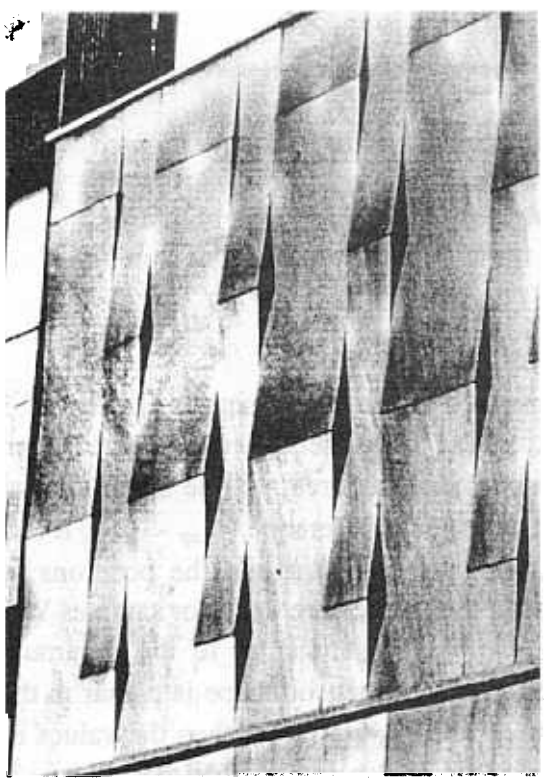

Fig. 1. The deformed facade cladding of the Finlandia Hall at Helsinki, made of Carrara marble.

Experimental Results

The *textures* - which can be sufficiently described by the c-axes pole figures - show variations between axial symmetric and girdle-like intensity distributions (see Fig. 2). The shape parameter T calculated from the pole figure tensor describes the texture differences quite well. It covers the range from $T = -0.824$ (sample WU5) to $T = 0.485$ (sample CA, see Fig. 2) indicating a well pronounced cluster-like and a moderate girdle-like intensity distribution as extreme cases. Because of the strong preferred orientations it must be assumed that the behaviour of the samples is anisotropic with respect to thermal dilatation - even highly anisotropic in some cases.

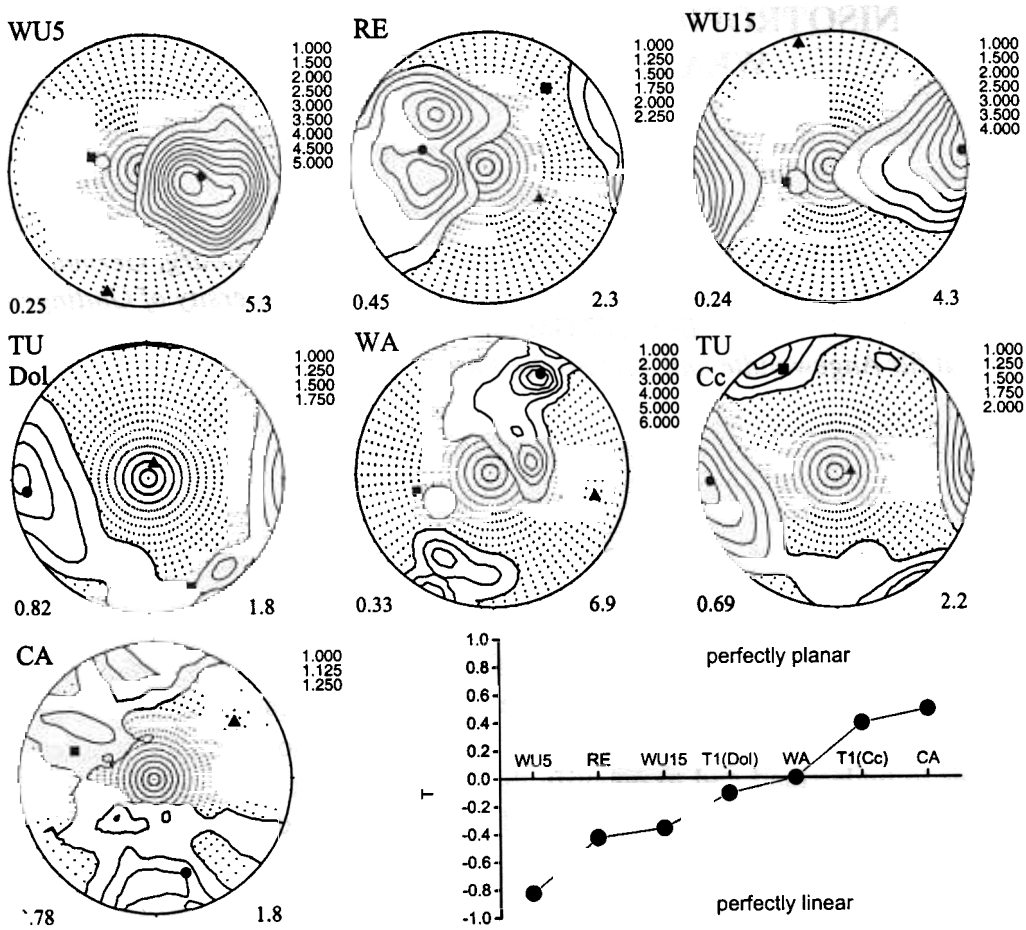

$$T = \left(\ln\frac{e_{int}}{e_{min}} - \ln\frac{e_{max}}{e_{int}}\right) \Big/ \left(\ln\frac{e_{int}}{e_{min}} + \ln\frac{e_{max}}{e_{int}}\right) \quad (e\text{: eigenvalues of the pole figure tensor})$$

Fig. 2. The c-axes [006] preferred orientations of the samples investigated (calculated from the ODF). Dots, squares and triangles refer to the maximum, intermediate and minimum principal directions of the pole figure tensor, respectively. The graph at the bottom gives the trend of the parameter T which characterizes the shape of the pole figure tensor.

Thermal expansion measurements were performed using a triple dilatometer [2]. Figure 3 illustrates the directional dependence of the thermal expansion coefficient α (i) obtained from thermal expansion experiments, α_{exp} (ii) modeled from the mineral textures and the single crystal constants applying the VOIGT model [3], α_{mod} (iii) as well as of their difference, α_{exp} - α_{mod}. It is a common observation that the patterns of α_{exp} and α_{mod} look quite similar and the positions of maximum and minimum agree more or less. Most pronounced differences are valid for samples WA and WU 15: the maximum of α_{exp} is elongated along a girdle perpendicular to the minimum whereas the plots of α_{mod} show such a trend for the minimum, *i.e.* the tensor shape is planar in the first case and linear in the second one. In all cases, the values of α_{exp} are larger than the values of α_{mod}, *i.e.* the difference is non-zero and is usually quite large. It is also remarkable that the α_{exp} - α_{mod} - distribution is anisotropic as well, and the patterns look different compared to the experimental and modeled ones. The latter observation is well illustrated by the positions of the maxima, see Fig. 3.

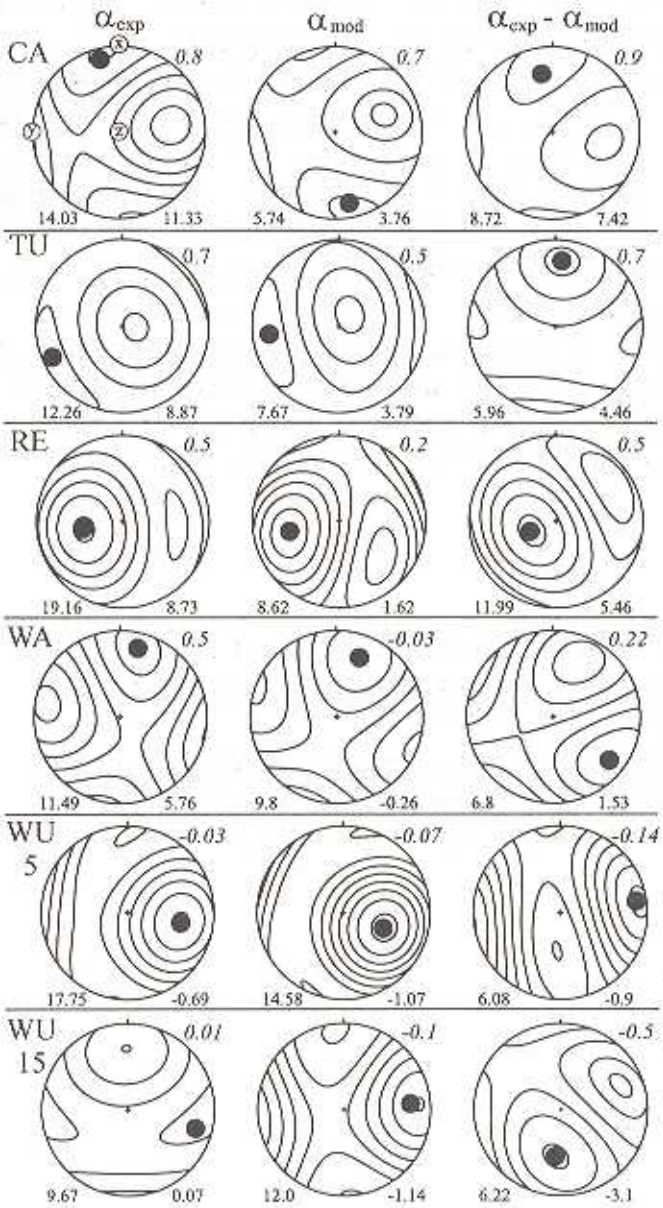

Fig. 3. The directional dependence of the thermal expansion coefficient α: experimentally determind (α_{exp}) and modeled from the textures (α_{mod}). The units are 10^{-6} K^{-1}. The minimum and maximum values are given at the bottom of the plot, as well as the anisotropy parameter $A_\tau = \alpha_{min}/\alpha_{max}$. The dot indicates the position of the maximum. The right column contains the difference $\alpha_{exp} - \alpha_{mod}$.

Discussion and conclusions

Judging the textures and the pronounced anisotropy of the thermal expansion coefficient α, the following conclusions can be evaluated: (i) for cluster-like c-axis distributions, the maximal thermal expansion can be observed in a single sample direction whereas the intermediate and minimum directions are connected by a girdle. Hence, measuring the thermal expansion in an arbitrary sample direction without knowledge of the texture, the probability to measure smaller values than the mean value is large because the cluster covers only a small area on the pole sphere. (ii) for girdle-like c-axis distributions the minimal thermal expansion is observed in a single sample direction and the intermediate and maximum directions are connected by a girdle. In this case, the probability to measure larger values than the mean value is large because the area of minimal values on the pole sphere is quite small. It is obvious, that large errors may arise in dependence on the type and strength of the texture, if the thermal expansion is estimated only in a single sample direction. Consequently, knowledge of the texture is obligatory for the proper determination of the dilatation behaviour of bulk rock.

The differences between the experimentally determined and modeled thermal expansion coefficients (α_{exp} - α_{mod}) are essentially addressed to the occurrence of microcracks. Microcracks usually originate in the late stage of tectonic history during uplift (stress-induced cracking) or in the late stage of cooling (thermal cracking). They are common in crystalline rocks. New cracks may be generated due to recent thermal treatment, *e.g.* alternating heating/cooling. It is assumed that the formation of new microcracks influences the thermal dilatation anisotropy much stronger than preexisting microcracks, and that microcrack formation is largely controlled by the texture. Evidence to support the conclusion comes from the observation that the topology of the α_{exp} - α_{mod} stereogram (Fig. 3) is clearly associated with the texture. This is true even for the sample with the lowest anisotropy of thermal dilatation, CA. If this relationship between texture and microcrack formation can be confirmed experimentally, it is also confirmed that the influence of the texture on the bulk rock thermal expansion anisotropy is double: (i) direct influence, which at least is based on the single crystal anisotropy (ii) indirect influence due to control of microcrack formation.

References

1. S. Siegesmund, A. Vollbrecht, K. Ullemeyer, T. Weiss, R. Sobott. Application of geological fabric analysis to characterize natural building stones - case study: Kauffung marble, Int. J. for Restoration of Buildings and Monuments, 1997, v.3, pp.269-292.
2. C. Widhalm, E. Tschegg, W. Eppensteiner. Anisotropic thermal expansion causes deformation of marble cladding, J. of Performance of Constructed Facilities ASCE, 1997, v10, pp.5-10.
3. H.J. Bunge, *Texture Analysis in Materials Sciences*, 1982, Butterworth, London.

INFLUENCE OF PARTICLE CONCENTRATION ON FERROFLUIDS MICROSTRUCTURE STUDIED BY SANS

M.V.Avdeev[a], Maria Balasoiu[a*], Doina Bica[b], L.Rosta[c], G.Torok[c], L.Vekas[b]

[a] *FLNPh, JINR, 114980, Dubna, Russia (*permanent address: ISS, Bucharest, R-76900, Romania)*

[b] *Laboratory of magnetic fluids, CFATR, Timisoara Branch of the Romanian Academy, Romania*

[c] *KFKI, H-1525, Budapest, Hungary*

Ferrofluids are dispersions of small, single-domain magnetic particles suspended in a fluid carrier (Fig.1). Aggregation through Van der Waals and magnetic forces is prevented by coating the particles with a surfactant layer. It is known that the stability and properties of magnetic colloidal solutions are considerably due to the degree of surfactant adsorption at the ferrophase surface. The micro-behavior of the surfactant molecules adsorbed at the surface of the particles is not yet completely understood. The data available in the literature [2-3] are insufficient to determine the features of the surfactant behavior under different conditions.

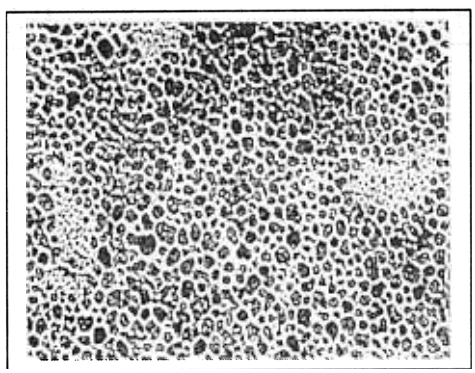

Fig.1 Electron microscopy image of a ferrofluid sample

The purpose of this work is to investigate the changes of the surfactant layer structure due to the variation of the colloid particles concentration by the SANS method . As is well known small angle neutron scattering (SANS) is an ideal method for investigating the structure of particles of about 1-100nm.

We have investigated a deuterated benzene ferrofluid sample of 19% particle volume fraction, with oleic acid as surfactant, prepared by the method of chemical condensation at the Institute of Complex Fluids Timisoara, Romania. The size distribution of magnetite particles analyzed by EM was determined to have a lognormal form with the mean diameter of about 100Å. By dilution with measured quantities of D-benzene were obtained the following volume fractions: 9.5%; 6.3%; 3.8%; 1.1%.

The SANS measurements were performed in the Q-range of $0.01944\ Å^{-1} \leq Q \leq 0.2778\ Å^{-1}$ with the SANS facility in function at the VVR-SM, KFKI-Budapest [4]. SANS experiment measures the coherent differential scattering cross section $d\Sigma(Q)/d\Omega$ as a function of the scattering vector $Q = (4\pi/\lambda)\sin\theta/2$, where λ is the neutron wavelength and θ is the scattering angle.

The experimental curves $d\Sigma(Q)/d\Omega$ versus Q, plotted on the logarithmic scale for each value of the particle volume concentration (Fig.2) were fitted with the theoretical expression of scattering from spherical particle with two components:

$$d\Sigma(Q)/d\Omega = \{d\Sigma(0)/d\Omega[\int(V_0+\eta V_1)^2 \quad D_N(R_0)dR_0]^{-1}\} \int[V_0\Phi(QR_0)+\eta V_1\Phi(Q(R+h))]^2 D_N(R_0)dR_0 + B, \quad (1)$$

where $d\Sigma(0)/d\Omega$ - is the scattering cross section at $Q = 0$; ρ_0, ρ_1, ρ_s - scattering density of the particle, of the surfactant and of the solution; $\eta = (\rho_1-\rho_s)/(\rho_0-\rho_1)$; $V_i = (4/3)\pi R_i^3$; $\Phi = (3\sin x - x\cos x)/x^3$; h - thickness of the surfactant layer, $h = R_1-R_0$; $D_N(R_0)$ - log-normal size distribution; σ - dispersion; B - the contribution of the incoherent and magnetic scattering.

Choosing the best fit of the experimental data for each particle concentration by the variation method of six parameters (R_0, δ, η, h, I(0), B) in the expression (1) we have obtained the following results (Tab.1):

Tab.1[6]

ϕ	R_0	σ	η	$d\Sigma(0)/d\Omega$	h	B
19%	40.9282	16.1338	-0.79477	59.8176	9.98534	0.06016
9.5%	40.6504	15.5454	-0.80239	46.712	11.4928	0.05011
6.3%	40.5262	15.6075	-0.80889	34.3885	12.368	0.03430
3.8%	41.4544	16.5211	-0.81581	19.1907	14.937	0.021426
1.1%	41.3777	17.6357	-0.80957	3.94212	17.8403	0.009456

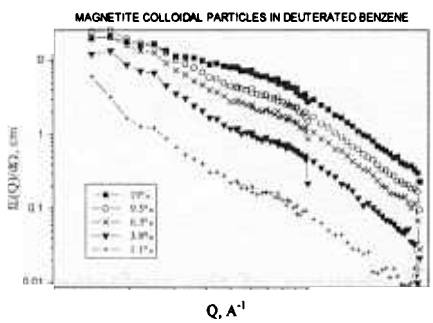

Fig.2 Experimental curves for C_6D_6 ferrofluid samples.

As we expected the values $d\Sigma(0)/d\Omega$ decrease with the lowering of the particle concentration (Fig.3). It is interesting to notice that h, the thickness of surfactant shell is increasing with the decrease of the particle concentration (Fig.5), the same time η, the degree of the solvent penetration in the surfactant shell is constant. Our results [6] referring to the lowering of the surfactant shell thickness are in agreement with those obtained by viscosity measurements at the Institute of Complex Fluids, Timisoara [7].
The variation of the surfactant shell thickness with particle concentration fits with the following exponential decay (see Fig.4):

$$h(\phi) = h_0 + 8.21\, e^{-(\phi-\phi_0)/t_1}$$

where t_1 is a constant .

As first explanation of the fact that h and R_g , the thickness of surfactant shell and radius of gyration, are changing with particle concentration it was presumed that with the

increasing of particle concentration the particles come closer and the "elastic" surfactant layer suffers effects as the partial bending of the oleic acid molecules' tails of the surfactant adsorbed on the same particle, and the interpenetration of surfactant chains.

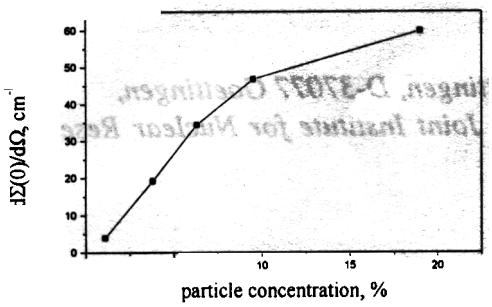

Fig.3 Variation of $d\Sigma(0)/d\Omega$ with the particle concentration.

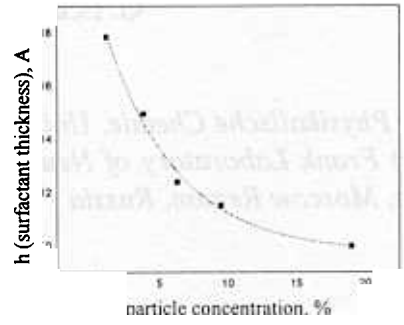

Fig.4 Variation of h, thickness of surfactant shell with particle concentration, ϕ.

To come to final conclusion it will be necessary further to analyze the experimental data taking into account the magnetic scattering, too.

References

[1] S.W.Charles and J.Popplewell, IEEE Trans on Magn., Vol. Mag-16, (1980) 172.
[2] P.C.Scholten, J.Magn.Magn.Mater.39(1983) 99.
[3] R.V.Mehta, P.S.Goyal, B.A.Dasannacharya, R.V.Upadhyay, V.K.Aswal, G.M.Sutariya., J.Magn.Magn.Mater.149 (1995) 47.
[4] M.Balasoiu, S.Borbely, D.Bica, G.Torok, L.Vekas, Experimental Report BNC, 1997.
[5] M.V.Avdeev, M.Balasoiu, D.Bica, S.Borbely, L.Rosta, G.Torok, L.Vekas, 8-th International Conference on Magnetic Liquids, 31 Juin-3 July, Timisoara, Book of Abstracts, 215-216(1998)
[6] M.Balasoiu, Thesis, *On the ferrofluids microstructure*, Bucharest, 1998.
[7] L.Vekas, D.Bica, D.Gheorghe, I.Potencz, M.Rasa, JMMM 201(1999) 159-162.

SMALL-ANGLE NEUTRON SCATTERING FROM TETRADECYLTRIMETHYLAMMONIUM BROMIDE IN NaBr AQUEOUS SOLUTIONS

G. Eckold * and N. Gorski */*

*) *Institut fuer Physikalische Chemie, Universitaet Goettingen, D-37077 Goettingen, Germany,* **) *Frank Laboratory of Neutron Physics, Joint Institute for Nuclear Research JINR, 141980 Dubna, Moscow Region, Russia*

Small angle neutron scattering (SANS) was used to characterize quantitatively the micelles of tetradecyltrimethylammonium bromide (TTABr) at a concentration of about 50 mM in aqueous (D_2O) solutions with added salt NaBr. It is shown that the shape of the micelles change from spheres to rod-like particles with increasing electrolyte concentration. The interparticle interaction becomes effectively screened if the salt concentration exceeds 0.1 M leading to a remarkable growth of the cylindrical micelles. Moreover, it is demonstrated that there is a gradual dehydration of the micelles due to the addition of NaBr.

SANS experiments were performed on the time–of–flight instrument MURN at the pulsed reactor IBR-2, JINR, Dubna, Russia. Using neutrons with wavelengths λ between 0.7 and 10 Å the accessible range of momentum transfer $Q=(4\pi/\lambda)\sin(\theta/2)$ extends from 0.009 to 0.25 $Å^{-1}$. The samples were contained in quartz glass cells (Hellma) with a path length of 1 mm. The temperature of the cells was kept constant at 20.0±0.1 °C by means of a thermostat. Conversion of the scattering intensities into absolute differential cross-sections was done by using vanadium as an internal calibration standard. Background scattering was subtracted by comparison with a reference sample of pure D_2O. The data treatment was done according to the standard procedures.

In Fig.1 the observed intensity distributions are shown for a number of TTABr-solutions with different NaBr-contents from 0.020 to 0.447 M along with the corresponding data for the pure TTABr-solution.

The intensity profile for the pure TTABr solution exhibits a well defined peak at $Q\approx0.046$ $Å^{-1}$. This peak is due the inter-particle structure factor S(Q) and indicates the presence of strong electrostatic interaction between TTABr micelles.

The average distance d between the micelles may be estimated from the position Q_{max} of this correlation peak according to $d=2\pi/Q_{max}=136.5$ Å. The number density n of the micelles is then calculated as $n=1/d^3=3.93\cdot10^{17}$ cm^{-3}. From the total TTABr-concentration C = 52.6 mM and the volume of a single surfactant molecule V=550 $Å^3$ we obtain the aggregation number $N=CN_A/n=80.7$ and the micelle volume $V_m=44400$ $Å^3$. Using the fact, that in a pure solution, free of NaBr, the TTABr-micelles are of spherical shape, their radius turns out to be $R \approx 22$ Å in good agreement with the SANS-results of variuos authors [1-4].

As can readily be seen from Fig.1, the addition of NaBr dramatically alters the intensity profile. The correlation peak at $Q_{max}=0.046$ $Å^{-1}$ is gradually reduced as the amount of salt is increased. At a NaBr-concentration of 0.098 M this peak has in fact completely disappeared. This finding is due to the fact that by addition of electrolyte (NaBr) the intermicellar electrostatic interactions are screened substantially and the structure factor is reduced to unity.

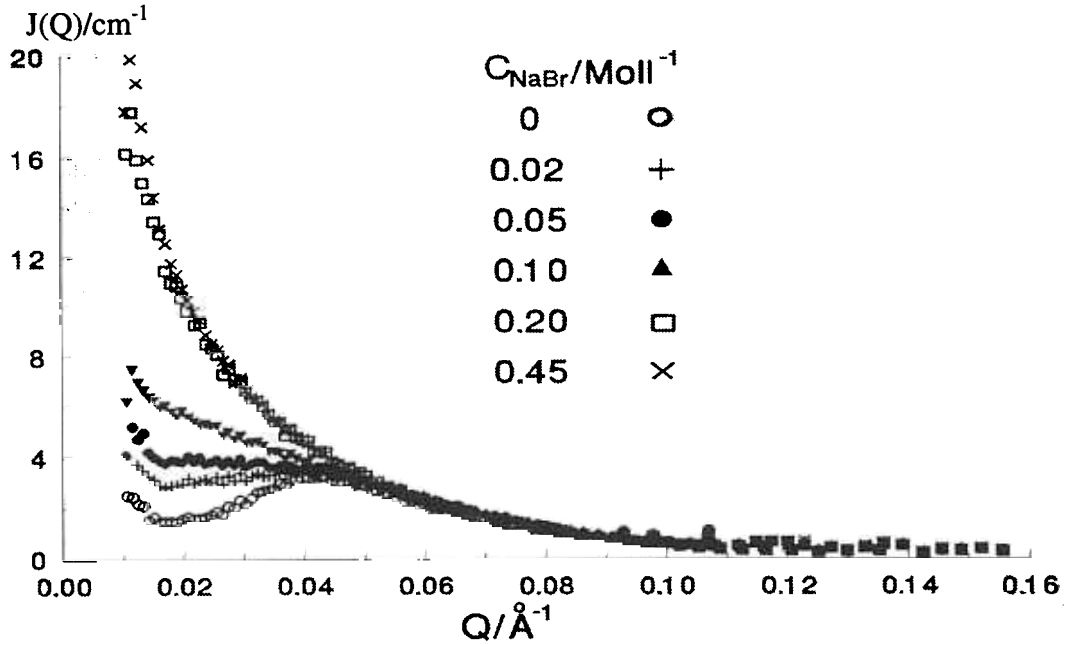

Fig. 1 Neutron scattering intensity profiles J(Q) vs. Q from D_2O solutions containing ≈50 mM TTABr with different NaBr concentrations

The radii of gyration R_g and R_c, the geometrical dimensions of the cylinder, R and L, and the aggregation number per unit micellar length, N/L, are determined according to eqations

$$\frac{d\ln(J(Q))}{dQ^2} = -\frac{R_g^2}{3} \quad (1), \qquad \frac{d\ln(J(Q)\cdot Q)}{dQ^2} = -\frac{R_c^2}{2} \quad (2), \qquad R_c = \frac{R}{\sqrt{2}} \quad (3),$$

$$R_g = \sqrt{\frac{R^2}{2} + \frac{L^2}{12}} \quad (4), \qquad \lim_{Q\to 0}(J(Q)\cdot Q) = \pi\cdot(\rho-\rho_s)^2\cdot C\cdot N_A\cdot\frac{N}{L}\cdot V^2 \quad (5)$$

for the different electrolyte concentrations. These data are collected in table 1.

Table 1: Characteristics of TTABr Micelles in Aqueous (D_2O) NaBr Solutions at 20 °C

C_{TTABr} - the surfactant concentration (mM), NaBr – the salt concentration (M),
R_g – the radius of gyration of the whole micelle, R_C – the radius of gyration of the cross sectional area of micelle, R – the radius of the cylindrical micelle, L – the length of the micelle, N/L – the aggregation number per unit micellar length.

C_{TTABr} (mM)	NaBr (M)	R_g (Å)	R_c (Å)	R (Å)	L (Å)	N/L ($Å^{-1}$)
52.4	0.020	25.5±0.4	15.4±0.5	21.8±0.7	70.7±3.0	1.77±0.08
52.0	0.0496	25.7±0.3	16.0±0.2	22.6±0.3	69.8±1.9	1.89±0.04
51.4	0.098	28.5±0.4	16.2±0.2	22.9±0.3	81.1±2.2	1.83±0.03
50,1	0.191	78.9±5.7	17.0±0.1	24.0±0.2	267±20	1.98±0.02
46.8	0.447	112.5±10.6	17.6±0.1	24.9±0.2	384±37	2.15±0.02

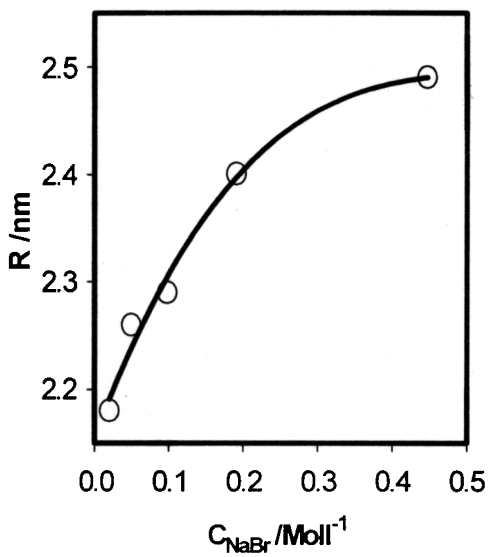

Interestingly, these radii increase with NaBr content from 21.8 ± 0.7 Å at 0.020 M to 24.9 ± 0.2 Å at 0.447 M as shown in Fig.2.
The apparent increase of the radii as determined from the SANS experiments is thus easily be explained by the (partial) dehydration of the hydrophilic head groups. The radius R_o of the bare micelles, however, does not change and is about
25 Å.

Fig.2: Variation of the apparent radius R of the cylindrical micelles vs. C_{NaBr}

The SANS investigations on the system TTABr+D_2O+NaBr at 20 °C and a surfactant concentration of about 50 mM reveal that the micelles exhibit a rod-like shape. As long as the salt concentrations do not exceed 0.1 M the lengths of the micelles are close to 70 – 80 Å and correlation effects due to the interparticle interaction are observed. At higher NaBr content long cylindrical objects are formed, characterized by radii of about 25 Å and lengths of several hundred Å. The apparent increase of surfactant volume with NaBr-concentration from about 415 Å^3 to 550 Å^3 indicates a (partial) dehydration of the -$N(CH_3)_3Br$ head-groups due to the presence of the electrolyte.
For the first time, the gradual stripping of the micelles from its surrounding solvent molecules by the addition of electrolytes could directly be observed. As already suspected by different authors, SANS experiments on D_2O-solutions with no or only minor salt content are likely to yield the properties of the hydrocarbon core of the micelle merely, rather than that of the whole object.

References

[1] Debye P. Ann. N. Y. Acad. Sci. **51** (1949) 575
[2] Zana R., Picot C., Duplessix R. J. Colloid Interface Sci. **93** (1983) 43
[3] Tabony J. Mol. Phys. **51** (1984) 975
[4] Gorski N., Gradzielski M., Hoffmann H. Langmuir **10** (1994) 2594

This work was supported by the Federal Ministry of Education and Science (BMBF) of the Federal Republic of Germany under grant No. 03-DU0GO4-6.

STRUCTURAL CHARACTERIZATION OF UNILAMELLAR LIPID VESICLES WITH ANCHORED ALKYLGLYCOSIDES AT HIGH WATER EXCESS FOR STUDYING CELL RECOGNITION PROCESSES

P. Jörchel[1], J. Gorshkova[2], G. Klose[1], H. Schmiedel[1]

1 Institute of Experimental Physics I, University of Leipzig, Linné-Str. 5, 04103 Leipzig, Germany

2 FLNP, Joint Institute of Nuclear Research, Dubna 141980, Russia

Glycosides play an important role for structural modification of membranes in the process of cell recognition. In extension to our experiments from April this year [1] (system POPC[1]/$C_{12}(EO)_3Glu$[2]) and former experiments [2 - 3] (POPC/$C_{12}E_4$[3]) now we carried out neutron scattering experiments with POPC vesicle membranes containing $C_{12}(EO)_3Glu$, $C_{14}(EO)_3Glu$[4], and $C_{16}(EO)_3Glu$[5], respectively.

The glycoside $C_{12}(EO)_3Glu$ can be considered as a derivative of $C_{12}E_4$ with higher steric requirements (see Fig.1). Furthermore, $C_{14}(EO)_3Glu$ and $C_{16}(EO)_3Glu$ are derived from $C_{12}(EO)_3Glu$ by lengthening the alkyl chain (see Fig.1).

Our attention is directed to the following three points:

- the influence of the exchange of one oxyethylen group by the glucopyranosyl fragment
- the influence of the alkyl chain length
- the influence of the molar ratio POPC/oxyethylen monoalkylether

on the structure of the vesicle membranes (thicknesses of the waterfree core and the water containing headgroup region, the number of water molecules fixed per amphiphile molecule, respectively).

We measured the scattering curves of the samples listed in table I. For measurement vesicles were prepared by extrusion with polycarbonate filters (pore diameter = 200 nm) 25 times, respectively. All measurements were carried out at room temperature (25 °C). The sample thickness was 2 mm in all cases. The measurements covered a q-range from 0.0864 nm^{-1} to 5.92 nm^{-1}.

---

[1] 1-Palmitoyl-2-oleoyl-sn-glycero-3-phosphocholine

[2] Glucopyranosyl-trioxyethylen-mono-dodecylether

[3] Tetra-oxyethylen-mono-dodecylether

[4] Glucopyranosyl-trioxyethylen-mono-tetradecylether

[5] Glucopyranosyl-trioxyethylen-mono-hexadecylether

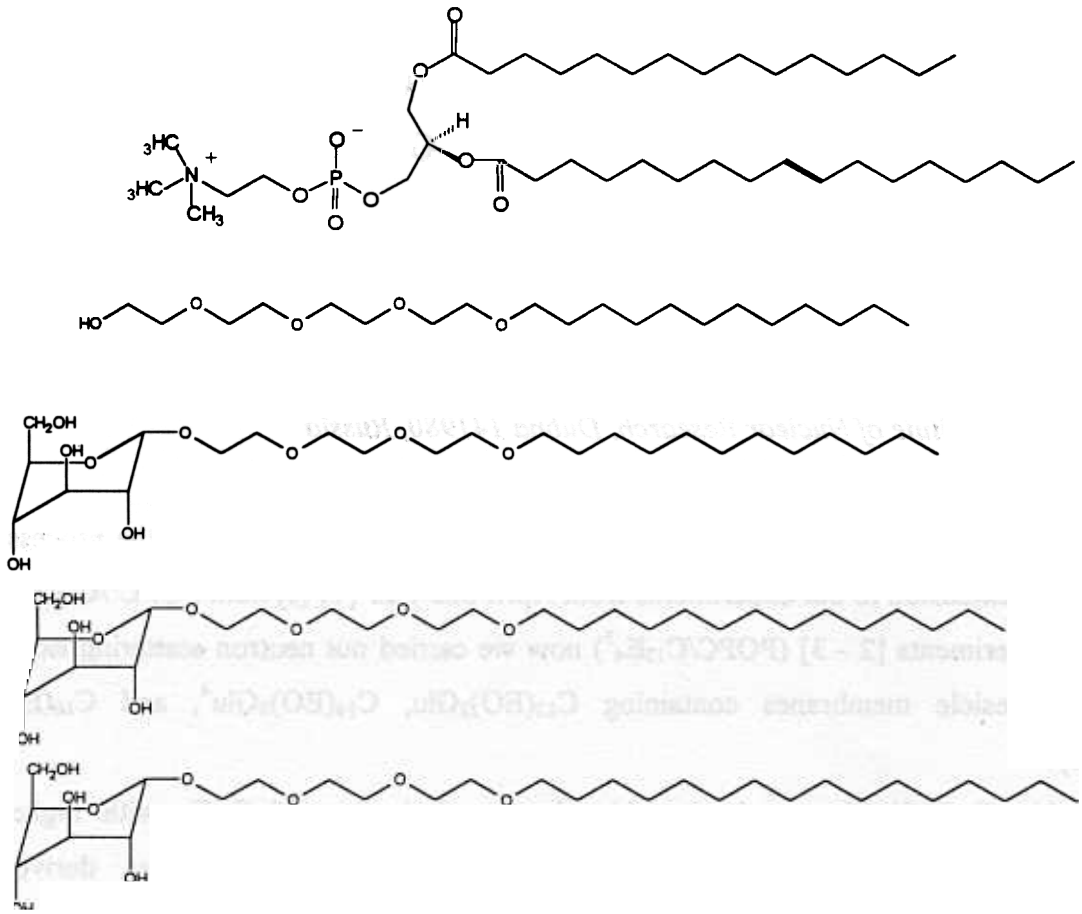

Figure 1: structural comparison of the components of the considered systems, POPC, $C_{12}E_4$, $C_{12}(EO)_3Glu$, $C_{14}(EO)_3Glu$, $C_{16}(EO)_3Glu$ (in the listed order)

Table I: measured samples (S ... $C_{12}E_4$ or $C_n(EO)_3Glu$, respectively)

Sample No.	content	$x_S = n_S/(n_S+n_{POPC})$	c(amphiphil) in mg/ml	t in minutes
1	POPC + $C_{12}(EO)_3Glu$ in D_2O	0.25	10	360
2	POPC + $C_{12}(EO)_3Glu$ in D_2O	0.50	10	360
3	POPC + $C_{14}(EO)_3Glu$ in D_2O	0.25	10	360
4	POPC + $C_{14}(EO)_3Glu$ in D_2O	0.50	10	360
5	POPC + $C_{16}(EO)_3Glu$ in D_2O	0.25	10	360
6	POPC + $C_{16}(EO)_3Glu$ in D_2O	0.50	10	360

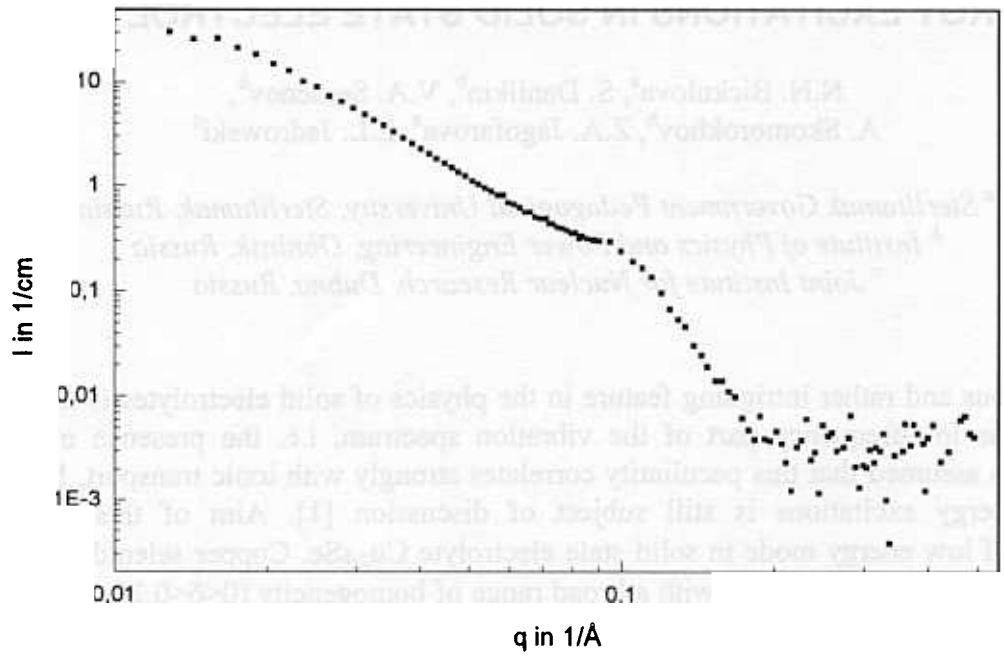

Figure 2: scattering curve of POPC/$C_{14}(EO)_3$Glu (x_S = 0.5)

The data of all samples shows a diffraction shoulder at 1 nm^{-1} which is caused by the presence of a small amount oligolamellar liposomes with a repeat distance of about 6.3 nm. There are small differnces in the shape of the scattering curves. A further and more elaborated data analysis will provide structural details about the inner structure of the membranes (see above: thicknesses of different region water content).

References:

[1] P. Jörchel, J. Gorshkova, M. Kiselev, G. Klose, H. Schmiedel: Structural characterization of unilamellar lipid vesicles with anchored alkylglycosides at high water excess for studying cell recognitation processes, experimental report at YuMo at FLNP Dubna, April 2000.

[2] P. Jörchel, M. Kiselev, G. Klose, H. Schmiedel: Determination of Structural Parameters and Hydration of Unilamellar Vesicles at high Water Excess from SANS Curves Using a Multiple-strip Model, experimental report at YuMo at FLNP Dubna, Dec. 1999.

[3] Schmiedel, H.; Jörchel, P.; Kiselev, M.; Klose, G.: J. Phys. Chem., in press.

LOW ENERGY EXCITATIONS IN SOLID STATE ELECTROLYTE $Cu_{2-x}Se$

N.N. Bickulova[a], S. Danilkin[b], V.A. Semenov[b],
A. Skomorokhov[b], Z.A. Jagofarova[a], E.L. Jadrowski[c]

[a] *Sterlitamak Government Pedagogical University, Sterlitamak, Russia*
[b] *Institute of Physics and Power Engineering, Obninsk, Russia*
[c] *Joint Institute for Nuclear Research, Dubna, Russia*

An ubiquitous and rather intriguing feature in the physics of solid electrolytes is the anomalous behavior of the low-frequency part of the vibration spectrum, i.e. the presence of low-energy excitation. It is assumed that this peculiarity correlates strongly with ionic transport, but the origin of the low-energy excitations is still subject of discussion [1]. Aim of this experiment is investigation of low energy mode in solid state electrolyte $Cu_{2-\delta}Se$. Copper selenide $Cu_{2-\delta}Se$ has a mixed ionic-electronic conductivity with a broad range of homogeneity ($0<\delta<0.25$). The peculiarity of this system is that a deviation from stoichiometry (δ) and temperature (T) correlate with the ionic transport. For example, Cu_2Se has superionic phase transition at 140°C with disordering of copper cations and $Cu_{1.75}Se$ belongs to the superionic phase at room temperature already.

Copper selenide in contrary to other solid state ionics shows the low energy mode at room temperature in the superionic ($Cu_{1.75}Se$) and non superionic Cu_2Se) phases [2-4]. Figure 1 demonstrates dynamic structure factor $S(Q,\omega)$ for Cu_2Se and $Cu_{1.75}Se$ at room temperature and two values of momentum transfer Q = 3.1 and 3.2 Å^{-1}.

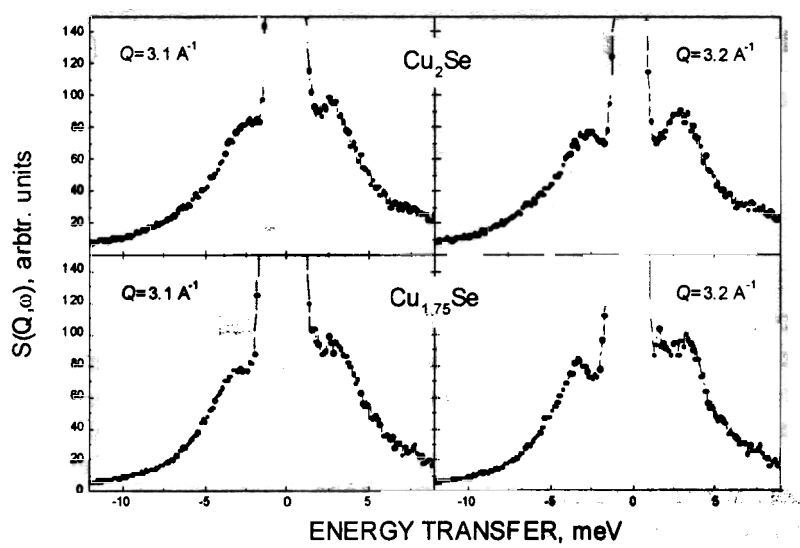

Figure 1. Dynamic structure of Cu_2Se and $Cu_{1.75}Se$ at room temperature and Q=3 and 3.2 Å^{-1}

Intensity, peak-position and width of the low-energy mode show pronounced Q-dependence when $S(Q,\omega)$ spectra of Cu_2Se and $Cu_{1.75}Se$ are the similar. Low frequency excitations are in evidence in both the superionic and non-superionic phases. The presence of the low frequency excitations in both phases of copper selenide is unexpected. Usually the low energy excitations is associated with localized vibrations of mobile ions in its non-superionic phase. Such excitations, however, have been believed to disappear upon transition the most of the solid electrolytes into their superionic phase.

One possible explanation of the unique behavior low energy mode in copper selenide is that only 1/8 part of Cu-cations is mobile in superionic phase [5]. There is assumption that fraction of mobile cations decreases with deviation of stoichiometry and there are no mobile cations in $Cu_{1.75}Se$. Other

assumption on origin of the low energy mode in $Cu_{2-\delta}Se$ is its associations with tunneling diffusion of the mobile cations. To study lattice dynamic of superionic conductors and check these assumptions we started the set experiments experiment on neutron scattering in copper selenide at various compositions and temperatures.

Preliminary results show that superionic phase transition in copper selenide via composition and temperature is non-equivalent (see fig 2).

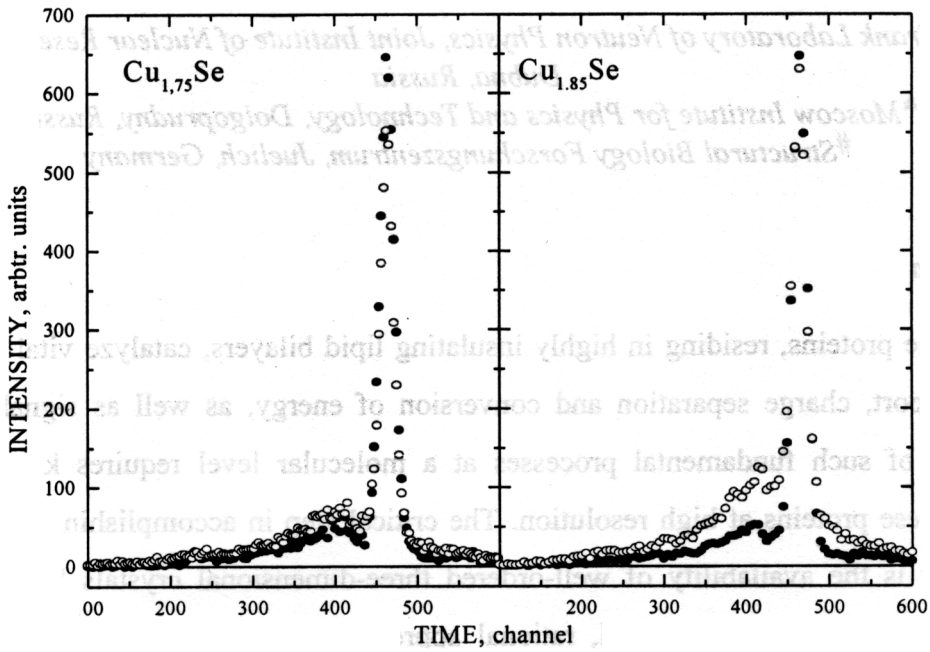

Figure 2. Inelastic neutron scattering spectra on $Cu_{1,75}Se$ и $Cu_{1,85}Se$ at T=20 °C (filled circles) and T=150 °C (empty circles) in time of flight scale. Initial neutron energy is 12 meV, scattering angle –71.2°. Peak at 460 channel corresponds to elastic neutron scattering, spectrum on the left from elastic peak to scattering with neutron energy gain, and from the right to the neutron energy loss scattering.

Figure 2 shows that INS spectra in $Cu_{1.75}Se$ do not change dramatically as temperature increases. Intensity of the spectrum corresponding to the neutron energy gain increases with the temperature due to Bose factor, quasi elastic peak decreases due to Debaye-Waller factor, intensity of the spectra with neutron energy loss is not changed practically. At the same time INS spectra of $Cu_{1,85}Se$ is changed essentially as temperature increases to 150 °C. Wide tails of quasielastic peak corresponding to the fast diffusion of the mobile copper cations appear in the INS spectra at 150 °C.

These results confirm assumption on decreasing of the mobile copper cations with deviation from stoichiometry. We need to note that this results is preliminary, data analysis in progress now. Further detailed experiments is invited also.

Reference

[1] M. B. Salamon (Ed.): Physics of Superionic Conductors, Springer-Verlag, Berlin (1979).

[2] N. Bickulova, S. Danilkin, V. Sememnov, E. Jadrovski,: Low frequency modes in $Cu_{2-\delta}Se$ superionic conductor; submitted to XVI Workshop on neutron scattering study of condensed matter, 13-17 September, 1999, Obninsk, Russia.

[3] T. Sakuma, K. Shibata: Journal of Physical Society of Japan, **58** (1989) 3061.

[4] T. Sakuma, K. Shibata, S. Hoshino: Solid State Ionics **40/41** (1990) 337.

[5] R. A. Yakshibaev, V. N. Konev, Soviet Solid State Physics **26** (1984) 3641-3645.

INVESTIGATIONS OF MECHANISM OF MEMBRANE PROTEINS CRYSTALLIZATION IN LIPIDIC CUBIC PHASE

G.Bobarykina*, R.Efremov*[&], V.Gordeliy*[#], A.Islamov*, A.Kuklin*
and G. Bueldt[#]

* *Frank Laboratory of Neutron Physics, Joint Institute of Nuclear Research, Dubna, Russia*
[&]*Moscow Institute for Physics and Technology, Dolgoprudny, Russia*
[#]*Structural Biology Forschungszentrum, Juelich, Germany*

1. Intoduction

Membrane proteins, residing in highly insulating lipid bilayers, catalyze vital reactions such as solute transport, charge separation and conversion of energy, as well as signal transduction. Understanding of such fundamental processes at a molecular level requires knowledge of the structures of these proteins at high resolution. The critical step in accomplishing of this by X-ray crystallography is the availability of well-ordered three-dimensional crystals [1]. E.Landau and J.Rosenbush [2] have devised a novel, rational approach to meet this goal using lipidic cubic phases. This membrane system, consisting of lipid, water and protein in appropriate proportions, forms a structured, transparent and complex three-dimensional lipidic array, which is pervaded by an intercommunicating aqueous channel bicontinuous system. Such matrices provide nucleation sites and support growth by lateral diffusion of protein molecules in the membrane.

Only this method of crystallization in cubic phase was successful in crystallization of an important membrane protein - bacteriorhodopsin (BR) [2]. This membrane protein is light-driven proton pump, which creates gradient of hydrogen ions. The energy of this gradient is used by cell for ATP synthesis to provide the *Halobium Salinarium* cells with energy.

Bacteriorhodopsin crystals were obtained from bicontinuous cubic phases, which consisted of monoolein (1-monooleoyl-*rac*-glycerol) or monopalmitolein (1-monopalmitoleyl-*rac*-glycerol) and water [3]. In both cases the intensively purple colored crystals are formed. Crystals of hexagonal morphology are appeared inside the MO matrix, while the MP system yields rhombic crystals.

However, it is not clear whether crystallisation of membrane proteins in lipidic cubic phase is a general method. Moreover, it is an open problem why lipidic cubic phase promote crystallization of membrane proteins.

Main aim of this work is to study phase behaviour of cubic phase formed by monoolein in course of BR crystallization. We expect that such investigation is necessary to understand how general is the behaviour of cubic phase in those cases when BR crystalls are growing.

2. Materials and methods

Standard conditions of BR crystallization [2] were used for the investigation of mechanism of the crystallization via small-angle neutron diffraction at the YuMO spectrometer, Dubna, Russia. 1-monooleoyl-*rac*-glycerol (C18:1) was purchased from Sigma Chemical and used without further purification.

Investigations of lipid phase behaviour at different protein concentrations (from 0.4 to 14 mg/ml), protein/buffer (250mM Na/K/P_i in D2O, 1.2% w/w octylglucoside, pD=6.0) rations and salt concentrations have been carried out. The samples were prepared by using the standard method for protein crystallization: 5 μl of BR buffer was added to 5mg of dry monoolein, centrifuged and then the phosphate salt was added and again centrifuged.

3. Results

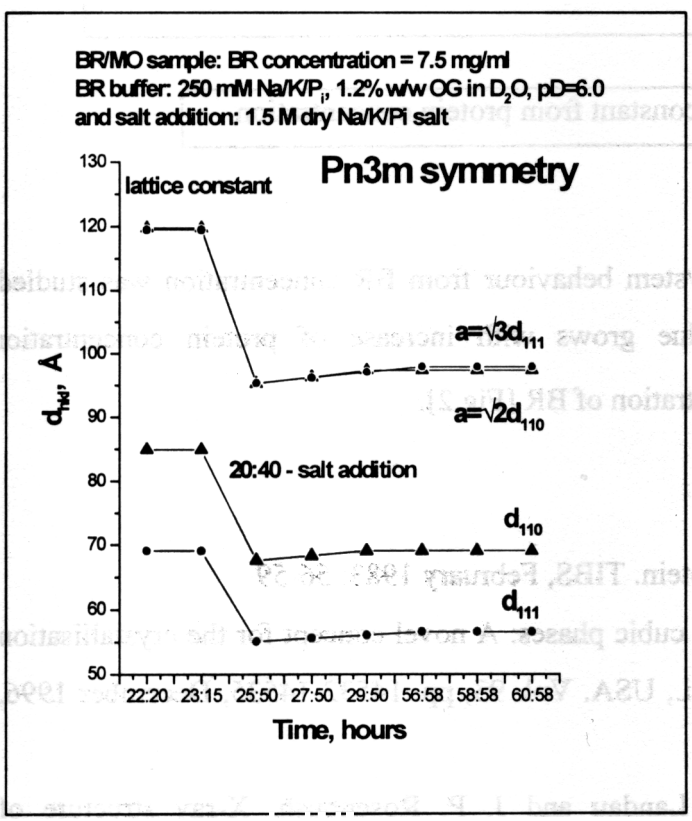

In this work the behaviour of BR/MO/buffer system in course of crystallization was studied by small angle neutron scattering (YuMO, Dubna, Russia).

We observed that investigated system forms cubic phase of Pn3m symmetry with lattice constant 16±2Å larger than that of MO/buffer system. The protein essentially influences this system.

Fig.1. The dependence of repeat distance d_{hkl} and lattice constant for BR/MO buffer system.

BR crystallization was initialising by salt addition. The addition of the salt influences on lattice constant, which is decreased by ~15Å [Fig.1], but not the symmetry of cubic phase. Main changes

occur during first 3 hours. It was shown that macroscopic phase symmetry is invariable in course of crystallization, the system does not undergo phase transitions [Fig.1].

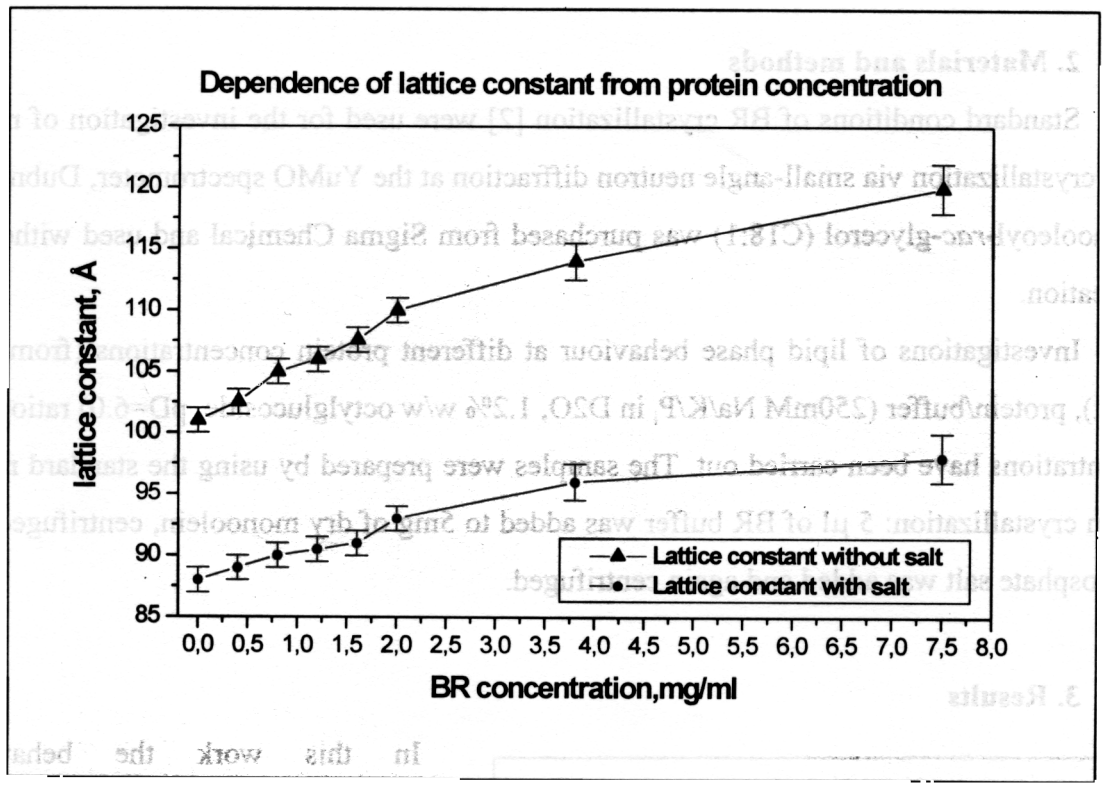

Fig.2. Dependence of lattice constant from protein concentration

Also dependence of BR/MO/buffer system behaviour from BR concentration was studied. We observed that the lattice constant value grows with increase of protein concentration approximately linearly up to 7.5mg/ml concentration of BR [Fig.2].

References:

1. H. Michel. Crystallization of membrane protein. TIBS, February 1983: 56-59
2. E. M. Landau and J. P. Rosenbush. Lipidic cubic phases: A novel concept for the crystallisation of membrane proteins. Proc. Natl. acad. Sci., USA. Vol. 93, pp. 14532-14535, December 1996, Biophysics.
3. E. Pebay-Peyroula, G. Rummel, E. M. Landau and J. P. Rosenbush. X-ray structure of bacteriorhodopsin at 2.5 Angstroem from Microcrystals Growth in Lipidic Cubic Phases. Science, vol. 277, 12 Sept., 1997.

THE STUDY OF THE UNBINDING OF MEMBRANES BY SANS

V. Gordeliy[1], U. Gorshkova[1], A.Islamov[1], V. Haramus[2]

[1] *Frank Laboratory of Neutron Physics, Joint Institute of Nuclear Research, Dubna, Russia*
[2] *GKSS Research Centre, Geesthacht, Germany*

1 Introduction

Intermembrane equilibrium distance is determined by the van der Waals short-range repulsion, long range electrostatic and undulation (repulsion) forces [1]. Superposition of these forces result in a global energy minimum, which can be shifted to infinite distance under change of the balance of the forces. It means that the transition has a sharp, first order character [2].

However, it has been argued that in presence of undulations the superposition does not work. The reason is that in presence of the undulations different parts of the surfaces of the opposite membranes are not placed at the same distance. Statistical mechanical treatments of the intermembrane interactions in this case were not successful [3]. Nevertheless, in spite of an analytical expressing of the intermembrane forces have not been derived it was shown that unbinding transition between a bound and a free (unbound) state should have a continuos character. It has been proved by renormalization group treatment [3], Monte-Carlo simulation [4] and mean field approach [5]. However, the character of the unbinding has never been experimentally rigorously examined.

2 Materials and methods

Synthetic dimyristoyl- phosphatidylcholine (DMPC) were used. The given amount of $CaCl_2$ in a $CaCl_2$ / D_2O solution was mixed with the lipid (about 1 wt %). The range of the salt concentrations from 0.0 mM to 1.0 mM was used. The measurement was carry out in gel and liquid phases at $T=15^0C$ and $T=55^0C$ respectively.

The samples were kept in quartz cells with a path length of 1.5 mm. For the control of the temperature the thermostate sample holder was used. Scattering data measured using the YuMO spectrometer are present as a function of the magnitude of the scattering vector q.

3 Results

The studies have shown that multilamellar membranes of DMPC in gel phase unbind when the concentration of $CaCl_2$ or $MgCl_2$ increases (Figure 1). It has been argued that this phenomenon can have a continuos character [3]. This prediction was never checked. Indeed, there is no experimental data on the unbinding of the mentioned above systems in liquid phase. As far as undulations are considerable only in liquid phase one can expect a continuos unbinding in this state of the membranes.

The aim of this project was to study in detail membrane unbinding in gel and liquid phases. It seems that SANS is the best method to do this. Indeed, our preliminaries SANS test have shown interesting features of this phenomenon. It is demonstrate in figure 1.

We have observed that the transition is quite sharp and occurs between 0.2 and 0.3 mM $CaCl_2$ in gel phase (see figure 2). The repeat distance is almost constant until the transition occurs. However, the intensity of the diffraction peaks and small angle part of the scattering curves change dramatically with the increase of the concentration of the ions (see Figure 1). It may mean a special type of a continuous unbinding. In any case it is a new observation.

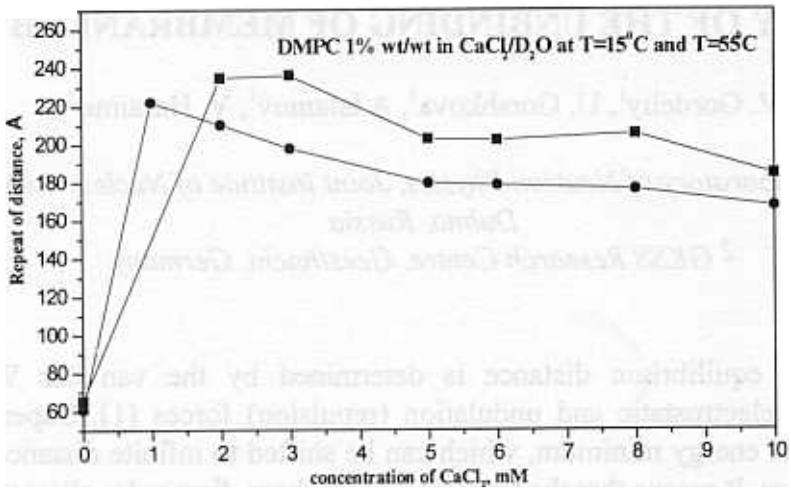

Figure 1: The repeat distance of the DMPC multilayers as a function of the CaCl2 concentration.

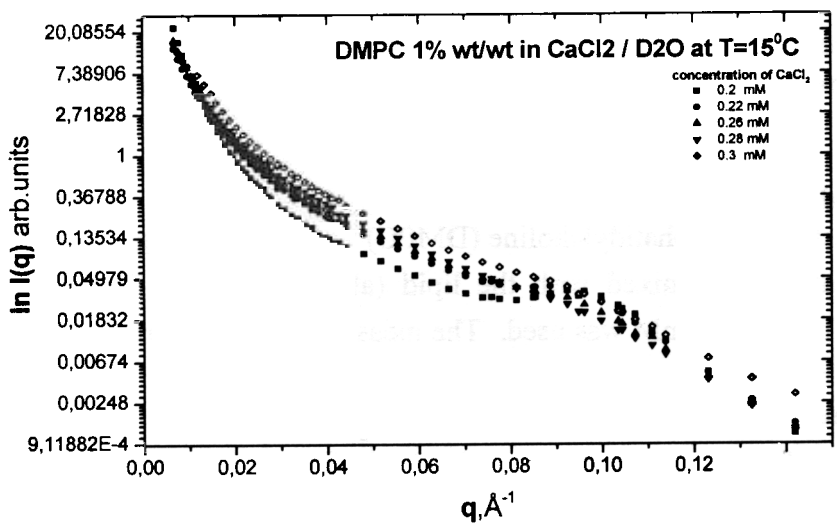

Figure 2: Scattering curves of DMPC/$CaCl_2$/D_2O mixture for the following concentration of the $CaCl_2$: 0.2mM, 0.22mM, 0.26mM, 0.28mM, 0.3mM

1. Izraelachvili, J.N., and H. Wennerstrцm. 1992. Entropic forces between amphiphilic surfaces in liquids. *J. Phys. Chem. 96: 520-531.*
2. Lipowsky R. 1995. Generic interection of flexible membranes. *In Handbook of Biological Physics. V 1B:521-602.*
3. Lipowsky R., and S. Libler. 1986. Unbinding transition of interacting membranes. *Phys. Rev. Lett. 56, 2541-2544.*
4. Lipowsky R., and B. Zelinska. 1989. Binding and unbinding of lipid membranes. A Monte Carlo Study. *Phys. Rev. Lett. 62, 1572-1575.*
5. Helfrich W. 1993. Mean field theory of n-layer unbinding. *J. Phys. II France 3:385-393.*

WATER MODERATOR OF A REACTOR IBR-2 WITH A CANYON ON A LATERAL SURFACE. A DESIGN AND PHYSICAL PARAMETERS.

A.A.Beliakov, V.I.Bodnarchuk, D.A.Korneev, V.F.Peresedov, E.P.Shabalin, S.P.Yaradaikin

Frank Laboratory of Neutron Physics
Joint Institute for Nuclear Research

The component of the new methane cryomoderator of a reactor IBR-2 - water premoderator - serves simultaneously as a thermal moderator for 9-th and 1-th channels. The radiation of neutrons in the direction of 9-th channel occurs from a lateral surface of a moderator. The specific feature of a reflectometer a REFLEX located on 9-th channel, consists that it "sees" neutrons, irradiated only from the limited region of a surface of a moderator. The form of this region represents the rectangular, extended along a vertical, with the horizontal size about 7 millimeters. With the purpose of increase of a flux on a sample, on a lateral surface of a moderator in a direction parallel to a wall of an active core of a reactor on distance 52 mm from it the vertical slot-hole pocket (canyon) by depth of 80 mm, width 15 mm and height 200 mm was created. The design data of a moderator and results of relative measurements of distribution of a flux of neutrons along a lateral surface as a function of distance from an active core of a reactor are resulted.

The water premoderator - integral part of a design of the new methane cryomoderator of a reactor IBR-2, represents a cavity filled with water at a room temperature. The casing of a premoderator structurally joint with a vacuum casing of a methane moderator represents a box fabricated from an aluminium alloy (see. fig. 1). The basic applicability of a water premoderator: a) to transform a spectrum of fast neutrons of fission in thermal and to "protect"

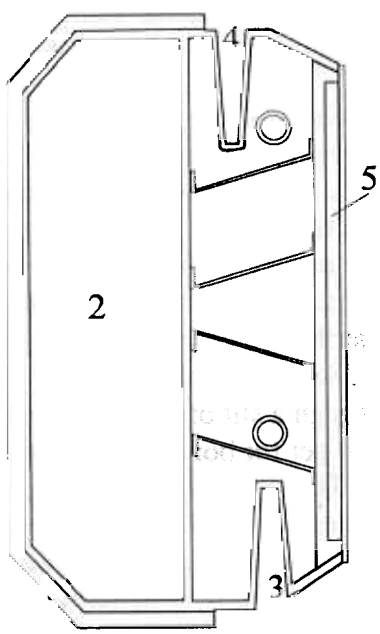

Fig. 1 Section of the cryomoderator in a horizontal plane. 1-cavity of a water premoderator; 2-cavity filled with a methane; 3, 4-slot-hole pockets (canyon) from the sides of channels 9 and 1 accordingly; 5-cavity filled B_4C

a methane from fast neutrons of an active zone of a reactor; b) to serve as a thermal moderator for 1 and 9 channels of a reactor IBR-2. The cavity, nearest to a reactor core, of a premoderator is filled with thickness of 10 mm by a powder B_4C. Such decision is traditional for water moderators of a reactor IBR-2 and is dictated by necessity to shield an active zone from thermal neutrons which are taking off from moderators. Thus, structurally water premoderator and methane cryomoderator make a single unit. The premoderator adjoins directly to an active core of a reactor. The further transformation of a spectrum of neutrons in "cold" is carried out by a solid-state methane moderator, contiguous to a water premoderator cooled up to temperatures 30-60K. The geometry of an arrangement of the cryomoderator on a reactor is those, that four beams (IV, V, VIa, VIb) (see. fig. 2) "look" at an obverse surface of a methane moderator. Except for

the listed beams there are two coaxial beams (I and IX), which "look" at lateral walls of a water warm premoderator from the opposite sides (axis of these beams are perpendicular to lateral surfaces of a premoderator).

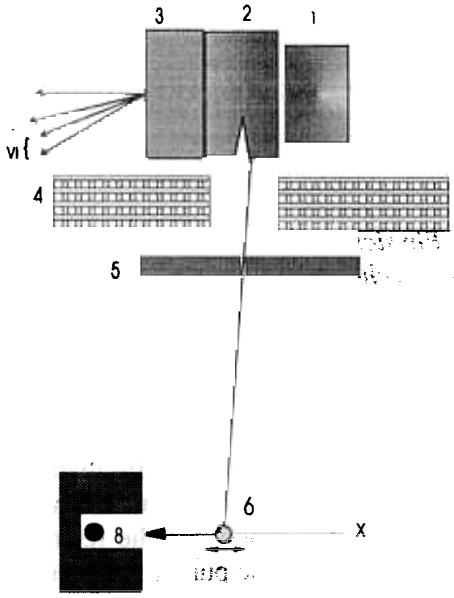

Fig. 2 Figures explaining the experiment by determination of distribution of density of a flux on a lateral surface of a premoderator on 9 channel IBR-2: 1-core of a reactor; 2-premoderators with a canyon; 3-methane moderators; 4-biological shields of a reactor with an aperture of shutter; 5- collimators with narrow (3 mm) vertical slit; 6- vanadium thin cylinder (scatterer) located on the mobile mechanism; 7-shields of the detector, 8-helium detectors; the Roman figures designate directions of the appropriate beams

On the 9-th channel of IBR-2 the neutron reflectometer REFLEX is located. The specific feature of a reflectometer consists that it "sees" neutrons, irradiated only from the limited region of a surface of a moderator. The form of this region represents the rectangular, extended along a vertical, with the horizontal size about 7 millimeters. Other part of a surface of a moderator in experiment is not used.

Taking into account this specific property of a reflectometer, with the purpose of increase of a flux on a sample, the design of a premoderator was complicated. Namely, on its lateral surface the vertical slot-hole pocket (canyon) by depth of 80 mm, width 15 mm and height 200 mm and located on distance 52 mm from a wall closed to the active reactor core was created (see a fig. 1). The similar pocket was created as well with opposite the side of a premoderator. It was supposed, that it will result to local in the field of a canyon to increase of a flux of irradiated neutrons.

In figure 2 the experiment on study of distribution of a flux of neutrons on a lateral surface of a premoderator from the side of 9 channel is shown. The collimator with a narrow vertical slit (width - 3.0, height - 150 of mm) was placed on distance of 7.5 meters from a

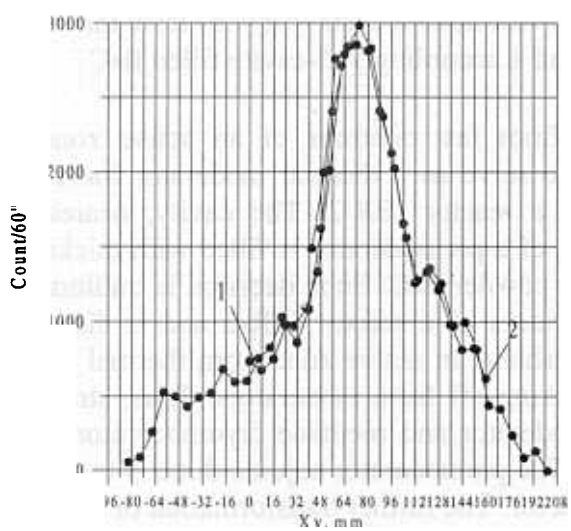

Fig. 3 Dependences of the count of the detector of the vanadium coordinate after subtraction of a background. The position of a maximum of count of the detector coincides with conyon position. The zero values of the count on the left and right borders of distribution correspond to coordinates of vanadium of which projection through a slit of a collimator on a premoderator get for borders of aperture of the shutter. The numeral on the diagram mark coordinates of vanadium in relation to which the spectral gain of a flux in a point of a maximum (see fig. 4) is determined

moderator in the experimental hall of the reactor directly with a wall of a ring corridor. On distance of 20.1 meters from a collimator the vanadium cylinder by a diameter of 5 mm and

height 100 mm was placed in order to scatter neutrons in the detector direction. The cylinder automatically with accuracy of 0.05 mm could move in a horizontal plane across a neutron beam. The neutrons scattered by vanadium were registered by the detector fixed in shield on distance 400mm from an average position of vanadium. The window in shield of the detector was oriented so, that the vanadium cylinder always was in a field of visibility of the detector. Obviously (see. fig. 2) that a projection of the vanadium cylinder through a slit of a collimator (vertical stripe like spot with width 5mm) on a surface of a premoderator moves synchronously with moving vanadium. Thus, the registration of scattered neutrons by the detector at various coordinates of vanadium carries out measurement of horizontal plane distribution of a flux on a surface of a premoderator. In figure 3 the measured distribution of neutron intensity is shown depending on coordinate of vanadium (integrated over a thermal

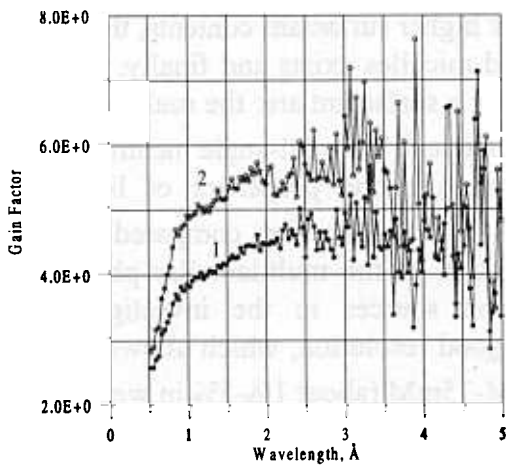

Fig. 4 Spectral gains in a local flux in a point appropriate to a position of a canyon on a premoderator concerning points outside a canyon. The curves 1, 2 correspond to points 1 2 in a fig. 2

neutron spectrum). From figure it is visible, that the distribution on a surface of a moderator of an integrated intensity has at the certain coordinates brightly expressed maximum. The gain in an intensity in these coordinates in relation to an average intensity behind its equal approximately to 3.5. In a fig. 4 the neutron wave length dependence of a gain in an intensity in maximum in relation to intensities behind its in coordinates 1 and 2 figures 2 is shown. It is visible, that at increase the relative gain grows and at 3 angstroms reachessize 4.5 and 5.5 for points 1 and 2 accordingly.

The received results have confirmed essential increase of a local flux of neutrons which are irradiated from a canyon area of a surface of a moderator. It will allow to use this area on a moderator for formation of a beam of neutrons on REFLEX and as result (see fig. 3,4) to lift luminosity of installation essentially.

The authors thank V.L.Aksenov for support, V.V.Golikov and A.D.Rogov for the useful remarks.

DMPC MEMBRANE SWELLING BY NONIONIC SURFACTANT $C_{12}E_8$: X - RAY DIFFRACTION STUDY

M.A. Kiselev*, D. Lombardo#, P. Lesieur#

* - *Frank Laboratory of Neutron Physics, JINR, 141980 Dubna, Russia*

\# - *LURE, Bat. 209-D, B.P. 34, F-91898 Orsay, France*

Mixed lipid/surfactant aggregates are currently of great interest because of their wide use for the development of new drug delivery systems. The phase state of a dilute aqueous lipid/surfactant mixture depends on the effective surfactant mole fraction in the aggregates. Mixed bilayers are formed up to the saturating fraction of the surfactant. For higher surfactant contents, the coexistence range of surfactant-saturated bilayers and lipid-saturated micelles exists and finally, only micelles are found. The main stages of membrane solubilisation by a surfactant are: the multilamellar phase, unilamellar phase, rod-like micelles, and spherical micelles/1/. Small-angle neutron and X-ray scattering are appropriate techniques to study the structure and properties of lipid/surfactant aggregates in the unilamellar or micellar phases/2,3,4/. X-ray diffraction compared with neutron diffraction is a more suitable method for the investigation of the multilamellar phase structure. Synchrotron sources have an advantage over neutron sources in the investigation of the multilamellar phase due to an extremely high flux and good resolution, which allows you to study diluted systems with a small lipid concentration of 15mM-75mM (about 1%-5% in weight)/5/.

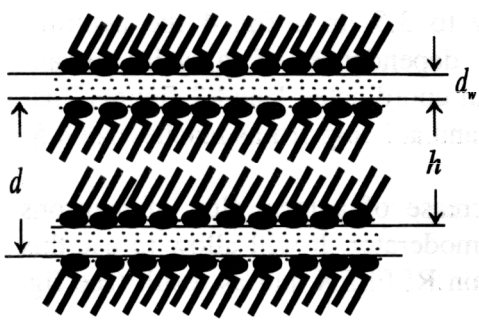

Fig. 1. The schematic representation of the gel $L_{\beta'}$ - phase of the DMPC multilamellar structure. The multilamellar structure consists of DMPC bilayers with the membrane thickness h and solvent layers with the solvent thickness d_W. The repeat distance of the DMPC membrane $d = h + d_W$. In the $L_{\beta'}$ - phase, the DMPC hydrocarbon chains tilte to the membrane surface.

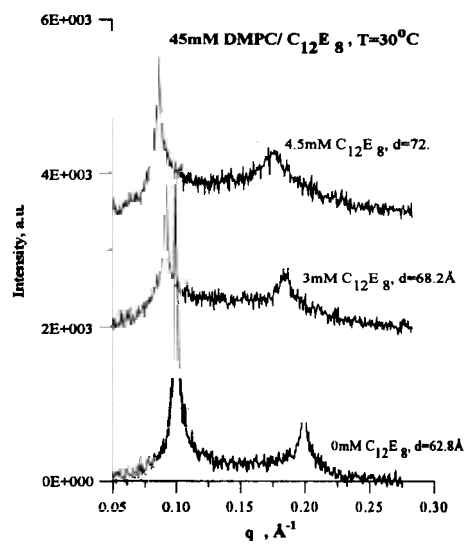

Fig. 2. The diffraction patterns recorded with the acquisition time 10min (0mM $C_{12}E_8$), 10min (3mM $C_{12}E_8$), 15min (4.5mM $C_{12}E_8$).

A highly diluted multilamellar phase of the DMPC/$C_{12}E_8$ system is characterized with the help of X-ray diffraction on beam line D22 of the synchrotron source DCI, LURE, France. The first stage of membrane solubilization, which is the transformation of multilamellar to lamellar phase, was studied for systems with the DMPC concentrations 30mM, 45mM, and 60mM as a function of surfactant concentration and temperature. Figure 2 presents the diffraction patterns recorded at T=30°C for the 45mM DMPC with the surfactant concentration 0mM (pure water), 3mM, and 4.5mM. The DMPC membrane repeat distance increases from 62.8±0.3Å at a 0 surfactant concentration to 68.2±0.3Å at the surfactant concentration 3mM, and to 72.3±0.4Å at 4.5mM. A decrease in the intensity of the diffraction peak with increasing surfactant concentration corresponds

to a decrease in the number of multilayers in the liposomes. All the measured membrane repeat distances for the 45mM DMPC as a function of surfactant concentration and temperature are presented in Fig. 3. An increase of d with increasing surfactant concentration describes membrane swelling. Membrane swelling is calculated as a derivative d of the surfactant concentration at constant temperature. The results of the calculation are presented in Fig. 4 for 30mM, 45mM, and 60mM lipid concentrations.

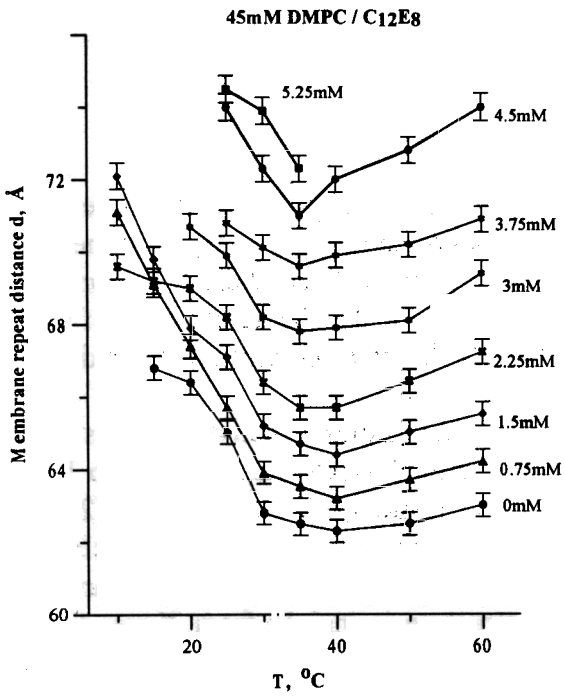

Fig. 3. The 45mM DMPC. The repeat distance as a function of temperature for the surfactant concentrations: 0; 0.75; 1.5; 2.25; 3; 3.75; 4.5; 5.25mM.

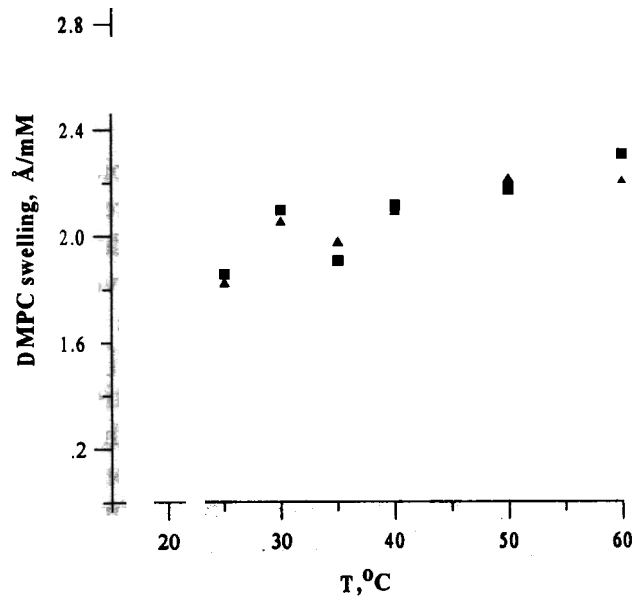

Fig. 4. DMPC membrane swelling as a function of temperature for 30mM DMPC (circles); 45mM DMPC (squares); 60mM DMPC (triangles).

It is found that membrane swelling is a temperature dependent parameter. DMPC membrane swelling has a tendency to increase from 1.25±0.15Å/mM at T=20°C to 2.26±0.20Å/mM at T=60°C. The swelling has a local maximum at T=30°C and a local minimum at T=35°C.

Acknowledgments: This study was supported by the TMR program for Large Instruments.

References

1. M.A. Kiselev, P. Lesieur, A. M. Kisselev, S.A. Kutuzov, L.I. Barsukov, T.N. Simonova, T. Gutberlet, G. Klose. Investigation of temperature sensitive mixed lipid/detergent systems at the YuMO spectrometer. JINR publication E3, 14-98-168 (1998), 52-57.

2. P. Lesieur, M.A. Kiselev, L.I. Barsukov, D. Lombardo. Temperature induced micelle to vesicle transition: kinetic effects in the DMPC / NaC system. J. Appl. Cryst. 33 (2000) 623-627.

3. T. Gutberlet, M. Kiselev, H. Heerklotz, G. Klose. SANS study of mixed POPC/$C_{12}E_n$ aggregates. Physica B, 381-383 (2000) 276-278.

4. H. Schmiedel, P. Joerchel, M.Kiselev, G. Klose. Determination of structural parameters and hydration of unilamellar POPC/$C_{12}E_4$ vesicles at high water excess from neutron scattering curves using a novel method of evaluation. J. Phys. Chem. B 105 (2001) 111-117.

5. M.A. Kiselev, P. Lesieur, D. Lombardo, A.M. Kisselev, T. Gutberlet. The investigation of temperature-sensitive phospholipid /surfactant systems via neutron and X-ray small-angle scattering and diffraction. Chemistry and Physics of Lipids, 107 (2000) 72.

STRUCTURE FACTOR OF DMPC UNILAMELLAR VESICLES: SAXS STUDY AT SYNCHROTRON

M.A Kiselev*, D. Lombardo#, A.M. Kisselev$, P. Lesieur#

* - *Frank Laboratory of Neutron Physics, JINR, 141980 Dubna, Moscow reg., Russia*
# - *LURE, Bat. 209-D, B.P. 34, F-91898 Orsay, France*
$ - *Physics Department, Cornell University, Ithaca, NY 14853, USA*

1. Introduction

Vesicles technology is a rapidly evolving field in basic and applied sciences and engineering. In addition, at present there are several industrial organizations engaged in the research and development of processes and products from vesicular materials. Thus, there is a strong driving force for the development of noninvasive and accurate methods for the characterization of vesicular dispersions. For potential applications of vesicular systems the size, polydispersity and dynamic properties are needed to be determined [1].

Of particular interest is application of the phospholipid vesicles as delivery agents of drugs, genetic materials and enzymes through living cell membranes. Vesicle size appears to be a key factor in their permeation through tumor microvessels and the residence in tumor tissues [2].

Today, the problem of accurate simultaneous determination of the vesicle radius, polydispersity and the internal membrane structure is not solved yet in SAXS and SANS experiments. Information about the internal membrane structure is mainly from X-ray diffraction experiments on multilamellar vesicles [3]. Large unilamellar vesicles are a more biologically appealing model of lipid bilayer than multilamellar vesicles. The new proposed methods (Schmidel's model and Pencer's approach) of the evaluation of the membrane thickness involve complementary techniques (freeze fraction cryomicroscopy and dynamic light scattering) to characterize the vesicle size and polydispersity [4,5].

A 40% sucrose buffer has been used in a SAXS investigation of a micelle to vesicle transition in a mixed DMPC/ionic surfactant system [6]. In this approach, the vesicle size and distribution were calculated directly from the SAXS curves. Sucrose solutions in water decrease the vesicle size and polydispersity and create appropriate experimental conditions for the investigation of vesicles via SAXS and SANS [7].

Different authors have reported the appearance of intervesicle interaction for vesicles at different lipid concentrations in the range of 3%-5% w/w. To clarify this problem, the SAXS experiment on vesicles with a low polydispersity was carried out in the range of scattering vectors $0.004Å^{-1} \le q \le 0.04Å^{-1}$ at a synchrotron source DCI (beam line D22). DMPC vesicles were prepared via extrusion through polycarbonate filter with the pores diameter 500Å for 15mM, 30mM, 45mM, 60mM, 75mM DMPC concentrations in the 40% sucrose buffer.

2. Results and discussion

The macroscopic cross section of monodispersed vesicles is

$$\frac{d\Sigma}{d\Omega}_{mon}(q,R) = n \cdot (\Delta\rho)^2 \cdot F(qR, d_l) \cdot S(qR), \qquad (1)$$

here n is the number of vesicles per unit volume, $F(qR,d_l)$ is the form factor of a hollow sphere in the approximation $R \ll d_l$ [5,6], R is the vesicle radius, d_l is the membrane thickness, $\Delta\rho$ is the X-ray contrast between the membrane and aqueous sucrose solution, and S(qR) is the structure factor of spherical vesicles in the Debye form

$$S(qR) = 1 - \frac{8V_v}{v}\left(8\pi \cdot \frac{R^2}{qR} \cdot Sin(2qR)\right) \qquad (2)$$

The experimentally measured macroscopic cross section $d\Sigma(q)/d\Omega$ was calculated via convolution of equation (1) with the vesicle distribution function G(R) by integration over the vesicle radius R_{min}=70Å to R_{max}=2000Å

$$\frac{d\Sigma}{d\Omega}(q) = \frac{\int_{Rmin}^{Rmax} \frac{d\Sigma}{d\Omega}_{mon}(q,R) \cdot G(R) \cdot dR}{\int_{Rmin}^{Rmax} G(R) \cdot dR} \qquad (3)$$

A nonsymmetrical Schulz distribution was used to describe vesicle polydispersity

$$G(R) = \frac{R^m}{m!} \cdot \left(\frac{m+1}{\bar{R}}\right)^{m+1} \exp\left[\frac{(m+1) \cdot R}{\bar{R}}\right] \qquad (4)$$

Finally, the $d\Sigma(q)/d\Omega$ values were corrected for the resolution function of the D22 spectrometer.

The polydispersity of vesicles P was defined as half width at half height (HWHH) of distribution function (4), $P = 1.18 \cdot \sqrt{\frac{1}{(m+1)}}$.

The SAXS curve for the DMPC concentration 15mM can be fitted well with S(q)≡1. Fitting with S(q)≡1 of the SAXS curve with the DMPC concentration 30mM gives overestimated results for the q range $0.004Å^{-1} \le q \le 0.008Å^{-1}$. The experimentally measured SAXS curves and the fitted curves with a structure factor in the Debye form are shown in Fig. 1. The obtained vesicles parameters are presented in Tab. 1. The experimental curves for the range of DMPC concentrations from 15mM to 75mM are fitted well with the introduced interaction as it is seen in Fig. 1. The application of different DMPC concentrations makes it possible to determine the accuracy of the evaluation of model parameters from the SAXS experiment. The evaluation of the membrane thickness from the q range $q \le 0.04Å^{-1}$ gives a big uncertainty in the value of the membrane thickness because this region of the scattering vector is just the begining of the Guinier region. No physical reason exists for the differences in the values of R, P, d_l for the different discussed concentrations of DMPC (for 75mM DMPC, $\frac{V_v}{v} = 0.106$). From the results presented in Table [1] the average model parameters are calculated for DMPC vesicles at T=30°C: $\bar{R} = 254 \pm 16Å$; P=0.29±0.07; d_l=36.6±4.1Å.

Figure 2 shows the calculated values of the structure factors $S_{av}(q)$ for all the DMPC concentrations presented in Figure 1. The average $S_{av}(q)$ functions were calculated with the Schulz distribution and vesicles parameters from Table 1. For 15mM DMPC, $|S_{av}(q)-1|<0.05$ for $q \ge 0.004$ $Å^{-1}$, and $S_{av}(q) \approx 1$ for $q \ge 0.006$ $Å^{-1}$, $|S_{av}(q)-1|<0.05$ for 30mM DMPC at $q \ge 0.006$ $Å^{-1}$. For the DMPC concentrations ≥45мМ, $|S_{av}(q)-1|>0.05$ at $q=0.008Å^{-1}$. The average structure factor $S_{av}(q)= 1$ for all the concentrations at $q \ge 0.02$ $Å^{-1}$ due to the system polydispersity. The influence of the structure factor is negligibly small for the Guinier region ($q \ge 0.02$ $Å^{-1}$), which is important for the determination of the membrane thickness.

3. Conclusions

Disregarding of structure factor calculations for the lipid concentrations ≥30mM (2% w/w) leads to errors in the calculation of the vesicle radius. At the same time, the structure factor correction is not important in the evaluation of the membrane thickness from the small angle experiment. For the lipid concentrations about 15mM (1% w/w) the structure factor correction is negligibly small. For the SANS experiment with polarized neutrons an increase of the scattering intensity is a problem due to decreasing of the polarized neutron flux. The use of samples with the lipid concentrations 5%-10% w/w is a much simple way to improve statistics in the SANSP experiment. The correct evaluation of vesicle structure factor is necessary in this case.

TABLE 1. The vesicle parameters evaluated from the model calculations of the SAXS curves. $\overline{R}$ is the average vesicle radius, P is the vesicle polydispersity, d_l is the membrane thickness at T=30°C.

DMPC concentration, mM	15	30	45	60	75
$\overline{R}$, Å	242±1	252±1	255±1	261±1	261±1
P	0.30	0.26	0.30	0.34	0.33
d_l, Å	40±5	35±5	35±5	36±5	37±5

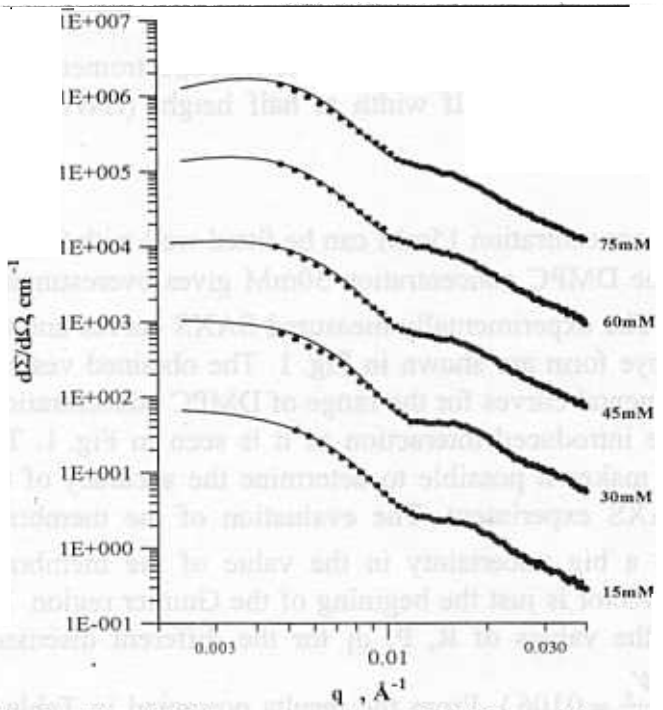

Fig. 1. The SAXS spectra from DMPC vesicles at T=30°C. The macroscopic cross section for the 15mM DMPC vesicles in absolute units. The macroscopic cross sections for 30mM, 45mM, 60mM, and 75mM are multiplied by 10, 100, 1000, 10000, respectively.

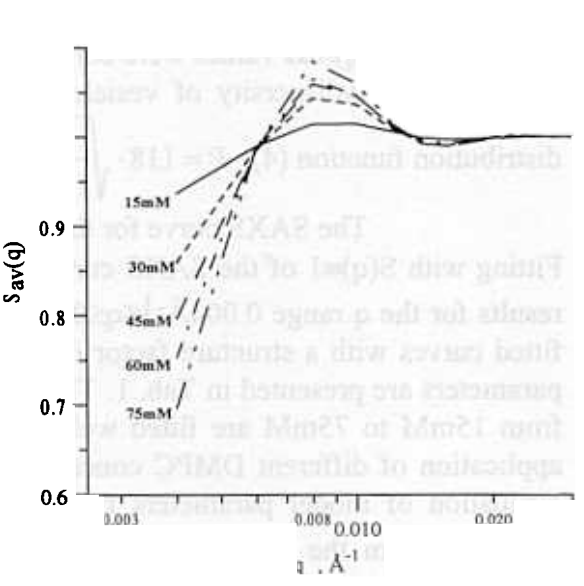

Fig. 2. The average structure factor of vesicles $S_{av}(q)$ calculated by the Debye model with the Schulz distribution for the 15mM, 30 mM, 45 mM, 60mM, and 75mM DMPC concentrations at T=30°C.

Acknowledgements: This study was supported by the TMR program for Large Instruments.

References

[1] Vesicles. ed. M. Rossoff. Marcel Dekker, Inc. 1996.
[2] A. Nagayasu, K. Uchiyama, and H. Kiwada. Adv. Drug Delivery Rev. 40 (1999) 75-87.
[3] J.F. Nagle, S. Tristram-Nagle. Biochim. Biophys. Acta 1469 (2000) 159-195.
[4] H. Schmiedel, P. Joerchel, M. Kiselev, G. Klose. J. Phys. Chem. 105 (2001) 111-117.
[5] J. Pencer, R. Hallet. Phys. Rev. E 61 (2000) 3003-3008.
[6] P. Lesieur, M.A. Kiselev, L.I. Barsukov, D. Lombardo. J. Appl. Cryst. 33 (2000) 623-627.
[7] M.A. Kiselev, P. Lesieur, A.M. Kisselev, D. Lombardo, M. Killany, S. Lesieur, M. Ollivon. Nucl. Instr&Methods A (2000), accepted for publication.

NEUTRON WAVE CHANNELING IN THE STRUCTURE Cu(30nm)/Ti(150nm)/Cu(100nm)/glass

V.L. Aksenov[a], Yu.V. Nikitenko[a], A.V. Petrenko[a], V.V. Proglyado[a], F. Radu[b], V. G. Syromyatnikov[c]

[a]*Frank Laboratory of Neutron Physics, Joint Institute for Nuclear Research, 141980 Dubna, Moscow Region, Russia*
[b]*National Institute of Physics and Nuclear Engineering, Department of Experimental Physics, 76900, P.O. Box MG-6, Magurele, Romania*
[c]*Petersburg Nuclear Physics Institute, Russian Academy of Sciences, 188350, Gatchina, St. Petersburg, Russia*

Propagation of neutrons in a channel with a nanometric cross section is a wave process (neutron wave channeling). A potential application of the channeling effect may be the creation of a highly collimated neutron beam with a super-narrow cross section (100 nm in diameter). The neutron guide is a matter-channel layer enveloped in layers, the walls, whose material has an optical density higher than that of the matter of the channel. Neutron waves propagate through the channel reflecting from the walls. Attenuation of the propagation is due to decoherence of the neutron wave possibly resulting from the curvature or changing of thickness of the channel and the roughness of the interface. In this connection, an important application of channeling is the study of violations in the rectilinearity of the interface in the length of the structure. In [1-2] experiments of neutron wave channeling in the structures (SiO_2+TiO_2)/Ti/Si and $Co_{0.95}Zr_{0.05}$/Al/ $Co_{0.95}Zr_{0.05}$ are discussed. In the experiments an increase in neutron transmission over the neutron guide was observed for a wave vector on the order of 10^{-2} Å^{-1}. The authors of the experiment claim that the growth of transmission is due to formation of a neutron wave with an increased amplitude caused, in its turn, by the coherent summation of 2π-multiple neutron waves with different amplitudes. The factor of growth of the amplitude of the resulting neutron wave in the neutron guide increases as the wall thickness of the neutron guide grows. At the same time, the beam divergence decreases together with a decrease of the wavelength interval over which it happens. This results in the growth of the influence of decoherent processes on the wave propagation and as a result, in a rise of the sensitivity of measurements to the probability of such processes. To study the channeling processes, the structures Cu(30nm)/Ti(150nm)/Cu(100nm)/glass (Fig. a.) and Cu(30nm)/Ti(150nm)/Cu(100nm) /glass with a 30 mm cadmium angle piece on the surface of the structure (Fig. b.) were chosen.

The structures were illuminated with a collimated neutron beam at a glancing angle of 2.55 mrad, the mean square deviation of the glancing angle being 20 μrad. The neutrons tunneled through a 30 nm copper layer into the titanium layer where they propagated.

Figure c. illustrates the dependence of the neutron reflection coefficient $R(\eta)$ on the perpendicular wavelength component $\eta = \lambda/\theta$ in the first structure. For η equal to 0.74, 0.91 or 1.58 Å/mrad, resonance downfalls (dips) on the reflection coefficient curve are seen (narrower dips, although not seen in the figure, also exist at $\eta < 0.74$). The dips are due to increasing neutron density and the related growth of neutron absorption in the titanium channel. Estimates show that the neutron density is reduced two times due to neutron absorption in the channel but at the same time, around the dips marked "2" it is 50 times larger than the density of neutrons in the incident beam. Figures d., e., f. show the dependence of the neutron transmission in the second structure $T(\eta)$ for the summation of counts over three, two or one channel of the detector, respectively (one channel equals 0.69 mm of the sensitive area of the linear detector, which corresponds to an angular interval of 0.26 mrad, the spatial resolution of the detector being on the order of 1.5 mm). From the results illustrated in Fig. d. it is seen that the large transmission maximums marked with "1", "2" or

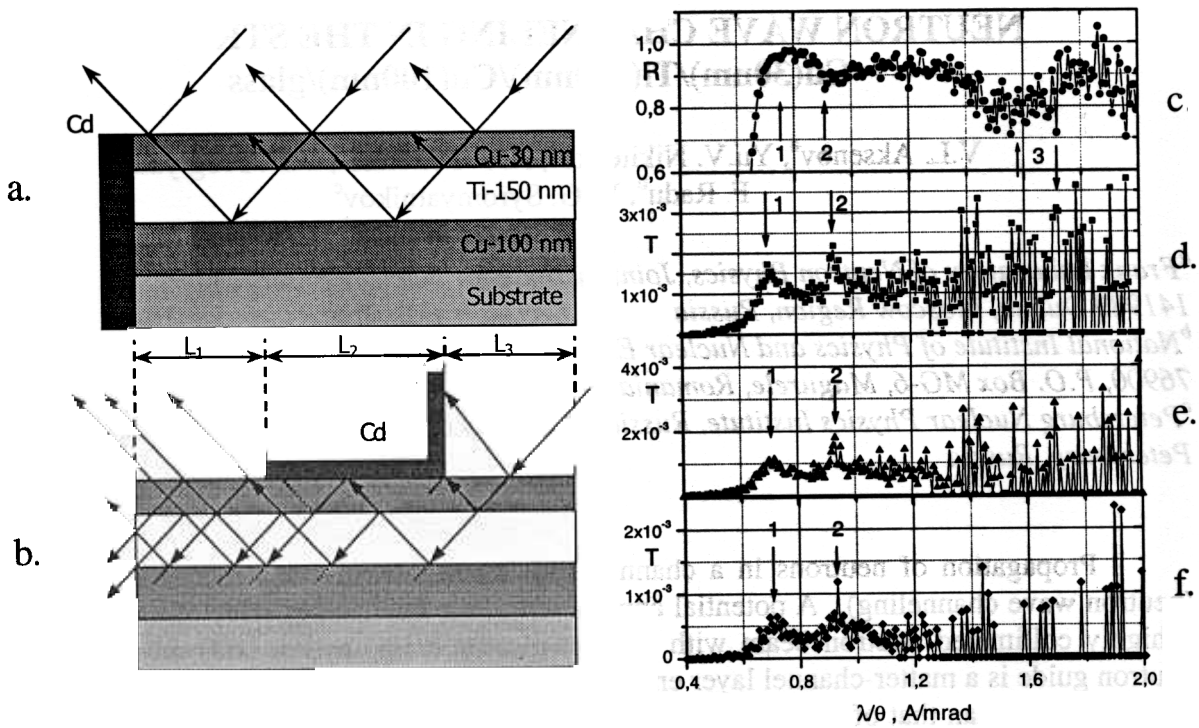

"3" are observed for η equal to 0.71, 0.93 or 1.67 Å/mrad. In the vicinity of the maximums "2" and "1" one will also see transmission oscillations with a smaller amplitude. The maximum "2" in Fig. d. virtually coincides with the minimum "2" in Fig. c. Thus, it is obvious that this maximum on T(η) is also due to an increase in the neutron density in the titanium channel. The maximum "1" in Fig. d. shifts (by 4%) with respect to the minimum at 0.74 Å/mrad in Fig. c. The maximum "3" in Fig. d. is extremely narrow and shifts (by 6%) from the center of the wide maximum at 1.58 Å/mrad in Fig. c. The entire process of channeling is as follows. In the 35 mm section of the titanium layer prior to cadmium a wave with an increased amplitude is formed at certain values of η. Then, in the titanium layer under the cadmium the neutron wave propagates and its amplitude decreases. In the 35 mm section of the titanium layer behind the cadmium the wave exits through the surface (tunneling through the copper layer) and through the exit cross section of the channel. In Fig. d. it is seen that the transmission maximums are on the background which increases linearly as η increases. Obviously, the magnitude of the background is determined by the flux of the incoherently propagating neutrons. It is seen that as the divergence of the registered neutrons decreases (Figs. e. and f.) the background decreases and equals a third of the peak for the data in Fig f. The transmission peaks themselves are of the order of 10^{-3}, which is about ten times larger than the intensity peaks observed in [1,2] and is caused by a higher neutron density in the channel because of a three times larger thickness of the first copper layer. Thus, the resonance modes corresponding to neutron channeling in the titanium layer at a distance larger than 30 mm are obtained.

1. Y.P. Feng, C.F. Majkrzak, S.K. Sinha, D.G. Wiesler, H. Zhang, H.W. Deckman, Phys. Rev. B 49 (1994) 10814.
2. A. Menelle, S.P. Pogossian, H.Le Gall, J.M. Desvignes, J. Ben Youssef, Physica B 234-236 (1997) 510.

NEUTRON SPATIAL BEAM-SPLITTING AND POLARIZATION ANALYSIS IN REFLECTOMETRY

V.L. Aksenov, S.V. Kozhevnikov, and Yu.V. Nikitenko

Frank Laboratory of Neutron Physics, Joint Institute for Nuclear Research, 141980 Dubna, Moscow Region, Russian Federation

Magnetically anisotropic layered structures are attractive because of their extended applications. Improvement of the methods of their investigation is thus an important problem. At reflection or refraction on the interface of magnetically noncollinear media neutrons experience spin-flip followed with spatial splitting of the neutron beam [1-5]. In [5] it is noted that a combined use of polarization analysis and the effect of beam splitting increases the efficiency of polarization measurements. This paper presents a more detail study of the problem.

The measurements were conducted with the SPN-1 spectrometer at the IBR-2 reactor in Dubna. The experimental setup comprises a polarizer, a spin-flipper in front of the sample, a spin-flipper behind the sample, an analyzer, and a position-sensitive detector (PSD). The sample is a magnetic film of Co (700 Å) on a glass substrate. The size of the sample is 100×50×5 mm^2. An external magnetic field of 220 Oe and 3.5 kOe is applied at an angle of $\beta=80^0$ to the plane of the sample. The spatial resolution of PSD is 1.5 ÷ 2.5 mm [6]. The glancing angle of the incident beam and the sample to detector distance changed and were $\theta_0=6.10\pm0.30$ mrad and $\theta_0=3.17\pm0.10$ mrad, and 3 m and 8 m, respectively.

The polarization efficiencies of the polarizer and analyzer are different from unity, which reduces the efficiency of the polarization analysis method [7]. Figures 1 a,b depict the neutron intensity distribution as a function of the glancing angle of the reflected beam θ (the wavelength interval is 2.55 ÷ 6.67 Å, $\theta_0=3.17$ mrad). The indices 1 and 2 mark the regions of off-specular reflection and the index 3 stands for the specular reflection region. In a parallel external magnetic field (black circles) the spin-flip effect is absent but the intensity of the reflected neutrons in the "off,on" regime of the spin-flippers is different from zero in the specular reflection region 3. This is a background intensity in the measurement of spin-flip-related coefficients. It is seen that in the off-specular region the background decreases 30 times. In an inclined magnetic field (open symbols) neutron spin-flip is present. However, since the external field is small (Fig. 1a) the splitting is weak and all the beams lie in the specular region. In a strong external magnetic field (Fig. 2b) spin-flip neutrons experience off-specular reflection. Figures 2 a,b show the reflectivities in the off-specular regions 1 and 2 in the field 3.5 kOe ($\theta_0=6.10$ mrad). It is seen that neutrons that experience the spin transition "+-" are reflected to region 1 while "-+" transition neutrons are reflected to the region 2.

In the specular region (Fig 1a) the *effect/background* ratio is $\eta=(0.6-0.25)/0.25=1.4$, where the "effect" is the spin-flip-related intensity of neutrons. In the off-specular region (Fig. 1b) for the "off,on" neutrons at 4.3 mrad $\eta=(0.2-0.01)/0.01=20$ while for the "on,off" neutrons at 2.0 mrad $\eta=(0.08-0.008)/0.008=10$. So, as is seen at beam splitting the effect decreases about three times, but the effect to background ratio increases about ten times. Obviously, the efficiency of measurements in the off-specular reflection region increases the more the smaller the *effect/background* ratio in the specular region. For example, if $\eta=1/10$, the measuring time decreases 10 times.

On the other hand, in the off-specular region beam polarization grows. Figures 2 c,d show the beam polarization at the exit of the polarizer P and the neutron beam polarization behind the sample P_s at off-specular reflection (for the transition "+-" the polarization is negative and the polarization dependence is shown with an opposite sign in the Figure). It is seen that the neutron beam polarization at the exit of the polarizer decreases as the neutron wavelength grows while the polarization of neutrons reflected from the sample increases with growing neutron wavelength and tends to unity.

Thus, a combined use of total polarization analysis and neutron beam spatial splitting increases significantly the efficiency of neutron reflection measurements from magnetically noncollinear structures.

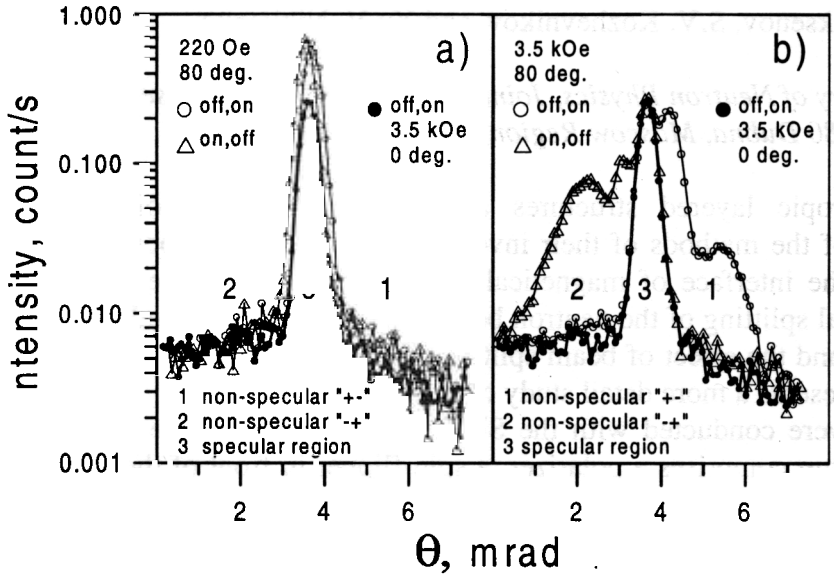

Fig.1. The neutron intensity as a function of the glancing angle of the reflected beam over the wavelength interval 2.55-6.67 Å.

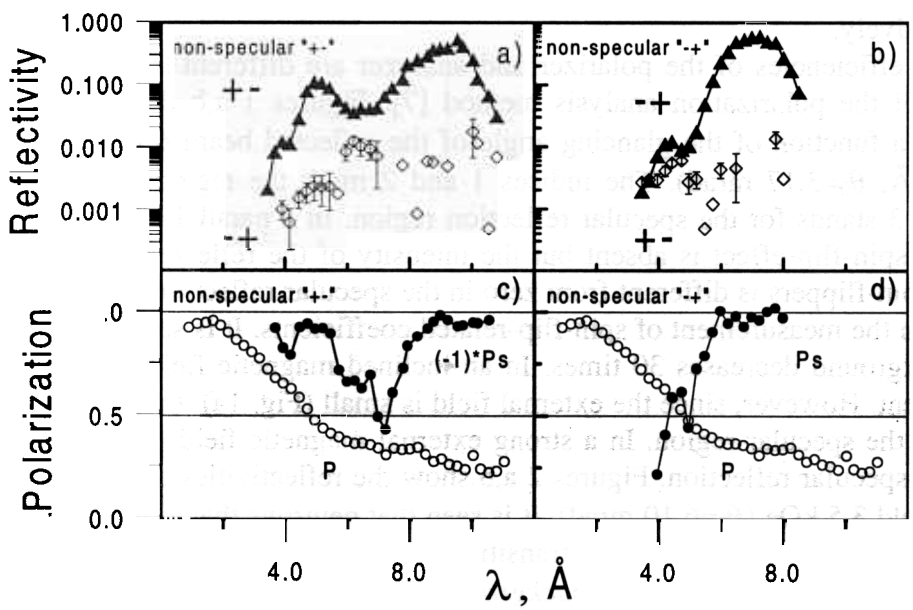

Fig. 2. The reflectivities (a,b) and the polarization degree of the beam (c,d) as a function of the neutron wavelength. P is the polarization of the beam falling on the sample; P_s is the polarization of the beam reflected from the sample.

[1] V.K. Ignatovich, Lett. JETP **28** (1978) 311 (in Russian).
[2] N.K. Pleshanov, Z. Phys. **94** (1994) 233.
[3] G.P. Felcher, S. Adenwalla, V.O. de Haan, A.A. van Well, Phys. **B 221** (1996) 494.
[4] V.L. Aksenov, E.B. Dokukin, S.V. Kozhevnikov, Yu.V. Nikitenko, A.V. Petrenko, J. Schreiber, Physica **B 234-236** (1997) 513.
[5] V.L. Aksenov, Yu.V. Nikitenko, S.V. Kozhevnikov, Phys. **B 297** (2001) 94.
[6] O.V.Fateev, G.A.Cheremukhina, S.P.Chernenko, Yu.V.Zanevskii, H. Lauter, V.V.Lauter, S.V.Kozhevnikov, Yu.V.Nikitenko, A.V.Petrenko, The position-sensitive detector for the spectrometer of polarized neutrons, Pribory i Tekhnika Experimenta **2** (2001) (in print).
[7] H. Fredrikze, R.W.E. van de Kruijs, Phys. **B 297** (2001) 143.

RBS INVESTIGATION OF MULTYLAYER STRUCRURES

A.P.Kobzev, A.Z.Kiss[a], A.Simon[a]

[a]*Institute of Nuclear Research of the Hungarian Academy of Sciences (ATOMKI), H-4001 P.O. Box 51, Debrecen, Hungary*

Artificial, synthetic compositionally modulated materials, such as Si/Ge multylayers, are not equilibrium structures. In particular, they have high interfacial gradients and sufficient atomic mobility, therefore changes in the composition profile are expected to occur even at moderate temperatures. The mechanism of their diffusion homogenization is still indefinite. First of all, the diffusion asymmetry (manifested in strong concentration dependence of interdiffusion coefficients) and strong porosity formation during diffusion mixing are the most important factors indicating the need of a better understanding of the above-mentioned process. Stability of the material, its resistance to composition changes, is obviously of importance for practical applications.

A study of the interdiffusion of the elements in amorphous Si/Ge multilayers has been carried out in cooperation with ATOMKI and the Department of Solid State Physics in Debrecen as part of a Co-ordinated Research Program of the International Atomic Energy Agency. This report is devoted to the studying of the elemental depth distributions in the amorphous Si/Ge multilayer structures prepared by DC magnetron sputtering from alternating elemental target onto (001) silicon wafers at the Department of Solid State Physics, University of Debrecen.

Si, Ge and O depth profiling in the Si/Ge multilayer structure consisting of 5 bilayers has been performed by the RBS and NRA methods[1,2]. The determination of the depth profiles of oxygen atoms in the investigated samples was carried out using the ^{16}O $(\alpha,\alpha)^{16}O$ nuclear reaction. A number of spectra were measured for the different angles of the incident beam with respect to the surface of the samples (φ ranging from 5^0 to 60^o) with 3.112 MeV helium ions.

Some of the measured spectra are shown in Fig.1. All silicon and germanium layers are seen in the spectrum as the separated peaks for $\varphi=6^o$. But the depth resolution is worse for deeper layers because of energy struggling. Nevertheless a layered structure with degraded interfaces is observed. From our analysis it is seen that all layers contain some oxygen impurity (10-13%), and a definite SiO_2 layer with a thickness of 177Å situated between the multilayer structure and the Si wafer is revealed. The oxygen peak shown in Fig. 1 corresponds to it (spectrum B). A sharp resonance in the ^{16}O $(\alpha,\alpha)^{16}O$ reaction for the 3.045 MeV is observed for all incident angles

except φ=60° (spectrum A, fig.1). For this incident angle and an initial energy of 3.112 MeV of ^{4}He ions resonance occurs in an oxygen free substrate.

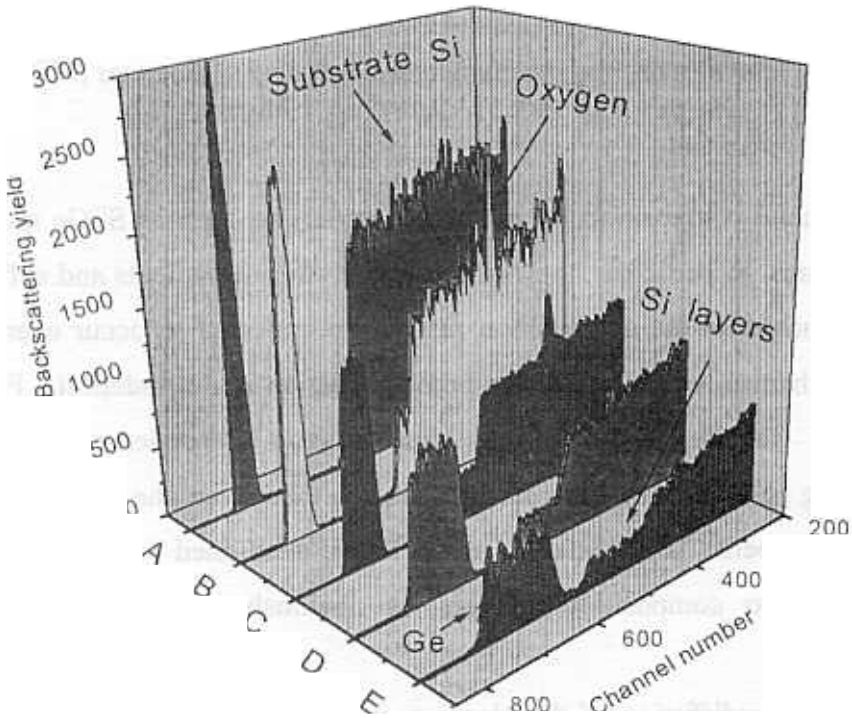

Fig.1 The backscattering spectra for the Si/Ge multylayer structure.
The incidence angle φ =6° –A, φ =10° – B, φ = 20° - C, φ =40° – D, φ = 60° – E.

Modelling has allowed us to determine the full thickness of the Ge-layer which is about 130 Å and that of the Si layer to be about 231 Å, including the mixed layers with the thickness 64.7 Å. It is essential that the same model has been used for the description of all the experimental spectra obtained at different incident angles. So, a complete structure of the sample has been reconstructed by this non-destructive technique.

Another sample consisting of three Si/Ge bilayers was investigated by the RBS method at an energy of 1 MeV. A better depth resolution has been reached because the stopping power increases for lower energies of ^{4}He ions. Figure 2 shows both the experimental and simulated spectra of ^{4}He ions scattered back at 170°, for an incident angle to the target surface of 10°, where the best resolution has been obtained. As it is seen there is fairly good agreement between the experimental and calculated spectra (every detail for an energy resolution of ΔE=15 keV). The elemental depth distribution derived from the RBS spectra is shown in the table.

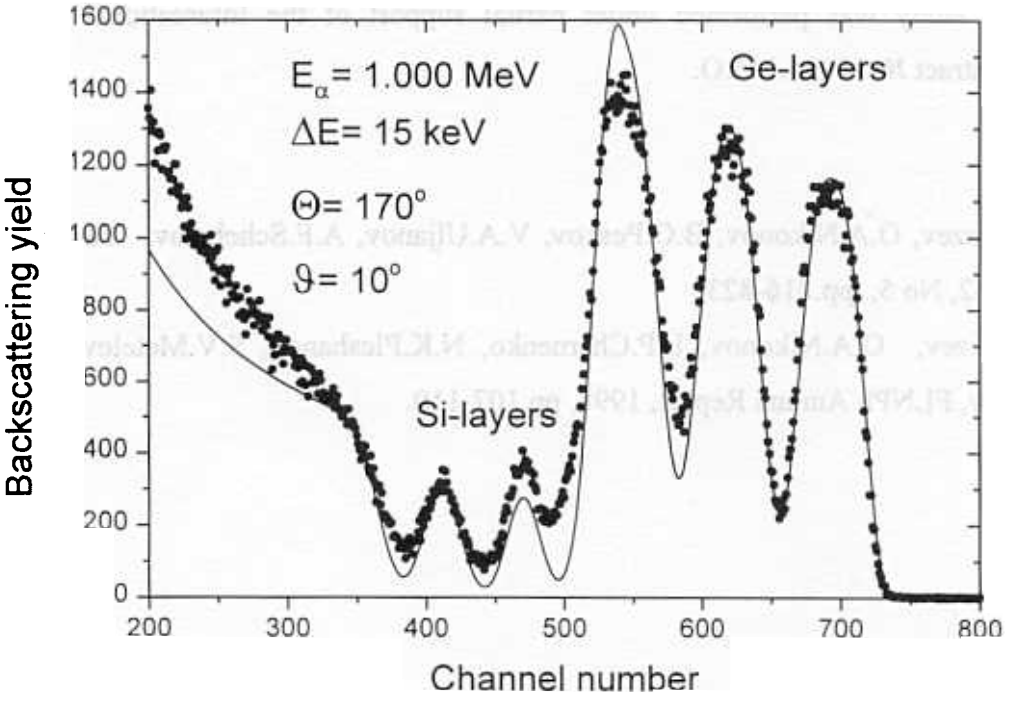

Fig. 2. The experimental (points) and calculated (line) backscattering spectra for three Si/Ge bilayer sample.

Depth Å	Element Concentrations (at %)	
	Ge	Si
100.5	0.00	100.0
147.2	50.0	50.0
296.3	100.0	0.00
343.1	50.0	50.0
429.5	0.00	100.0
476.3	50.0	50.0
618.5	100.0	0.00
665.3	50.0	50.0
755.7	0.00	100.0
802.5	50.0	50.0
942.5	100.0	0.00
989.3	50.0	50.0
2000	0.00	100.0

The thickness of the full period obtained from this measurement is 320 Å. It consists of a Ge layer with a thickness of 143 Å, a Si layer with a thickness of about 90 Å and two layers of

mixed content with a thickness of about 47 Å. As interdiffusion at room temperature is practically zero, the mixed layer refers to surface roughnesses.

This study was performed under partial support of the International Atomic Energy Agency, contract № 10036.1/ RO.

References

[1] A.P.Kobzev, O.A.Nikonov, B.G.Peskov, V.A.Uljanov, A.F.Schebetov. Yadernaya Fizika. 1999, Vol. 62, No 5, pp.816-823.

[2] A.P.Kobzev, O.A.Nikonov, L.P.Chernenko, N.K.Pleshanov, S.V.Metelev, A.F.Schebetov, V.A.Uljanov, FLNPh Annual Report, 1998, pp.107-110.

SURFACE EXCITATIONS IN THIN HELIUM FILM IN SILICA AEROGELS.

I.V.Bogoyavlenskii, A.V.Puchkov, H.J.Lauter*, and Andrei Skomorokhov

Institute for Physics and Power Engineering, 249020, Bondarenko sq.1, Obninsk, Russia
Institute Laue Langevin, F-38042, Grenoble Cedex 9, France

Liquid helium attracts the attention of experimentalists and theorists nowadays even more than as previously. The long term studies of the excitation spectrum of bulk liquid helium on DIN-1M, DIN-2PR, and DIN-2PI spectrometers (IBR-30 and IBR-2 reactors) brought interesting results [1] in parallel with the investigations at other neutron centres. During the last years the interest in this field widened from bulk helium to helium in confined geometries. So properties of helium in porous media like exfoliated or powdered graphite, zeolites, sponge, vycor glass, aerogels, and xerogels were explored. It turns out that liquid helium properties in porous media differ from those of bulk helium and depend on geometrical parameters and type of porous media [2]. It appears that the surface properties of the media have great influence on the helium adjacent to the confinement. Neutron scattering studies of thin liquid helium films on different substrates are started now to get an understanding of these properties

Neutron scattering data, taken from helium films on graphite show the existence of the ripplons at the liquid-gas interface of the film and of excitation, which have the character of 2-dimentional rotons at the solid-liquid interface of the film, called layered-phonon-roton modes [3]. In very thin films only these two excitations may exist, whereas in the example of a 4-monolayer film parts of the bulk phonon-roton curve are visible.

The interest to study the excitations in a ^{4}He film adsorbed on silica aerogel is, that ^{4}He films in the aerogel shows a different behavior compared to films on other substrates as e.g. graphite. Apart from this, bulk helium in aerogel, graphite or vycor shows a different exponent for the temperature dependence of the superfluid component near the lambda-transition. This may be related again to the different interface properties of the helium film excitations on the fractal aerogel surface.

The results presented here are the first attempt of the investigation of liquid helium films on the DIN-2PI spectrometer.

The incident neutron energy was 2.58 meV. The range of scattering angles and of momentum transfers was 11° - 133° and 0.2-2.0A^{-1}, respectively. The aerogel sample had been annealed at 600C under a pressure of ~10^{-4} torr during 3 days. The MAX ORANGE cryostat has been used together with the special sample-stick for the filling of the aerogel sample with helium gas under pressure-temperature control. The measurement was carried out at a sample temperature of T=1.55K. Three different coverages have been tested: corresponding to a monolayer (20 l of normal

pressure helium gas), a 2-3 layer film (58 l), and a filling of 68 l, a coverage at which the signal from the bulk roton is just appearing. It should be mentioned that the first layered part of the helium film adjacent to the aerogel substrate is amorphous and is added to the aerogel substrate.

Fig.1 shows the experimental dynamic structure factor of aerogel+helium at constant angle at T=1.55K. No background was subtracted. The scattered intensity at the angle of 133° picks up the signal from the roton region near the momentum transfer of $Q=1.9A^{-1}$. At T=1.55K the energy of the bulk roton (BR) and the layer roton (LR) are very close. Perhaps the influence of the bulk roton appears already at the 58 l-coverage due to its high intensity.

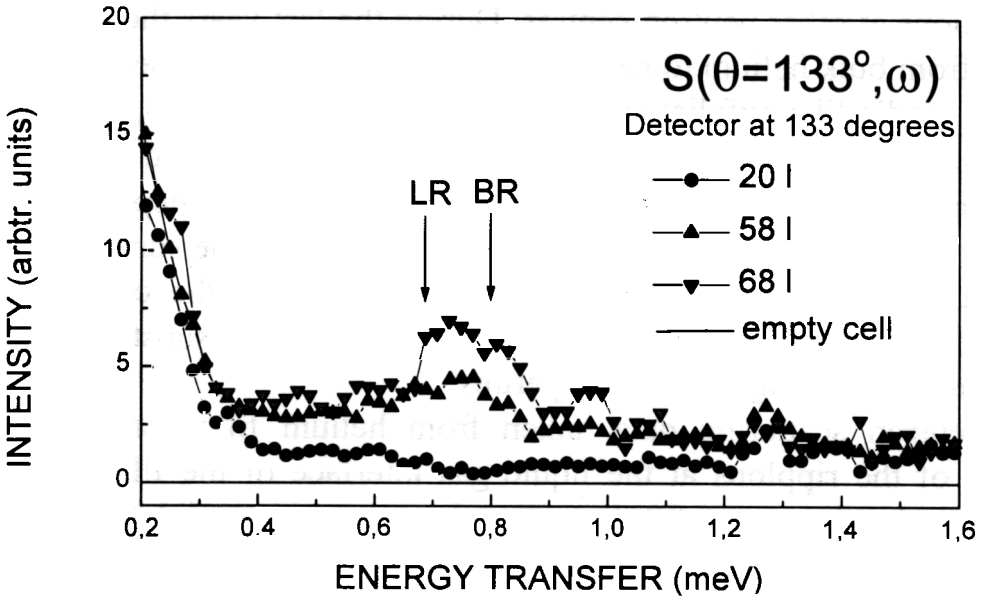

Fig.1. Experimental dynamic structure of a thin 4He film adsorbed on silica aerogel for three coverages at T=1.55K. No difference between the 20 l-coverage spectrum and the empty cell spectrum was found. The scattering angle corresponds to a momentum transfer near the "roton minimum". No background was subtracted. Arrows mark the values of the bulk roton (BR) energy [3] and the layer roton (LR) energy [3].

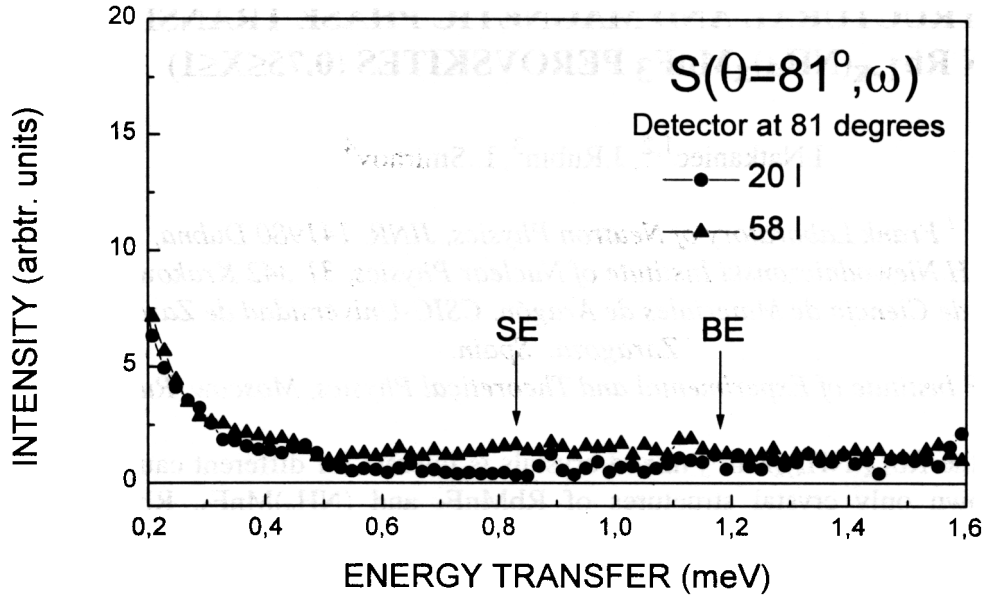

Fig.2. Experimental dynamic structure of thin 4He film adsorbed at silica aerogel for two coverages at T=1.55K. The scattering angle corresponds to a momentum transfer near the "maxon" region. The energy values of the bulk excitation (BE) [4] and the surface excitation (SE) [3] differ considerably. No background was subtracted.

The first experiment on the DIN-2PI spectrometer with thin helium films shows the good performance of this spectrometer even without cold source. In particular the very low background is an absolute necessary feature to observe the very small signals.

REFERENCE

1. I.V.Bogoyavlenskii, A.V.Puchkov and A.Skomorokhov, "The association between temperature dependence of liquid ^{4}He scattering law and the phenomena of the Bose condensation", Physica B276-278 (2000) 465.
2. M.Chan, N.Mulders and J.Reppy, Physics Today (August 1996) 30.
3. B.Clements, H.Godfrin, E.Krotscheck, H.J.Lauter, P.Leiderer, V.Passiouk, "Excitations in a thin liquid ^{4}He film from inelastic neutron scattering", Phys.Rev.B53 (1996) 12242.
4. I.V.Bogoyavlenskii, A.V.Puchkov, A.N.Skomorokhov and S.V.Poupko, "Neutron scattering study of ^{4}He $S(Q,w)$ at the phonon-maxon region", Physica B234-236(1997)324.

STRUCTURAL AND MAGNETIC PHASE TRANSITIONS IN $Rb_{1-x}(NH_4)_xMnF_3$ PEROVSKITES ($0.75 \leq X \leq 1$)

I.Natkaniec[1,2], J.Rubin[3], L.Smirnov[4]

[1] *Frank Laboratory of Neutron Physics, JINR, 141980 Dubna, Russia*
[2] *H.Niewodniczanski Institute of Nuclear Physics, 31-342 Krakow, Poland*
[3] *Instituto de Ciencia de Materiales de Aragón, CSIC-Universidad de Zaragoza, Zaragoza, Spain.*
[4] *SSC RF Institute of Experimental and Theoretical Physics, Moscow, Russia.*

The study of the $Rb_{1-x}(NH_4)_xMnF_3$ mixed crystals is interest for different causes. Until recent time there are known only crystal structures of $RbMnF_3$ and $(NH_4)MnF_3$. $RbMnF_3$ has the cubic perovskite structure (space group Pm3m, Z=1) with Rb ion at the body centre which is surrounded by 12 ions of F on the cube edges and 4 ions of Mn on the cube vertex. $RbMnF_3$ do not undergo the phase transition in wide interval of the temperature from 50 to 300 K [1,2]. $(NH_4)MnF_3$ is isomorphous to $RbMnF_3$ at high temperatures but undergoes phase transition at 183 K from orientational disordered cubic phase to the orientational ordered orthorhombic crystal structure with space group Pnma, Z=4 [3,4]. Ionic radii of ammonium and rubidium are very close and on the one hand it is possible to expect that $RbMnF_3$ and $(NH_4)MnF_3$ will form the solid solution in wide concentration region. On the other hand by the analogy with the mixed crystals of the type of $K_{1-x}(NH_4)_xI$ [5], $K_{1-x}(NH_4)_xSCN$ [6], $Rb_{2-x}(NH_4)_xSO_4$ [7] it is possible to expect that the $Rb_{1-x}(NH_4)_xMnF_3$ mixed crystals will form the phase diagram with the region of orientational glass at low temperatures.

The measurements of the inelastic incoherent neutron scattering (IINS) and neutron powder diffraction (NPD) are carried out on the $Rb_{1-x}(NH_4)_xMnF_3$ mixed crystals with the concentrations x=0.75 and 1.0 at 20, 100 and 200 K. The NPD spectra and the IINS spectra for $(NH_4)MnF_3$ at 25, 100 and 200K are presented in Figs. 1 and 2(a,b). The NPD spectra are measured at different Bragg angles in order to have the possibility to obtain diffraction spectra with good resolution and to fix crystal structure transformation with the help of the detector at big Bragg angle and to obtain magnetic reflection on big interplane distances with the help of the detector on small Bragg angle.

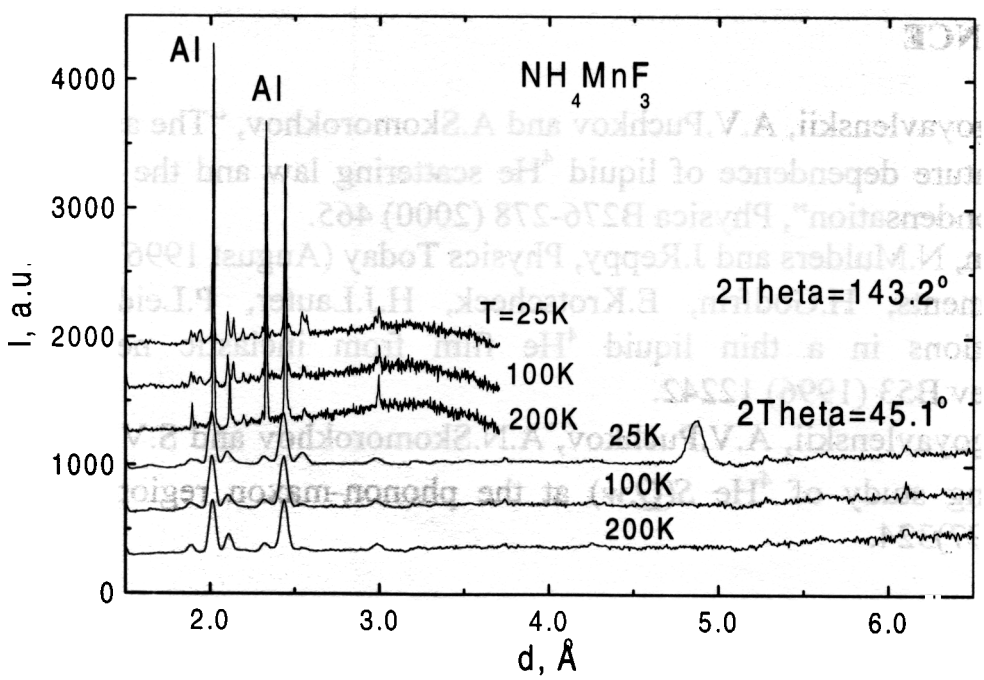

Fig. 1. The NPD spectra from $(NH_4)MnF_3$ at different temperatures and Bragg angles.

In accordance with determined crystal stuctures of different phases of $(NH_4)MnF_3$in [4] diffraction profile of NPD at 200 K is satisfactorily described by cubic perovskite structure with lattice parameter a=4.2364 Å, at 100 K it is described by orthorhombic lattice with parameters a=5.9539, b=8.5572 and c=5.9585 Å and at 25 K magnetic orthorhombic phase is observed with lattice parameters a=5.9524, b=8.5579 and c=5.9577 Å. Magnetic reflections are observed near 4.8 and 2.5 Å, showing antiferromagnetic ordering.

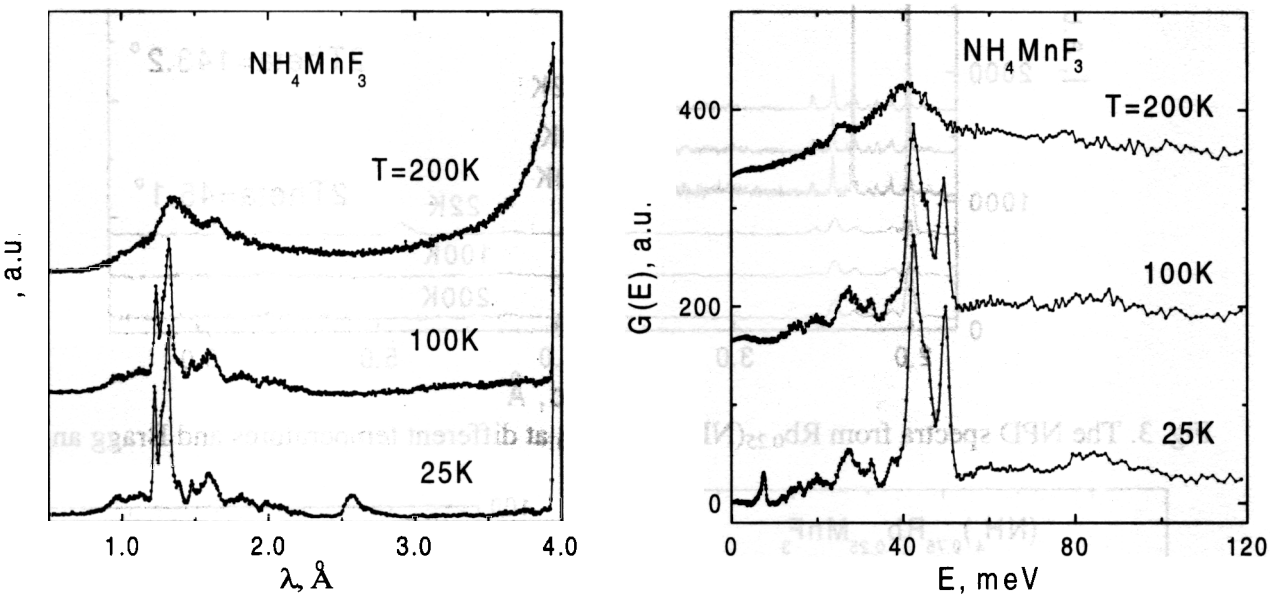

a) b)

Fig. 2. The IINS spectra (a) and G(E) spectra (b) for $(NH_4)MnF_3$ at different temperatures.

The IINS spectrum of $(NH_4)MnF_3$ at 200 K has the significant contribution of quasielastic incoherent neutron scattering (QINS) (see Fig. 2a) that confirms that in the cubic phase ammonium ions are orientationally disordered. The contribution of QINS intensity is absent in the IINS spectra at 100 and 25 K that is confirms orientational ordering of ammonium ions in the orthorhombic phase. The spectra of generalized phonon density of states G(E) for $(NH_4)MnF_3$ at 25, 100 and 200 K are presented in Fig.2b. At temperatures 25 and 100 K in orthorombic phase G(E) presents in energy region 10-35 meV the translational lattice modes and in the energy region 35-50 meV the librational modes in accordance with the results of [4]. However there is difference between G(E) spectra at 25 and 100 K which is concluded in the absence of assymetric peak near 7.6 meV. If one take attention that difference between NPD spectra of $(NH_4)MnF_3$ at 25 and 100 K is in the absence of magnetic reflections so it is possible to do the conclusion that the energy near 7.6 meV can be described to magnetic excitations or spin wave modes..

The substitution of 25% ammonium ions by rubidium in $(NH_4)MnF_3$ do not change the succession of phase transitions from orientational disordering cubic perovskite phase to orientational ordering orthorhombic phase with successive magnetis phase transition in antiferromagnetic phase. This conclusion succeeds from the NPD spectra obtained at 200, 100 and 22 K and are presented in Fig.3. The spectra of IINS intensities and G(E) of $Rb_{0.25}(NH_4)_{0.75}MnF_3$ are presented in Fig. 4(a,b) respectively. The IINS and G(E) spectra for $Rb_{0.25}(NH_4)_{0.75}MnF_3$ are analogous to appropriate spectra of $(NH_4)MnF_3$ but at 22 and 100 K its are more smeared. The energy of spin wave mode is approximately 7.9 meV. Earlier authors of [8] measured spin-wave dispersion relation for $RbMnF_3$ and obtained approximate value of the energy on the boundary of Brillouein zone 8.6 meV. If one takes attention that Neel temperature for $RbMnF_3$ is higher than for NH_4MnF_3 then the value 7.6 meV is real for spin wave energy of NH_4MnF_3 on the boundary of Brillouin zone.

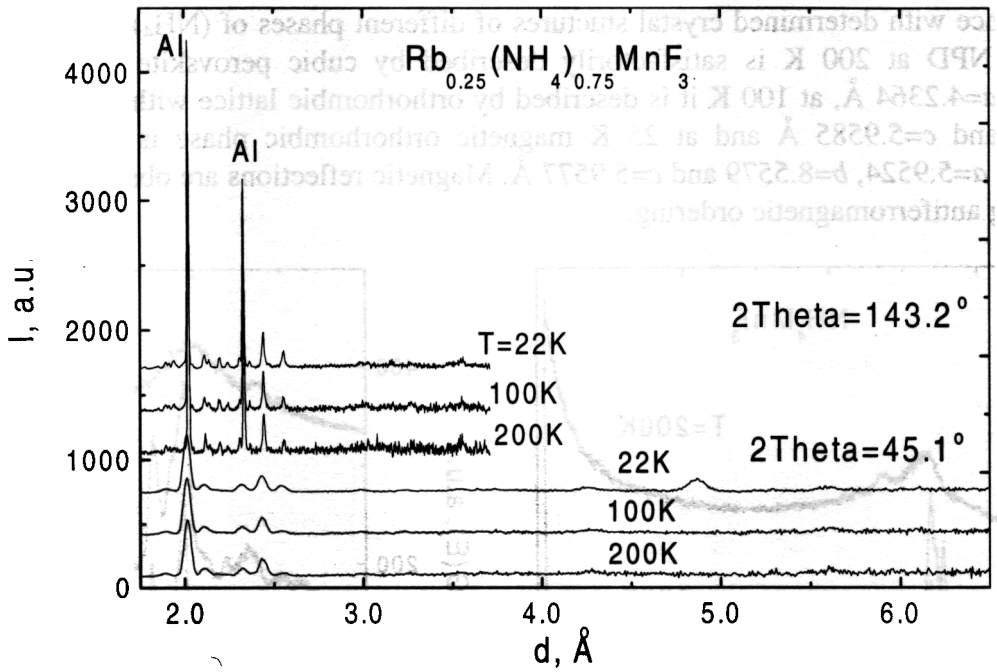

Fig. 3. The NPD spectra from $Rb_{0.25}(NH_4)_{0.75}MnF_3$ at different temperatures and Bragg angles.

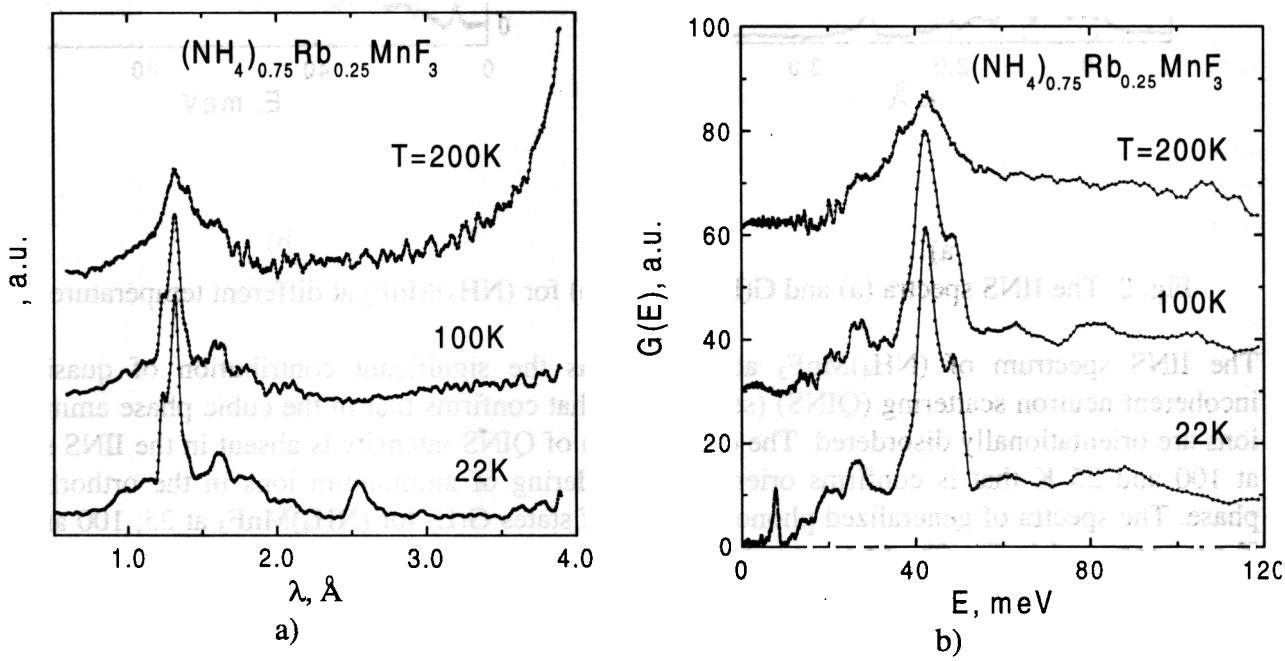

Fig. 4. The IINS spectra (a) and G(E) spectra (b) for $Rb_{0.25}(NH_4)_{0.75}MnF_3$ at different temperatures.

References:

1. C.G.Windsor, R.W.H.Stevenson, Proc.Phys.Soc., **87**, 501 (1966).
2. D.T.Teaney, V.L.Moruzzi, B.E.Argyle, J.Appl.Phys., **37**, 1122 (1966).
3. M.A.Laguna, M.L.Sanjuan, V.M.Orera, J.Rubin, E.Palacios, M.C.Pique, J.Bartolome, J.F.Berar, J.Phys.:Condens.Matter, **5**, 283 (1993).
4. J.Rubin, E.Palacios, J.Bartolome, J.Rodriguez-Carvajal, J.Phys.:Condens.Matter, **7**, 563 (1995).
5. I.Natkaniec, L.S.Smirnov, Physica B **234&236** (1997) 409-411.
6. I.Natkaniec, L.S.Smirnov, A.I.Solov'ev. Physica B **213&214** (1995) 667-668.
7. I.Natkaniec, M.L.Martinez-Sarrion, L.Mestres, L.S.Smirnov, L.A.Shuvalov, Physica B, Condens.Matter, **241-243**, 487 (1998).
8. C.G.Windsor, R.W.H.Stevenson, Proc.Phys.Soc., **87**, 501 (1966).

Phonons in coarse grained and plastically deformed vanadium

S.Danilkin[1], M. Jung[2], H. Wipf[2]

[1] *Institute of Physics and Power Engineering, 249020 Obninsk, Russia*
[2] *Technische Universitat Darmstadt, D-64289 Darmstadt, Germany*

Aim of the study was to observe changes in the vibrational density of states ($g(\varepsilon)$) of vanadium due to deviations from perfect crystalline order. We investigated differences in the $g(\varepsilon)$ between plastically deformed and well-annealed vanadium. Vanadium is most suitable material for measurements of $g(\varepsilon)$ because it scatters neutrons nearly exclusively incoherently.

The measurements were done with DIN-2PI spectrometer at incident energy of neutrons 10 meV in scattering angle range of 70 ÷ 130°. Samples were vanadium plate of 1 mm thickness and the same material after the cold deformation (90 %). The second sample was consisted of 10 plates to have the same total thickness as the annealed vanadium sample. The time-of-flight spectra of two vanadium samples normalised by the area of the elastic peak are shown in Fig. 1. The spectrum of the deformed vanadium has higher intensity in the low energy region at $\varepsilon \approx 4$ meV.

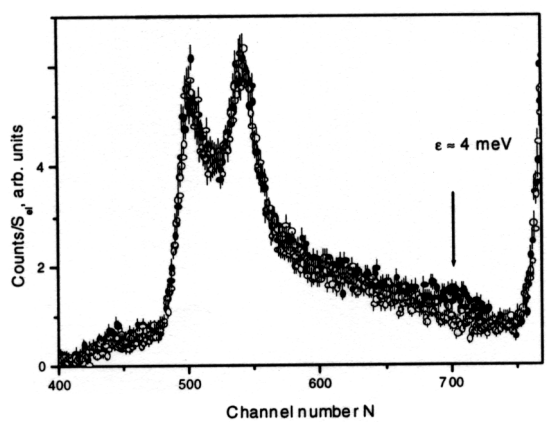

Fig. 1 INS spectrum of deformed (•) and annealed (#) vanadium

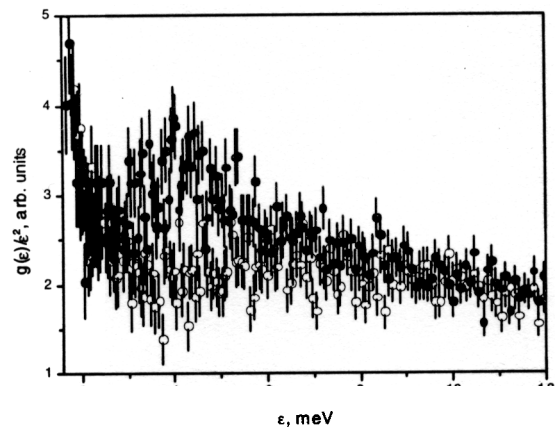

Fig. 2 Function $g(\varepsilon)/\varepsilon$ of deformed (•) and annealed (#) vanadium

These additional modes are also seen in the $g(\varepsilon)$ of deformed vanadium, but they are less pronounced there. To observe the deviation of $g(\varepsilon)$ from the Debye spectrum the function $g(\varepsilon)/\varepsilon^2$ was calculated for both samples (Fig. 2). This function for the annealed vanadium has a nearly linear behaviour in the energy range 2 ÷ 12 meV while that of deformed vanadium has a pronounced peak at $\varepsilon \approx 4$ meV. At frequencies lower then 2 meV the increase of intensity is connected with

contribution from the elastic line. The similar excess soft modes designated as the "boson peak" were observed earlier in different glasses and amorphous alloys [1]. INS study of austenitic steels showed that an enhancement of the low-frequency VDOS may also be induced by cold plastic deformation - the distinct increase of the VDOS in the low-frequency range between 8 and 16 meV was observed after cold plastic deformation (70%) in Fe-18Cr-10Mn-16Ni-0.5N alloy [2]. Also these changes are in fact very similar to those found for nanocrystalline materials [3, 4] demonstrated recently that the low-frequency increase of the $g(\varepsilon)$ results predominantly from atoms in or at grain boundaries or surfaces.

References

A. Meyer, J. Wuttke et al., Phys. Rev. B, **53**, 12107 (1996).

2. S.Danilkin, V.Minaev, V.Sumin: Preprint No. FEI-2371, 1994, Institute of Physics and Power Engineering, Obninsk, Russia.
3. U.Stuhr, H.Wipf, K.H.Andersen, H.Hahn, Phys. Rev. Lett. **81**, 1449 (1998)
4. A.Kara, T.Rahman, Phys. Rev. Lett. **81**, 1453 (1998)

Quasielastic scattering investigation of liquid phosphorus oxychloride $POCl_3$

A.G.Novikov[a], O.V.Sobolev[b]

[a]State Scientific Centre of RF – Institute of Physics and Power Engineering. 249020, Obninsk, Kaluga reg., Russia.

[b]Frank Laboratory of Neutron Physics, Joint Institute for Nuclear Research, 141980, Dubna, Moscow Reg., Russia.

In the frame of neutron scattering experiments on liquid $POCl_3$ [1] we have measured and analysed the quasielastic component of its common double-differential scattering cross section (DDSCS). The detail description of the procedure and results of analysis will be published [2]. Now we give short information, concerning with these questions.

For separation of quasielastic component from the total DDSCS and its subsequent analysis the following procedures were performed:

- time-of-flight DDSCS were transformed into energy scale and then by interpolation into the form $S(Q,\varepsilon)$ at Q = const, where $S(Q,\varepsilon)$ is the scattering law (or dynamic scattering function) and ε - energy transfer.;
- from the total DDSCS the inelastic contribution was removed; it was shown by calculations and practically [3,4], that for $S(Q,\varepsilon)$ in the vicinity of quasielastic peak the inelastic contribution can be considered as a flattened background with relatively small amplitude, so the approximation appropriate for $S(Q,\varepsilon)$ can be written:

$$S(Q,\varepsilon) = \{S_q(Q,\varepsilon) + [a + b\varepsilon]\} \otimes R(Q,\varepsilon) \qquad (1)$$

where the expression in square brackets represents inelastic scattering effects and sign $\otimes$ means the convolution of natural scattering law with resolution of spectrometer $R(Q,\varepsilon)$, measured by special vanadium sample.

The shapes and halfwidths (full width at halfmaximum, FWHM) of quasielastic peaks arise from a number of effects, including coherent and incoherent scattering, translation and rotation components of diffusion motions (the detail expressions for DDSCS of quasielastic scattering on molecular liquids with mixed (coherent and incoherent) scattering are given in [5,6]). It turned out, that in our case some alleviation takes place, because according to results of [7] on peak widening of Rayleigh scattering effects of rotation diffusion in liquid $POCl_3$ are expected to be negligible. This conclusion can be conformed by the estimation of rotation diffusion coefficient in liquid $POCl_3$ on the basis of Einstein – Stokes law for rotation motion [8]:

$$D = kT/8\pi\eta R^3 \qquad (2)$$

Substituting in (2) viscosity (for room temperature η = 1.06 cP [9]) and effective radius of $POCl_3$ molecule ($R_{eff} \approx 3$ A), we find: $D_{rot} \approx 1.3 * 10^{10}$ c^{-1} and

$$\Delta E_{rot} = 2D_{rot} * h \sim 0.02 \text{ meV}.$$

Keeping in mind the resolution of our spectrometer for elastic scattering ($\Delta E_o \sim 0.1 \div 0.13$ meV), we are led to conclusion, that these effects can not be observed under our experimental conditions. So, the later analysis of experimental quasielastic DDSCS will be performed under assumption, that we deal only with effects of translation diffusion. In so doing, we have supposed, the quasielastic peaks are superposition of two components, hypotically corresponding to coherent and incoherent contributions:

$$S_q(Q,\varepsilon) = \{1/\pi \Sigma_{i=1,2}\, c_i(Q)\Delta E_i(Q)/(\varepsilon^2+\Delta E^2{}_i)\} \otimes R(Q,\varepsilon), \qquad (3)$$

with their own Q-dependened weights and halfwidths $c_i(Q)$, $\Delta E_i(Q)$, which are shown on fig. 1 and 2. It follows from fig. 8, that the common integral intensity of quasielastic scattering (the sum of coherent and incoherent contributions: $c_1(Q)+c_2(Q) = \int_{-\infty}^{\infty} S_q(Q,\varepsilon)d\varepsilon$)) is not far from diffraction results [1].

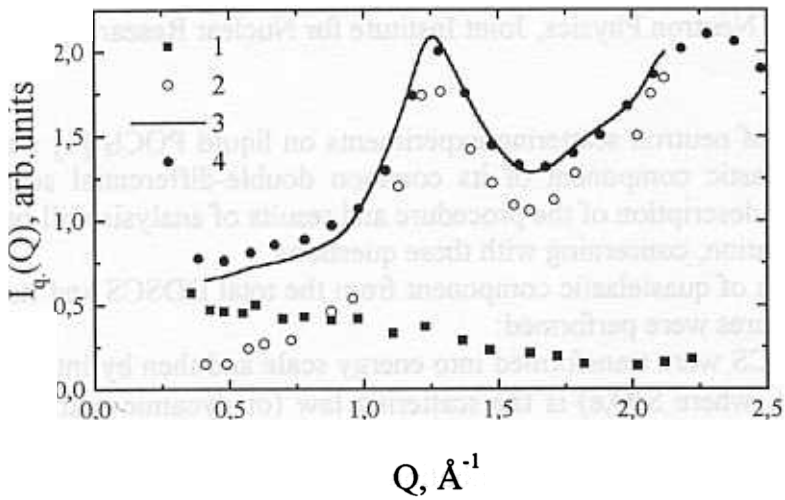

Fig. 1. Integral intensity of quasielastic scattering.
1 – incoherent component; 2 – coherent component; 3 – sum of coherent and incoherent components; 4 – angular differential scattering cross section (diffraction experiment, see [1]).

The curve 1 of fig.1 gives the integral intensity of incoherent quasielastic scattering, which can be expressed as [10]:

$$S_q(Q) \sim \Sigma_s/4\pi \exp\{-u^2Q^2\}\,, \qquad (4)$$

where $W = u^2Q^2$ is Debye - Waller factor and u^2 - mean – sqare amplitude of molecular vibration, infered from analysis of this curve, is:

$(u^2)^{1/2} = (0.55 \pm 0.05)$Å.

Now draw our attention to fig. 2. Curve 1 corresponds to the common halfwidth of quasielastic peak (in one-Lorentzian representation). The main contribution in the intensity of this peak arises from coherent scattering, so, its halfwidth demonstrates some evidence of oscillatory behaviour, being distinctive feature of coherently scattering liquids [11] (its first minimum coincides with the position of the fist structure factor maximum, $Q \sim (1.2 - 1.3)$ Å^{-1}, see [1]). We did not try to describe this curve by Scold model [12], because it contains a remarkable portion of incoherent scattering. Curve 2 of fig. 2 shows the halfwidth of incoherent quasielastic peak (two-Lorentzian representation). In small Q-region curves 1 and 2 are near each other (coherent effects are weak), but then they come apart, and curve 2 tends to flatten, what is commonly understood, as an evidence of jump diffusion process, which is distinctive for highly associated liquids. Fitting curve 2 by mixed diffusion model [13], assuming the diffusion process to be superposition of two mechanisms: continuous and jump ones, we get parameters of model: common selfdiffusion coefficient D, coefficient of collective diffusion (diffusion of particle together with nearest surrounding) D_o and the residence time of molecule at the temporary equilibrium position τ_0:

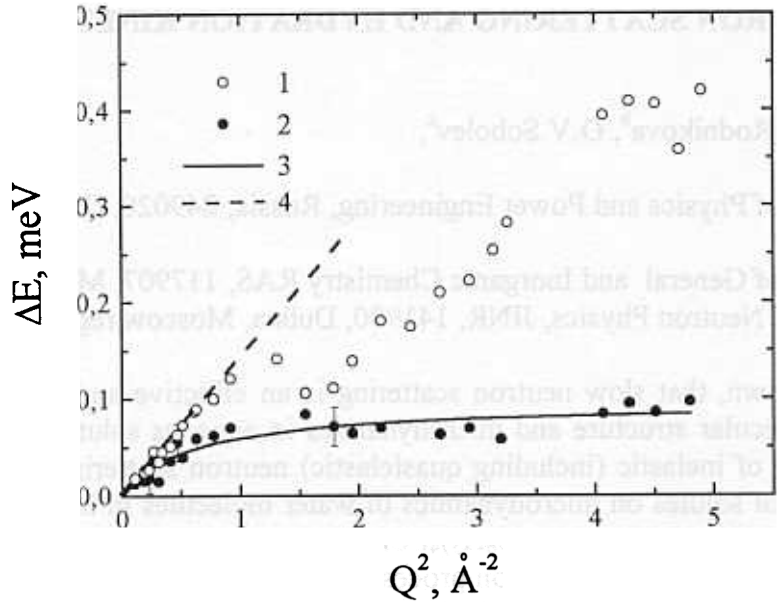

Fig. 2. Halfwidths of quasielastic peaks.
1 – common halfwidth of quasielastic peak (one – Lorentzian description); 2 – halfwidth of incoherent component of quasielastic peak; 3 – description of incoherent quasielastic peak halfwidth with the model of mixed diffusion.

$D = (2.3 \pm 0.8)$ см^2/с;
$D_o \sim 0.02$ см^2/с;
$\tau_0 = (7 \pm 1)*10^{-12}$ с.

The sizable errors of the parameters given arise from the procedure of decomposition, as well as from restricted experimental statistics.

The work was performed under financial support of Russian Federation Program "Actual Directions in Condensed Matter Physics", project "Neutron studies".

References

1. A.Novikov, D.Seliverstov, O.Sobolev. Annual Reportn of FLNP, JINR, Dubna, 1999, p. 89-90.
2. A.Novikov, O.Sobolev. J. of Mol. Liquids. (in press).
3. S.Iskanderov, A.Novikov. Rus. J. Phys. Chem. 56 (1982) 1469.
4. A.G.Novikov, M.N.Ivanovskii, V.V.Savostin, A.L.Shimkevich, O.V.Sobolev, M.V.Zaezjev. J. Phys.: Cond. Matter. 8 (1996) 3525.
5. F.Bermejo, F.Batallant, E.Enciso, R.White, A.Dianoux, W.Howells. J. Phys.: Cond. Matt. 2 (1990) 1301.
6. F.Bermejo, M.Alvarez, M.Garcia-Hernandez at al. J. Phys.: Cond. Matt. 3 (1991) 851.
7. R.Pappalardo, A.Lempicki. J. Appl. Phys. 43(1972) 1699.
8. G.Sposito. J. Chem. Phys. 74 (1981) 6943.
9. K.C.Krasnov. Molecular constants of inorganic compounds. Leningrad, "Nauka", 1977, 448 p., (in russian).
10. I.Gurevich, L.Tarasov. Low-energy neutron physics. North-Holland, Amsterdam, 1968, 608 p.
11. J.Copley, S.Lovesey. The Dynamic Properties of Monatomic Liquids. Rep. Prog. Phys. 38 (1985) 461.
12. K.Skold. Phys. Rev. Lett. 19 (1967) 1023.
13. V.Oskotskii. Sov. Phys. Solid State. 5 (1963) 789.

INELASTIC NEUTRON SCATTERING AND HYDRATION KINETICS IN AQUEOUS SOLUTIONS

A.G.Novikov[a], M.N.Rodnikova[b], O.V.Sobolev[c]

[a]SSC RF – Institute of Physics and Power Engineering, Russia, 249020, Obninsk, Kaluga reg., Russia.
[b]Kurnakov Institute of General and Inorganic Chemistry RAS, 117907, Moscow, Russia.
[c]Frank Laboratory of Neutron Physics, JINR, 141980, Dubna, Moscow reg., Russia

It is well known, that slow neutron scattering is an effective and adequate instrument for investigation of molecular structure and microdynamics in aqueous solutions. Last years we have performed a number of inelastic (including quasielastic) neutron scattering experiments, aimed to clarify an influence of solutes on microdynamics of water molecules in ionic (LiCl, CsCl, [1]) and hydrophobic ($(CH_3)_4NCl$, $(C_4H_9)_4NCl$, $(C_6H_5)_4PCl$, [2,3]) aqueous solutions. From results of these experiments the information about diffusion processes (coefficients of self- and collective diffusion, residence times of molecules, static and dynamic hydration numbers) and vibration-rotation dynamics (in the form of generalyzed frequency distribution, GFD) for water molecules, incorporated in hydration shells was extracted. Basing on these data the comparative analysis of ionic and hydrophobic hydration effects was performed with the conclusion, that the ionic hydration destroys the hydrogen bond network in surrounding water, and conversely hydrophobic one retains it to be untouched.

The dynamical information, above mentioned, corresponds to the equilibrium state of solutions under study. But for chemical kinetics it is more important to understand a way, which proceed transition processes in solutions, when a disturbance of equilibrium takes place, for example, by instant appearance of a charge on one of solute and to be able to describe the time-space picture of transition from old equilibrium state of a solution to new one. This problem, known in contemporary literature as "fast hydration dynamics" (FHD) takes last decade much attention and is under intensive investigation experimentally [4], theoretically [5] and by molecular dynamics (MD) simulation [6]. The frequently used characteristic for description of the transition processes mentioned is called as time correlation function of hydration energy S(t). At present there are some theories, dealing with FHD, which give the relation between S(t) and GFD **g (ω)** of hydration water molecules. In particular (see [5]):

$$S(t) = 1 - kT\left\langle (\delta V)^2 \right\rangle^{-1} \int d\omega\, g(\omega) \frac{(1-\cos(\omega t))}{\omega^2} \qquad (1)$$

where $(\delta V)^2 = \mathbf{kT(1-1/\varepsilon) / a}$ – mean-square fluctuations of interaction potential and **a** – radius of sphere beyond which ranges the solution can be considered as structureless continuum with dielectric constant ε.

Our fist attempt to use this relation in combination with GFD for water molecules, obtained by us, demonstrates the qualitative agreement between experimental and calculated (by MD and theory) S(t) curves (see fig. 1). So, there are grounds to believe, the inelastic neutron scattering method among with information about the equilibrium microdynamics of aqueous solutions can be applied for investigation of transition processes, associated with fast hydration dynamics.

The work was performed under financial support of Russian Federation Program "Actual Directions in Condensed Matter Physics", project "Neutron studies".

References

1. A.Novikov, M.Rodnikova, O.Sobolev. J. Mol. Liquids. **82**, 83, (1999).

2. A.G.Novikov, M.N.Rodnikova, V.V.Savostin, O.V.Sobolev. Chem. Phys. Letters. **259**, 391, (1996)
3. A.Novikov, M.Rodnikova, J.Barthel, O.Sjbolev. J. Mol. Liquids.**79**, 203, (1999).
4. S.Rosenthal, X.Xie, M.Du, G.Fleming. J. Chem. Phys. **95**, 4715, (1991).
5. R. Stratt, M.Cho. J. Chem. Phys. **100**, 6700, (1994).
6. M.Maroncelli, G.Fleming. J.Chem. Phys. **89**, 5044, (1988).

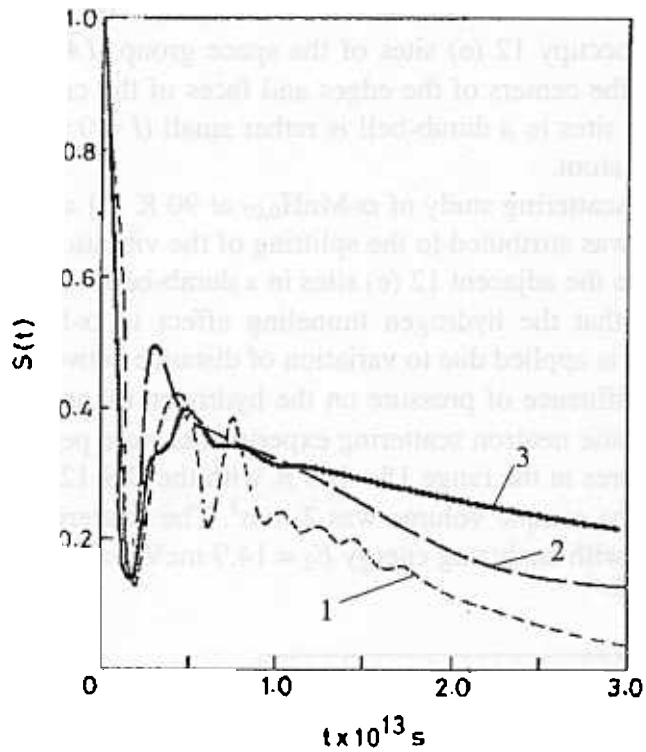

Fig.1. Time correlation function of hydration energy S(t):
1 – MD simulation [6];
2 – theoretical calculation [5];
3 – calculation by equation (1) with the use of the experimental g(ω).

THE EFFECT OF PRESSURE ON HYDROGEN TUNNELING IN α-Mn

V.E.Antonov[a], V.P.Glazkov[b], D.P.Kozlenko[c], B.N.Savenko[c], V.A.Somenkov[b], V.K.Fedotov[c]

[a] *Institute of Solid State Physics RAS, 141432 Chernogolovka Moscow Reg., Russia*
[b] *Russian Research Center "Kurchatov Institute", 123182 Moscow, Russia*
[c] *Frank Laboratory of Neutron Physics, JINR 141980 Dubna Moscow Reg., Russia*

Recently it was shown that under pressure the solubility of hydrogen in α-Mn increases up to a few atomic percent [1]. A neutron diffraction investigation of α-$MnH_{0.07}$ [2] revealed that hydrogen atoms randomly occupy 12 (e) sites of the space group ($I\bar{4}3m$) which form dumb-bells situated rather far apart, at the centers of the edges and faces of the cubic unit cell of α-Mn. Since the distance between 12 (e) sites in a dumb-bell is rather small (l = 0.68 Å) each dumb-bell can be occupied by the only one H atom.

In inelastic neutron scattering study of α-$MnH_{0.07}$ at 90 K [3] a strong peak at 6.3 meV was observed in INS spectra. It was attributed to the splitting of the vibrational ground state of hydrogen due to tunneling between the the adjacent 12 (e) sites in a dumb-bell.

One would expect that the hydrogen tunneling effect in α-$MnH_{0.07}$ may undergo sharp changes if external pressure is applied due to variation of distance between the adjacent H positions.

To investigate the influence of pressure on the hydrogen tunneling effect in α-$MnH_{0.07}$ and α-$MnH_{0.04}$, incoherent inelastic neutron scattering experiments were performed at high pressures up to 3 GPa and low temperatures in the range 15 - 100 K with the DN-12 spectrometer using sapphire anvil high pressure cells. The sample volume was 2 mm^3. The scattering angle was $2\theta = 90°$. The pyrolytic graphyte analyzer with analyzing energy E_2 = 14.9 meV was used for experiments.

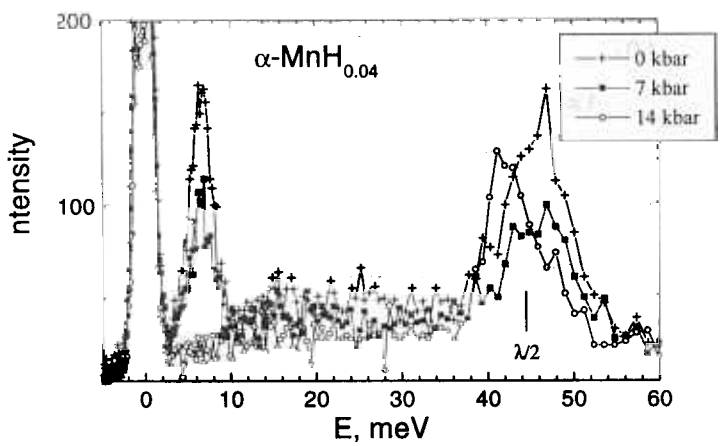

Fig. 1. Inelastic neutron scattering spectra of α-$MnH_{0.04}$ at different pressures obtained with the DN-12 spectrometer using pyrolytic graphite analyzer.

The INS spectra of α-$MnH_{0.04}$ at different pressures are shown in Fig. 1. Hydrogen tunneling peak becomes smaller with the pressure increase. At pressures higher than 10 kbar it completely disappears. In the pressure range up to 10 kbar the tunneling peak position in INS spectra remains nearly the same with the pressure increase. These results show that application of external pressure suppresses the hydrogen tunneling effect in α-Mn.

The work has been supported by Russian Foundation for Basic Research, grant № 00-02-17199.

1. V.E.Antonov et al., Scripta Materialia 34, 1331 (1996).
2. V.K.Fedotov et al., J. Phys.: Condens. Matter 10, 5255 (1998).
3. A.I.Kolesnikov et al., Physica B 263-264, 421 (1999).

NEUTRON DIFFRACTION STUDY OF PYRIDINIUM PERRHENATE AT AMBIENT AND HIGH PRESSURES.

L. Bobrowicz-Sarga [1,2], J. Wąsicki[1], A.I. Beskrovnyi[2], P.Czarnecki[1] I. Natkaniec[2,3] W. Szczepański[1]

[1]*Institute of Physics, A. Mickiewicz University, 61-614 Poznań, Poland*
[2]*Frank Laboratory of Neutron Physics, JINR, 141980 Dubna, Russia*
[3]*H. Niewodniczański Institute of Nuclear Physics, 31-342 Kraków, Poland*

Pyridine, Py = C_5H_5N, forms salts with many strong mineral and organic acids. These salts belong to a family of molecular – ionic crystals where a solid – solid transition related to changes in ion dynamics occurs. It has recently been found that ferroelectricity exist in pyridinium tetrafluoroborate, perchlorate and perrhenate [1-3]. At atmospheric pressure these salts reveal two solid – solid transitions, and a higher one appears to be the Curie point of the intermediate ferroelectric phase. Both phase transitions are connected with the ordering of the cation and anion reorientations.

As a continuation of our study of pyridinium salts, we report here the results of the neutron powder diffraction study of pyridinium perrhrnate as a function of temperature and pressure. Pyridinium perrhenate, $[C_5\ NH_6\ ]^+[ReO_4]^-$, (hereafter denoted as $PyReO_4$) reveals two structural transitions, at 250 and 333 K. The x-ray diffraction study performed at room temperature shows that the salt crystallises in the orthorombic system, space group $Cmc2_1$. At 333 K, the ferroelectric crystal transforms to Cmcm symmetry and at 250 K, to the space group Pbca.

Neutron scattering experiments were carried out using the time of flight spectrometer NERA-PR installed on the IBR-2 pulsed neutron source of JINR in Dubna. The studied polycrystalline sample at ambient pressure was placed in the cryostat cooled by a close–cycle helium refrigerator permitting temperature changes from 20 – 300 K within an accuracy of 0.5 K. Measurements of neutron scattering spectra as a function of hydrostatic pressure have been performed on the same spectrometer with the aid of a high pressure set-up. The high-pressure helium gas arrangement consist of a U-11GC gas compressor (UNIPRESS, Poland), GNC-400 high-pressure cell and a top loaded cryostat with adjustable temperature in the 78-350 K temperature range. The polycrystalline sample was a cylindrically shaped by an additional aluminium container inserted into the high-pressure cell. The use of helium gas as a pressure-transmitting medium enables the achievement of purely hydrostatic conditions inside the cell. Measurements under high pressure were carried out in the temperature range 90 –310 K and pressures from 0.01 to 370 MPa. Part of the diffraction spectra, between 300 and 350 K at ambient pressure, were measured on the DN-2 diffractometer at the IBR-2 reactor of JINR in Dubna.

The neutron powder diffraction spectra made it possible to determine the experimental intermolecular distances d used in the calculation of unit cell parameters with the AUTOX program [4]. At each temperature, the measured interplanar distances are adequately described by the orthorombic unit cell. Figure1 shows the temperature dependence curves of elementary unit cell parameters. A monotoneus change of all elementary unit cell parameters up to 250 K indicates that the crystalline symmetry of $PyReO_4$ remains unchanged in the temperature range 25-250 K. All phase transitions are clearly seen on the temperature dependence curves of lattice parameters. The phase transition at 250 K, from low-temperature phase III to intermediate phase II, is marked by jumps of the parameters a and c and smaller jumps of the parameters b and volume V. At 333 K the

crystal transforms from phase II to high-temperature phase I. This phase transition corresponds to small discontinuous change of all elementary unit cell parameters.

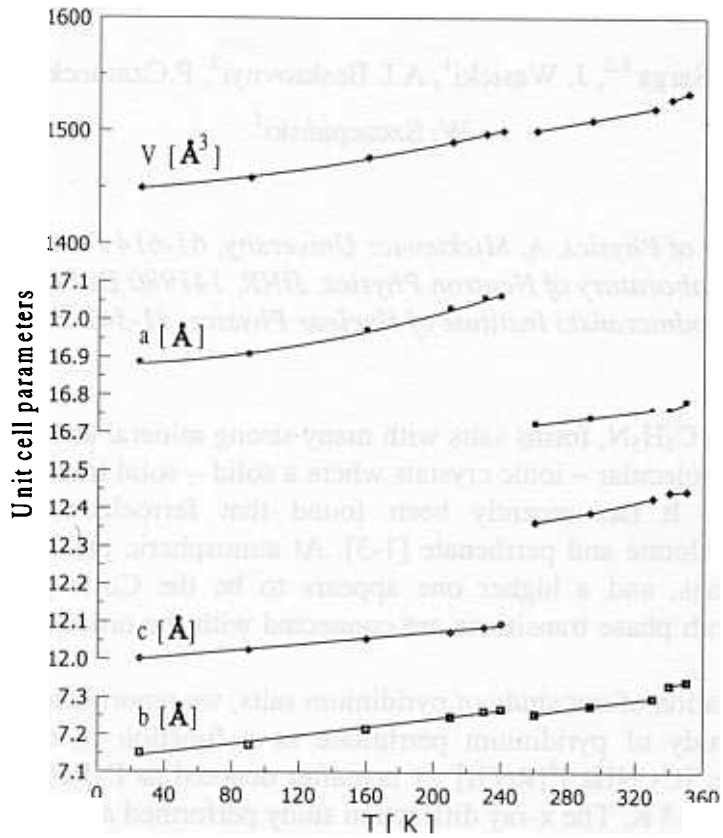

Fig.1. The temperature dependence of the elementary unit cell parameters of $PyReO_4$.

The temperature dependence of the elementary unit cell volume was used to determine the isobar thermal expansion coefficient α from the relative slope of the V_p (T) curves. The values of the parameters α for three phases of the $PyReO_4$ crystal are collected in Table1.

Table1. The isobar thermal expansion coefficient for three phases of $PyReO_4$.

		$\alpha=1/V(dV/dT)_p$ [1/K] x10^{-3}
$PyReO_4$	Phase I	0.347 (p=0.1 MPa)
	Phase II	0.175 (p=0.1 MPa)
	Phase III	0.163 (p=0.1 MPa)

It has recently been observed by some authors (by dielectric and NMR methods) that the new phase transition takes place due to high pressure. To examine the influence of high pressure on the phase transition, the neutron diffraction spectra as a function of hydrostatic pressure were measured at the temperature: 90, 230, 260, and 310 K. Figure 2 presents the most interesting result obtained at the temperature 230K. The upper diffraction spectrum corresponding to the low-temperature phase III was measured in the cryostat cooled by a helium refrigerator. Taking the high-pressure cell background (the lowest spectrum) into account, the spectrum obtained at 80 MPa can be identified as the spectrum of phase III.

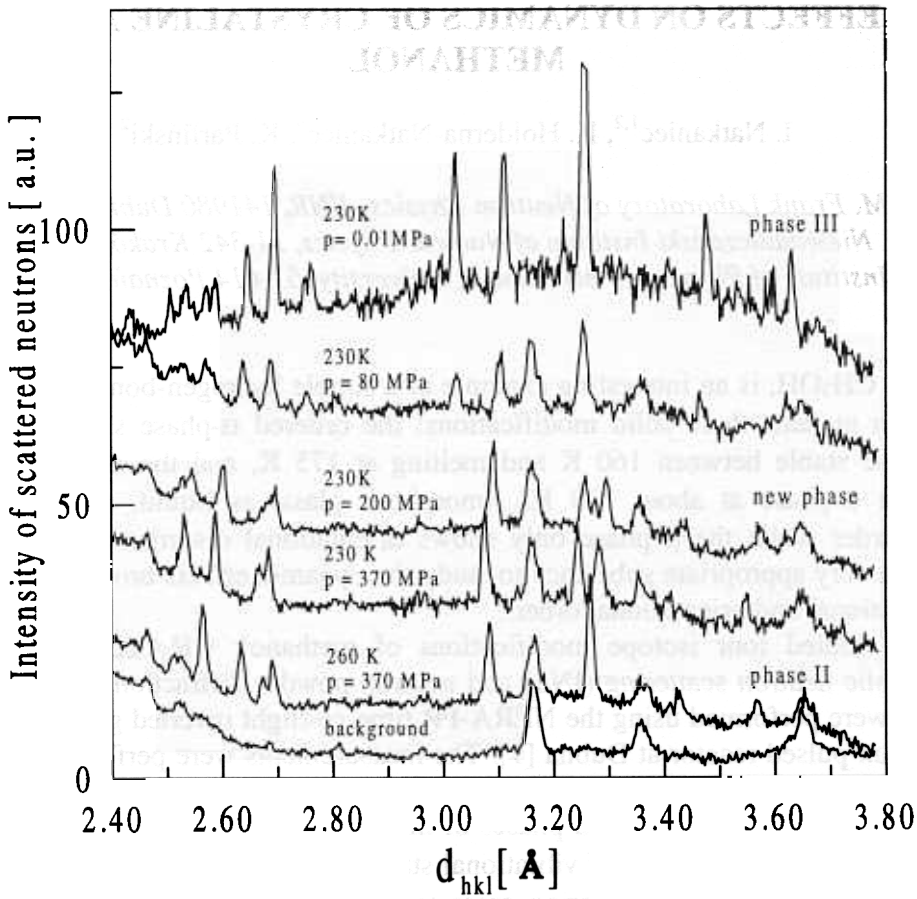

Fig.2. The neutron powder diffraction spectra of pyridinium perrhenate measured with a close-cycle helium refrigerator set-up at ambient pressure (upper spectra at 0.1 MPa) and with a high-pressure set-up.

Visual examination of the spectra measured at 200 and 370 MPa indicate that they differ from this one characteristic for phase III as well as for phase II (spectrum at 260 K). From this we may conclude that the $PyReO_4$ crystal reveals a structural transition to the new phase at 230 K and about 200 MPa. At 230 K and 370 Mpa, the crystal remains in the same phase and then transforms to phase II at equal pressure but higher temperature.

Acknowledgments

The authors express their sincere thanks to Mr. T.Sarga and Mr S.I. Bragin for their help with neutron scattering measurements.

References

[1] P. Czarnecki, W. Nawrocik, Z. Pająk and J. Wąsicki, Phys.Rev.**B 49**, 1511 (1994).
[2] P. Czarnecki, W. Nawrocik, Z. Pająk and J.Wąsicki, J.Phys.Cond. Matter, **6**, 4955 (1994).
[3] J. Wąsicki, P. Czarnecki, Z. Pająk, W. Nawrocik and W. Szczepański, J.Chem.Phys.**107**, 576 (1997)
[4] V.B. Zlokazov, Comput. Phys Commun., **85**, 415 (1995)

ISOTOPIC EFFECTS ON DYNAMICS OF CRYSTALINE AND VITREOUS METHANOL

I. Natkaniec[1,2], K. Hołderna-Natkaniec[3], K. Parliński[2]

[1] *I.M. Frank Laboratory of Neutron Physics, JINR, 141980 Dubna, Russia.*
[2] *H. Niewodniczański Institute of Nuclear Physics, 31-342 Kraków, Poland.*
[3] *Institute of Physics, A. Mickiewicz University, 61-614 Poznań, Poland.*

Methanol, CH_3OH, is an interesting example of a simple hydrogen-bonded organic crystal. It is known to exist in at least three solid modifications: the ordered α-phase stable below 160 K, the disordered β-phase stable between 160 K and melting at 175 K, and the amorphous phase, which transforms to the α-phase at about 130 K. Amorphous glass, as liquid, shows translational and orientational disorder while the β-phase only shows orientational disorder of plastic crystals. This makes methanol a very appropriate substance to study the dynamic effects brought forward due to loss of long-range positional and orientational order.

We have studied four isotope modifications of methanol: CH_3OH, CH_3OD, CD_3OH and CD_3OD, by inelastic neutron scattering (INS) and neutron powder diffraction (NPD), simultaneously. The experiments were performed using the NERA-PR time-of-flight inverted geometry spectrometer at the IBR-2 high flux pulsed reactor at Dubna [1]. The measurements were performed at temperature 20 K, over a wide range of momentum and energy transfer. These allow us to investigate the vibrational spectra up to 2000 cm^{-1} for all condensed phases of methanol whose structures were controled by the NPD method. The generalized density of vibrational states - G(ω) (weighed over square amplitudes of atom vibrations and their neutron scattering cross-sections) for the crystalline α-phase at 20 K, is shown in Fig. 1.

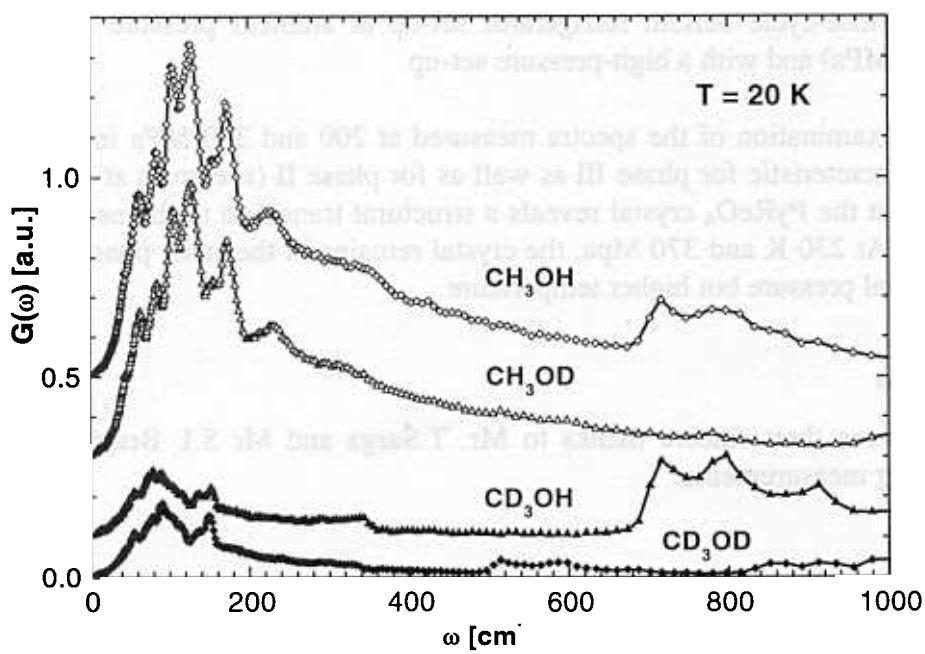

Fig. The weighed densities of vibrational states G(ω) of crystalline methanol in the solid α-phase at 20 K for differently deuterated molecules.

The glass samples were prepared by fast quenching of room temperature liquid samples (in a liquid nitrogen bath) just before placing them into the measuring cryostat well, which was cooled to about 20 K. The sample container was an aluminum plate 16x7 cm^2 of ca.1 mm internal thickness. A comparison of the G(ω) spectra of vitreous and crystalline samples of CH_3OD and CD_3OH, is shown in Fig. 2.

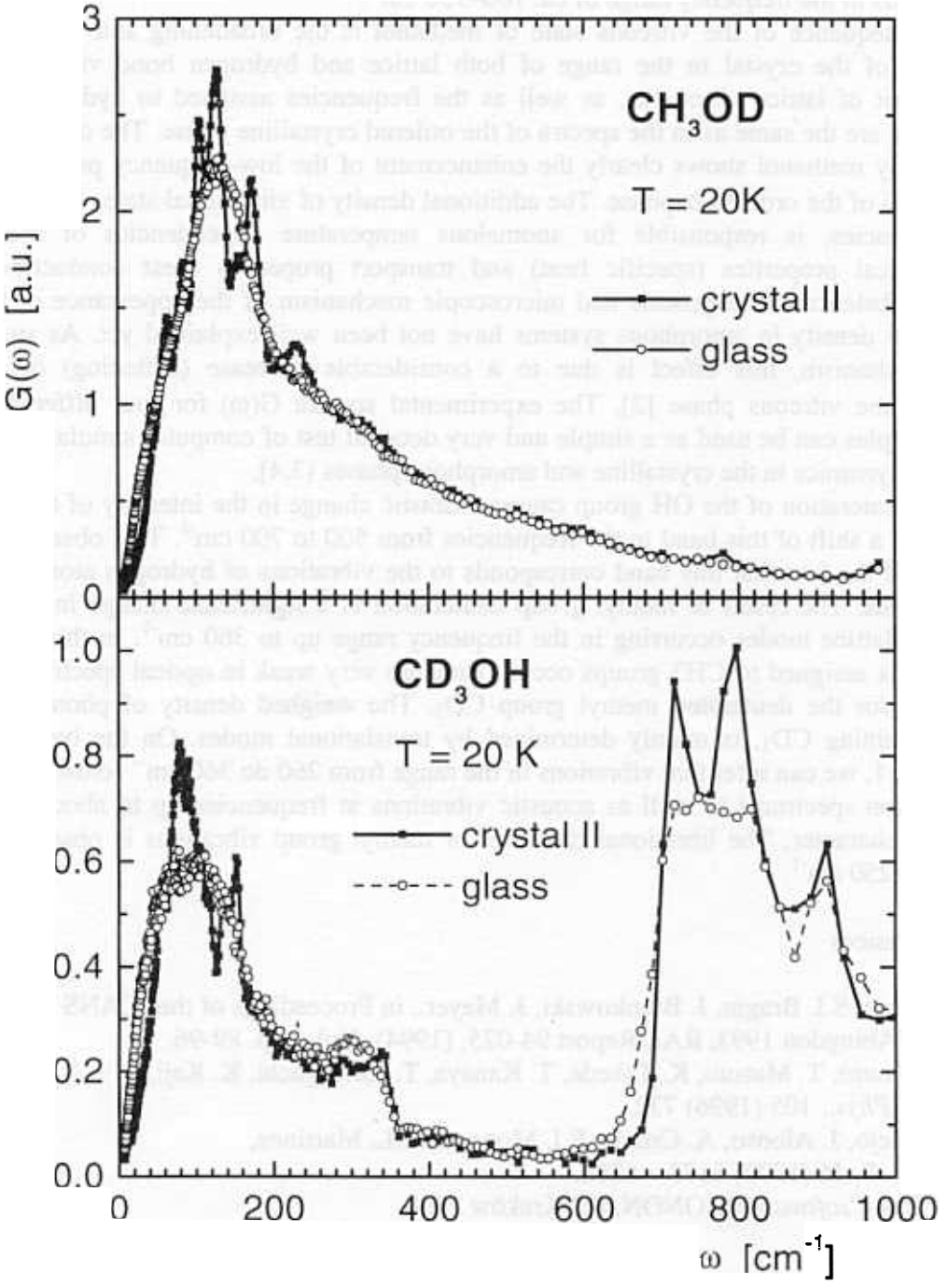

Fig. 2. The weighed densities of vibrational states G(ω) for vitreous and crystalline methanol at 20 K and for partly deuterated CH_3OD and CD_3OH molecules.

The intensities of the G(ω) spectra presented in figures 1 and 2 were normalised to equal mass and volume of the sample, and equal number of neutrons incident on the sample.The different isotope modifications of methanol molecules allow as to study the contribution of methyl group rotations and hydroxyl dynamics to lattice dynamics. Wide range of energy transfer allows one to display the effects of disorder in the whole frequency range of lattice dynamics up to ca. 400 cm^{-1}, and on the dynamics of hydrogen bonds in the frequency range of ca. 700–950 cm^{-1}.

A consequence of the vitreous state of methanol is the broadening and smoothing of bands characteristic of the crystal in the range of both lattice and hydrogen bond vibrations. The high-frequency limit of lattice vibrations, as well as the frequencies assigned to hydrogen bonds, in the vitreous phase are the same as in the spectra of the ordered crystalline phase. The density of vibrational states of glassy methanol shows clearly the enhancement of the low-frequency part comparing to the reference G(ω) of the ordered α-phase. The additional density of vibrational states in the vitreous phase at low-frequencies, is responsible for anomalous temperature dependencies of the macroscopic thermodynamical properties (specific heat) and transport properties (heat conduction), typical of amorphous substances. The genesis and microscopic mechanism of the appearance of the additional vibration state density in amorphous systems have not been well explained yet. As suggested in the proposed mechanism, this effect is due to a considerable decrease (softening) of the librations frequency in the vitreous phase [2]. The experimental spectra G(ω) for four differently deuterated methanol samples can be used as a simple and very detailed test of computer simulations of molecular glass former dynamics in the crystalline and amorphous phases [3,4].

The deuteration of the OH group causes a drastic change in the intensity of the band at 700 to 950 cm^{-1}, and a shift of this band to the frequencies from 500 to 700 cm^{-1}. This observation is a direct confirmation f the fact that this band corresponds to the vibrations of hydrogen atoms in the chain of hydrogen bonds. The result of methyl group deuteration is a significant change in the intensity and frequency of lattice modes occurring in the frequency range up to 360 cm^{-1}. In this range the strong libration bands assigned to CH3 groups occur. They are very weak in optical spectroscopy and in the IINS spectra for the deuterated methyl group CD_3. The weighed density of phonon states, for the samples containing CD_3, is mainly determined by translational modes. On the basis of the spectra shown in Fig. 1, we can infer that vibrations in the range from 260 do 360 cm^{-1} (close to the limit of the lattice vibration spectrum) as well as acoustic vibrations at frequencies up to about 90 cm^{-1}, have a translational character. The librational character of methyl group vibrations is observed in the range from ~100 to 250 cm^{-1}.

References

[1]. I. Natkaniec, S.I. Bragin, J. Brankowski, J. Mayer., in Proceedings of the ICANS XII Meeting, Abingdon 1993, RAL Report 94-025, (1994), Vol. I., p. 89-96.

[2]. O. Yamamuro, T. Matsuo, K. Takeda, T. Kanaya, T. Kawaguchi, K. Kaji, *J. Chem. Phys.*, 105 (1996) 732.

[3]. F.J. Bremejo, J. Alonso, A. Criado, F.J. Monpean, J.L. Martinez, *Phys. Rev. B*, **46** (1992) 6173 – 6286.

[4]. K. Parliński, *software* PHONON, IFJ Kraków 2000.

COMPUTER SIMULATION AND NEUTRON SCATTERING INVESTIGATION OF DYNAMICS OF UREA: $CO(NH_2)_2$ AND $CO(ND_2)_2$

I. Natkaniec[1,2]. K. Parliński[2], K. Hołderna-Natkaniec[3], J. Mayer[2]

[1] *I.M. Frank Laboratory of Neutron Physics, JINR, 141980 Dubna, Russia.*
[2] *H. Niewodniczański Institute of Nuclear Physics, 31-342 Kraków, Poland.*
[3] *Institute of Physics, A. Mickiewicz University, 61-614 Poznań, Poland.*

Physical and chemical properties of urea NH_2-CO-NH_2 have been studied for many years. The crystal structure of urea is relatively simple and has been resolved as one of the first structures of organic compounds. Under normal pressure the tetragonal structure of crystalline urea of the D^3_{2h} symmetry with two molecules in the elementary unit does not change with temperature varied from the melting point to that of liquid helium [1]. The chemical singularity of this structure is the fact that each oxygen atom from the CO group accepts four hydrogen bonds N-H...O.

Computer simulations of the dynamics of molecular crystals are much in demand but very difficult because of the degree of complication of their structure. This dynamics includes lattice modes corresponding to mutual vibrations of molecules and vibrations of atoms in molecules (internal modes), also dependent on the crystal field. Recently, the programs for simulation of structure and dynamics of molecular crystals based on generalised semi-empirical field force methods and the "*ab initio*" calculations based on the methods of quantum chemistry have been tested. The authors of [2] presented results of computer simulation of the dispersion curves for deuterated urea obtained by a combination of these two calculation methods.

Here we report a comparison of the calculated phonon densities of state weighted by the amplitudes of atoms vibrations in the given modes - $G(\omega)$, with the experimental one, which can be determined from the spectra of inelastic neutron scattering on polycrystalline samples. The spectra of inelastic neutron scattering on the powdered samples of $CO(NH_2)_2$ and $CO(ND_2)_2$ were performed at 20 K, on a NERA spectrometer [3] at the pulse reactor IBR-2 in Dubna. The experimental densities of phonon states $G(\omega)$ were determined in the approximation of single-phonon scattering for frequencies up to 1000 cm^{-1}. A satisfactory agreement was obtained between the calculated and experimental results in the range of the lattice modes frequencies (see Fig. 1, below 220 cm^{-1}). These spectra are very little dependent on deuteration of the urea molecule. The significant isotopic shifts were observed for the internal vibrations in the range from 300 to 1000 cm^{-1}. The frequencies of these vibrations calculated by the *ab initio* method are in a worse agreement with experiment than those of lattice vibrations. However the calculated intensities of internal bands and their isotopic shifts permit a reliable interpretation of the experimental spectra.

1. S. Swaminathan, B.M. Craven, R.K. McMullan, Acta Cryst. **B40** (1984) 300-306.
2. K. Parlinski, G. Chapuis, J. Chem. Phys., **110** (1999) 6406-6411.
3. I. Natkaniec, S.I. Bragin, J. Brankowski, J. Mayer., in Proceedings of the ICANS XII Meeting, Abingdon 1993, RAL Report 94-025, (1994), Vol. I., p. 89-96.

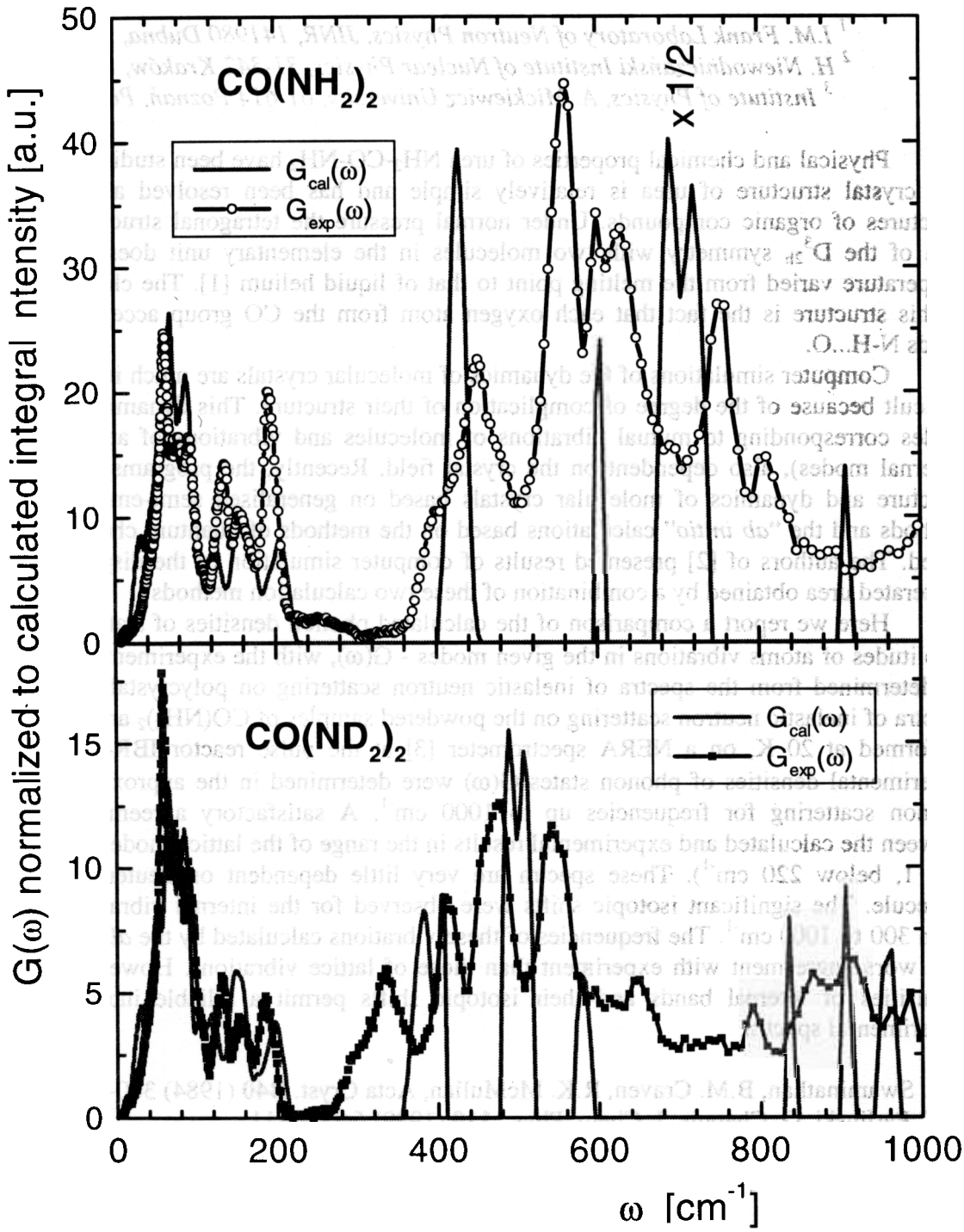

Fig. Calculated and experimental neutron scattering weighted vibrational density of states of crystalline urea at 20 K.

INVESTIGATION OF THE NEUTRON-ELECTRON INTERACTION

E.L.Enik, L.V.Mitsyna, V.G.Nikolenko, S.S.Parzhitskii, A.B.Popov, G.S.Samosvat, R.V.Khariuzov

Frank Laboratory of Neutron Physics, JINR, Dubna

The problem of refining of the length of the neutron-electron interaction, b_{ne}, remains topical since its existing experimental estimates lie beyond the error limit and also, because it is necessary to know this length to clarify the physical nature of the mean square charge radius of the neutron.

To model more precisely the experiments under preparation to measure b_{ne} from the inelastic scattering of neutrons on a single-atom noble gas, the algorithm describing the angular distribution of neutrons scattered on gas atoms in thermal motion was improved.

The Monte-Carlo calculation of the neutron scattering anisotropy for a "precise" gas sample of argon was repeated and the results were compared with the analytical calculation by the formulas from [1]. The results are illustrated in Fig.1.

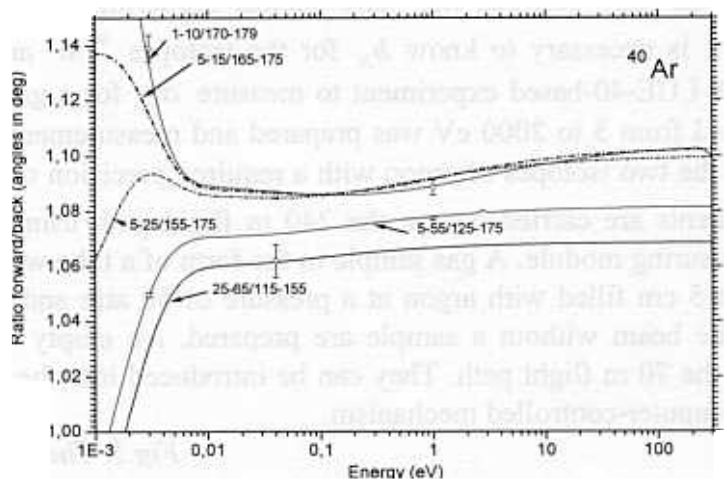

Fig.1. The angular anisotropy of neutron scattering on argon. The curves are the result of analytical calculation for the intervals of forward/backward scattering angles marked with arrows (in degrees). The points represent some variants of the Monte-Carlo calculation.

Figure 1 shows that the analytical and Monte-Carlo calculations agree well and that depending on the value of scattering angles (or their intervals) the effect of the n,e-interaction contribution may reach a value of 1.5%. In addition, an experimental setup with a 5 cm radius neutron beam and a ring detector of ^3He counters (pressure 10 atm and thickness 3 cm) arranged along a radius of 35 cm with respect to the beam axis as illustrated in Fig. 2 was calculated. Figure 3 illustrates the results of the Monte-Carlo calculation for the chosen geometry when a real scattering area from which neutrons come to the detectors has a length of about 90 cm. For comparison, the results of analytical calculations for a "precise" sample and an interval of angles close to the chosen geometry of the setup are presented.

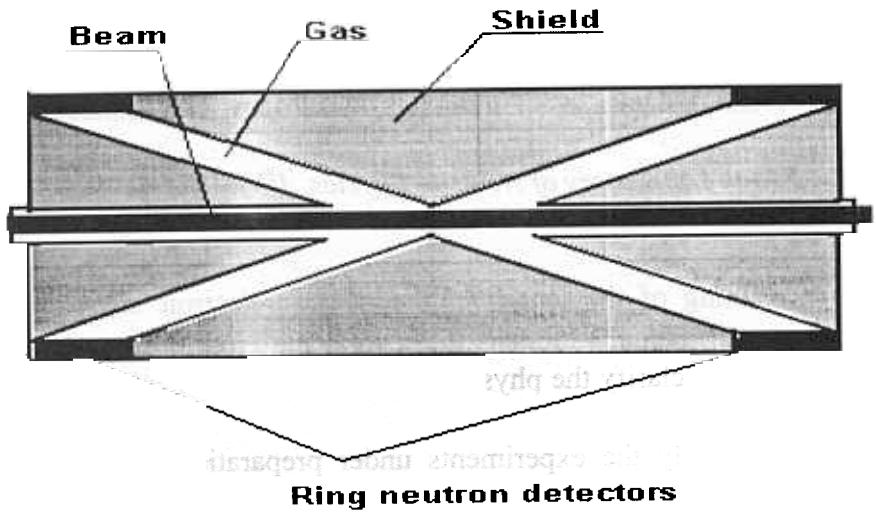

Fig. 2. The scheme of the experimental setup for the measurement of the energy dependence of the angular anisotropy of neutrons scattered on argon.

In the experiment the ratio between n,e- and nuclear scattering-length, b_{ne} / b_N, will be extracted. To obtain b_{ne} it is necessary to know b_N for the isotopes ^{40}Ar and ^{36}Ar present in natural argon. An IBR-30+LUE-40-based experiment to measure σ_{tot} for a gas sample of natural argon in the energy interval from 5 to 2000 eV was prepared and measurements started. This will allow us to obtain b_N for the two isotopes of argon with a required precision using known thermal point data. The measurements are carried out on the 240 m flight path using a battery of ^{3}He counters and a 16-exit measuring module. A gas sample in the form of a tube with a length of about 100 cm and a diameter of 5 cm filled with argon at a pressure of 50 atm and an exact copy of a vacuum tube to imitate the beam without a sample are prepared. An empty and an argon-filled container are installed on the 70 m flight path. They can be introduced into the collimated neutron beam with the help of a computer-controlled mechanism.

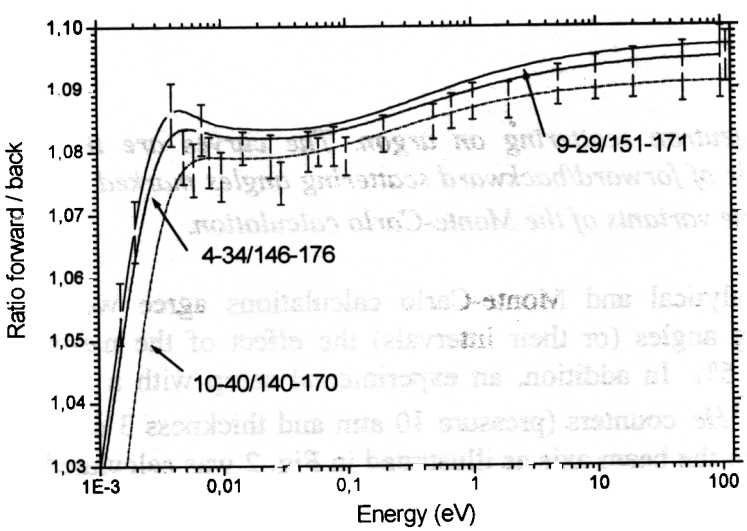

Fig.3. The energy dependence of the angular anisotropy of neutrons scattered on argon. The points are the Monte-Carlo calculation for the setup shown in Fig. 2. The curves are the analytical calculation for realistic intervals of angles for a "precise" sample.

References

1. G.G.Bunatian, V.G.Nikolenko, A.B.Popov, G.S.Samosvat, T.Yu.Tretyakova, Zeit.Phys., **A359**, p.337, 1997.

INVESTIGATION OF INTERFERENCE MINIMA NEAR s-WAVE RESONANCES OF ^{238}U

T.L.Enik, L.V.Mitsyna, G.S.Samosvat *(FLNP, JINR, Dubna, Russia)*
V.V.Sinitsa *(IPPE, Obninsk, Russia)*

1.Introduction

Because of the importance of ^{238}U for nuclear technology, its neutron total and capture cross sections (σ_t and σ_γ respectively) have been measured many times (see, for example [1]). We only know, however, two published works where the scattering cross section σ_s in ^{238}U resonances was studied: in [2] σ_s around the 6.67 eV resonance was only measured and in [3] the scattering resonance area of many resonances was only obtained.

Meanwhile, the interference minima below the resonance energies of s-wave resonances in even-even targets are of a certain interest because very small values of σ_s or the coherent scattering cross section are realized, if the minimum is close to thermal neutron energies (the last phenomenon was observed in [4]).

2.Experiment

Measurements were carried out on a 250.8 m flight path of the Dubna booster IBR-30 using a neutron spectrometer UGRA with a time resolution of ~24 ns/m [5]. A neutron beam with a cross section of 22×12 cm^2 hit a 195 mm diameter of metallic uranium sample depleted with a ^{235}U isotope with a thickness of 3 or 1 mm. The scattered neutrons were detected by two batteries of ^3He-counters which could be set at any of nine positions providing a scattering angle between 25^0 and 155^0 with a $\pm 4^0$ incertainty. The measurement process (choice of the necessary scatterer, angles of detectors, angle between the plane of the scatterer and the beam axis, accumulation of spectra and monitor counts) were made automatically on line with a computer.

3.Analysis

If a nucleous has the neutron scattering cross section $\sigma_s(E)$ at energy E, the yield of the scattered neutrons is:

$$I(E) = p(E)\sigma_s(E)\gamma(E,\alpha,\beta). \qquad (1)$$

Here $p(E)$ includes the neutron flux, detector efficiency and sample dimensions, $\gamma(E,\alpha,\beta)$ is the probability of the neutron entering a flat sample at angle α to a normal experiences scattering and leaves the sample at angle β to a normal. In our case, $p(E)$ depends weakly on E and can be considered as different constants around different resonances. The function $\gamma(E,\alpha,\beta)$ is:

$$\gamma(E,\alpha,\beta)=\begin{cases}\dfrac{1-e^{-nd\left(\frac{\sigma_t}{\cos\alpha}+\frac{\sigma_t'}{\cos\beta}\right)}}{nd\left(\dfrac{\sigma_t}{\cos\alpha}+\dfrac{\sigma_t'}{\cos\beta}\right)} & \textit{for reflection geometry}\\[2ex] \dfrac{e^{\frac{nd\sigma_t'}{\cos\beta}}-e^{\frac{nd\sigma_t}{\cos\alpha}}}{nd\left(\dfrac{\sigma_t}{\cos\alpha}-\dfrac{\sigma_t'}{\cos\beta}\right)} & \textit{for "transmission geometry"}\end{cases}$$

It is obtained by the integration over the sample thickness d. In (2) the total cross sections σ_t and σ_t' correspond to the energy E and $E[(A+\cos\vartheta)/(A+1)]^2$ of the incident and outcoming neutrons, respectively (A is the target mass number and ϑ is the scattering angle). Of course, $\gamma(E,\alpha,\beta)$ is only valid for small $nd\sigma_s$ as it does not take into account multiple scattering.

In order to compare the experimental data with calculations it is necessary to take into account the Doppler and resolution broadening. The first correction was made by means of replacing $I(E)$ in (1) by

$$I^D(E)=\frac{1}{\Delta\sqrt{\pi}}\int_{E-3\Delta}^{E+3\Delta} e^{\left(\frac{E-E'}{\Delta}\right)^2} I(E')dE'$$

with $\Delta=0.0206\sqrt{E}$ eV (E is in eV). The second correction was made by means of replasing $I^D(t)$ being the function of time-of-flight by the weighed average

$$I_R^D(t)=\sum_{i=-7}^{11} I^D(t-i)F(i). \qquad (4)$$

Here, $F(i)$ is normalized time resolution function of the spectrometer, t and i are the integer standing for the 1 mcs channels of the measured spectrum and the histogram $F(i)$. The function (4) plus the constant background B were fitted to the measured spectra in small regions near well isolated resonances by varying the parameters p and B. In (1) the cross section $\sigma_s(E)$ was calculated in the one-level approximation taking into account one or several nearest resonances.

4.Results and discussion

Because of a poor resolution we have chosen to analyse only three low-energy resonances. Raw data for them are partially shown in Fig.1 for two sample thicknesses nd and two scattering angles ϑ. Heavy distortions of the usual resonance form are striking especially for $\vartheta=25^0$ although they are weaker for the sample with nd=0.0048 b^{-1} which was fixed normal to the beam. Due to strong competition with radiative capture the resonance 6.674 eV looks very weak even in comparison with potential scattering. It was hopeless in these conditions to obtain a good fit to the whole resonance with our imperfect correction function $\gamma(E,\alpha,\beta)$ which must be, however, acceptable for describing resonance wings.

The main goal of the discussed investigations is to obtain the experimental values of $\sigma_s(E)$ around the interference minima at $E_{min}=E_0-\Gamma_n/(2k_0R')$. It can be done using equations (1)–(4) but only for the cases when it is possible to neglect multiple scattering, i.e. when $nd\sigma_s/\cos\alpha$ is small. We estimate this conditions for nd=0.0144 b^{-1} and $\alpha=45^0$ as $\sigma_s<15$–20 b which is well fulfilled practically everywhere. So for resonance wings, instead

of (1)–(4) the following spectrum of counts can be used $N_i = C\sigma_{si}\gamma_i + B$, where for each resonance C and B are constants. Then, if we know σ_{sm} at a certain energy E_m corresponding to the channel m, the following takes place:

$$\sigma_{si} = \frac{N_i - B}{N_m - B}\,\frac{\gamma_m}{\gamma_i}\,\sigma_{sm} \qquad (5)$$

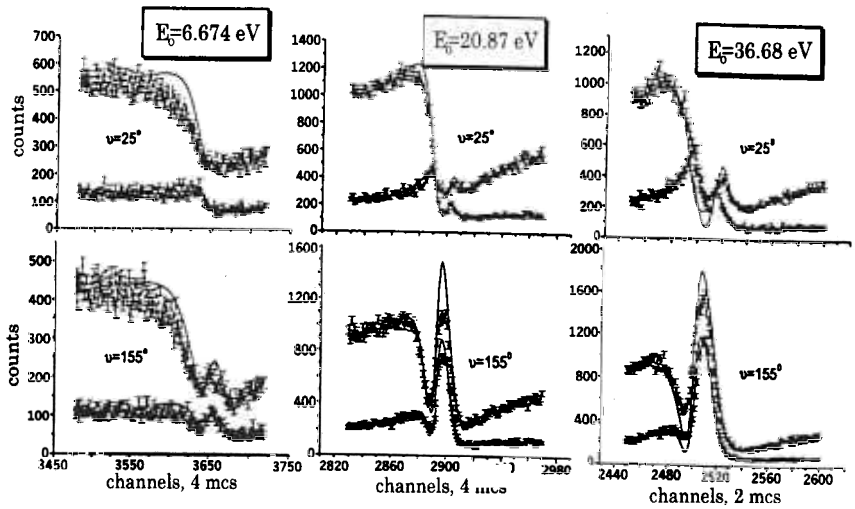

Fig.1. The time-of-flight spectra of neutrons scattered by ^{238}U. Upper spectrum in each diagram relates to the sample with nd=0.0144 b^{-1} and α=45° (120 hours of running), lower spectrum relates to nd=0.0048 b^{-1} and α=0° (96 hours of running). Solid lines are the fits to the wings (30–50 channels left and 50–80 channels right)

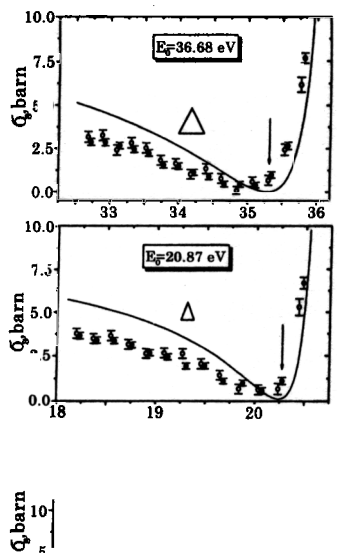

Three values of E_m on the high-energy wings of resonances are chosen and the cross sections σ_{sm} are obtained for them from the well-known file JENDL-3. The values of both quantities are presented in the table. This gives us the possibility to achieve the declared aim using formula (5). The results are shown in Fig.2. The base of each triangle is a double half-width of the local energetic resolution and the arrows indicate the theoretical position E_{min} (without Doppler effect) of the σ_s minima. The solid lines are the calculated results from the file JENDL-3. The squares for the 6.674 eV resonance are our rough estimation of the result [2]. Fig.2 allows us to say that the

Fig.2. The scattering cross sections near the resonances. Black points relate to the ϑ=155° measurements, light points relate to the ϑ=90° measurements

E_0, eV	E_{min}, eV	E_m, eV	σ_{sm}, b
6.674	6.525	8.05	11.2
20.87	20.28	23.05	14.2
36.68	5.29	39.50	23.7

measured and calculated σ_s are in moderate agreement. Some difference can be explained, besides the finite resolution of the setup, by any possible inaccuracies in the obtaining both results.

References

[1] D.K.Olsen, G.de Saussure, R.B.Perez, E.G.Silver, F.C.Difilippo, R.W.Ingle, H.Weaver. Nucl. Sci. Eng., 1977, v.62, p.479.

[2] P.Stavelov, F.Poortmans, L.Mewissen, E.Cornelis. Nucl. Sci. Eng., 1978, v.66, p.349.

[3] M.Asghar, C.M.Chaffey, M.C.Moxon. Nucl. Phys., 1966, v.85, p.305.

[4] Yu.A.Alexandrov. JINR 3-3442, p.112, Dubna, 1967 (in Russian).

[5] B.I.Voronov, T.L.Enik, V.A.Ermakov, V.I.Konstantinov, E.I.Litvinenko, L.V.Mitsyna, G.S.Samosvat, A.A.Smirnov, V.A.Trepalin, R.V.Kharjuzov. JINR Communication P13-97-36, Dubna, 1997 (in Russian); T.L.Enik, R.V.Kharjuzov, L.V.Mitsyna, G.S.Samosvat. Nucl. Instr.Meth., 2000, v.A440, p.777.

PARITY VIOLATION AND INTERFERENCE EFFECTS IN ANGULAR DISTRIBUTIONS OF FISSION FRAGMENTS

V.P. Alfimenkov, N.A.Bazhanov, L.Lason[1], Yu.D.Mareev, V.V.Novitskii, L.B.Pikelner, T.L.Pikelner, M.I.Tsulaia, A.N.Chernikov

Frank Laboratory of Neutron Physics, JINR, Dubna
[1]Lodz University, Poland

In the year 2000 investigations of the parity violation and interference effects in the angular distributions of fragments of the resonance neutron induced fission of heavy nuclei continued.

The angular correlations in resonance neutron induced fission can be written as

$$W(\mathbf{P}_f) = 1 + \alpha_{pv}(\sigma_n \cdot \mathbf{P}_f) + \alpha_{fb}(\mathbf{P}_f \cdot \mathbf{P}_n) + \alpha_{lr}(\mathbf{P}_f \cdot [\sigma_n \cdot \mathbf{P}_n]),$$

where $\mathbf{P}_f$ and $\mathbf{P}_n$ are the unit vectors of the momentums of the light fission fragments and neutrons that caused the fission, σ_n is the unit pseudovector in the direction of neutron polarization. The coefficients α_{pv}, α_{fb}, and α_{lr} characterize respectively the effects of parity violation, forward-backward and left-right asymmetry in the emission of the fragments. There exist theories [1, 2] describing these coefficients as a function of the parameters of s- and p-wave resonances and also, of the matrix elements of the weak interaction for the coefficient α_{pv}. The experimental investigations of the reported effects over the region of resonance energies were conducted by joint groups of PINP (Gatchina) and FLNP JINR (Dubna) in the recent years. The generalized results of the investigations of all the effects for ^{235}U are published in [3] and the experiments with ^{233}U nuclei completed in 1999 are described in [4]. In 2000, measurements of ^{239}Pu were carried out.

One of the specific features of the transverse cross section of fission and radiative neutron capture in ^{233}U and ^{235}U nuclei is a high density of neutron resonances and a small number of reduced neutron widths. For s-resonances the average spacing between resonances is about 0.5 eV and the average reduced widths is about 10^{-4} eV. These two facts make it almost impossible to observe directly p-wave resonances in which the existence of the cetrifugal barrier results in that the cross section of compound state formation in the area of 10 eV neutron energy is smaller than in s-wave resonances 4 – 5 orders of magnitude. Parallel investigations of the above-mentioned effects make it possible to determine the positions of unknown p-resonances and do the assessment of their main parameters. Figure 1 depicts the energy behavior of all three effects over the neutron energy range from thermal to 15 eV for ^{233}U. A distinctly seen structure of the effects (fb) and (lr) has made it possible to determine the parameters of 18 p- resonances. As it is seen in Fig. 1 the parity violation effects are noticeably weaker. However, we managed to assess the value of three matrix elements. The obtained values lie in the interval from 10^{-4} to 10^{-3} eV.

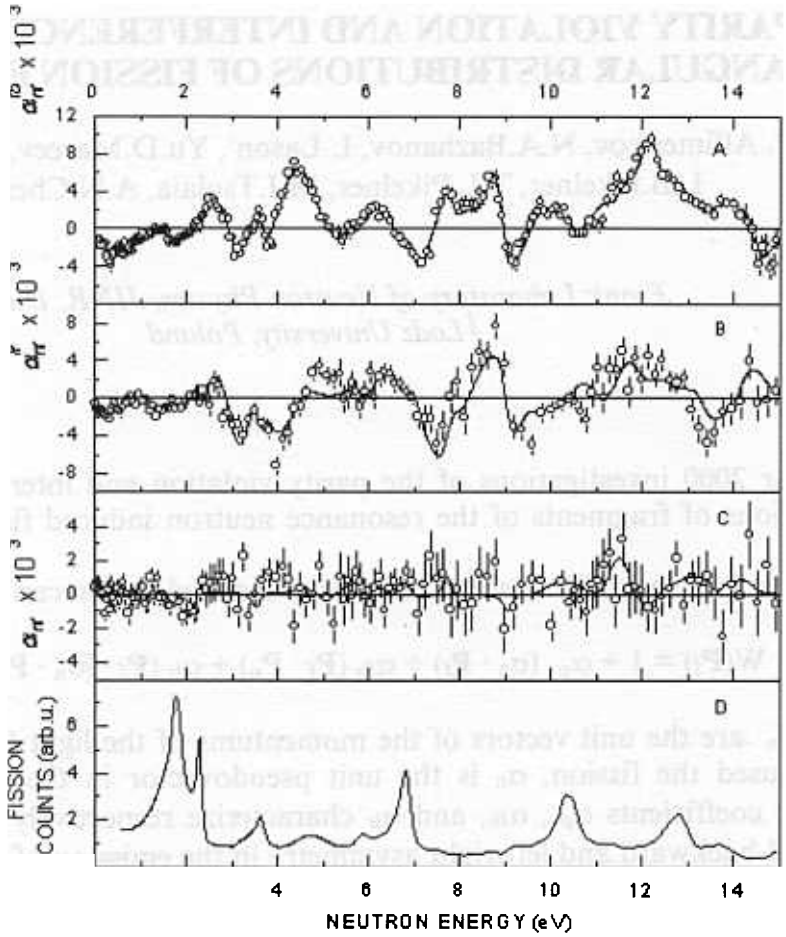

Fig. 1.

The measurements of ^{239}Pu started in 1999 and continued through the year 2000 have their pluses and minuses. The positive side is that it has a noticeably smaller density of levels than uranium isotopes. The average distance between resonances is 2.3 eV. This simplifies joint processing of the obtained spectra because the contribution of neighboring resonances to the analyzed section decreases. At the same time, however, it leads to a decrease in the effect that depends on the distance between the mixing levels. In this connection in the year 2000, we continued to collect statistics on the measurement of the left-right asymmetry and parity violation in the resonance neutron-induced fission of ^{239}Pu with the POLIANA facility at the IBR-30 reactor.

References

[1] Sushkov O.P., Flambaum V.V., Usp.Fiz.Nauk, 1982, v. 136, p. 3.
[2] Bunakov V.E., Gudkov V.P., Nucl. Phys., 1983, v.A 401, p.93.
[3] Alfimenkov V.P.,Chernikov A.N., Lason L. et al. Nucl. Phys., 1999, v.A645, p. 31.
[4] Alfimenkov V.P., Gagarskii A.M., Golosovskaia S.P. et al., Jad.Fiz, 2000, v.63, p.598.

Improving Explosive Nucleosynthesis Models Via (n,α) Measurements

P. E. Koehler[1], Yu. M. Gledenov[2], J. Andrzejewski[3], K. H. Guber[4], S. Raman[1], T. Rauscher[5]

[1] *Physics Division, Oak Ridge National Laboratory, Oak Ridge, Tennessee 37831*
[2] *Frank Laboratory of Neutron Physics, Joint Institute for Nuclear Research, 141980 Dubna, Russia*
[3] *Department of Nuclear Physics and Radiation Safety, University of Lodz, 90-236 Lodz, Pomorska St. 149, Poland*
[4] *Computational Physics and Engineering Division, Oak Ridge National Laboratory, Oak Ridge, TN 37831*
[5] *Departement für Physik und Astronomie,Universität Basel, CH-4056 Basel, Switzerland*

Recently, there has been much interest [1-5] in the astrophysical rates for reactions between α particles and intermediate to heavy nuclei. These reactions often can play an important role in the nucleosynthesis occurring in massive stars at high temperatures and in explosive scenarios such as supernovae. For example, photodisintegration processes such as (γ,α) reactions play an essential role in the nucleosynthesis of the proton-rich intermediate to heavy elements in the so-called *p*-process [6,7]. A better understanding of the nucleosynthesis occurring in these environments should lead to improved stellar models and impact related areas such as the origin of isotopic anomalies in meteorites [1]. Possible *p*-process contributions to s-only isotopes are also relevant for high-precision tests of *s*-process models [8]. There is scant experimental information on the rates for these reactions and the few data which have been measured are sometimes very different from theoretical predictions. Direct determinations of these rates via experiments are extremely difficult and it is very unlikely that the rates for most of the needed reactions will be determined by direct experiments. Theoretical calculations are hampered by large uncertainties in the α+nucleus optical potential in the astrophysically relevant energy range. Traditional methods for improving optical potentials, such as elastic scattering of α particles [9], have been of limited usefulness because the potentials must be extrapolated from measurements made at energies well above the astrophysically interesting range. A series of low-energy (n,α) cross-section measurements may offer the best opportunity for enabling global improvements in the α+nucleus optical potential for astrophysics applications because; i) the Q-values for (n,α) reactions are such that the relative energy between the α particle and the residual nucleus are in the astrophysically interesting range, so no extrapolation is necessary; ii) scaling the sample size to that employed in a previous measurement [10] using predicted cross sections [11], we calculate that as many as 30 nuclides across a wide range of masses should be accessible to measurements, and iii) a recent study [3] has shown that calculated (α,n) rates, via the α transmission coefficients, are sensitive to the α-potential used in the model. By detailed balance arguments, (n,α) reactions should display the same sensitivity. The data presented herein are the first (n,α) cross section measurements in this mass range over the broad range of energies of interest to

nuclear astrophysics. It is intended that they represent the first in a series of measurements aimed at a global improvement in the calculation of rates for α-induced reactions of interest to explosive nucleosynthesis models.

The experiments were performed at the Oak Ridge Electron Linear Accelerator (ORELA) white neutron source. The ORELA was operated at a repetition rate of 525 Hz, a power of 6 - 8 kW and a pulse width of 8 ns. A compensated ionization chamber (CIC) [10] was used as the detector. Although a CIC can have poorer pulse-height resolution than, for example, a gridded ionization chamber, it reduces γ flash effects by several orders of magnitude, allowing measurements to be made to much higher neutron energies (500 keV in the present case) than in previous experiments [12]. The source-to-sample distance was 8.835 m and the neutron beam was collimated to 10 cm in diameter at the sample position. The $^{6}Li(n,\alpha)^{3}H$ reaction was used to measure the energy dependence of the flux and to normalize the raw counts to absolute cross section. The data for ^{147}Sm [13] in the unresolved region are shown in Fig. 1, together with cross sections calculated by three statistical model codes [11,14,15] frequently used for astrophysical applications. The theoretical cross sections are renormalized by the constant factors given in the figure. The older calculations of Ref. [11] are much closer to the data than the more recent calculations of Refs. [14,15] which are roughly a factor of 3 different from the data in opposite directions. The comparison to our new data provides important clues to problems with the α potentials in the models.

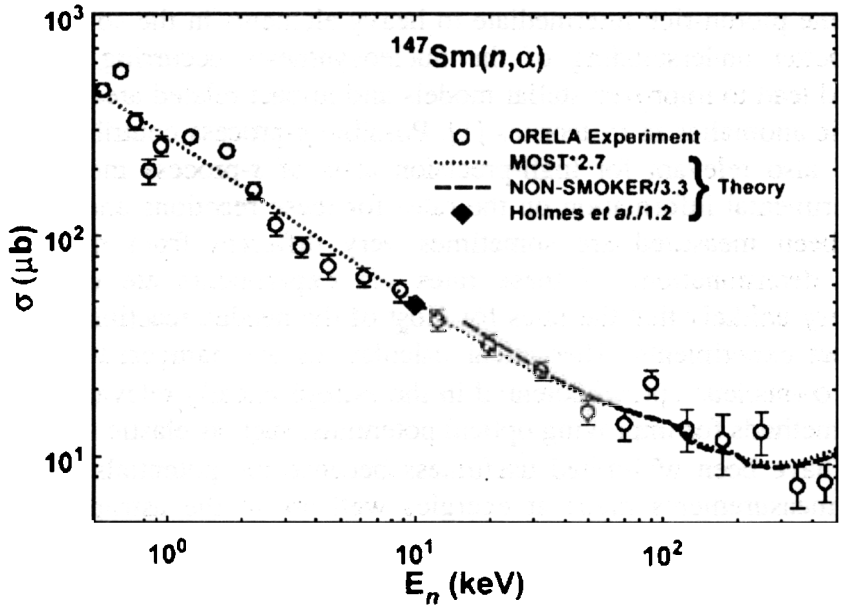

Fig.1. Cross sections for the ^{147}Sm (n,α) reactions in the unresolved region. Shown are the measurements of the present work (circles with error bars depicting one-standard-deviation statistical uncertainties) and calculations by Holmes et al. [11] (diamonds), as well as calculations using the newer statistical model codes NON-SMOKER [14] (long-dashed curves), and MOST [15] (dotted curves).

We studied theoretically [13] the dependence of the calculated ^{147}Sm (n,α) reaction rates on the optical α potential as well as the nuclear level density. The NON-SMOKER [14] code was used to calculate the astrophysical reaction rates

^{147}Sm (n,α) using two different optical α+ nucleus potentials and three different level density prescriptions, in addition to the standard NON-SMOKER potential and level density. Differences of about a factor of 30 can be accounted for in the variation of the optical potential alone. The different level density prescriptions can change the cross section by a factor of about 1.5, by far smaller than the effect of the α potential. However, we want to emphasize that this is not a systematic study of the sensitivity but merely presented to illuminate the source of the differences in the results from various statistical model calculations. Although it is possible to obtain an α potential by fitting the current experimental data, such a potential probably would be of limited usefulness. For example, it has recently been shown [5] that a potential constructed to give good agreement with the experimental data for the ^{144}Sm (α,γ) reaction can be off by as much as a factor of 100 compared to the data for the ^{70}Ge(α,γ) reaction. More experimental data are needed across as wide a range of masses and energies as possible to constrain the several parameters thought to be needed to define a global α potential. The proper treatment of the statistical model of nuclear reactions involving α particles poses a very important problem in nuclear astrophysics today. It is especially crucial for a better understanding of the nucleosynthesis occurring in stellar explosions such as supernovae and the origin of the *p*- nuclides. We have demonstrated the feasibility of a new approach for reducing the main uncertainty in the calculation of rates for reactions involving α particles. It is evident that further experimental data of the type presented herein are needed to more fully explore this problem if the statistical model and the explosive nucleosynthesis calculations which in large part rely on them are to be improved.

References

1. S. E. Woosley and W. M. Howard, Astrophys. J. Lett. **354**, (1990) L21.

2. T. Rauscher, F. -K. Thielemann, and H. Oberhummer, Astrophys. J. Lett. **451**, (1995) L37.

3. R. D. Hoffman, S. E. Woosley, T. A. Weaver, T. Rauscher, and F.-K. Thieleman, Astrophys. J. **521**, (1999) 735.

4. T. Rauscher, in Nuclei in the Cosmos, edited by N. Prantzos and S. Harissopulos (Editions Frontieres, Gif-sur-Yvett, 1998), p. 484.

5. E. Somorjai, Zs. Fulop, A. Z. Kiss, C. E. Rolfs, H.-P. Trautvetter, U. Greife, M. Junker, M. Arnould, M. Rayet, S. Goriely, T. Rauscher, H. Oberhummer, and P. Mohr, Astron. Astrophys. **333**, (1998) 1112.

6. S. E. Woosley and W. M. Howard, Astrophys. J., Suppl. **36**, (1978) 285.

7. M. Rayet, M. Arnould, M. Hashimoto, N. Prantzos, and K. Nomoto, Astron. Astrophys. **298**, (1995) 517.

8. K. H. Guber, R. R. Spencer, P.E. Koehler, and R. R. Winters, Phys. Rev. Lett. **78**, (1997) 2704.

9. P. Mohr, T. Rauscher, H. Oberhummer, Z. Mate, Z. Fulop, E.Somorjai, M. Jaeger, and G. Staudt, Phys. Rev. C **55**, (1997) 1523.

10. P.E. Koehler, J.A. Harvey, and N.W. Hill, Nucl. Instr. and Meth. **A361**, (1995) 270.

11. J.A. Holmes, S.E. Woosley, W.A. Fowler, and B.A.Zimmerman, At. Data Nucl. Data Tables **18**, (1976) 305.

12. J. Kvitek and Y. P. Popov, Nucl. Phys. **A154**, (1970) 177.

13. Yu. M. Gledenov, P. E. Koehler, J. Andrzejewski, K. H. Guber, and T. Rauscher, Phys. Rev. **C 62** (2000) 042801(R).

14. T. Rauscher and F.-K. Thielemann, in Stellar Evolution, Stellar Explosions, and Galactic Chemical Evolution, edited by A. Mezzacappa (Institute of Physics, Bristol, 1998), p.519.

15. S. Goriely, in Nuclei in the Cosmos, edited by N. Prantzos and S. Harissopulos Editions Frontieres, Gif-sur-Yvette, 1998), p. 314.

Level density and radiative strength functions of dipole transitions below B_n in $^{185,187}W$ and $^{191,193}Os$

V.A.Bondarenko[a], J.Honzátko[b], V.A. Khitrov[c], A.M. Sukhovoj[c], I.Tomandl[b]
[a] *Nuclear Research Center, LV 2169 Salaspils, Latvia*
[b] *Nuclear Physics Institute, CZ-25068 Řež near Prague, Czech Republic*
[c] *Frank Laboratory of Neutron Physics, Joint Institute for Nuclear Research 141980 Dubna, Russia*

1 Introduction

Information on the properties of the excited states of heavy non-magic nuclei for the excitation region from 1-3 MeV to the neutron binding energy, B_n, can be derived from an analysis of the energy dependence of the level density, ρ, and reduced probability (strength function) f of their excitation after the decay of compound states. Up to now, there have been no methods which would allow the determination of these parameters without some additional information (for example, model assumptions with an unknown precision). Therefore, main information on the level density was obtained [1] from analyses of the products of nuclear reactions with the use of different potentials of the optic model to predict an unknown probability of nucleon emission with further excitation of an arbitrary low-lying level. New possibilities are provided by the investigation of two-step γ-cascades between the neutron resonance and given low-lying levels.

Unlike other compound nucleus reaction with yields proportional to the level density, the intensity of two-step γ-cascades (to one or several final levels) is, on the whole, inversely proportional to the level density of the nucleus. Theoretically there is an infinite number of possible ρ and f values which provide precise reproduction of experimental cascade intensities and total radiative widths of neutron resonances. However, due to a unique property of this experiment, the interval of probable estimates of ρ and f is limited by certain minimum and maximum values for all excitation energies of the nucleus. As it was shown in [2], these intervals are narrow enough in order to verify different models of nucleus. This is the main difference of the data used below from, for instance, that on spectra of primary γ-transitions where the interval of theoretically possible values is always infinite. It is obvious that analysis by the method [2] requires experimental cascade intensities with sufficiently small statistic and systematic errors.

2 Experimental data

Two-step γ-cascades following thermal neutron capture in the $^{184,186}W$ and $^{190,192}Os$ target nuclei were measured at the Light-Water Reactor LWR-15 in Řež near Prague. The $\gamma-\gamma$ coincidences were measured [3] with $HPGe$ detectors of sufficiently enough efficiency, which enabled us to achieve 5 to 10 times higher statistics than in earlier experiments in Dubna and Riga. This allowed us to obtain the spectra where up to 80-90% of cascade intensities are resolved as pairs of peaks, i. e., the main portion of the experimental intensity can be related to quite defined cascades which excite individual intermediate levels and can be analysed using the technique of nuclear spectroscopy. The use of the algorithm [4] for the determination of quanta ordering in the resolved cascades allowed us to estimate [5] the dependence of the cascade intensity on the energy of their intermediate levels (Fig. 1).

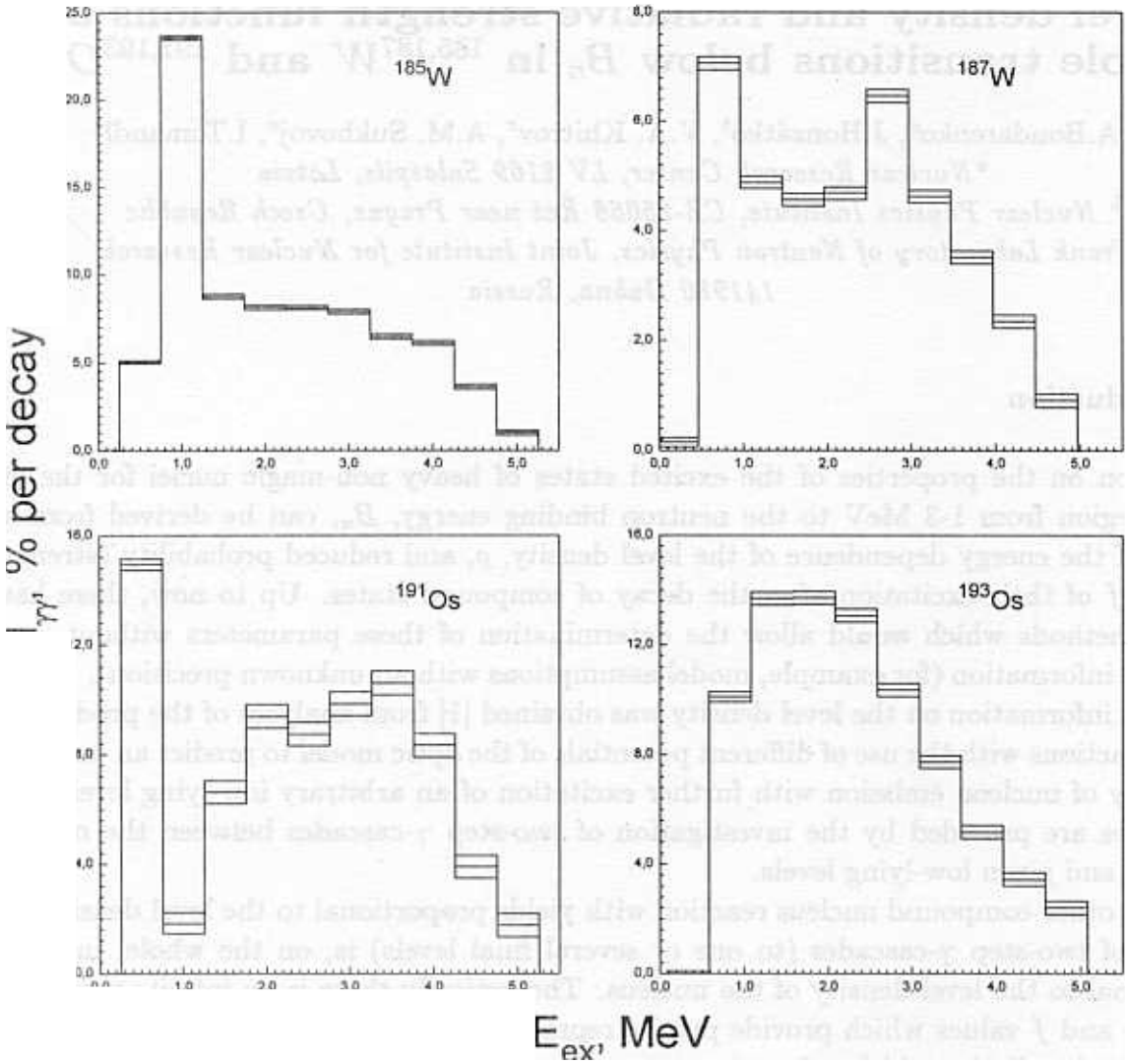

Fig. 1. The total experimental intensities (in % per decay) of two- step cascades (summed in energy bins of 500 keV) with ordinary statistical errors as a function of the primary transition energy.

Most probably, systematic error of this result does not exceed [6] 5-10%.

Specific dependence of the cascade intensities on the density ρ of their intermediate levels and radiative strength functions f of cascade transitions in conjunction with the known total radiative strength function of the capture state allow the determination [2] of the probable interval of ρ and f values. The corresponding results are shown in Figs. 2 and 3. intermediate levels per 100 keV observed earlier. As it is described in [2], the "best" values and intervals of their probable variations (which allow the reproduction of the experimental intensities (Fig. 1) within the precision of the experiment) are determined here as a mean value and dispersion of ensembles of random ρ and f obtained in Monte-Carlo simulations. A simple iterative algorithm was used for this purpose: we set some different initial values for the level density and partial radiative widths and then distorted them by means of random functions. If these distortions improve the agreement between the experimental and calculated cascade intensities and total radiative widths of the capture state at this stage of the iterative procedure, then the distorted values are used as initial parameters in the next iteration. Repeated iterative calculations for the W and Os isotopes and the nuclei studied earlier [2]

leads to convergent in probability of "best" values independently on the initial ρ and f values in the realized random process.

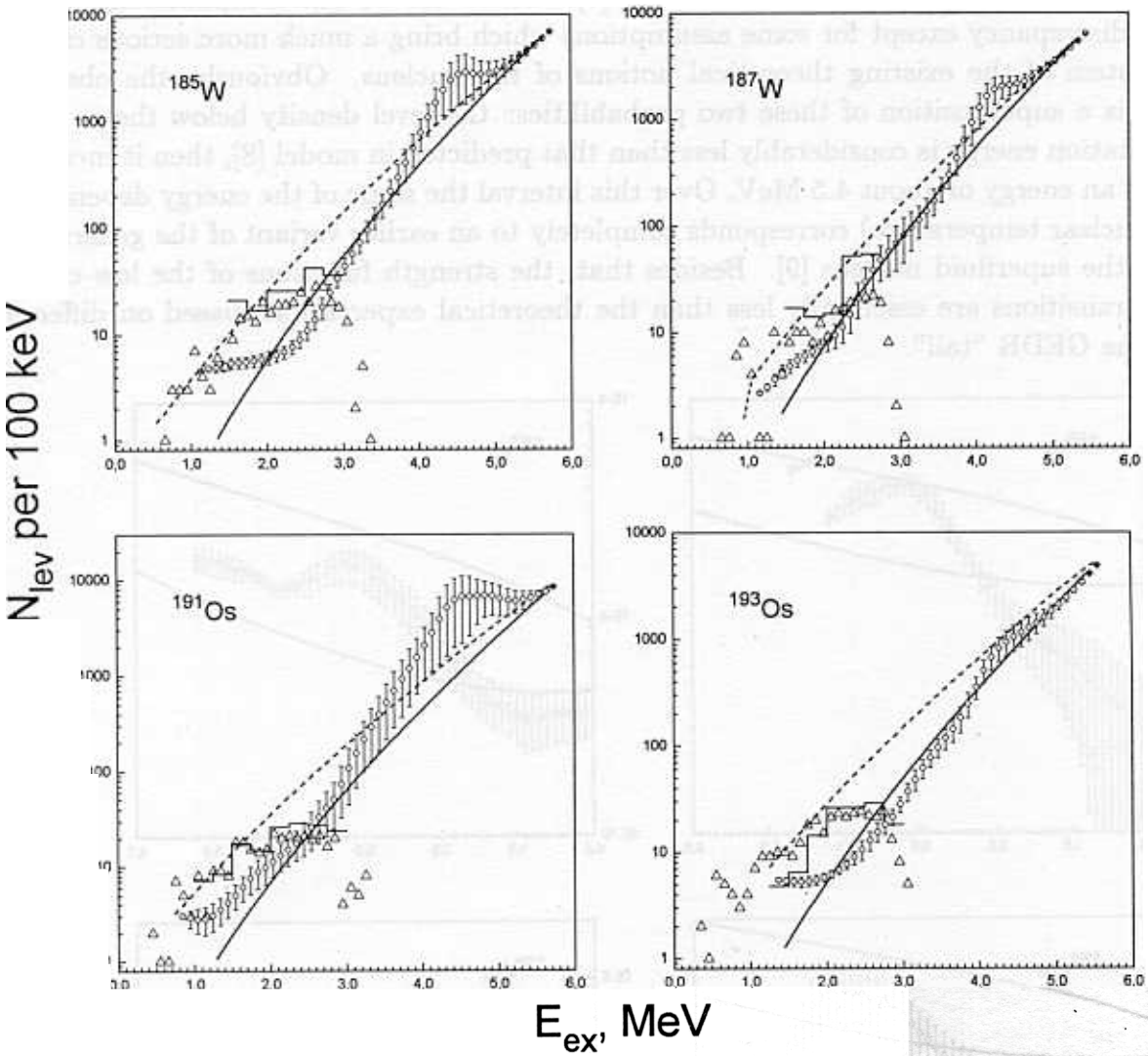

Fig. 2. The interval of probable values of the level density enabling the reproduction of the experimental intensity of two-step cascades and total radiative widths of capture states in $^{184,186}W$ and $^{190,192}Os$. The dashed and solid lines represent the predictions [8] and [9], respectively. The histogram represents the data [6], triangles show the number of cascade intermediate levels per 100 keV observed earlier.

Even-odd nuclei with $A > 180$ are characterized by considerable local fluctuations of the intensities of primary transitions to low-lying levels. This circumstance and the necessity to average the cascade intensities (Fig. 1) over the 0.5 MeV energy interval lead to "breaking" of the strength functions in Fig. 3.

3 Possible interpretation of the results of analysis

The experimental intensities of two-step cascades in $^{185,187}W$ and $^{191,193}Os$ are noticeably larger than the theoretical values calculated according to the models of level density and radiative strength functions which consider nucleus as a Fermi-liquid [7] or Fermi-gas [8]. This

means that the level density excited in the (n,γ) reaction is considerably less than the predicted in the model [8] or that the dependence of the strength function f on the γ-transition energy is much stronger than it follows from [7]. There are no other explanations of the observed discrepancy except for some assumptions which bring a much more serious change in the system of the existing theoretical notions of the nucleus. Obviously, the observed situation is a superposition of these two probabilities: the level density below the $\simeq 2-3$ MeV excitation energy is considerably less than that predicted in model [8], then it increases rapidly to an energy of about 4.5 MeV. Over this interval the slope of the energy dependence (due to nuclear temperature) corresponds completely to an earlier variant of the generalized model of the superfluid nucleus [9]. Besides that, the strength functions of the low-energy primary transitions are essentially less than the theoretical expectations based on different ideas of the GEDR "tail".

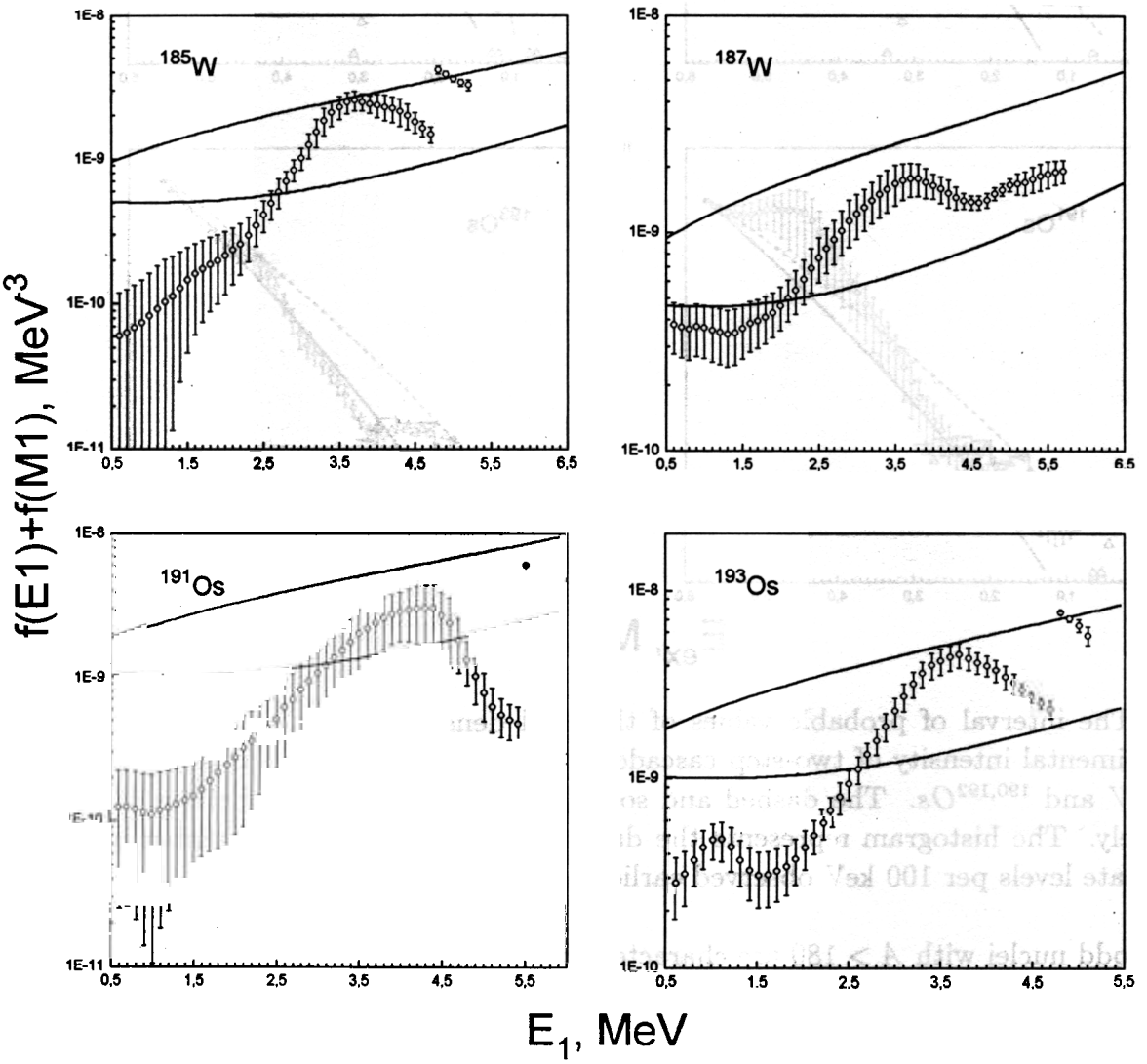

Fig. 3. The probable interval of the sum strength functions $f(E1)+f(M1)$ (points with error bars) providing the reproduction of the experimental data. The upper and lower curves represent the extrapolation of the GEDR "tail" into the region below B_n and the prediction of the model [7] for $E1$ transitions in the sum with $f(M1) = const$ values, respectively.

Unfortunately, at present the analysis [2] can be only carried out under the assumption of similar shapes of the energy dependence of strength functions for the primary and sec-

ondary transitions with equal multipolarities. A comparison between the experimental and calculated two-step cascades to different final levels of the investigated nuclei shows that, most probably, this assumption leads to some overestimation of the level density above the energy of several MeV and to underestimation — at low excitations. This fact in conjunction with the circumstance that some part of the cascades cannot be unambiguously placed in the decay scheme results in a discrepancy for the data in Fig. 1 below the excitation energy 2 MeV.

The simplest interpretation of the observed discrepancy between the experiment and models [7,8] can be obtained from the specific shape of the dependence of ρ on E_{ex}. The dependence of ρ on the excitation energy for all of these nuclei demonstrates a step-like structure at the 2 MeV excitation energy and in addition, a similar structure at $\simeq$ 4 MeV. This result agrees with the qualitative predictions [9] by A.Ignatyuk of the step-like dependence of the level density on the excitation energy. The only discrepancy is that the width of the step-like structure in our data is approximately 2 MeV instead of $\simeq$ 1 MeV in [9]. Theoretical notions of A.Ignatyuk are based on the fact that breaking of a nucleon pair requires a certain excitation energy. Each of these damped "steps" are due to the complication of the structure of the wave function by two quasiparticles as the excitation energy increases. From the data shown in Fig. 2 and notions of model [9] it follows that the next structure of the step-like type should be expected at an excitation energy of about 6.5-7.0 MeV, i. e., after the capture of the neutron with an energy of $\approx$ 1 MeV. This means that the estimated interaction cross sections of neutrons with nuclei can include an additional uncertainty. A similar conclusion about the step-like structure of the level density above the neutron binding energy is made in an analysis of the interaction cross section of neutrons with actinides described in details in [10]. The novelty of the suggested methods of analysis [6,7] and the data obtained within these methods assume, naturally, the necessity of further experimental and theoretical studies of the results discussed in present article.

This work was supported by the RFBR Grant N^o 99-02-17863.

References

1. M.I. Svirin, G.N. Smirenkin, Yad. Fiz, **47** (1988) 84
2. E.V.Vasilieva, V.A. Khitrov, A.M.Sukhovoj, Physics of Particles and Nuclei, **31(2)** (2000) 170
3. J. Honzátko et al., Nucl. Instr. and Meth. **A376** (1996) 434
4. Yu.P. Popov, A.M. Sukhovoj, V.A. Khitrov, Yu.S. Yazvitsky, Izv. AN SSSR, Ser.Fiz. **48** (1984) 1830
5. S.T. Boneva, V.A. Khitrov, A.M. Sukhovoj, A.V. Vojnov, Z. Phys. **A338** (1991) 319
   S.T. Boneva, V.A. Khitrov, A.M. Sukhovoj, A.V. Vojnov, Nucl. Phys. **A589** (1995) 293
6. A.M. Sukhovoj, V.A.Khitrov, Yad. Fiz. **62(1)** (1999) 24
7. S.G. Kadmenskij, V.P. Markushev, W.I. Furman, Sov. J. Nucl. Phys. **37** (1983)165
8. W. Dilg, W. Schantl, H. Vonach, Nucl. Phys. **A217** (1973) 269
9. A.V. Ignatyuk, Report IAEA INDC-233(L), IAEA, Vienna 1985
10. V.M.Maslov, Phys. of Atomic Nuclei **63(2)** (2000) 161

WEEKLY CYCLES OF ELEMENT POLLUTANTS IN AIR OF THE GREATER CAIRO AREA (EGYPT) STUDIED BY NEUTRON ACTIVATION ANALYSIS

M.V. Frontasyeva, A.B. Ramadan*, T.Ye. Galinskaya

Frank Laboratory of Neutron Physics, Joint Institute for Nuclear Research, Dubna, Russia
** National Center for Nuclear Safety and Radiation Control, Cairo, Egypt*

Why is the weather different in working days and in week-ends? Why is it gloomy during the holidays? This variability, noted by Canadian and United States inventories [1] and later nicknamed the "Sunday effect" [2], is characterized by high late-week pollution levels as opposed to the early week levels. According to the interpretation of numerous data offered by American scientists studying the weekly cycles of air pollutants, precipitation, and tropical cyclones in the coastal Atlantic region of the USA, it is connected to a greater extent, with human activity rather than natural phenomena.

As an example of curiosity, the cyclic anthropogenic impact on air pollution in the Greater Cairo Area of Egypt is demonstrated in our work. It is based on the results of elemental analysis of limited number of air filters used to study air pollution in the Greater Cairo Area, a densely populated and industrial district of Egypt. This area differs from the above-mentioned region of the USA not only by its climatic conditions, but also by its week-ends, corresponding in the Arabic world to Thursday and Friday! As well as high concentration of anthropogenic aerosols have been identified over the North Atlantic Ocean [3] associated with the urbanised eastern seaboard of North America, we have noted that Cairo with its suburbs (the Greater Cairo Area), a megapolice encompassing 16 million people, produces a strong weekly pollution cycle.

Results for a total of 30 elements are reported, including lead, cadmium and copper determined by total reflection fluorescence analysis (TXRF) at NCNSRC, Cairo, Egypt.

A seven-day cycle was revealed, with the last two days of the week for the Arabic world (Tuesday-Wednesday) experiencing the highest values of pollutants and with the lowest values associated with the beginning of the week (Saturday-Sunday). It is an excellent extra testing of a hypothesis of weekly cycles of air pollutants, along with precipitation, and tropical cyclones. The weekly cycles of air pollution noted in our work for the Arabic world with its week-ends on Thursday-Friday *(Fig. 1)* are in good agreement with a similar behavior of air pollution in the Christian world with its week-ends on Saturday-Sunday [1].

A pronounced increase of major and trace element concentrations, including heavy metals, rare earth elements and actinides along the valley with the prevailing wind direction, from the north to the south of the Greater Cairo Area was observed in the period under examination *(Fig. 2)*.

The air filters were collected in winter months December-January of 1997-1998 at three aerosol stations located in the north-south direction of 27 km. Total particulate suspended matter has been sampled with high-volume samplers operating at a flow of about 25 m^3/h by pumping 540 m^3 of air through Whatman-41 cellulose filters of 25 x 25 cm in size. Initially measured for the man-made and natural radionuclides, filters then were subdivided, and part of the material was subject to instrumental neutron activation analysis using epithermal neutrons (ENAA) at IBR-2 pulsed fast reactor in Dubna, Russia. Neutron flux density and temperature in the channels of irradiation of the pneumatic system REGATA are shown in *Table 1*. One should note that the high fluxes of epithermal and fast neutrons of IBR-2 reactor are especially favorable for determination of the radionuclides with large resonance integrals.

Table 1. Characteristics of the irradiation channels

Irradiation site	$\phi_{th}x10^{12}$ (n/cm^2s) E=0.55eV	$\phi_{epi}x10^{12}$ (n/cm^2s) E=0.55÷10^5eV	$\phi_{fast}x10^{12}$ (n/cm^2s) E=0.1÷25MeV	$<E_{fast}>$MeV (n/cm^2s) E=0.1÷25MeV	Tempe-rature, °C
Ch1 Cd coated	0.023	3.31	4.32	0.88	70
Ch2	1.23	2.96	4.10	0.92	60

Short-lived radionuclides were determined using small parts of filters (2.5 x 2.5 cm) which were irradiated in channel 2. Long-lived radionuclides were determined using activation with the epithermal neutrons in channel 1.

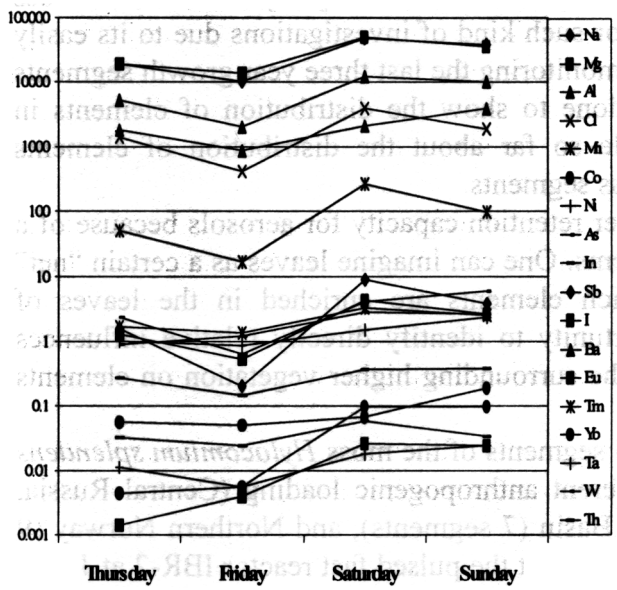

Fig. 1. Irregularity of aerosol elemental content of the South of the Greater Cairo Area

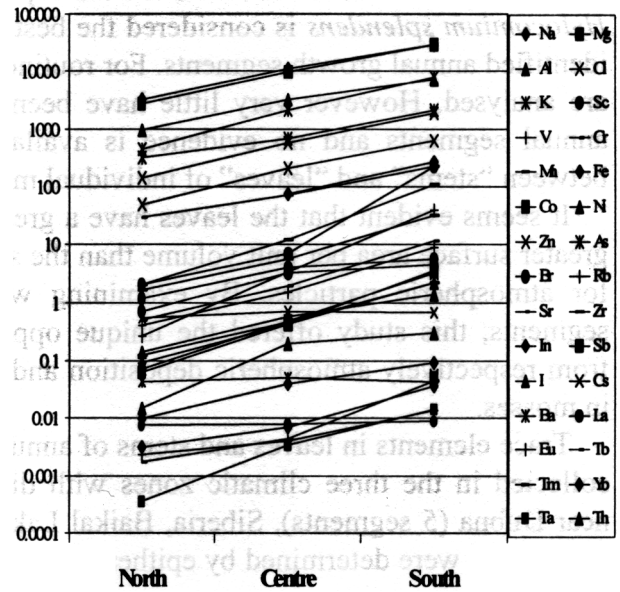

Fig. 2. The Greater Cairo Area aerosol elemental content.

Further investigations will allow us to create coloured geographical maps of temporal and spatial air pollution patterns for the examined periods of time.

This pilot study showed the possibility of obtaining information on air pollution elements using segments of the same air filters exposed for radionuclide determination at the National Center for Nuclear Safety and Radiation Control in Cairo.

REFERENCES

[1] CERVENY, R.S., BALLING, R.C., Jr. Weekly cycles of air pollutants, precipitation and tropical cyclones in the coastal NW Atlantic region. Nature, 394/6, 561- 563 (1998).

[2] GRAEDEL, T.E., FARROW, L.A., WEBER, T.A. Photochemistry of the "Sunday Effect". Environ. Sci. Technol. 11, 690-694 (1977).

[3] ANDERSON, B.E. et al. The impact of U.S. continental outflow on ozone and aerosol distributions over the Western Atlantic. J. Geophys. Res. 98(D12), 23477-23489 (1993).

STUDY OF TRACE ELEMENTS IN ANNUAL SEGMENTS OF MOSS BIOMONITORS USING EPITHERMAL NEUTRON ACTIVATION ANALYSIS: LINK WITH ATMOSTHERIC AEROSOL

Ye.V. Yermakova, M.V. Frontasyeva, E. Steinnes*, K. A. Rahn**

Joint Institute for Nuclear Research, Dubna, Russia
**Norwegian University of Science and Technology, Trondheim, Norway*
***University of Rhode Island, Centre for Atmospheric Chemistry Studies, Narragansett, USA*

Analysis of naturally growing moss as biomonotor is a well established technique for surveying deposition of metals from atmospheric pollution sources [1-3]. The feather moss *Hylocomium splendens* is considered the best for such kind of investigations due to its easily identified annual growth segments. For routine monitoring the last three year growth segments are analysed. However very little have been done to show the distribution of elements in annual segments and no evidence is available so far about the distribution of elements between "stems" and "leaves" of individual moss segments.

It seems evident that the leaves have a greater retention capacity for aerosols because of a greater surface area per unit volume than the stems. One can imagine leaves as a certain "net" for atmospheric particles. By examining which elements are enriched in the leaves of segments, this study offered the unique opportunity to identify directly relative influences from respectively atmospheric deposition and the surrounding higher vegetation on elements in mosses.

Trace elements in leaves and stems of annual segments of the moss *Hylocomium splendens* collected in the three climatic zones with different anthropogenic loading (Central Russia, near Dubna (5 segments), Siberia, Baikal Lake Basin (7 segments), and Northern Norway (9 segments)) were determined by epithermal activation at the pulsed fast reactor IBR-2 at JINR, Dubna.

Data obtained for 32 elements (Na, Mg, AL, Cl, K, Ca, Sc, V, Cr, Mn, Fe, Co, Ni, Zn, As, Br, Rb, Sr, Mo, Cd, Sb, I, Cs, Ba, La, Ce, Sm, Hf, Ta, W, Th, U) were used for the analysis of the inter-annual variations of elemental concentrations in leaves and stems of annual segments.

The major finding is that even through concentrations of elements varied considerably over leaves and stems, leaves/stem ratios for individual segments varied so little that they could be considered characteristic for each element. Plots of elemental concentrations of paired moss leaves and stems from all three places (Central Russia, Siberia, and Northern Norway) showed clearly that the grouping of elements is systematic and geochemically meaningful: elements with the highest leaves/stem ratios are those typically associated with atmospheric aerosol or deposition (lithophilic and chalcophilic elements such as Al, Sc, V, and Sb), whereas elements with the lowest leaves/stem ratios are those typically linked with plant material (K, Zn, Rb, Cs). Intermediate elements with mixed properties are those enriched in plants but also in the atmosphere (Mn, Ca, Mg, Ba, etc.) (**Fig. 1**).

By examining which elements are enriched in the leaves of segments, this study allows one to identify relative atmospheric/plant influences on elements in moss directly, assuming that leaves have a greater effect from aerosol because of a greater surface area per unit volume than stems. The observed grouping of elements (**Fig. 1**) is consistent with this picture: the

"atmospheric" Al-group is enriched in leaves, the "plantlike" K-group is enriched in stems, and the "mixed" Mn-group shows similar concentrations in leaves and stems.

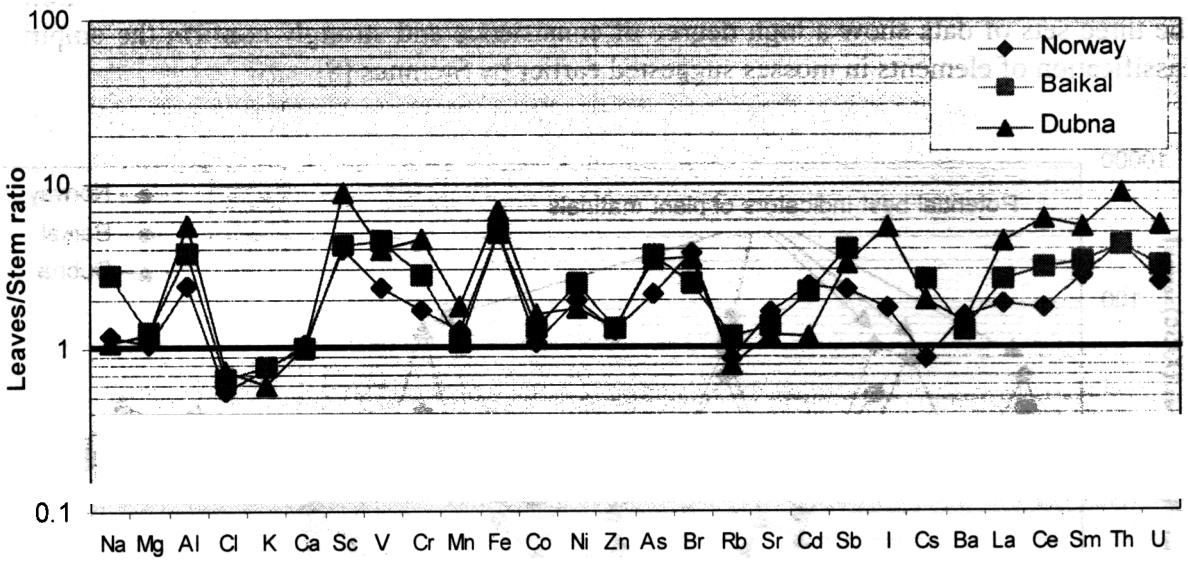

Fig.1. Mean Leaves/Stem ratio of element concentrations

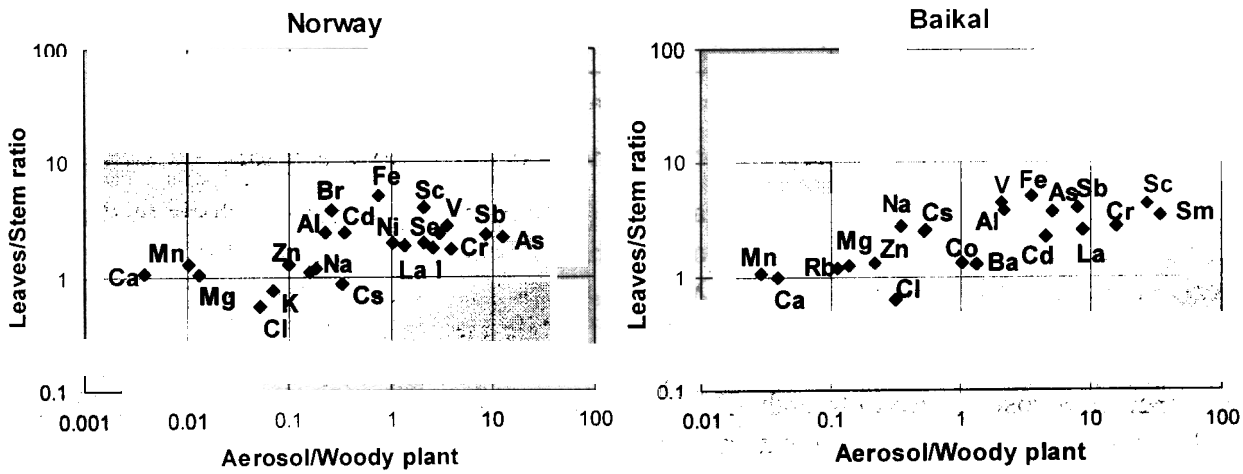

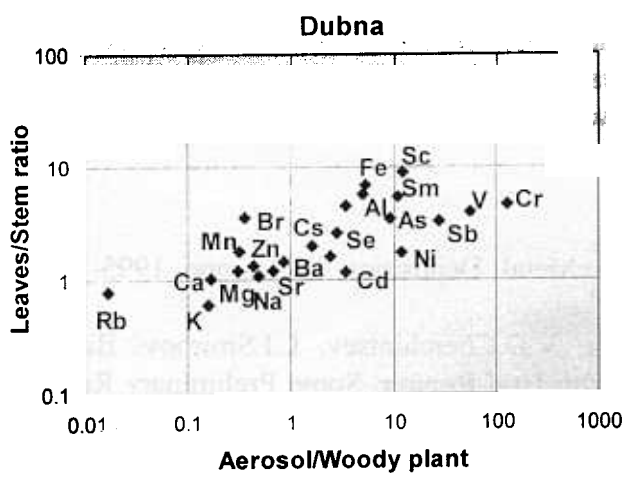

Fig.2. Leaves/Stem ratio in moss versus aerosol/plant ratio

To test these groups further, an independent index of atmospheric/plant ratios (Aerosol/Woody plant) was calculated for the elements concerned and compared with the leaves/stem ratios in the moss (**Fig. 2**) using literature data for aerosols from Moscow (4), Baikal (5) and Norway (6), and Bowen's global averages for woody plants (7). The degree of correlation between the two ratios is remarkable. The three plots in **Fig. 2** show that only a few of the many elements determined in mosses are pure atmospheric

indicators. They are found at the upper right end of the plot, and include V, Cr and Sb, and possibly some other pollution and crustal elements. For elements found between the lower left and the middle of the plot mosses are not satisfactory as indicators of atmospheric pollution. The three sets of data show a high degree of consistence and strongly confirm the empirical classification of elements in mosses suggested earlier by Steinnes [8].

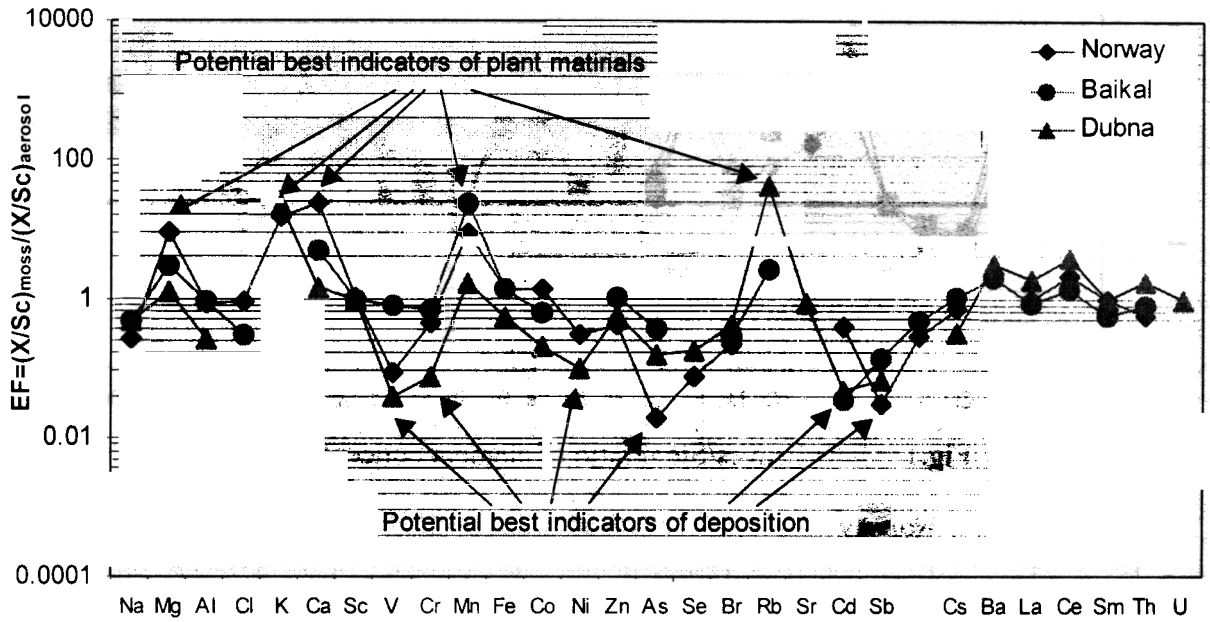

Fig 3. Enrichment factor of elements in moss versus aerosol

Potential best indicators of plant materials (non-crust origin) can be distinguished by comparing the moss average composition with that of atmospheric aerosol (**Fig. 3**). Here the enrichment factor X is defined as $EF=(X/Sc)_{moss}/(X/Sc)_{urban\ aerosol}$. In this plot purely crustal elements not enriched in plants will plot at EF=1 while elements with EF<1 predominate in the relevant aerosol. Since atmospheric deposition of an element is clearly connected to its presence in aerosols, elements with EF<<1 in **Fig. 3** can be considered as good pollution indicators. The potential best indicators of atmospheric pollution as indicated from **Fig. 3** are thus: for Norway V, Ni, As and Sb; for the Baikal Lake Basin Cl (emission from the Baikalsk Cellulose-Paper Plant), Cd and Sb; and for Dubna V, Cr, Co, Ni, As, Cd and Sb. It should be noted that elements showing extremely low EF values in the plot are typically those that have a pollution origin and at the same time show a low retention capacity in the moss.

References

Å.Rühling, E.Steinnes. Atmospheric Heavy Metal Deposition in Europe 1995-1996. *NORD Environment*, 1998:15, 67 p.

2. M.V.Frontasyeva, E.Steinnes, S.M.Lyapunov, V.D.Cherchintsev, L.I.Smirnov. Biomonitoring of Heavy Metal Deposition in the South Ural Region: Some Preliminary Results obtained by Nuclear and Related Techniques, *J.Radioanal.Nucl.Chem.*, Vol.245, No.2 (2000) 415-420.

3. M.V.Frontasyeva, Ye.V.Yermakova, E.Steinnes. Reliability of Mosses (*Hylocomium Splendens*, *Pleurozium Schreberi* and *Calliergon Geganteum*) as Biomonitors of Heavy Metal Atmospheric Deposition in Central Russia. *FLNP JINR Annual Report-1999*, 2000-81, p. 178-180, 2000.
4. A.A.Volokh. Experience in Controlling Air Pollution with Metals and Organic Compounds in Urban and Background Territories. In Geochemical Investigations of Towns' Aglomerations. "Minpriroda", Moscow, 1998, p.40-58 (in Russian).
5. K.A.Rahn, T.V.Khodzhe, U.Tomza. A Study of Trace Elements in Atmospheric Aerosols of the Eastern Siberia Using Neutron Activation and Synchrotron Radiation X-ray Fluorescence Analysis, *Nuclear Instruments and Methods in Physics Research*, A 448, 2000 p. 413-418.
6. K.A.Rahn. The Chemical Composition of the Atmospheric Aerosol. *Technical Report*, Graduate School of Oceanography, University of Rhode Island, 1976, 265 p.
7. H.J.M. Bowen: Environmental Chemistry of the Elements, pp.92-93, Academic Press, London 1979.
8. E.Steinnes. Aspects of Biomonitoring Air Pollutants Using Mosses. In "Plants as Biomonitors. Indicators for Heavy Metals in the Terrestrial Environment". VCH, Weinheim,1993, p.381-394.

5. PUBLICATIONS

CONDENSED MATTER PHYSICS

Diffraction

1. Andrianov A.V., Kosarev D.I., Beskrovnyi A. I. Helical magnetic ordering in Tb completely suppressed by uniaxial tension: Evidence of electronic topological transition and support for the nesting hypothesis. Phys. Rev., 2000, v.B62, p.13844.
2. Babushkina N.A., Belova L.M., Taldenkov A.N., Aksenov V.L., Balagurov A.M., Pomjakushin V.Yu., Sheptyakov D.V., Gorbenko O.Yu., Kaul A.R., Kugel K.I., Khomskii D.I. Isotopically driven transitions in LaPrCaMnO system. Physica B, 2000, v.280 , pp.323-324.
3. Balagurov A.M., Fischer P., Pomjakushin V.Yu., Sheptyakov D.V., Aksenov V.L. Atomic and magnetic structure of perovskite manganites: A-cation size and oxygen isotope substitution effects and homogeneity of magnetic state. Physica B, 2000, v.276-278, pp.536-539.
4. Balagurov A.M., Pomjakushin V.Yu., Sheptyakov D.V., Aksenov V.L., Fischer P., Keller L., Gorbenko O.Yu., Kaul A.R., Babushkina N.A. Long scale phase separation versus homogeneous magnetic state in $(La_{1-y}Pr_y)_{0.7}Ca_{0.3}MnO_3$: a neutron diffraction study. Physical Review B, 2000 (in press).
5. Balagurov A.M., Raspopina E.V., Sikolenko V.V., Lyubutin L.S., Stepin L.S., Gribanov A.V., Andre G., Bouree F., Duh H.M. Neutron diffraction study of the $U(Pd_{1-x}Fe_x)_2Ge_2$ magnetic structure. J. of Magnetism and Magnetic Materials, 2000, v.210, pp.225-232.
6. Balagurov A.M., Fischer P., Pomjakushin V.Yu., Sheptyakov D.V., Aksenov V.L. Atomic and magnetic structure of perovskite manganites: A-cation size and oxygen isotope substitution effects and homogeneity of magnetic state. Physica B: Physics of Condensed Matter, 2000, v.276-278, pp.536-539.
7. Balagurov A.M., Pomjakushin V.Yu., Sheptyakov D.V., Aksenov V.L., Babushkina N.A., Belova L.M., Gorbenko O.Yu., Kaul A.R. A-cation size and oxygen isotope substitution effects on $(La_{1-y}Pr_y)_{0.7}Ca_{0.3}MnO_3$ structure. Eur. Physical Journal, B, 2001, v.19, p.215.
8. Balagurov A.M., Beskrovnyi A.I., Mironova G.M., Pole A.V., Simkin V.G. “Diffraction experiments at the IBR-2 pulsed reactor with methane cold neutron source” JINR Communication, P3-2000-220, 2000, Dubna.
9. Balagurov A.M., Pomjakushin V.Yu., Sheptyakov D.V., Aksenov V.L., Fischer P., Keller L., Gorbenko O.Yu., Kaul A.R., Babushkina N.A. Long scale phase separation versus homogeneous magnetic state in $(La_{1-y}Pr_y)_{0.7}Ca_{0.3}MnO_3$: a neutron diffraction study. Phys. Rev. B, 2000, in press.
10. Bramnik K.G., Miehe G., Ehrenberg H., Fuess H., Abakumov A.M., Shpanchenko R.V., Pomjakushin V.Yu., Balagurov A.M. Preparation, structure and magnetic studies of a new $Sr_{11}Re_4O_{24}$ double oxide. Solid State Chemistry, 2000, v.149, pp.49-55.
11. Chernyshov D.Yu., Sheptyakov D.V., Smirnov M.B., Trounov V.A. Crystal structure and lattice dynamic effects of rare-earth hexaborides under hydrostatic pressure. Physica B, 2000, v.276-278, pp.320-321.
12. Duginov V.N., Gritsaj K.I., Amato A., Baines Ch., Herlach D., Pomjakushin V.Yu., Zimmermann U., Ponomarev A.N., Krivosheev I.A., Nezhivoy A.A., Gribanov A.V., Nikiforov V.N., Seropegin Yu.D. Study of the magnetic properties of $Ce_3Pd_{20}Si_6$ compound. Physica B, 2000, v.289-290, pp.43-46.
13. Fischer P., Frey G., Koch M., Koennecke M., Pomjakushin V., Schefer J., Thut R., Schlumpf N., Buerge R., Greuter U., Bondt S., Berruyer E. High-resolution powder diffractometer HRPT for thermal neutrons at SINQ. Physica B, 2000, v.276-278, pp.146-147.
14. Glazkov V.P., Savenko B.N., Somenkov V.A, Sheptyakov D.V., Shilstein S.Sh. Investigation of Nd_2CuO_4 crystal structure at high pressure by neutron diffraction. High Pressure Research, 2000, v.17, pp.201-207.
15. Kozlenko D.P, Glazkov V.P., Savenko B.N., Somenkov V.A., Hull S. Structural study of ND_4Br at high pressure. High Pressure Research, 2000, v.17, pp.251-260.
16. Kozlenko D.P., Belushkin A.V., McGreevy R.L., Savenko B.N., Zetterström P. A study of orientational disorder in NaCl-type phase I of ND_4I by reverse Monte Carlo and maximum entropy methods. JINR Communication, 2000, E14-2000-221, Dubna.
17. Kozlenko D.P., Glazkov V.P., Savenko B.N., Somenkov V.A. Hull S. Structural study of ND_4I at high pressures and low temperatures. High Pressure Research, 2000, v.17, pp.235-249.
18. Kozlenko D.P., Savenko B.N., Glazkov V.P., Somenkov V.A., Hull S. Structure and dynamics of ammonium halides under high pressure. Physica B, 2000, v. 276-278, pp. 226-227.
19. Lobanov M.V., Balagurov A.M., Pomjakushin V.Ju., Fisher P., Gutmann M., Abakumov A.M., D'yachenko O.G., Antipov E.V., Lebedev O.I., Van Tendeloo G. Structural and magnetic properties of the colosal magnetoresistance perovskite $La_{0.85}Ca_{\_0.15}MnO_3$. Physical Review B, 2000, v.61, pp.8941-8949.
20. Pomjakushin V.Yu., Balagurov A.M., Raspopina E.V., Sikolenko V.V., Gribanov A.V., Schenck A., Amato A., Zimmermann U., Lyubutin I.S. Modulated structure of $U(Pd_{1-x}Fe_x)_2Ge_2$ studied by μSR J.Phys.:Condens. Matter, 2000, v.12, pp.7969-7981.

21. Ponomarev A.N., Ivanter I.G., Krivosheev I.A., Nezhivoy A.A., Nikolsky B.A., Duginov V.N., Gritsaj K.I., Olshevsky V.G., Herlach D., Pomjakushin V.Yu., Zimmermann U. Magnetic field acting on muons in textured and single crystalline holmium. Physica B, 2000, v.289-290, pp.236-239.
22. Putilin S.N., Antipov E.V., Abakumov A.M., Rozova M.G., Lokshin K.A., Pavlov D.A., Balagurov A.M., Sheptyakov D.V., Marezio M. Effect of fluorination and high pressure on the structure and properties of the Hg-bearing superconducting Cu mixed oxides. Physica C, 2000, v.338, pp.52-59.
23. Raspopina E.V., Balagurov A.M., Pomjakushin V.Yu., Sikolenko V.V., Gribanov A.V., Amato A., Schenck A. Magnetic structure of $U(Pd_{1-x}Fe_x)_2Ge_2$ studied by μSR: comparison with neutron diffraction data. Physica B, 2000, v.289-290, pp.282-285.
24. Schefer J., Boehm M., Keller L., Medarde M., Horisberger M., Fischer P., Pomjakushin V., Doenni A. Application of composite neutron germanium monochromators at SINQ: neutron powder diffraction (HRPT) and single crystal diffraction (TriCS). Physica B, 2000, v.276-278, pp.302-304.
25. Voronin V.I., Teplykh A.E., Medvedeva I.V., Kuchin A.G., Sheptyakov D.V., Glazkov V.P., Savenko B.N. Magnetic and structural properties of $Y_2Fe_{15.3}Si_{1.7}$ alloy under high pressure. High Pressure Research, 2000, v.17, pp.193-200.

Textures and stresses

1. Bestmann M., Kunze K., Matthews A. Evolution of a calcite marble shear zone complex on Thassos Island, Greece: Microstructural and textural fabrics and their kinematic significance. Journal of Structural Geology, 2000, v.22, pp.1789-1807.
2. Bokuchava G.D., Schreiber J., Shamsutdinov N., Stalder M. Residual stress studies in graded W/Cu materials by neutron diffraction method, Physica B, 2000, v.276-278, pp.884-885.
3. Burilichev D.E., Ivankina T.I., Klima K., Locajicek T., Nikitin A.N., Pros Z. Investigation of rock samples by neutron diffraction and ultrasonic sounding. Physica B, 2000, v.276-278, pp.837-838.
4. De Wall H., Bestmann M., Ullemeyer K. Anisotropy of diamagnetic susceptibility in Thassos marble: a comparison between measured and modelled data. Journal of Structural Geology, 2000, v.22, pp.1761-1771.
5. Frischbutter A., Neov D., Scheffzuek Ch., Vrana M., Walther K. Lattice strain measurements on sandstones under load using neutron diffraction. Journal of Structural Geology, 2000, v.22, pp.1587-1600.
6. Ivankina T.I., Nikitin A.N., Abramova V.I., Arkhipov I.K., Levin D.M.. Development of the model of texture formation in a plastically deformed iron-copper composite. Zavodskaya laboratoria, 2000, v.3, p.19-25.
7. Ivankina T.I., Nikitin A.N., Telepnev A.S., Ullemeyer K., Sobolev G.A., Sukhoparov V.A., Walther K. Textures and physical properties of marbles deformed at 20-250°C. High Pressure Research, 2000, v.17, pp.335-346.
8. Ivankina T.I., Yudin V.E.. Indexing of the diffraction spectra of multiphase materials. Metodicheskie rekomendatsii. 2000, Moscow, MSU, p. 14.
9. Leiss B., Weiss T. Fabric anisotropy and its influence on physical weathering of different types of Carrara marbles. Journal of Structural Geology, 2000, v.22, pp.1737-1745.
10. Locajicek T., Pros Z., Klima K., Nikitin A.N., Ivankina T.I., Ullemeyer K., Smirnov Y.P., Guberman D.M., Kouznetzov Y.I. P-wave elastic anisotropy and texture of amphibolites from the Kola super deep borehole KSDB-3. IGCP Project 408: The results of the study of the deep substance and physical processes in the Kola super deep borehole section down to a depth of 12261 m. Apatity: Poligraph, 2000, pp.122-125.
11. Nikitin A.N., Ullemeyer K., Ivankina T.I. Texture analysis of geologic materials by neutron diffraction. JINR News, 2000, v.3, pp.16-19.
12. Nikitin A.N.. The anisotropy and texture of materials. Course of lectures. Uchebnoe posobie. 2000, Moscow, MSU, 267 p.
13. Scheffzuek Ch., Walther K., Frischbutter A. Strain measurements on geomaterials by neutron time-of-flight diffraction. Materials Science Forum, 2000, v.347-349, pp.542-547.
14. Siegesmund S., Ullemeyer K., Weiss T., Tschegg E.K. Physical weathering of marbles caused by anisotropic thermal expansion. International Journal of Earth Sciences, 2000, v.89, pp.170-182.
15. Taran Yu.V.,Schreiber J., Mikula P., Lukas P., Neov D., Vrana M. Neutron diffraction investigation of low and high cycle fatigue austenitic stainless steel. Materials Science Forum, 2000, v.347-349, pp.322-327.
16. Taran Yu.V.,Schreiber J., Wright J.S. The time-of-flight diffraction measurements of residual stresses in a shape welded steel tube. Materials Science Forum, 2000, v.347-349, pp.640-645.
17. Ullemeyer K., Braun G., Dahms M., Kruhl J.H., Olesen N.-Ř., Siegesmund S. Texture analysis of a muscovite-bearing quartzite: a comparison of some currently used techniques. Journal of Structural Geology, 2000, v.22, pp.1541-1557.
18. Ullemeyer K., Spalthoff P., Leiss B., Weber K. TOF texture investigations of geological samples. Physica B 2000, v.276-278, pp.878-879.
19. Walther K., Scheffzuek C., Frischbutter A. Neutron time-of-flight diffractometer "EPSILON" for strain measurements: layout and first results. Physica B, 2000, v.276-278, pp.130-131.

Small angle scattering

1. Avdeev M., Garamus V., Rosta L., Smirnova I., Smirnova N. SANS study of micelle formation in aqueous mixed solutions of sodium and magnesium dodecylsulfates. Physica B, 2000, v.276-278, pp.339-342.
2. Bakeeva R. F., Kudriavcev D. B., Zaharova L., Kudriavceva L.A., Rajewska A., Sopin V. F. Micellar liquid crystalline and polymer systems based on surfactant and polyethyleneimine as nanoreactors for transfer of phosphorous group. Liquid Crystals, 2000 (in press).
3. Cherezov V., Cheng A., Petit J.-M., Diat O., Caffrey M. Biophysics and synchrotron radiation. Where the marriage fails. X-ray damage of lipid membranes and mesophases. Cellular and Molecular Biology, 2000, v.46, pp.1133-1145.
4. Eckold G., Gorski N. Small-angle neutron scattering from tetradecyltrimethylammonium bromide in NaBr aqueous solutions. Colloids and Surfaces A, 2000(in press).
5. Merta J., Garamus V.M., Kuklin A.I., Willumeit R., Stenius P. Determination of the structure of complexes formed by a cationic polymer and mixed anionic surfactants by small-angle neutron scattering. Langmuir, 2000; v.16, pp.10061-10068
6. Sinko K., Cser L., Mezei R., Avdeev M., Peterlik H., Trimmel G., Schubert U., Fratzl P. Structure investigation of intelligent aerogels. Physica B, 2000, v.276-278, pp.392-393.
7. Uhrikova D., Balgavy P., Kucerka N., Islamov A., Gordeliy V. Kuklin A. Small-angle neutron scattering study of the n-decane effect on the bilayer thickness in extruded unilamellar dioleoylphosphatidylcholine liposomes. Biophysical Chemistry, 2000, v.88, pp.165-170.

Reflectometry, polarized neutrons

1. Aksenov V.L., Cser L., Gundorin N.A., Nikitenko Yu.V., Popov Yu.P. Observation of neutron standing waves at total reflection of polarised neutrons by method of precision gamma-spectroscopy. Physica B, 2000, v.276-278, p.809.
2. Aksenov V.L., Gundorin N.A., Nikitenko Yu.V., Popov Yu.P.., Cser L. Observation of neutron standing waves at total reflection of polarized neutrons by the method of precision gamma-spectroscopy. Poverkhnost, 2000, v.6, p.7.
3. Aksenov V.L., Kozhevnikov S.V., Nikitenko Yu.V. Refraction of polarized neutrons on boundaries of a magnetic film. Physica B, 2000, v.276-278, p.958.
4. Aksenov V.L., Kozhevnikov S.V., Nikitenko Yu.V. Spin-flipped transmission of polarized neutrons through a Co film on glass. Physica B, 2000, v.276-278, p.956.
5. Aksenov V.L., Kozhevnikov S.V., Nikitenko Yu.V., Lauter H. Reflection and refraction of spin-flip neutrons in a Fe-Gd structure. Physica B, 2000, v.276-278, p.179.
6. Aksenov V.L., Nikitenko Yu.V. Neutron interference in layered structure at grazing–incidence reflection. Neutron standing waves: application, status, perspectives. Physica B, 2001 (in press).
7. Aksenov V.L., Nikitenko Yu.V., Kozhevnikov S.V. Spin-flip spatial neutron beam-splitting in magnetic media. Physica B, 2001 (in press).
8. Aksenov V.L., Nikitenko Yu.V, Kozhevnikov S.V., Radu F., Krus R., Rekveldt T. Generation of neutron standing waves at total reflection of polarized neutrons. Povekhnost, 2000, v.8, p.10.
9. Aksenov V.L., Nikitenko Yu.V., Radu F., Gledenov Yu.M., Sedyshev P.V. Observation of resonance enhanced neutron standing waves through (n,γ) reaction, Physica B, 2000, v.276-278, p.916.
10. Gutberlet T., Kiselev M., Heerklotz H., Klose G. SANS study of mixed POPC/$C_{12}E_n$ aggregates. Physica B, 2000, v.381-383, pp.276-278.
11. Kiselev M.A., Grysunov Yu.A., Dobretsov G.E., Komarova M.N. The size of the human albumin molecule in solutions. Biofizika, 2001 (in print).
12. Kiselev M.A., Lesieur P., Kisselev A.M., Lombardo D., Killany M., Lesieur S. Sucrose buffer as perspective medium to study the vesicle structure: SAXS and SANS study. J. Alloys and Compounds, 2001 (in press).
13. Kiselev M.A., Lesieur P., Kisselev A.M., Lombardo D., Killany M., Lesieur S., Ollivon M. A sucrose solutions application to the study of model biological membranes. Nuclr. Inst&Method, 2001 (in press).
14. Kiselev M.A., Lesieur P., Kisselev A.M., Olivon M. Ice formation in model biological membranes in the presence of cryoprotectors. Nuclr. Inst&Method A, 2000, v.448, pp.255-260.
15. Kiselev M.A., Lesieur P., Lombardo D., Kisselev A.M., Gutberlet T. The investigation of temperature-sensitive phospholipid /surfactant systems via neutron and X-ray small-angle scattering and diffraction. Chemistry and Physics of Lipids, 2000, v.107, p.72.
16. Kiselev M.A., Lesieur P., Lombardo D., Kisselev A.M., Ollivon M. A structure of phospholipid vesicles in the presence of cryoprotectors. Chemistry and Physics of Lipids, 2000, v.107, pp.72-73.
17. Korneev D.A., Bodnarchuk V.I., Peresedov V.F., Zhuravlev V.V., Schebetov A.F. Inelastic mode of polarised reflectometer REFLEX-P for observation of surface phonons and magnons. Physica B, 2000, v.276-278, pp.314-315.

18. Korneev D.A., Bodnarchuk V.I., Yaradaikin S.P., Peresedov V.F., Ignatovich V.K., Menelle A., Gaehler R. Reflectometry studies of the coherent properties of neutrons. Physica B, 2000, v.276-278, pp.973-974.
19. Kravtsov E, Lauter-Pasyuk V., Lauter H.J., Toperverg B., Nikonov O., Petrenko A., Milyaev M.A., Romashev L., Ustinov E. Interface formation and magnetic ordering in Fe/Cr hybrid nanostructures. Physica B, 2000 (in press).
20. Lauter-Pasyuk V., Lauter H.J., Lorenz M., Petrenko A., Nikonov O., Aksenov V.L., Leiderer P. Magnetic field distribution around flux-lines in $YBa_2Cu_3O_7$ superconducting thin films in a parallel field. Physica B, 2000, v.276-278, p.776-777.
21. Lauter-Pasyuk V., Lauter H.J., Toperverg B., Nikonov O., Kravtsov E., Milyaev M.A., Romashev L., Ustinov V. Magnetic off-specular neutron scattering from Fe/Cr multilayers. Physica B, 2000, v.283, pp.194-198.
22. Lesieur P., Kiselev M.A., Barsukov L.I., Lombardo D. Temperature induced micelle to vesicle transition: kinetic effects in the DMPC / NaC system. J. Appl. Cryst., 2000, v.33, pp.623-627.
23. Nikitenko Yu.V., Kozhevnikov S.V., Toperverg B., Nikonov O., Lauter-Pasyuk V., Lauter H. Towards 3D polarization analysis in neutron reflectometry. Physica B, 2000 (in press).
24. Schmiedel H., Joerchel P., Kiselev M., Klose G. Determination of structural parameters and hydration of unilamellar POPC/$C_{12}E_4$-vesicles at high water excess from neutron scattering curves using a novel method of evaluation. J. Phys. Chem., 2001 (in press).
25. Toperverg B., Lauter-Pasyuk V., Lauter H., Nikonov O., Ausserri D., Gallot Y. Morphology of off-specular neutron scattering pattern from islands on a lamellar film. Physica B, 2000, v.283, pp.60-64.

Inelastic scattering of neutrons

1. Baran J., Pawlukojc A., Majerz I., Malarski Z., Sobczyk L., Grech E. Vibrational spectra of the adduct of 1,8-bis(dimethylamino) naphthalene with dichloromaleic acid (DMAN*DCM). Spectrochimica Acta A, 2000, v.56, pp.1801-1812.
2. Bobrowicz-Sarga L., Czarnecki P., Lewicki S., Natkaniec I., Wasicki J. Neutron diffraction study of thermal expansion and compressibility of piridinium nitrate and tetrafluoroborate. Materials Science Forum, 2000, v.321-324, pp.1107-1112.
3. Cser L., Hoiderna-Natkaniec K., Natkaniec I., Pawlukojc A. Neutron spectroscopy and QC modeling of the low-frequency internal vibrations of mesitylene. Physica B, 2000, v.276-278, pp.296-297.
4. Glazkov V.P., Kozlenko D.P., Savenko B.N., Somenkov V.A. Vibrational spectra of ammonia halides NH_4I and NH_4F at high pressures. JETP, 2000, v.90, pp.319-323.
5. Glazkov V.P., Somenkov V.A., Syrykh G.F., Savenko B.N. Splitting of libration mode frequencies in the vicinity of orientation phase transition in NH_4Br. High Pressure Research, 2000, v.17, pp.289-295.
6. Hoiderna-Natkaniec K., Natkaniec I., Pawlukojc A., A., Khavryuchenko V.D. Neutron spectroscopy and QC modeling of methyl dynamics in 1- and 2-methyl-naphthalene crystals, Physica B, 2000, v.276-278, pp.292-293.
7. Kazimirov V.Yu., Rieder E.E., Sarin V.A., Smirnov M.B., Belushkin A.V., Shuvalov L.A. Investigation of ferroelectric phase transition in DMAAS crystals: neutron diffraction, neutron spectroscopy, theoretical model. Ferroelectrics, 2000, v.235, pp.35-46.
8. Lushnikov S.G., Belushkin A. V., Gvasaliya S.N., Natkaniec I., Shuvalov L.A., Smirnov L.S., Dolbinina V.V. Neutron scattering study of the $Cs_5H_3(SO_4)_4*0.5H_2O$ crystal and its deuterated analog. Physica B, 2000, v.276-278, pp.483-484.
9. Lushnikov S.G., Gvasalia S.N., Siny I.G., Sashin I.L., Schmidt V.N., Uesu Y. Temperature dependence of the generalized vibrational density of states of sodium bismuth titanate in the ferroelectric phase. Solid State Communications, 2000, v.116, pp.41-45.
10. Majerz I., Pawlukojch A., Sobczyk L., Dziembowska T., Grech E., Szady-Cheimieniecka A. The infrared, Raman and inelastic neutron scattering studies on 5-nitro-N-salicylideneethylamine. Journal of Molecular Structure, 2000, v.552, pp.243-247.
11. Malenkov G.G., Averkiev A.A., Bobrowicz-Sarga L., Bragin S.I., Natkaniec I., Smirnov L.S. Neutron scattering study of heavy water and ice under hydrostatic Ar pressure. Materials Science Forum, 2000, v.321-324, pp. 872-877.
12. Malenkov G.G., Zheligovskaya E.A., Averkiev A.A., Natkaniec I., Smirnov L.S., Bobrowicz –Sarga L., Bragin S.I. Dynamics of hydrogen-bonded water networks under high pressure: neutron scattering and computer simulation, High Pressure Research, 2000, v.17, pp.273-280.
13. Mikuli E., Migdai-Mikuli A., Natkaniec I., Mayer J. Phase transition and water dynamics of $[Mn(H_2O)_6](ClO_4)_2$ studied by differential scanning calorimetry and neutron scattering methods. Z. Naturforsch., 2000, v.55a, pp.1-6.
14. Natkaniec I., Martinez Sarrion M.L., Mestres L., Smirnov L.S. Ammonium dynamics and structural phase transition in $Rb_{1-x}(NH_4)_xI$ solid solutions at 20K. Physica B, 2000, v.276-278, pp.294-295.
15. Osborn R., Goremychkin E.A., Sashin I.L., Murani A.P. Anomalous magnetic response of $Ce_{1-x}La_xAl_3$. Journal of Appl. Physics, 2000, v.87, pp.5131.

16. Pawlukojc A., Natkaniec I., Malarski Z., Leciejewicz J. The dynamical pattern of the 2-aminopyrazine-3-carboxylic acid molecule by inelastic and incoherent neutron scattering, Raman spectroscopy and ab initio calculations. Journal of Molecular Structure, 2000, v.516, pp.7-14.
17. Sheka E., Barthel H., Khavryutchenko V., Natkaniec I., Nikitina E., Weis J. INS and IR studies of intermolecular interaction at the silicone-fumed silica interface I. Silicones, Phys. Low-Dim. Struct., 2000, v.7-8, pp.127-158.
18. Sheka E., Natkaniec I., Khavryutchenko V., Nikitina E., Barthel H., Weis J. INS study of intermolecular interaction at the silicone-fumed silica interface. Physica B, 2000, v.276-278, pp.244-246.
19. Shuvalov L.A., Natkaniec I., Smirnov L.S. Dynamic and static orientational disorder in mixed $K_{1-x}(NH_4)_xI$ crystals. Crystallography Reports, 2000, v.45, pp.270-276.
20. Wasicki J., Kozlenko D.P., Lewicki S., Goc R., Savenko B.N. Ammonium ions dynamics in NH_4Br at high pressure - measurements and simulations. High Pressure Research, 2000, v.18, pp.359-363.

Accelerated ions and ❍SR

1. Didyk A.Yu., Kobzev A.P., Orelovich O.L., Semina V.K. Track effects in silicon irradiated by swift high energy heavy ions. JINR Communication E14-2000-107, 2000, Dubna, JINR.
2. Pogrebnjak A.D., Kobzev A.P., Gritsenko B.P., Sokolov S., Bazyl E., Sviridenko N.V., Valyaev A., Ivanov Yu. F. Effect of Fe and Zr ion implantation and high-current electron irradiation treatment on chemical and mechanical properties of Ti-V-Al alloy. Journal of Applied Physics, 2000, v.87, pp. 2142-2148.
3. Popov Yu.P., Voinov A.V., Parzhitski S.S., Gundorin N.A., Serov D.G., Kobzev A.P., Sedyshev P.V. Measurements of a partial cross section for the reaction $^{58}Ni(n,\gamma_o)\ ^{59}Ni$. Physics of Atomic Nuclei. v.63, 2000, pp. 525-529.

Miscellaneous

1. Aksenov V.L., Ossipyan Yu.A., Forro L., Khasanov S., Chernyshev V.V., Shakhmatov V.S. Fullerene molecule strain in RbC_{60}. Physics Letters A, 2000, v.268, pp.395-398.
2. Aksenov V.L., Ossipyan Yu.A., Shakhmatov V.S. Symmetry groups of carbon nanotubes. Particles and Nuclei, Letters, 2000, v.1, pp.44-47.

Participation in conferences

1. Avdeev M.V., Balasoiu M., Bica D., Rosta L., Torok G., Vekas L. Influence of particle concentration on ferrofluids microstructure studied by SANS. 8th European Magnetic Materials and Applications Conference, June 7-10, 2000, Kyiv, Ukraine.
2. Aksenov V.L., Ossipyan Yu.A., Shakhmatov V.S. Symmetry groups of carbon nanotubes. International Symposium on Fullerenes and Fullerene- Like Structures in Condensed Matter, 6-8 June, 2000, Minsk, Belarussia.
3. Aksenov V.L., Shakhmatov V.S. Phase transitions in fullerene crystals. XXVIII International Winter School of Physicist. Courovka-2000, February 28 - March 4, 2000, Ekaterinburg, Russia.
4. Balagourov A.M. Atomic and magnetic structure of $(La_{1-y}Pr_y)_{0.7}Ca_{0.3}MnO_3$: A-cation size and oxygen isotope substitution effects and homogeneity of magnetic state. M2S-HTSC-VI, 2000, February 20-25, Houston, USA.
5. Balagourov A.M. Magnetic and structural macroscopic phase separation in the perovskite manganites: A-cation size and isotope effects. ISRF-III, 2000, June 14-17, Dubna, Russia.
6. Balagurov A.M. Magnetic and structural macroscopic phase separation in the perovskite manganites: A-cation size and isotope effects. ISRF-III, 2000, June 14-17, Dubna, Russia.
7. Balagurov A., Pomjakushin V., Sheptyakov D., Fischer P. Structural long-range phase separation in perovskite manganites. ECM-XIX, 2000, August 25 – 31, Nancy, France.
8. Balagurov A.M. Magnetic and structural macroscopic phase separation in the perovskite manganites: A-cation size and isotope effects. ASR-2000, 2000, October 31 - November 02, Tokai, Japan.
9. Balagurov A.M. New developments of TOF neutron diffraction at the IBR-2 pulsed reactor. ICANS-XV, 2000, November 06-09, Tsukuba, Japan.
10. Baran J., Pawlukojc A., A., Majerz I., Malarski Z., Sobczyk L., Grech E. Vibrational spectra of the adduct of 1,8-bis(dimethylamino)naphthalene with dichloromaleic acid (DMAN*DCM). EUCMOS XXV, August 27-September 1, 2000, Coimbra, Portugal.
11. Brokmeier H.-G., Jansen E.M., Spalthoff P., Signorell J.A., Turner, Bolmaro R.E. Magnesium SiC reinforced composites - texture and residual strain investigation by simulation and experiments. Int. Congr. 'Magnesium Alloys and their Applications', September 26-28, 2000, Munich, Germany.
12. Brokmeier H.-G., Jansen E.M., Spalthoff P., Signorelli J.A., Turner G., Bolmaro R.E. Texture and residual strains of ceramic reinforced magnesium composites. Experiments and Simulations. THERMEC-2000, December 4- 8, 2000, Las Vegas, USA.

13. Brokmeier H.-G., Jansen E.M., Spalthoff P., Signorelli J.A., Turner G., Bolmaro R.E. Magnesium SiC reinforced composites - texture and residual strain investigation by simulation and experiments. Int. Congr. 'Magnesium Alloys and their Applications'. September 26-28, 2000, Munich, Germany.
14. Brokmeier H.-G., Jansen E.M., Spalthoff P., Signorelli J.A., Turner G., Bolmaro R.E. Texture and residual strains of ceramic reinforced magnesium composites. Experiments and Simulations. THERMEC-2000, December 4-8, 2000, Las Vegas, USA.
15. Budzynski P., Tarkowski P., Jartych E., Kobzev A.P. Evolution of mechenical properties in tool steel implanted with high energy nitrogen ions. III International Simposium "Ion Implantation and Other Application of Ions and Electrons", June 12-15, 2000, Dolny, Poland.
16. Dlouha M., Natkaniec I., Rubin J., Smirnov L.S., Vratislav S. Structural and magnetic phase transitions in $(NH_4)_xRb_{1-x}MnF_3$ perovskites ($0.75<x<1$). EPDIC-7, May 20-23, 2000, Barcelona, Spain.
17. Fedotov W.K., Antonov W.E., Bashkin I.O., Natkaniec I., Hansen T., Hasanov S.S. Neutron investigation of new high pressure phase of SeH_2. PTHP, June 13-17, 2000, Chernogolovka, Russia.
18. Fedotov W.K., Antonov W.E., Ivanov A., Kolesnikov A.I., Sashin I.L., Hansen T. Crystallographic structure and lattice vibration of high pressure phases of Co-H system. PTHP, June 13-17, 2000, Chernogolovka, Russia.
19. Fedotov W.K., Antonov W.E., Kolesnikov A.I., Natkaniec I., Sashin I.L. Structure, lattice dynamics and giant tunneling effect in б-Mn. PTHP, June 13-17, 2000, Chernogolovka, Russia.
20. Frischbutter A., Scheffzuek C., Walther K. Last- und Restspannungszustaende in Quarz und Dolomit - bestimmt mittels Neutronendiffraktion. 8th symposium on 'Tectonics, Structural and Crystalline Geology', October 4-6, 2000, Freiburg, Germany.
21. Groeger H., Leiss B., Ullemeyer K., Lebit H. Quantitative texture analyses of deformed amphibolites and biotite schists. 8th symposium on 'Tectonics, Structural and Crystalline Geology', October 4-6, 2000, Freiburg, Germany.
22. Hewat A., Martinez Sarrion M.L., Mestres L., Natkaniec I., Smirnov L.S., Shuvalov L.A. Diffraction study of x-T phase diagram of the $(NH_4)_xRb_{2-x}SO_4$ mixed crystals. EPDIC-7, May 20-23, 2000, Barcelona, Spain.
23. Hoiderna-Natkaniec K., Kiodzicski P., Natkaniec I., Pawlukojch A., Szyczewski A. Neutron scattering investigations of vibrational spectra of testerone and progesterone. XII PCMC, September 20-23, 2000, Krakow, Poland.
24. Ivankina T.I. Neutron diffraction investigations of local strains and microstresses in rocks. International conference "Physical properties of rocks at high pressure" dedicated to the 100th anniversary of M.P.Volarovich, 4-5 October 2000, Moscow.
25. Ivankina T.I., Nikitin A.N., Locajicek T., Pros Z., Klima K., Burilichev D.E. Texture and P-wave anisotropy of olivine xenoliths determined by neutron diffraction and ultrasonic sounding. XVII General Assembly of the European Seismological Commision, September 10-15, 2000, Lisbon, Portugal.
26. Ivankina T.I., Nikitin A.N., Sobolev G.A., Scheffzuek Ch., Frischbutter A. Intracrystalline strain of calcite measured with neutron diffraction under temperature and uniaxial load. XVII General Assembly of the European Seaismological Commision, September 10-15, 2000, Lisbon, Portugal.
27. Kazansky V.I., Lobanov K.V., Zharikov A.V., Nikitin A.N., Ivankina T.I. Investigation of the rocks-analogues from the Kola Superdeep borehole and surface based on geological and neutron methods. Plenary Meeting of IGSP Project 408, September 24-28, 2000, Prague, Czech Republic.
28. Kiselev M.A., Kisselev A.M., Lombardo D., Lesieur P. DMPC membrane swelling by nonionic surfactant $C_{12}E_8$: X-ray small-angle diffraction study. 5th International School and Symposium on Synchrotron Radiation in Natural Science, June 12-17, 2000, Ustron Jaszowiec, Poland.
29. Kiselev M.A., Lesieur P., Kisselev A.M., Lombardo D., Killany M., Lesieur S. Sucrose buffer as perspective medium to study the vesicle structure: SAXS and SANS study. 5th International School and Symposium on Synchrotron Radiation in Natural Science. June 12-17, 2000, Ustron Jaszowiec, Poland.
30. Kiselev M.A., Lesieur P., Kisselev A.M., Lombardo D., Killany M., Lesieur S., Ollivon M.A sucrose solutions applicatiion to the study of model biological membranes. XIII Russian Conference on Application of Synchrotron Radiation, July 17-21, 2000, Novosibirsk, Russia.
31. Kiselev M.A., Lesieur P., Lombardo D., Kisselev A.M., Ollivon M. A structure of phospholipid vesicles in the presence of cryoprotectors. 41st International Conference on the Biochemistry of Lipids, September 13-16, 2000, Halle, Germany.
32. Kiselev M.A., Lesieur P., Lombardo D., Kisselev A.M., Gutberlet T. The investigation of temperature-sensitive phospholipid /surfactant systems via neutron and X-ray small-angle scattering and diffraction. 41st International Conference on the Biochemistry of Lipids. September 13-16, 2000, Halle, Germany.
33. Kobzev A.P., Kravtcov E.A., Romashev L.N., Semerikov A.V., Ustinov V.V. Using of the high-grade layered structure for the deminstration of the depth resolution of the RBS method. III International Simposium "Ion implantation and other application of ions and electrons", June 12-15, 2000, Kazimierz Dolny, Poland.
34. Kozlenko D.P., Savenko B.N., Glazkov V.P., Somenkov V.A., Hull S. Structural study of ammonium halides ND_4I and ND_4Br at high pressure and low temperature. International Workshop on "Crystallography at high pressure and high temperature using X-rays and neutrons". September 30 –October 3, 2000, Spring-8, Japan.
35. Kozlenko D.P., Savenko B.N, Glazkov V.P., Somenkov V.A., Hull S. Neutron diffraction study of ND_4I and ND_4Br at high pressure and low temperature. 19th European Crystallographic Meeting, 25-31 August 2000, Nancy, France.

36. Lauter-Pasyuk V., Lauter H.J., Toperverg B., Nikonov O., Kravtsov E., Milyaev M.A., Romashev L., Ustinov V. Magnetic neutron off-specular scattering for the direct determination of the coupling angle in exchange couple multilayers. International conference on Magnetism, August 6-11, 2000, Recife, Brasil.
37. Locajicek T., Pros Z., Klima K., Nikitin A.N., Ivankina T.I., Ullemeyer K., Smirnov Yu.P., Kuznetsov Yu.I. P-wave elastic anisotropy and texture of amphibolites from the Kola Superdeep borehole KSDB-3. Plenary Meeting of IGSP Project 408, September 24-28, 2000, Prague, Czech Republic.
38. Martinez Sarrion M.L., Mestres L., Natkaniec I., Pawlukojc A., Smirnov L.S. The participation of the NH_4^+ ion in ferroelectric phases of AA'BX_4 type compounds. EPDIC-7, May 20-23, 2000, Barcelona, Spain.
39. Martinez-Sarrion M.L., Mesterss L., Herraiz M., Balagurov A.M., Beskrovnyi A.I., Smirnov L.S., Vasilovskii S.G. $Bi_{2.5+x}Li_{0.5-x}Nb_2O_9$ (x=0.04) – new compound with Aurivillius type structure. X-ray and neutron powder diffraction study. EPDC-7, May 20-23, 2000, Barcelona, Spain.
40. Natkaniec I. Neutron scattering investigation at the IBR-2 reactor at 2000 and perspectives for the following year. PSNS-IV, September 24-26, 2000, Krakow, Poland.
41. Natkaniec I., Dianoux A-J., Martinez Sarrion M.L., Mestres L., Smirnov L.S., Shuvalov L.A. The peculiarities of ammonium dynamics in the $Rb_{1-x}(NH4)_xI$ mixed crystals. ISRF-III, June 14-17, 2000, Dubna, Russia.
42. Natkaniec I., Dianoux A-J., Martinez Sarrion M.L., Mestres L., Smirnov L.S., Shuvalov L.A. Transition from quantum tunneling to orientational glass and ordered crystal dynamics of ammonium in $Rb_{1-x}(NH_4)_xI$ mixed salts. VIII F-PSDTMM, September 13-17, 2000, Choch Castle, Poland.
43. Natkaniec I., Hoiderna-Natkaniec K., Kalus J. Neutron Spectroscopy and Computing Simulations of Lattice Dynamics and Internal Vibrations of Differently Deuterated p-Xylene. VIII F-PSDTMM, September 13-17, 2000, Choch Castle, Poland.
44. Natkaniec I., Hoiderna-Natkaniec K., Parlicski K. Dynamics of crystalline and vitreous methanol, XII PCMC, September 20-23, 2000, Krakow, Poland.
45. Natkaniec I., Hoiderna-Natkaniec K., Parlicski K. Neutron scattering investigations and computational modeling of dynamics of urea: $CO(NH_2)_2$ and $CO(ND_2)_2$. 4th PSNS September 24-26, 2000, Krakow, Poland.
46. Natkaniec I., Hoiderna-Natkaniec K., Parlicski K. Lattice and internal dynamics of crystalline and glassy methanol: H - D isotope effects. ISNSICM-7, May 11-13, 2000, Poznac, Poland.
47. Natkaniec I., Smirnov L.C., Telepniev A.S., Sukhoparov W.A., Bragin S.I. Neutron studies of D2O in the area of meta-stability of ice-IV phase. PTHP, June 13-17, 2000, Chernogolovka, Russia.
48. Natkaniec I., Smirnov L.C., Telepniev A.S., Sukhoparov W.A., Bragin S.I., Kobelev G.W. In situ neutron investigation of heavy water phases at high pressure range up to 5 kbar. PTHP, June 13-17, 2000, Chernogolovka, Russia.
49. Nikitenko Yu.V. Neutron spin precession for structurum investigations of lawered structure. International Workshop on neutron spin-echo spectroscopy, October 16-17, 2000, HMI, Berlin, Germany.
50. Nikitin A.N. Neutron diffraction investigations of the texture and anisotropy of rocks at elevated temperatures and pressures. International conference "Physical properties of rocks at high pressure" dedicated to the 100th anniversary of M.P.Volarovich, 4-5 October 2000, Moscow.
51. Nikitin A.N., Ivankina T.I. Texture measurements of geological materials: a study by neutron diffraction. Plenary Meeting of IGSP Project 408. September 24-28,2000, Prague, Czech Republic.
52. Pawlukojc A., Leciejewicz J., Parker S.F., Tomkinson J. Neutron spectroscopy and ab initio study of hydrogen bonds dynamics in L-serine and L-threonine. EUCMOS XXV, August 27-September 1, 2000, Coimbra, Portugal.
53. Pomjakushin V.Yu., Balagurov A.M., Zakharov A.A. Concomitance of magnetic ordering and supercondu ctivity in low oxygen mobility La_2CuO_{4+x} single crystals. 6th International Conference on Materials and Mechanisms of Superconductivity and High Temperature Superconductors, February 20-25, 2000, Houston, USA.
54. Popov Yu.P., Voinov A.V., Parzhitski S.S., Kobzev A.P., Gundorin N.A., Serov D.G., Sedyshev P.V., Sedysheva M.V. Analysis of the pertial radiative neutron capture cross section by ^{58}NI nucleys. ISSIN-8. May 17-20, 2000 Dubna, Russia.
55. Reehuis M., Smirnov L.S., Sarin V.A., Georgiev D.G., Natkaniec I., Baranov A.I., Dolbinina V.V., Shuvalov L.A. Ammonium dynamics in crystal structure of phase II of $(NH_4)_3H(SO_4)_2$. NCC-II, May 22-26, 2000, Chernogolovka, Russia.
56. Scheffzuek, Ch., Walther, K., Frischbutter, A., Zhukov, R.A. Strain/stress measurements on dolomite rocks using neutron TOF diffraction and the determination of its orientation functions. Stress Evaluation Meca-SENS by Neutron and Synchrotron Radiation, December 13-14, 2000, Reims, France.
57. Shchennikov V.V., Berger I.F., Glazkov V.P., Kozlenko D.P., Tikhomirov S.V., Voronin V.I. Neutron Diffraction Investigation of Pressure – Induced Phase Transiiton in Ternary Mercury Compounds. International Workshop on "Crystallography at High Pressure and High Temperature using X-rays and Neutrons", September 30 –October 3 2000, Japan.
58. Ullemeyer K., Siegesmund S., Rasolofosaon P.N.J. Elastic Properties of Rocks from the TRANSALP Seismic Traverse. 8th symposium on 'Tectonics, Structural and Crystalline Geology', October 4-6, 2000, Freiburg, Germany.

NEUTRON NUCLEAR PHYSICS

Reviews

1. Alexandrov Yu. A, Furman W.I., Ignatyuk A.V., Kazarnovsky M.V., Konovalov V.Yu., Kornilov N.V., Pikelner L.B., Plyaskin V.I., Popov Yu.P., Rauch H., Waschkowski W., Zamyatnin Yu.S. Landolt-Bцrnstein Numerical Data and Functional Relationships in Science and Technology, Group 1: Elementary Particles, Nuclei and Atoms, Volume 16: Low Energy Neutron Physics, Subvolume A: Low Energy Neutrons and Their Interaction with Nuclei and Matter, Part 1.— Springer-Verlag, Berlin Heidelberg, 2000

Exsperimental research

1. Alfimenkov V.P., Gagarsky A.M., Golosovskaya S.P. et al. Parity violation and interference effects in the angular distributions of fission fragments from the resonance neutron induced fission of ^{233} U, Jad. Fiz., 2000, v.63, p.598.
2. Baek W.Y., Kim G.N., Cho M.H., Ko I.S., Namkung W., Grigoriev Yu.V., Faikov-Stanczyk H., Shvetsov V.N., Furman W.I. Investigation of γ-multiplicity spectra and neutron capture cross-sections of ^{232} Th in the energy region 21.5-215 eV. Nuclear Instruments and Methods in Physics Research B **168** (2000) 453-461
3. Bondarenko I.V., Frank A.I., Balashov S.N., Masalovich S.V., Nosov V.G., Geltenbort P., Hшghшj P., Cimmino A., Klein A.G. *UCN gravity spectrometry using neutron interference filter.* NIM A, 440 (2000), pp. 591-596, 2000.
4. Bondarenko V.A., Khitrov V.A., Sukhovoj A.M., Honzatko J., Tomandl I., Cascade gamma-decay of the ^{191}Os compound nucleus, JINR preprint E3-99-343, Dubna, 1999.
5. Boneva S.T., Vasilieva E.V., Sukhovoj A.M., Khitrov V.A., Cascade γ -decay of the ^{190}Os compound nucleus. Izv. RAN, ser. fiz., 64(3) (2000) 593-599
6. Boneva S.T., Vasilieva E.V., Sukhovoj A.M., Khitrov V.A., Two-step γ-cascades following thermal neutron capture in ^{187}Os. Izv. RAN, ser. fiz., 64(3) (2000) 585-592
7. Boneva S.T., Vasilieva E.V., Sukhovoj A.M., Khitrov V.A., Two-step γ-cascades after the thermal neutron capture in ^{139}La. Izv. RAN, ser. fiz., 64(5) (2000) 942-949
8. Borzakov S.B., Andreev A.N., Dermendjiev E., Filip A., Furman W.I., Panteleev Ts., Ruskov I., Zamyatnin Yu.S., Zeinalov Sh., Measurements of Delayed Neutron Yields from Thermal-Neutron-Induced Fission of ^{235}U, ^{233}U, ^{239}Pu and ^{237}Np.// ЯФ.— 2000.— т.63, N4.— с.589–597.
9. Borzakov S.B., Panteleev Ts., Pavlov S.S., Ruskov I.N., Zamyatnin Yu.S. Study of Delayed Neutron Decay Curves From Thermal Neutron Induced Fisiion of ^{235}U and ^{239}Pu. // Progress in Nuclear Energy, to be published
10. Borzakov S.B., Zamyatnin Yu.S., Panteleev Ts., Pavlov S.S., Ruskov I. Investigation of delay neutron decay curves at thermal neutron induced fission // VANT, Series: Jad. Konstanty, 1999, issue 2, p. 5–11
11. Bunatian G.G. et al, Zeit.Phys.A359, p.337, 1997
12. Enik T.L., Kharjuzov R.V., Mitsyna L.V., Samosvat G.S. The UGRA Spectrometer for the Measurement of the Neutron Electric Polarizability. Nucl. Instr. Meth., 2000, v.**A440**, p.777.
13. Enik T.L., Mitsyna L.V., Samosvat G.S., Sinitsa V.V. Investigation of Interference Minima Near s-Wave Resonances of ^{238}U. ISINN-8. Abstracts, E3-2000-71, Dubna, 2000, p.103.
14. Faikov-Stanczyk H., Grigoriev Yu. V., Kitaev V. Ya., Panteleev Ts. Ts. «*Study of a resonance self-shielding effect in the α-value of ^{235}U, ^{239}Pu in the neutron resonance energy range*», ANNUAL REPORT 2000, Obninsk, ed. by Kuzminov B.D.
15. Frank A.I., Gaehler R. *Time focusing of neutrons.* Jad.Fiz., 2000, v.63,p.605-608.
16. Georgiev G.P., Zamyatnin Yu.S., Pikelner L.B., Faikow-Stanczyk H., Grigoriev Yu.V., Muradyan G.V., Janeva N.B. Determination of the parameters of ^{149}Sm neutron resonances in the energy range 15 – 300 eV. VANT, Series: Jad. Konstanty, 1999, issue. 1, 1999, p. 3.
17. Gledenov Yu.M., Koehler P.E., Andrzejewski J., Guber K., Rausher T.. ^{147}Sm(n,α) cross section measurements from 3 eV to 500 keV: Implications for explosive nucleosynthesis reaction rates. Phys. Rev. C**62** (2000) 042801.
18. Gledenov Yu.M., Sedysheva M.V., Khuukhenkhuu G., Guohui Zhang, Guoyou Tang, Jinxiang Chen, Xuemei Zhang, Zemin Chen, Yingtang Chen. Twin ionization chamber for studies of (n,p), (n,α) reactions. JINR Communications E13-2000-89 (Dubna, 2000) 1-8.
19. Grigoriev E. P., V. A. Khitrov, A. M. Sukhovoj and E. V. Vasilieva A search for the γ-decay of the ^{168}Er compound in the (n,2γ) reaction, by Fizika B (Zagreb) vol. 9 (2000) no.4, pp 147-168
20. Grigoriev Yu.V., Zhuravlev B.V., Synitsa V.V., Ilchev G.L., Faikow-Stanczyk H., Kim G.N. *«Investigations of the neutron cross sections of ^{232}Th at the energies 20 eV – 10 keV».* VOPROSY ATOMNOI NAUKI I TEKHNIKI, Series: Jad. Konstanty, issue, 2000, p.
21. Grigoriev Yu.V., Sinitsa V.V., Borzakov S.B., Ilchev G.L., Panteleev Ts.Ts., Faikow-Stanczyk H., Janeva N.B. *«Investigations of the neutron cross section and the value of alpha for U-235 over the energy range from 1meV to 2 eV».* VOPROSY ATOMNOI NAUKI I TEKHNIKI, Series: Jad. Konstanty, issue 1, 2000, pp.3 – 6.

22. Gritzay O.O., Libman V.A., Murzin A.V., Nikolenko V.G., Popov A.B., Samosvat G.S., Waschkowski W. Preliminary Measurements of the Neutron Total Cross Section of ^{208}Pb at 24 keV and the Neutron Polarizability. ISINN-8. Abstracts, E3-2000-71, Dubna, 2000, p.65.
23. Khitrov V.A., Sukhovoj A.M., New technique for a simultaneous estimation of the level density and radiative strength functions of dipole transitions at $E_{ex} < B_n$ -0.5 MeV, JINR preprint E3-2000-133, Dubna, 2000.
24. Kolachevsky N.N. *et al.*, Quantum Electronics, **30**(1), 81 (2000).
25. Korneev D.A., Bodnarchuk V.I., Yaradaikin S.P., Peresedov V.F., Ignatovich V.K., Mennelle A., Gaehler P., Reflectometry studies of the neutron coherent properties. Phisica B, v. **276**, p. 973, 2000.
26. Mitchell G.E., Bowman J.D., Crawford B.E., Delheij P.P.J., Frankle, C.M. Iinuma M., Knudson J.N., Lowie L.Y., Masaike A., Matsuda Y., Penttila S., Postma H., Roberson N.R., Seestrom S.J., Sharapov, E.I. Stephenson S.L., Yen Y.-F., and Yuan V.W., Phys. Rev. C **61**, 045503 (2000).
27. Pokotilovski Yu.N., "Abnormally large neutron polarizability or long-range strong-interaction potential at fast neutron scattering by heavy nuclei?", Eur. Phys. Journ., A8 (2000) 299-302.
28. Pokotilovski Yu.N., "Interaction of ultracold neutrons with liquid surface modes as a possible reason for neutron energy spread during long storage in fluid wall traps", Phys. Lett., A255 (1999) 173-177.
29. Pokotilovski Yu.N., "On the form of long-range potential observed at fast neutron scattering by heavy nuclei", Jad. Fiz., 63 (2000) 1996-1999; Physics of At. Nucl, 63 (2000) 1903-1906.
30. Pokotilovski Yu.N., "Possibility for low temperature fluid-wall neutron bottle with very low neutron upscattering losses", Nucl. Instr. Meth., A425 (1999) 320-322.
31. Pokotilovski Yu.N., "Quasielastic neutron scattering by diffusive adsorbed hydrogen as a possible cause of the energy spreading of ultracold neutrons during long storage in traps", Pis'ma v ZhETF, 69 (1999) 81-86; JETP Lett., 69 (1999) 91-96.
32. Pokotilovski Yu.N., "Quasielastic scattering of ultracold neutrons as possible reason for their energy spreading during long storage in closed traps", Eur. Phys. Journ., B8 (1999) 1-4.
33. Popov Yu.P., Voinov A.V., Parzhitski S.S., Gundorin N.A., Serov D.G., Kobzev A.P., Sedyshev P.V., «Measurrements of a Partial Cross Section for the Reaction ^{58}Ni(n,γ_0)^{59}Ni «, Physics of Atomic Nuclei, **52**, (2000), pp.525 – 529. (ЯФ **63,** (2000), 583 – 588).
34. Pospisil S., Becvar F., Granja Bustamante C., Kubasta J., Telezhnikov S.A. Secondary gamma Transitions in ^{159}Gd after Neutron Capture at Isolated Resonances J. Res. Natl. Inst. Stand. Technol. 105, 173 (2000)
35. Prokofjevs P., Simonova L.I., Balodis M., Berzins J., Bondarenko V.A., Wirth H.F., von Egidy T., Doll C., Ott J., Schauer W., Hoff R.W., Casten R.F., Gill E.L., Honzatko J., Tomandl I., Boneva S.T., Khitrov V.A., Sukhovoj A.M., Burke D.G., Kvasil J., Mackova A., Nuclear structure of ^{166}Ho studied in neutron-capture, (d,p), and (d,^{3}He) reactions, Phys. Rev. C**61**(4) (2000) 044305-1.
36. Prokofjevs P., Simonova L.I., Balodis M., Berzins J., Bondarenko V.A., Honzatko J., Tomandl I., Boneva S.T., Khitrov V.A. and Sukhovoj A. M. , The gamma -gamma coincidence measurement of ^{166}Ho from the (n,gamma) reaction, Fizika B (Zagreb), V.**9** (2000) 97-110.
37. Sharapov E.I., Bowman J.D., Crawford B.E., Delheij P.P.J., Frankle C.M., Iinuma M., Knudson J.N., Lowie L.Y., Lynch J.E., Masaike A., Matsuda Y., Mitchell G.E., Penttila S., Postma H., Roberson N.R., Seestrom S.J., Shimizu H.M., Stephenson S.L, Yen Y.-F., and Yuan V.W., Phys. Rev. C **61**, 025501(2000).
38. Stephenson S.L., Bowman J.D., Corvi F., Crawford B.E, Delheij P.P.J., Frankle C.M., Iinuma M., Knudson J.N., Lowie L.Y., Masaike A., Masuda Y., Matsuda Y., Mitchell G.E., Penttila S., Postma H.,. Roberson N.R, Seestrom S.J., Sharapov E.I., Shimizu H.M., Yen Y.-F., Yuan V.W., and Zanini L., Phys. Rev. C **61**, 045501 (2000).
39. Sukhovoj A.M., Khitrov V.A., Information capacity of the spectroscopy of the states of deformed nuclei up to the excitation energy 3-4 MeV. Izv. RAN, ser. fiz., 64(3) (2000) 576-584
40. Vasilieva E.V. Sukhovoj A.M., Khitrov V.A., Influence of the structure of excited states on the process of cascade gamma-decay at energy below neutron binding energy. Part. Nucl., 2000, v.**31**, pp.350-384.
41. Yen Y.-F., Bowman J.D., Bolton R.D., Crawford B.E., Delheij P.P.J., Hart G.W., Frankle C.M., Haseyama T., Iinuma M., Knudson J.N., Masaike A., Masuda Y., Matsuda Y., Mitchell G.E., Penttila S.I., Roberson N.R., Seestrom S.J., Sharapov E.I., Shimizu H.M., Smith D.A., Stephenson S.L., Szymanski J.J., Yoo H., and Yuan V.W., Nucl. Instrum. Methods Phys. Res. A**447**, 472 (2000).
42. Zhang Guohui, Tang Guoyou, Chen Jinxiang, Shi Zaomin, Liu Guanzhi, Zhang Xuemei, Chen Zemin, Gledenov Yu.M., Sedysheva M., Khuukhenkhuu G. Differential cross-section measurement for the ^{6}Li(n,t)^{4}He reaction at 3.67 and 4.42 MeV. Nucl. Sci. Eng **134** (2000) 312-316.
43. Zhang Xuemei, Chen Zemin, Chen Yingtang, Tang Guoyou, Zhang Guohui, Chen Jinxiang, Gledenov Yu.M., Khuukhenkhuu G. Measurements and Calculations of the ^{39}K and ^{40}Ca (n,α) Cross Sections at E_n = 4.5 to 6.5 MeV. Nucl. Sci. Eng **134** (2000) 86-96.
44. Zhang Xuemei, Chen Zemin, Chen Yingtang, Yuan Jing, Tang Guoyou, Zhang Guohui, Chen Jinxiang, Gledenov Yu.M., Khuukhenkhuu G., Sedysheva M. Dispersion relations for (n,n), (n,p), and (n,α) reactions on ^{39}K and ^{40}Ca. Phys. Rev. **C61** (2000) 054607.

Theoretical investigations

1. Ignatovich V.K., Ignatovitch F.V., Andersen D.R., Algebraic description of multilayer systems with resonances. Particles and Nuclei Lett. **3** [100], pp. 48-61, 2000. in Proc. Int. Sem. on Fission, Castele of Pont d'Oye, Haabay-la-Neuve, Belgium, 6-8 Oct.,1999, editted by Wagemans C., Serot O., D'hondt P., p. 95, World Scientific, Singapore, 2000.
2. Tretyakova T.Yu. , Lanskoy D.E. Structure of neutron-rich Λ- hypernuclei, Eur. Phys. J. A 5 391-398 (1999)
3. Ignatovich V.K. In: Proceedings of the seminar dedicated to the 80th anniversary of M.I.Podgoretskii, p. 67-84. JINR, Dubna, 2000.
4. Lyuboshits V.V., Lyuboshits V.L. T-ivariance and polarization effects in the reactions $p + 3He \rightarrow p+ + 4He$ and $p+ + 4He \rightarrow p + 3He$. Jad. Fiz., 2000, v.**63**, issue 5, pp. 837-843 (Physics of Atomic Nuclei , 2000, v.**63**, No. 5, pp. 767-773) .
5. Lyuboshits V.V., Lyuboshits V.L. Transport scattering cross section and Aaronov-Bom effect on a torroidal solenoid. Preprint JINR ОИЯИ P4-2000-48 , Dubna, 2000 ; Zh.Exp. i Teor.Fiz (ZhETP), 2000, v. **118**, issue 4 (10), pp. 777-786 (Journal of Experimental and Theoretical Physics, 2000, v. **91**, No. 4, pp. 673-681) .

Applied research

1. Dovgun O., Frontasyeva M.: Heavy metal atmospheric deposition study in the Lake Baikal area. Book of Abstracts, Fifth Int. Symposium and Exhibition on Environmental Contamination in Central and Eastern Europe, 12-14 September 2000, Prague, Czech Rep., p.179.
2. Feofanov Y.V., Smirnov L.I., Frontasyeva M., Cherchintsev V.D., Lyapunov S.M., Steinnes E.: Atmospheric deposition of heavy metals in the South Ural Mountains, Russia. Book of Abstracts, Fifth Int. Symposium and Exhibition on Environmental Contamination in Central and Eastern Europe, 12-14 September 2000, Prague, Czech Republic, p.286.
3. Frontasyeva M.V. and Lyapunov S.M.: Comparative assessment of INAA, AAS and XRF used to study multi-element material characterization in Geolofy, Ecology and Medicine. Collaborative experience of two laboratories in Russia). Technical report, IAEA, Physics Section NAPC (October 13-18, 2000).
4. Frontasyeva M.V., Nikonov V.V., Steinnes E.: Atmospheric deposition of trace metals studied by moss and lichens analysis: some examples from Russia. Book of Abstracts (Invited Talk), 2nd Int.Workshop on Biomonitoring of Atmospheric Pollution (with emphasis on trace elements), Azores islands, August 28-September 3, 2000, p. 28.
5. Frontasyeva M.V., Pavlov S.S., Strelkova L.P., Steinnes E., Kirpichnikova N.V., Bogdanov A.V.: How does Konakovo thermo power plant affect the environment? Book of Abstracts, VIII Int. Seminar on Interaction of Neutrons with Nuclei (Dubna, May 17-20, 2000), p. 127.
6. Frontasyeva M.V., Pavlov S.S.: Analytical Investigations at the IBR-2 reactor in Dubna. *Preprint of JINR*, E14-2000-177, Dubna, 2000 (submitted to the Proc. VIII Int. Seminar on Interaction of Neutrons with Nuclei (Dubna, May 17-20, 2000)
7. Frontasyeva M.V., Steinnes E., Lyapunov S.M., Cherchintsev V. D., Smirnov L.I.: Biomonitoring of heavy metal deposition in South Ural region: Some preliminary obtained by nuclear and related techniques. *J. Radioanal. Nucl. Chem*., v. 245, No.2, 415-420, 2000.
8. Frontasyeva M.V., Yermakova Ye.V., Steinnes E.: Reliability of mosses *(Hylocomium splendens, Pleurozium schreberi* and *Calliergon geganteum)* as biomonitors of heavy metal atmospheric deposition in Central Russia. *FLNP JINR Annual Report*, 2000-81, p. 178-180, 2000.
9. Kirova-Cheshkova R., Frontasyeva M.V., Strelkova L.P., Antonov A., Mitrikov M.: Heavy metal atmospheric deposition in the Rodopi Mountains (South Bulgaria). Book of Abstracts, VIII Int. Seminar on Interaction of Neutrons with Nuclei (Dubna, May 17-20, 2000), p. 112.
10. Lucaciu A., Cuculeanu V., Frontasyeva M., Steinnes E.: Atmospheric deposition of heavy metals in Transilvania Plateau of Romania studied by the moss biomonitoring technique employing Nuclear and related analytical techniques. Book of Abstracts, Fifth Int. Symposium and Exhibition on Environmental Contamination in Central and Eastern Europe, 12-14 September 2000, Prague, Czech Republic, p.239.
11. Morzhukhina S.V., Uspenskaya V.V., Chermnikh L.P., Khodakovsky I.L., Frontasyeva M.V, Gundorina S.F.: Nuclear and related analytical techniques used to study anthropogenic impact on the River Sister in the vicinity of the town of Klin (Moscow Region, Russia). Book of Abstracts, VIII Int. Seminar on Interaction of Neutrons with Nuclei (Dubna, May 17-20, 2000), p. 128 (submitted to NATO ASI Series, Kluwer Academic Publishers, 2000).
12. Mosulishvili L.M., Kirkesali Ye.I., Belokobylsky A.I., Khizanishvili A.I., Frontasyeva M.V., Gundorina S.F., Oprea C.D.: Epithermal neutron activation analysis of blue-green algae Spirulina Platensis as a matrix for selenium-containing pharmaceuticals. Preprint of JINR, E14-2000-225, Dubna, 2000 (submitted to J. Radioanal. Nucl. Chem.)
13. Oprea C., Timofte L., Cozma F., Pavlov S.S., Smirnov L.I., Stan O.: Atmospheric deposition of trace elements in Southern and Western Carpatians studied by the analysis of moss samples using neutron activation analysis and atomic absorption Spectrometry. Book of Abstracts, VIII Int. Seminar on Interaction of Neutrons with Nuclei (Dubna, May 17-20, 2000), p. 116.
14. Ostrovnaya T.M.: Tables for Identification of Nuclides Formed in Nuclear Reactors. Preprint JINR, E14-2000-178, 2000, pp. 1-47.

15. Stan O.A., Lucaciu A., Frontasyeva M.V., Steinnes E.: New results from air pollution studies in Romania. *Preprint of JINR*, E14-2000-126, Dubna, 2000. (Delivered at Fifth Int. Symp. and Exhibition on Environmental Contamination in Central and Eastern Europe, 12-14 September, 2000, Prague, Czech Republic, p. 192).
16. Stan O.A., Zhang Zh.H., Frontasyeva M.V., Steinnes E.: Selection of appropriate moss biomonitors for studying atmospheric elemental deposition in China. *FLNP JINR Annual Report*, 2000-81, p. 181-183, 2000.
17. Yermakova Ye., Frontasyeva M., Steinnes E., Pavlov S.S.: Epithermal Neutron Activation Analysis of Mosses used to monitor heavy metal atmospheric seposition in Tula Region. Book of Abstracts, Fifth Int. Symposium and Exhibition on Environmental Contamination in Central and Eastern Europe, 12-14 September 2000, Prague, Czech Rep., p.191.

Reports at Schools and Conferences

1. Ali M.A., Khitrov V.A., Sukhovoj A.M., On Stepwise Change in Heavy Nuclei Properties at 3-5 MeV Excitation Energy, Proc. Nuclear and Particle Physics Conference, 13-17 Nov 1999, Cairo, Egypt, Ed. M.N.H. Comsan, K.M. Hanna, NRC, Atomic Energy Authority Egypt, 2000, pp. 451-466.
2. Ali M.A., Khitrov V.A., Sukhovoj A.M., Possible dominance of vibrational-type excitations of heavy nucleus at 1-2 < E_{ex}< 3-5 MeV. In: Capture gamma-ray spectroscopy and related topics, Santa Fe, USA,1999, Ed. by Weder S., AIP, pp. 632-634.
3. Beer H., Sedyshev P.V., Mohr P., Stadler W., Oberhummer H., Rochow W., Popov Yu.P. Neutron capture of ^{22}Ne, ^{30}Si, and ^{40}Ar at thermonuclear energies. In: 10 Int. Symp. Capture Gamma-Ray Spectroscopy and Related Topics, Santa Fe 1999. AIP Conf. Proc. **529** Ed. by S. Wender (New York 2000) 450-457.
4. Bondarenko V.A., Honzatko J., Khitrov V.A., Sukhovoj A.M., Tomandl I. Direct experimental estimates of radiative strength functions of low-energy primary gamma-transitions in ^{191,193}Os, In: Capture gamma-ray spectroscopy and related topics, Santa Fe, USA,1999, Ed. by Weder S., AIP, pp. 626-628.
5. Bondarenko V.A., Khitrov V.A., Simonova L.I., Sukhovoj A.M. On different character of cascade gamma-decay of near-magic and deformed compound nuclei, In: Capture gamma-ray spectroscopy and related topics, Santa Fe, USA, 1999, Ed. by Weder S., AIP, pp.635-636.
6. Boneva S.T., Khitrov V.A., Sukhovoj A.M., Vasilieva E.V. Two-step gamma-cascades of the ^{188,190}Os compound nuclei decay, In: Capture gamma-ray spectroscopy and related topics, Santa Fe, USA, 1999, Ed. by Weder S., AIP, pp. 624-625.
7. Borzakov S. B., Faikov-Stanczyk H., Grigoriev Yu. V., Ilchev G. L., Janeva N. B., Panteleev Ts. Ts., Sinitsa V. V. *«The measurement of neutron cross-section and the* $\alpha = \sigma_\gamma/\sigma_f$ *value for* ^{235}*U within the energy range 1 meV–2 eV».* VIII International Seminar on Interaction of Neutrons with Nuclei: NEUTRON SPECTROSCOPY, NUCLEAR STRUCTURE, RELATED TOPICS, Dubna, May 17-20, 2000
8. Borzakov S. B., Faikov-Stanczyk H., Grigoriev Yu. V., Ilchev G.L., Kim G.N., Kitaev V. Ya., Panteleev Ts. Ts., Sinitsa V. V., Zhuravlov B.V. *«The measurement of the* ^{232}*Th radiation capture cross-section within the 20 eV– 10 keV energy range»*. VIII International Seminar on Interaction of Neutrons with Nuclei: NEUTRON SPECTROSCOPY, NUCLEAR STRUCTURE, RELATED TOPICS, Dubna, May 17-20, 2000
9. Borzakov S. B., Faikov-Stanczyk H., Grigoriev Yu. V., Telezhnikov S. A., Panteleev Ts. Ts., Smotritsky L. M. *«Gamma-ray transitions of the* ^{118}*Sn observed in radiative capture of thermal neutrons»*. VIII International Seminar on Interaction of Neutrons with Nuclei: NEUTRON SPECTROSCOPY, NUCLEAR STRUCTURE, RELATED TOPICS, Dubna, May 17-20, 2000
10. Borzakov S.B., Panteleev Ts., Strelkov S.V., Grigoriev Yu.V., The Search for Dineutron in the Interaction of Thermal Neutrons with the Deutrons, ISINN-8, Dubna, May 17-20, 2000, Preprint JINR E3-2000-71, Dubna, 2000.
11. Florek M., Konovalov V.Yu., Pikelner L.B., Zamyatnin Yu.S., Zeinalov Sh.S. The ^{234}U Neutron Induced Fission Cross-Section Near the Thermal Point.— In: Proceedings of the XIV International Workshop on Nuclear Fission Physics, 12–15 October, 1998.— Obninsk, 2000.— p. 146–149.
12. Florek M., Konovalov V.Yu., Zamyatnin Yu.S., Zeinalov Sh.S. Neutron Induced Fission Cross-Section of ^{243}Am in the Energy Region from 0.8 to 50 eV.— In: Proceedings of the XIV International Workshop on Nuclear Fission Physics, 12–15 October, 1998.— Obninsk, 2000.— p. 243–248.
13. Frank A.I., Balashov S.N.,.Bodnarchuk V.N, Bondarenko I.V., Cimmino A., Geltenbort P., Hшghшj P., Klein A., Korneev D. , Kozlov A.V., Masalovich S.V. *Neutron multilayers structures for fundamental experiments in UCN optics.* Proceeding SPIE v.3767, 2000
14. Frank A.I., Bondarenko I.V., Balashov S.N., Masalovich S.V., Nosov V.G., Gelternbort P., Hшghшj P., *Diffraction of UCN on a Moving Grating*, VIII International Seminar on Interaction of Neutrons with Nuclei (ISINN-8), 2000. pp 448.
15. Frank A.I., Bondarenko I.V., Kozlov A.V., Hшghшj P.H., Ehlers G. *Larmor Clock and Measuring of Neutron Interaction Time with Quantum Objects* . VIII International Seminar on Interaction of Neutrons with Nuclei (ISINN-8), 2000. p.215
16. Gledenov Yu.M., Machrafi R., Oprea A.I., Salatski V.I., Sedyshev P.V., Szalanski P.I. Angular Correlation in ^{35}Cl(n,p)^{35}S Reaction. In: Proc. Second International Yugoslav Nuclear Society Conference. Belgrade, Yugoslavia,

Sept. 28-Oct. 1, 1998, ed. D.P.Antiж (The VINИA Institute of Nuclear Sciences Printing-House, 1999), p.565-574.
17. Gledenov Yu.M., Mashrafi R., Oprea A.I., Salatski V.I., Sedyshev P.V., Sedysheva M.V. Angular distribution in $^{35}Cl(n,p)^{35}S$ at the resonance E_n=398 eV. 8 International Seminar on Interaction of Neutrons with Nuclei. Neutron Spectroscopy, Nuclear Structure, Related Topics. ISINN-8, Dubna, May 17-20, 2000 (Abstracts) E3-2000-71, 105.
18. Gledenov Yu.M., Sedysheva M.V., Xuemei Zhang, Zemin Chen, Yingtang Chen, Guohui Zhang, Guoyou Tang, Jinxiang Chen, Khuukhenkhuu G. Measurements of the $^{39}K(n,\alpha)^{36}Cl$ and $^{40}Ca(n,\alpha)^{37}Ar$ cross sections at E_n=4.5-6.5 MeV. 8 International Seminar on Interaction of Neutrons with Nuclei. Neutron Spectroscopy, Nuclear Structure, Related Topics. ISINN-8, Dubna, May 17-20, 2000 (Abstracts) E3-2000-71, 68.
19. Khitrov V.A., Sukhovoj A.M., Cascade gamma- decay of heavy compound nucleus. Experimental picture for excitation energy region $E_{ex}=B_n$, In: Capture gamma-ray spectroscopy and related topics, Santa Fe, USA,1999, Ed. by Weder S., AIP, pp. 637-638.
20. Khitrov V.A., Sukhovoj A.M., Direct experimental estimation of level density of heavy nucleus observed in reaction (n, 2gamma) at E_{ex}<3-5 MeV, In: Capture gamma-ray spectroscopy and related topics, Santa Fe, USA,1999, Ed. by Weder S., AIP, pp. 534-536.
21. Khitrov V.A., Sukhovoj A.M., Furman W.I., Gundorin N.A., Matveev D.V., Serov D.G., On Possibility to Obtain New Data on Structure of Excited States of Fissile Compound-Nuclei ^{236}U and ^{240}Pu. In: VIII International Seminar on Interaction of Neutrons with Nuclei, Dubna, 17-20 May 2000, E3-2000-192, Dubna, 2000, p. 387-391.
22. Khitrov V.A., Sukhovoj A.M., On the Ratio of Level Densities with Different Parity in the Excitation Energy Range up to B_n. In: VIII International Seminar on Interaction of Neutrons with Nuclei, Dubna, 17-20 May 2000, E3-2000-192, Dubna, 2000, p. 43-50.
23. Khitrov V.A., Sukhovoj A.M., On the Ratio of Level Densities with Different Parity in the Excitation Energy Range up to B_n. In: VIII International Seminar on Interaction of Neutrons with Nuclei, Dubna, 17-20 May 2000, E3-2000-192, Dubna, 2000, p. 43-50.
24. Khitrov V.A., Sukhovoj A.M., Two-step cascades and the real possibility of improving the accuracy in calculating the gamma-decay parameters of heavy nucleus, In: Capture gamma-ray spectroscopy and related topics, Santa Fe, USA,1999, Ed. by Weder S., AIP, pp. 629-631.
25. Khitrov V.A., Sukhovoj A.M., Two-Step gamma-Cascades from the ^{39}K(n,gamma) and $^{79}Br(n,\gamma)$ reactions. In: VIII International Seminar on Interaction of Neutrons with Nuclei, Dubna, 17-20 May 2000, E3-2000-192, Dubna, 2000, p. 382-386.
26. Koehler P.E., Gledenov Yu.M., Andrzejewski J. Improving explosive nucleosynthesis calculations through (n,α) measurements. 8 International Seminar on Interaction of Neutrons with Nuclei. Neutron Spectroscopy, Nuclear Structure, Related Topics. ISINN-8, Dubna, May 17-20, 2000 (Abstracts) E3-2000-71, 61.
27. Kopach Yu., Mutterer M., Singer P., Klemens M., Hotzel A., Schwalm D., Thirolf P., Hesse M., Goennenwein F., «Neutron Decay of Ternary Particles in Spotaneous Fission of », in Proc. 2nd Int.Conf. on Fission and Properties of Neutron-Rich Nuclei, 28.06-2.07.1999, St.Andrews, Scottland, editted by Hamilton J.H., Phillips W.R., Carter H.K., p. 316, World Scientific, Singapore, 2000.
28. Kopach Yu., Mutterer M., Singer P., Klemens M., Hotzel A., Schwalm D., Thirolf P., Hesse M., Goennenwein F., «Angular Correlations with Gamma-Rays and Neutrons in Ternary Fission of », in Proc. Int. Sem. on Fission, Castele of Pont d'Oye, Haabay-la-Neuve, Belgium, 6-8 Oct.,1999, editted by Wagemans C., Serot O., D'hondt P., p. 95, World Scientific, Singapore, 2000.
29. Kopach Yu., Mutterer M., Singer P., Klemens M., Hotzel A., Schwalm D., Thirolf P., Hesse M., Goennenwien F., «Anisotropy of Gamma-Ray Emission in Binary and Ternary Spontaneous Fission of », in Proc.4th Int. Conf. on Dynamical Aspects of Nuclear Fission, Casta-Papernicka, Slovakia, 19-23 Aug 1998, editted by Oganessian Yu., Kliman J., Gmuca S., p.405, World Scientific, Singapore, 2000.
30. Kopach Yu., Mutterer M., Singer P., Klemens M., Hotzel A., Schwalm D., Thirolf P., Hesse M., Goennenwein F., «Emission of and in Spontaneous Ternary Fission of », in Proc.4th Int.Conf. on Dynamical Aspects of Nuclear Fission, Casta-Papernicka, Slovakia, 19-23 Aug 1998, editted by Oganessian Yu., Kliman J., Gmuca S., p. 136, World Scientific, Singapore, 2000.
31. Kopach Yu.N.. Popov A.B., Furman W.I., Tambovtsev D.I., Kozlovsky L.K., Gonin N.N., Kliman J., «Progress and Present Status of Investigation of Fission Fragment Angular Anosotropy in the Slow Neutron Induced Fission of », in Proc.4th Int.Conf. on Dynamical Aspects of Nuclear Fission, Casta-Papernicka, Slovakia, 19-23 Aug 1998, editted by Oganessian Yu., Kliman J., Gmuca S., p.393, World Scientific, Singapore, 2000.
32. Kopach Yu.N.. Popov A.B., Furman W.I., Tambovtsev D.I., Kozlovsky L.K., Gonin N.N., Kliman J., «Angular Anisotropy of Fission Fragments from the Resonance Neutron Induced fission of Aligned Target and Role of $J^{\pi}K$ Fission Channels», in Proc. Int. Sem. on Fission, Castele of Pont d'Oye, Haabay-la-Neuve, Belgium, 6-8 Oct.,1999, editted by C.Wagemans, O.Serot, P.D'hondt, p. 95, World Scientific, Singapore, 2000.
33. Olejniczak U., Gundorin N.A., Pikelner L.B., Przytula M., Serov D.G., Compound Nuclear States from Resonance Radiative Neutron Capture in Antimony and Tantalum. Proc. 9 Intern. Conf. on Nuclear Reaction mechan., Ed. Gadioli E., Varenna, 2000, p. 145.

34. Popov Yu.P., A.V.Voinov, S.S.Parzhitski, A.P.Kobzev, N.A.Gundorin, D.G.Serov, P.V.Sedyshev, M.V.Sedysheva. «Analysis of the Partial Neutron Capture Cross Sections by ^{58}Ni nucleus». Proc. ISINN-8, JINR E3-2000-192, p.75-81, Dubna, 2000.
35. Popov Yu.P., Voinov A.V., Parzhitski S.S., Kobzev A.P., Gundorin N.A., Serov D.G., Sedyshev P.V., Sedysheva M.V. New experimental possibility of neutron spectra investigation in the neutron energy interval 10-100 keV. 8 International Seminar on Interaction of Neutrons with Nuclei. Neutron Spectroscopy, Nuclear Structure, Related Topics. ISINN-8, Dubna, May 17-20, 2000 (Abstracts) E3-2000-71, 120.
36. Sharapov E.I., Bowman J.D., Crawford B.E., Delheij P.P.J., Frankle C.M., Iinuma M., Knudson J.N., Lowie L.Y., Lynch J.E., Masaike A., Matsuda Y., Mitchell G.E., Penttila S., Postma H., Roberson N.R., Seestrom S.J., Shimizu H.M., Stephenson S.L., Yen Y.-F., and Yuan V.W., ISINN-8: VIII International Seminar on Interaction of Neutron with Nuclei, Report E3-2000-192, p.86, Dubna 2000.
37. Tambovtsev D.I., Kozlovsky L.K., Gonin N.N., Furman W.I., Kopach Yu.N., Popov A.B., Kliman J., «Investigations of Fission Fragments Angular Anisotropy for Low Energy Neutron Induced Fission of Aligned Target», in Proc. 14th Int. Workshop on Nuclear Fission Physics, Oct 1999, p. 176, 2000.
38. Tretyakova T.Yu. , Lanskoy D.E. Neutron-rich Λ-hypernuclei: σ admixture and production in the (K^-,π^+) reaction, in Proc. Of VII International Conference on Hypernuclear and Strange Particle Physics HYP2000, Torino, Italy, 2000, to be published in Nucl. Phys. A
39. Tretyakova T.Yu., Tretyakova S.P., Calabretta L., Itkis M.G., Kozulin E.M., Kondratiev N.A., Maiolino C., Pokrobski I.V., Prokhorova E.V. Rusanov A.Yu., «Investigation of the Fusion-Fission Reaction », in Proc. Int.Conf. on Nuclear Physics «Nuclear Shells - 50 Years», Dubna, Russia, 1999, editted by Oganesian Yu.Ts.and Kalpakcheeva R., p.151, World Scientific, Singapore, 2000.
40. Voinov A.V., Popov Yu.P., Parzhitski S.S., Kobzev A.P., Gundorin N.A, Serov D.G., Sedyshev P.V., Sedysheva M.V. Analysis of the partial neutron capture cross sections of ^{58}Ni(n,γ)^{59}Ni reaction. 8 International Seminar on Interaction of Neutrons with Nuclei. Neutron Spectroscopy, Nuclear Structure, Related Topics. ISINN-8, Dubna, May 17-20, 2000 (Abstracts) E3-2000-71, 46.
41. Voinov A.V., Popov Yu.P., Sedyshev P.V., Kobzev A.P., Serov D.G., Parzhitski S.S., Gundorin N.A., Sedysheva M.V. Measurement of the partial radiative neutron capture cross section on ^{63}Cu. 8 International Seminar on Interaction of Neutrons with Nuclei. Neutron Spectroscopy, Nuclear Structure, Related Topics. ISINN-8, Dubna, May 17-20, 2000 (Abstracts) E3-2000-71, 100.
42. Voinov A.V., Yu.P.Popov, S.S.Parzhitski, A.P.Kobzev, N.A.Gundorin, D.G.Serov, Experimental Checking for Possibility of the Neutron Spectrum Measurement in Neutron Energu Interval 10-150 keV. Proc. ISINN-8, JINR E3-2000-192, p.445, Dubna, 2000.
43. Tambovtsev D.I., Kozlovsky L.K., Gonin N.N., Doroshenko A.Yu., Kopach Yu.N., Popov A.B., Furman W.I. Measurement of the superfine bond constant in the crystal URN», 15th Int.Workshop on Nuclear Fission Physics, 2-5 Oct, 2000.

THE IBR-2 SPECTROMETER COMPLEX AND COMPUTATION INFRASTRUCTURE

1. Levchanovski F., Gebauer B., Schulz Ch.. A PCI DAQ Board for a Two-Dimentional High-Resolution Delay Line Detector. Book of Abstracts of the Second Intern. Workshop on Data Acquisition Systems for Neutron Experimental Facilities. June 5-7, 2000, Dubna, Russia, p.17.
2. Butenko V., Levchanovski F., Prikhodko V. RTOF-Correlator of the Parallel-Serial Type for Fourier Diffractometers at Steady-State Neutron Sources, ibid. p.20.
3. Zhuravlev V.et al. Control System of Neutron Beam Choppers on the Physical Instruments at the IBR-2 Reactor, ibid., p.21.
4. Drozdov V.. Four-Processor Block for the Measurement and Acquisition of Correlation Spectra from the High Resolution Spectrometer FSD, ibid. p.26.
5. Ermilov V.G.et al. System for Diagnostic and Monitoring of the IBR-2 Reactor State. Data Acquisition and Storage, ibid. p.30.
6. Kirilov A.. Current State and Prospects of the IBR-2 Instrument Control Software, ibid. p.36.
7. Litvinenko E.. The Implementation of NeXus Data Format in OpenG2 Software Package, ibid. p.39.
8. Litvinenko E., Semenov R.. The Experience with TACO Testing, ibid. p.40.
9. Murashkevich S., Kirilov A.. DAQ Control in the SONIX Control Software, ibid. p.41.
10. Petukhova T., Kirilov A.. Stepper-Motor in the SONOX Control Software, ibid. p.42.
11. Astakhova N., Kirilov A.. Sample Environment Characteristics Visualization Program in the SONIX Control Software, ibid. p.43.
12. Astakhova N., Kirilov A.. Temperature Control in the SONIX Control Software, ibid. p.44.
13. Salamatin I., Astakhova N., Kirilov A.. Remonte Control of the YuMO Instrument, ibid. p.45.
14. Petukhova T.. The Software Control System of X-ray Diffractometers DRON and SAX, ibid. p.46.
15. Levchanovski F., Nikiforov A.. The Software for Spectra Accumulation on the Basis of the DSP TMS320C40 Signal Processor for Neutron Spectrometers at the IBR-2 Pulsed Reactor, ibid. p.48.
16. Avdeev M., Prikhodko A.. C^{++} Library Instrument to Treat Experimental numbers Taking the Errors Propagation

into Account, ibid. p.49.
17. Avdeev M., Prikhodko A.. EXPDATLIB C^{++} Library Based on STL. Instrument to Treat Experimental Data, ibid. p.50.
18. Levchanovski F., Polyakov V.. MEZZANINES: The Way for a Common Specification for Interfaces Between Layers in the Neutron Spectrometers DAQ Systems, ibid. p.56.
19. Gebauer B., Schulz Ch., Richter G., Levchanovski F., Nikifiriv A.. Development of a Hybrid MSGC Detector for Terminal Neutron Imaging with a MHz Data Acquisition and Histogramming System. In Proc. of the Imaging 2000 Conference, June 28 – July 1,2000, Stockholm Sweden (Submitted to NIM).
20. Zhidkov E.P., Litvinenko E.. Some Methods of Neutron Scattering Data Analysis, Computer Physics Communication 127 (2000), 229-241.
21. Fromme M., Hoffmann-Schulz G., Litvinenko E., Ziem P.. BEAN – A New Standard Program for Data Analysis at BER-II, Proc. of XIth IEEE NPSS Real Time Conference, Santa Fe, USA, 1999, 354-358.

6. PRIZES

JINR Prizes:

Experimental Physics Research*:*

Encouraging Prize:

V.L.Aksenov, A.M.Balagurov, D.V.Sheptyakov, E.V.Antipov, S.N.Putilin. «Neutron Diffraction Study of the Atomic Structure and Physical Properties of High-T_c Mercury-Based Superconductors as a Function of Anion Composition and External Pressure»

Physics Instruments and Methods:

Encouraging Prize:

Yu.M.Gledenov, V.I.Salatskii, P.V.Sedyshev, M.V.Sedysheva, R.Mashrafi, G.Khuukhenkhuu, Cheng Zemin, Tang Gyouy, V.A.Vesna, P.Szalanski. «Gas-Filled Detectors for Research of Neutron-Induced Charged Particle Emission Reactions»

***FLNP Prizes*:**

In Nuclear Physics:

First Prize:

E.V.Vasilieva, A.M.Sukhovoj, V.A.Khitrov. «Influence of the Excited States Structure of Heavy Nuclei on the Process of Cascade γ-Decay at Energies around the Neutron Binding Energy»

Second Prize:

A.V.Strelkov et al. «Neutron Quantum States in the Gravitational Field of Earth»

V.P.Alfimenkov, L.Lason, Yu.D.Mareev, V.V.Novitskii, L.B.Pikelner, V.M.Tsulaya, M.I.Tsulaya, A.N.Chernikov. «Spatial Parity Violation and Interference Effects at ^{233}U Fission»

In Condensed Matter Physics:

First Prize:

V.L.Aksenov, Yu.V.Nikitenko, S.V.Kozhevnikov, N.A.Gundorin, Yu.P.Popov, Yu.M.Gledenov, P.V.Sedyshev. «Observation of the Field of Neutron Standing Waves by Registering Spin-Reoriented Neutrons, Gamma-Quanta, and Charged Particles»

Second Prize*:*

N.I.Gorskii et al. «SANS Studies of the Properties of Self-Organizing Systems»

Third Prize:

V.V.Sikolenko, V.V.Sumin et al. «Neutron Investigations of the Lattice Structure and Dynamics of a Solid Solution of Hydrogen in α-Mn»

E.V.Raspopina, A.M.Balagurov, V.Yu.Pomjakushin, V.V.Sikolenko et al. «Neutron Diffraction and μSR Studies of the Modulated Magnetic Structure $U(Pd_{1-x}Fe_x)_2Ge_2$»

7. SEMINARS

Date	Authors	Title
20.01.2000	I.Natkaniec (FLNP JINR)	Neutron investigations and computer modeling of molecular crystal dynamics
27.01.2000	V.V.Nesvizhevsky (ILL, Grenoble)	1. Observation of neutron quantum states in the gravitational field of the earth. 2. Experiments of small UCN heating. 3. The new UCN channel at the ILL reactor
02.06.2000	1. V.L.Aksenov 2. A.V.Belushkin 3. E.P.Shabalin (FLNP JINR)	<u>European Neutron Source Project</u> 1. Research objectives for the neutron sources of the fourth generation. 2. The project status and JINR participation. 3. The project of the target and moderators.
09.11.2000	V.N.Pervushin D.V.Proskurin (BLTP JINR) M.Pavlowski (Zoltan Inst., Warszaw)	Quantum-field theory of the cosmic evolution of the Universe
14.12.2000	V.M.Dubovik (BLTP JINR)	Quantum gravitation and low-energy interactions
28.12.2000	A.V.Strelkov (FLNP JINR)	Monitoring of intense neutron beams with the help of a proportional counter

8.1. STRUCTURE OF LABORATORY AND SCIENTIFIC DEPARTMENTS

Directorate:
Director:
V.L.Aksenov
Deputy Directors:
A.V.Belushkin
W.I.Furman
Scientific Secretary:
V.V.Sikolenko

Reactor and Technical Departments
Chief engineer: V.D.Ananiev
IBR-2 reactor
Chief engineer: A.V.Vinogradov
IBR-30 booster + LUE-40
Head: S.A.Kvasnikov
Mechanical maintenance division
Head: A.A.Belyakov
Electrical engineering department
Head: V.P.Popov
Design bureau
Head: V.I.Konstantinov
Experimental workshops
Head: A.N.Kuznetsov

Scientific Departments and Sectors
Condensed matter department
Head: V.L.Aksenov
Nuclear physics department
Head: V.N.Shvetsov
Department of IBR-2 spectrometers complex
Head: A.V.Belushkin
Department of IREN
Head: A.P.Sumbaev
Nuclear Safety and applied research
Head: E.P.Shabalin

Administrative Services
Deputy Director: S.V.Kozenkov
Secretariat
Finances
Personnel

Scientific Secretary Group
Translation
Graphics
Photography
Artwork

CONDENSED MATTER DEPARTMENT

Sub-Division	Title	Head
Diffraction sector. Head: A.M.Balagurov		
Group No.1	HRFD	V.Yu.Pomjakushin
Group No.2	DN-2	A.I.Beskrovnyi
Group No.3	DN-12	B.N.Savenko
Group No.4	NSVR	K.Ullemeyer
Small-angle neutron scattering group. Head: V.I.Gordeliy		
Neutron optics sector. Head: V.L.Aksenov		
Group No.1	SPN-1	Yu.V.Nikitenko
Group No.2	REFLEX	D.A.Korneev
Inelastic scattering group. Head: I.Natkaniec		

NUCLEAR PHYSICS DEPARTMENT

Sub-Division	Title	Head
Group No.1	Polarized neutrons and nuclei	Yu.D.Mareev
Group No.1	Neutron spectroscopy	A.B.Popov
Group No.3	Nuclear fission	Sh.S.Zeinalov
Group No.4	Thermal polarized neutrons	M.I.Tsulaya
Group No.5	Proton and α-decay	Yu.M.Gledenov
Group No.6	Properties of γ-quanta	A.M.Sukhovoy
Group No.7	Neutron structure	G.S.Samosvat
Group No.8	Ultra-cold neutrons	V.N.Shvetsov
Group No.9	Neutron optics	A.I.Frank
Group No.10	Neutron activation analysis	M.V.Frontasyeva
Group No.11	Theory	Yu.A.Alexandrov

DEPARTMENT OF IBR-2 SPECTROMETERS COMPLEX

Sub-Division	Title	Head
Sector No.1	Electronics	V.I.Prikhodko
Group No.1	Analogous electronics	A.A.Bogdzel
Group No.2	Digital electronics	V.F.Levchanovsky
Group No.3	Software	A.S.Kirilov
Group No.4	Local networks	G.A.Sukhomlinov
Group No.5	Technology	A.B.Melnichuk
Sector No.2	Spectrometers	V.V.Zhuravlev
Group No.1	Development	G.A.Varenik
Group No.2	Samples environment	A.P.Sirotin
Group No.3	Detectors	J.Sokolovsky

8.2. USER POLICY

The IBR-2 reactor usually operates 10 cycles a year (2500 hrs.) to serve the experimental programme. A cycle is established as of 2 weeks of operation for users, followed by a one week period for maintenance and machine development. There is a long shut-down period between the end of June and the middle of October.

All experimental facilities of IBR-2 are open to the general scientific community. The User Guide for neutron experimental facilities at FLNP is available by request from the Laboratory's Scientific Secretary.

Condensed matter studies at IBR-2 have undergone some changes in accordance with the experience gained during the last several years. It was found to be necessary to establish specialized selection committees formed of independent experts in their corresponding fields of scientific activities. The following four committees were organized:

1. Diffraction *Chairman* - V.A.Somenkov - Russia	3. Neutron optics *Chairman* - A.I.Okorokov - Russia
2. Inelastic scattering *Chairman* - W.Nawrocik - Poland	4. Small angle scattering *Chairman* - L.Cser - Hungary

Dr. Ekaterina V.Raspopina is responsible for the user policy. Deadline for proposal submission is May 16.

The IBR-2 beam schedules are drawn up by the head of the Condensed Matter Department together with instruments responsibles on the basis of experts recommendations and are approved by the FLNP Director or Deputy Director for condensed matter physics. The schedules are sent to Chairmen of Selection Committees.

After the completion of experiments, "Experimental Report" forms are filled out by experimenter(s) and submitted to the Scientific Secretary.

The Application Form and other information about FLNP are available by WWW: http://nfdfn.jinr.ru/~sikolen/usepol.html

Contact address:

***Dr. E.Raspopina**, Frank Laboratory of Neutron Physics*
Joint Institute for Nuclear Research
141980 Dubna, Moscow region, Russia
Tel.: (+7)-095-926-22-53, Fax: (+7)-09621-65085; (+7)-09621-65484;
E-mail: katrin@nf.jinr.ru

8.3. MEETINGS AND CONFERENCES

In 2000, FLNP organized the following meetings:

1.	VIII International Seminar on Interaction of Neutrons with Nuclei (ISINN-7)	May 11-14	Dubna
2.	III International Seminar «Ferroelectrics-relaxors»	June 23-26	Dubna

In 2001, FLNP will organize the following meetings:

1.	IX International Seminar on Interaction of Neutrons with Nuclei (ISINN-9)	May 17-20	Dubna
2.	School on Neutron Scattering and Synchrotron Radiation	March 19 - April 27	Dubna
3.	IBR-2 in XXI century	May 25	Dubna

8.4. COOPERATION

List of Visitors from Non-Member States of JINR in 2000

Name	Organization	Country	Dates
R.Machrafi	Univ.Mohamed V.Rabat	Morocco	01.01-25.08
D.Protopopescu	Univ. of New Hamphire, Durham	USA	01.01-27.01
Zhang Zhaohui	IHEP, Beijing	China	01.01-28.01
O.Nikonov	ILL, Grenoble	France	09.01-28.01
V.Lauter	ILL, Grenoble	France	12.01.27.01
H.-J.Lauter	ILL, Grenoble	France	16.01-21.01
M.Jung	TU, Darmstadt	Germany	16.01-27.01
T.Wieder	TU, Darmstadt	Germany	19.01-23.01
V.V.Nesvizhevsky	ILL, Grenoble	France	23.01-28.01
Hany Ahmed Abdel Meguid Amer	NCNSRC, Cairo	Egypt	31.01-06.02
B. Titze-Jaensch	FRZ, Juelich	Germany	04.02-09.02
H.Wagner	FRZ, Juelich	Germany	07.02-09.02
M.Stalder	IfzP, Dresden	Germany	24.02-09.03
Fawzi Ibrahim Ali Asfour	NRC, AEA, Cairo	Egypt	24.02-24.05
A.Bogdan	Univ. of Helsinki	Finland	18.03-23.03
R.K.Heenan	Rutherford Appleton Laboratory	UK	07.04-17.04
F.Haussler	Leipzig University	Germany	08.04-14.04
P.Joercel	Leipzig University	Germany	10.04-16.04
V.Lauter	ILL, Grenoble	France	13.04-22.04
K.Bramnik	TU, Darmstadt	Germany	14.04-19.04
K.Mishima	RRI, Kyoto Univ.	Japan	16.04-18.04
K.Kobayashi	RRI, Kyoto Univ.	Japan	16.04-18.04
H.-J.Lauter	ILL, Grenoble	France	16.04-20.04
M.Stalder	IfzP, Dresden	Germany	14.05-30.05
O.Steinsvol	Inst. for Energy Technology, Kjeller	Norway	14.05-26.05
A.-T.Skjeltop	Inst. for Energy Technology, Kjeller	Norway	19.05-26.05
I.-A.Skjeltorp	Inst. for Energy Technology, Kjeller	Norway	19.05-26.05
Gou Cheng	Inst. of Atomic Energy,	China	06.06-09.06

	Beijing		
Yang Tonghua	Inst. of Atomic Energy, Beijing	China	06.06-09.06
Ye Chuntang	Inst. of Atomic Energy, Beijing	China	06.06-09.06
O.Nikonov	ILL, Grenoble	France	18.06-29.06
V.Lauter	ILL, Grenoble	France	18.06-29.06
H.-J.Lauter	ILL, Grenoble	France	18.06-29.06
E.T.Knijnenburg	TU, Delft	The Netherlands	21.06-21.06
H.T.Wolterbeek	TU, Delft	The Netherlands	21.06-21.06
T.I. Van der Meer	TU, Delft	The Netherlands	21.06-21.06
A.J. Van der Meer	TU, Delft	The Netherlands	21.06-21.06
M.Hoelzel	GSI, Darmstadt	Germany	19.07-29.07
M.Rudalics	University of Linz	Austria	30.07-09.09
K.Walther	GeoFRZ, Potsdam	Germany	10.08-18.08
A.Tressaud	ICMCB-CNRS, Pessac	France	14.09-17.09
A.Bulou	Lab. De Phys. de l'ETAT Cond., Le Mans	France	14.09-17.09
R.B.Lahoz	Ins. Ciencia de Materiales, Zaragoza	Spain	14.09-17.09
E.Steinnes	Univ. of Trondheim	Norway	30.09-03.10
Zhang Zhaohui	IHEP, Beijing	China	02.10-16.10
R.E. El-Din	NRC, AEA, Cairo	Egypt	02.10-10.10
R.Tamm	TU, Dresden	Germany	22.10-10.11
Medhat Moustafa El-Sayed	NRC, AEA, Cairo	Egypt	30.10-01.01
Abdel Rasik Hussein	NRC, AEA, Cairo	Egypt	08.11-14.11
Mohey Mahomud	NRC, AEA, Cairo	Egypt	08.11-14.11
G.Klose	Leipzig Univ.	Germany	08.11-16.11
V.Lauter	ILL, Grenoble	France	08.11-21.11
H.-J.Lauter	ILL, Grenoble	France	11.11-14.11
J.Schreiber	IfzP, Dresden	Germany	12.11-25.11
Adnan Hafez Murbut	University of Bagdad	Iraq	17.11-17.11
P.Pal	TU, Berlin	Germany	17.11-17.11
F.Haussler	Leipzig Univ.	Germany	19.11-22.11
U.Dallborg	Leipzig Univ.	Germany	19.11-22.11
W.Gudowski	Royal Inst. of Technol., Stockholm	Sweden	23.11-24.11
Gyinyun Kim	Pohang Univ. of Science & Technol.	Korea	03.12-13.12
Dae Won Lee	Pusan National University	Korea	03.12-13.12
Youn Soo Kang	Pusan National Univ.	Korea	03.12-23.12
H.Groeger	Goettingen Univ.	Germany	03.12-17.12
T.Straessle	PSI, Villigen	Switzerland	04.12-11.12
P.Joercel	Leipzig Univ.	Germany	06.12-10.12
B.Kalska	Uppsala Univ.	Sweden	07.12-13.12
J.Watanabe	RIKEN, Tokyo	Japan	10.12-24.12

8.5. EDUCATION

The objective of the FLNP educational program is the training of specialists in the field of neutron methods for condensed matter and nuclear physics research. In the year 2000 in Moscow State University named after M.V.Lomonosov the neutron diffraction department opened and it is a basic department for FLNP. In addition to the students of this department, the students of the MSU Interfaculty Center «Structure of Matter and New Materials» carry out their diploma work in FLNP. In the Center the students from the Chemical Faculty of MSU, Higher College of Materials Sciences under MSU, Tula State University, Tula Pedagogical University, Tver State Univesity and other universities of Russia and JINR member-states do the course. A total of 14 students and 8 post-graduates took the course in the year 2000. The reported year saw the eighth graduation of students.

In the year 2000, the First Spring School on Neutron Scattering for Condensed Matter Research was organized by FLNP in cooperation with MSU. The participants listened to the lectures by eminent scientists and did a series of practical works at the IBR-2 reactor and other JINR facilities under the guidance of FLNP specialists. It is planned to hold the school annually.

8.6. PERSONNEL

Distribution of the Personnel per Department as of 01.01.2001

Theme	Departments	Main staff
-0974-	Nuclear Physics Department	58
-1031-	Condensed Matter Physics Department	45
-1012-	IBR-2 Spectrometers Complex Department	50
-0993-	IREN Department	28
-1007-	Nuclear Safety Sector	14
-0851-	IBR-2 Department	51
	Mechanical and Technical Department	61
	Electric and Technical Department	34
	Central Experimental Workshops	39
	Design Bureau	8
	FLNP infrastructure:	
	Directorate	6
	Services and Management Department	18
	Scientific Secretary Group	7
	Staff Management Group	5.5
	Supplies Group	3
Total		**428.5**

Personnel of the Directorate as of 01.01.2001

Country	People
Azerbaijan	1
Armenia	1
Bulgaria	4
Egypt	1
Germany	4
Georgia	2
Iraq	1
Kazakhstan	1
Morocco	1
Mongolia	3
Poland	6
Romania	3
Russia	21
Ukraine	2
TOTAL	**51**

8.7. FINANCE

Financing of the FLNP Scientific Research Plan in 2000 (th. USD)

No.	Theme	Financing plan, $ th.	Expenditures for 12 months, $ th.	In % of FLNP budget
I	**Condensed matter physics**	**4054.2**	**1917.0**	**47.3**
	-1031-	2468.9	1450.4	58.7
	-0851-	959.9	236.3	24.6
	-1012-	625.4	230.3	36.8
II	**Neutron nuclear physics**	**1117.7**	**694.4**	**62.1**
	-0974-	618.2	340.2	55.0
	-0993-	499.5	354.2	70.9
III	**Elementary particle physics**			
	-1007-	**6.1**	**21.6**	**354.1**
IV	**Relativistic nuclear physics**		**6.7**	
	-1008-	**41.5**		**16.1**
V	**TOTAL:**	**5219.5**	**2639.7**	**50.6**